Synthesis and Characterisation of Functionalised Perylene Diimides

Ben Alexander Llewellyn, MSci

Thesis submitted to the University of Nottingham for the degree of Doctor of Philosophy

July 2016

Declaration

Except where specific reference is made to other sources, the work presented in this thesis is the original work of the author. It has not been submitted for any other degree except for a small section of Chapter 4 which was submitted for a Masters project at the University of Nottingham. Some of the results have already been published.

Signed:

Ben A. Llewellyn

Date:

Abstract

This thesis describes the synthesis of three series of perylene diimides (PDIs) by functionalisation at all four possible regions of the molecule. The synthesised compounds were then probed by optical, electrochemical and photophysical methods in order to fully elucidate their properties.

Chapter 1 gives an overview of the structure, synthesis, properties and applications of PDIs and introduces the main topics investigated in this thesis.

Chapter 2 describes the synthesis of two of the first examples of PDIs with an absorption maximum in the near infrared. This was achieved by functionalisation of the bay area with a secondary amine followed by thionation of the imide carbonyls. One of the synthesised PDIs displays a highly unusual black colour, demonstrating absorption of light across an impressive range of the sun's emission spectrum, suggesting excellent potential for incorporation into light harvesting devices.

Chapter 3 details the synthesis of seven multichromophoric systems composed of PDIs and boron dipyrromethenes (BODIPYs). The number and position of the BODIPYs is varied along with the structure of the BODIPYs themselves by addition of methyl- and catecholate groups. The absorption and emission properties of the systems were investigated in order to elucidate any energy or electron transfer processes occurring. Energy transfer results in fluorescence solely from the PDI chromophore, rather than the BODIPY, whilst electron transfer was found to quench emission. Communication across the core of the PDI was observed between the BODIPY moieties, shown by cyclic voltammetry, whilst spectroelectrochemical methods demonstrated the effects of oxidation and reduction upon the absorption of the molecules.

Chapter 4 reports on the synthesis of a pair of PDIs symmetrically and asymmetrically substituted with a platinum acetylide complex. Transient absorption spectroscopy and singlet oxygen generation measurements confirmed the formation of the triplet excited state of the PDI, due to the 'heavy atom' effect, induced by the presence of the platinum complex covalently bound to the PDI.

Acknowledgments

Firstly I would like to thank Professor Neil Champness for being an excellent supervisor providing advice, support and encouragement with good humour throughout the four and a half years I have worked for him. I've learnt so much and had a lot of fun.

Dr Stephen Davies has not only spent many hours performing cyclic voltammetry, spectroelectrochemistry and EPR spectroscopy on the compounds I have synthesised but has also taught me huge amounts about the measurements being undertaken and suggested many possible routes for my projects to follow. He was even persuaded to carry out the emission measurements despite this being his least favourite pastime.

I would like to thank Dr Will Lewis, Dr Stephen Argent and Dr Connie Pfeiffer who all patiently (and repeatedly) explained crystallography the new way, the old way and the really old way respectively.

During my PhD I have taken full advantage of the NMR and mass spectrometry facilities available in the School which are so well run and maintained by Dr Adrienne Davies, Shaz Aslam, Kev Butler, Graham Coxhill, Ben Pointer-Gleadhill and Dr Mick Cooper, who must receive a special thanks for running so many HRMS in a very short time.

I would also like to thank Dr Tim Easun for emission spectroscopy, Dr Xue-Zhong Sun and Professor Mike George for transient absorption measurements, Professor Andrew Beeby for singlet oxygen generation measurements, Stephen Boyer for elemental analysis and Dr Jonathan McMaster for advice on DFT.

The overriding reason I have enjoyed my PhD has been the people I have worked with so I would like to thank; Nic for all of the help since our days as project students

together, extensive proof reading and a little bit of competition, Anna for teaching me so much about PDIs before she left, my project students Sarah and Monksey for both being excellent and enthusiastic (with amusingly different personalities), Tim for his relentless cheerfulness, Lixu for her mother-in-law stories, Harry for demonstrating that it is possible to succeed in life with very little effort, Sam for sharing my definition of ‘a couple of pints’, Charlie for not leaving me behind too much on the bike, Dan for being a great fumehood partner, Phil for all his great jokes about Germany, Simon, Irina, Tom, Vics, Barry, Ben, Harry, Razan and Andrea for making B52 such an excellent place to work!

Contents

List of Abbreviations

5DI	Pentarylene Diimide
abs	Absorption
B_2Pin_2	Bis(pinacolato) Diboron
BHJ	Bulk Heterojunction
BODIPY	Boron Dipyrromethene
BPin	Pinacol Boron
c	Concentration
CV	Cyclic Voltammetry
D-A	Donor-Aceptor
DCB	Dichlorobenzene
DCM	Dichloromethane
DCTB	*trans*-2-[3-(4-*tert*-Butylphenyl)-2-methyl-2-ropenylidene]malononitrile
DDQ	2,3-dichloro-5,6-dicyanobenzoquinone
DFT	Density Functional Theory
DSSC	Dye Sensitised Solar Cell
em	Emission
EPR	Electron Paramagnetic Resonance
ESI	Electrospray Ionisation
Fc/Fc^+	Ferrocene/Ferrocenium
FI	Field Ionisation
FRET	Fluorescence Resonance Energy Transfer
HDI	Hexarylene Diimide
HOMO	Highest Occupied Molecular Orbital
ICT	Intramolecular Charge Transfer
IPA	Isopropyl Alcohol
ISC	Intersystem Crossing
LUMO	Lowest Unoccupied Molecular Orbital

MALDI	Matrix-Assisted Laser Desorption/Ionisation
MeOH	Methanol
MO	Molecular Orbital
MS	Mass Spectrometry
NDI	Naphthalene Diimide
NIR	Near Infrared
NMP	N-Methyl-2-Pyrrolidone
NMR	Nuclear Magnetic Resonance
OFET	Organic Field Effect Transistor
OLED	Organic Light Emitting Diode
OPV	Organic Photovoltaic
PCE	Power Conversion Efficiency
PDA	Perylene Dianhydride
PDI	Perylene Diimide
PDT	Photodynamic Therapy
PET	Photoinduced Electron Transfer
PMI	Perylene Monoimide
QDI	Quaterrylene Diimide
SWIR	Short Wave Infrared
TA	Transient Absorbance
TBAH	Tetrabutylammonium Hydroxide
TDI	Terrylene Diimide
TEA	Triethyl Amine
TFA	Trifluoroacetic Acid
TOF	Time of Flight
TTET	Triplet-Triplet Energy Transfer
UV	Ultraviolet
ε	Extinction Coefficient
λ	Wavelength

Chapter 1. Introduction

1.1. Perylene Diimides

Perylene diimides (PDIs) were first synthesised over a century ago by Kardos.[1] Since that time their high chemical and thermal stability, intense absorbance in the UV/vis range, high fluorescence with up to 100% quantum yields, excellent n-type semiconductivity and synthetic versatility have led to the creation of a vast field of research.[2-4] This thesis details the synthesis and optical, electrochemical and photophysical analysis of three different series of PDIs, therefore, this introduction will concentrate only on PDIs in general with a more detailed introduction, including more specific information, given at the start of each chapter.

1.1.1. Structure and Synthesis

The basic structure of PDI consists of two naphthalene rings joined together by single bonds, making up the perylene core, functionalised at the peri-positions (3-, 4-, 9- and 10-) with dicarboxylic acid imide groups, Figure 1.1. There are three main areas of interest on the PDI which can all undergo further functionalisation; the imide-, ortho- and bay-regions. The planar aromatic core of the PDI results in strong π-π stacking interactions, with a stacking distance crystallographically measured to be 3.34 to 3.55 Å,[5] leading to a reduction in the solubility of the molecules.

Substitutions at the imide-region of the PDI displace the stacking between the PDIs, due to steric bulk, disrupting the π-π interactions thus increasing the solubility. This approach was pioneered by Langhals and co-workers[6] with their 'swallow-tail' branched alkyl chains, since then many other solubilising groups have been used with ortho-substituted anilines proving particularly effective.[7] PDIs have even been solubilised in water *via* imide-functionalisation with, for example, phosphate

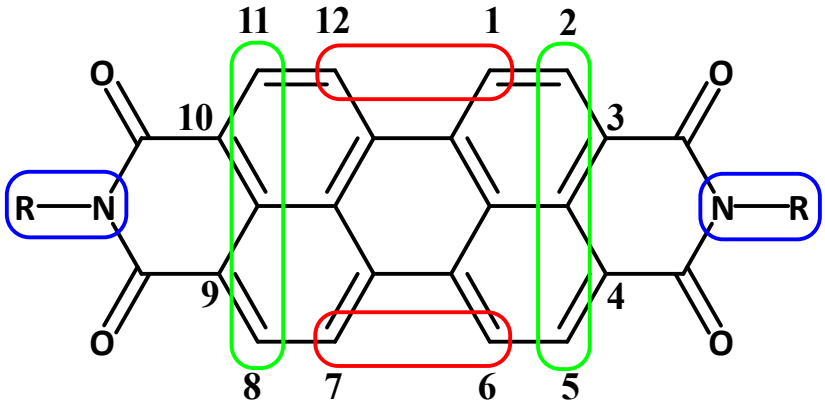

Figure 1.1. Structure of PDI with numbering system and imide- (blue), ortho- (green) and bay- (red) regions highlighted.

surfactants,[8] ammonium cations[9] and cyclodextrins.[10] One major advantage of substitution at this position is that it has no effect on the absorption or redox properties of the PDI due to a node in the HOMO and LUMO at the imide nitrogen, Figure 1.2.[11] The fluorescence, however, can be quenched by photoinduced electron transfer (PET) caused by electron rich substituents at the imide-position.[12]

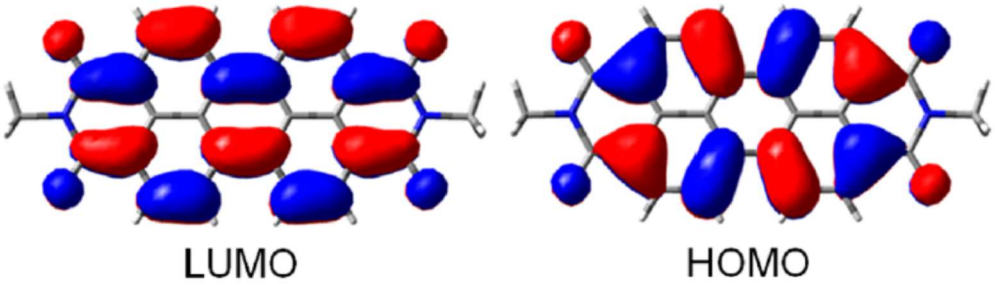

Figure 1.2. DFT calculated HOMO and LUMO of an unsubstituted PDI showing the node at the imide nitrogens.[3]

Imide-substitutions are usually carried out by an imidization of the parent perylene dianhydride (PDA) with the appropriate amine. Imidazole is often used as a solvent in the case of anilines whilst alcohols, such as isopropyl alcohol (IPA), are commonly used in the case of aliphatic amines. *N,N'*-asymmetrically substituted PDIs have been synthesised from PDA *via* mono potassium salts[13] or monoanhydride diesters[14] vastly increasing the scope of the PDI systems being synthesised. Imide-substitution is not

only used as a tool to increase the solubility of PDIs but also to synthesise highly complex PDI-containing systems such as photoisomerisable dimers,[15] rotaxanes,[16] molecular triangles,[17] self-assembled tetrahedrons[18] and 'on/off' fluorescence probes[19] to name but a few.

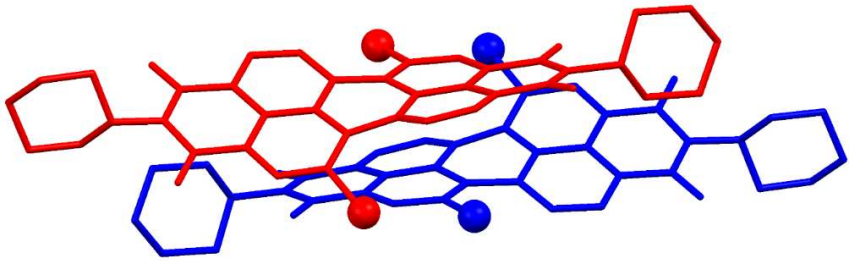

Figure 1.3. X-ray crystal structure of 1,7-dibromo PDI showing the disruption of the π-π stacking by displacement of the molecules, due to imide-substitution, and twisting of the core caused by bay-functionalisation.

Substitutions at the bay-area of PDIs not only introduce interesting functionality to the molecules but also cause a steric twisting of the PDI core, disrupting the π-π stacking and increasing the solubility, Figure 1.3. These substitutions are usually performed by halogenation; first realised in the 1980s with the tetra-chlorination of PDA with sulfuryl chloride in nitrobenzene.[20] More recently, bromination has become the most common route to introducing functionality to the bay-area by the reaction of PDA with bromine, in boiling concentrated sulfuric acid, giving dibromo PDIs.[21] The use of harsher conditions, such as oleum rather than sulfuric acid as the solvent and longer reaction times, leads to tetra-bromo PDIs.[22] Bromination post-imidization allows for the use of much milder conditions (dichloromethane at reflux) and leads to the selective formation of di- and mono-brominated PDIs.[23] Octa-bromination and chlorination, with 5,5-dimethyl-1,3-dibromohydantoin and chlorosulfonic acid respectively, have been used to synthesise PDIs with potential for further functionalisation at every position on the core of the molecule.[24, 25]

A major problem with dibromination of PDIs is the unavoidable formation of two isomers; the 1,6-isomer has two bromine atoms on opposite sides of the same naphthalene ring whilst the bromine atoms in the 1,7-isomer are connected to opposing naphthalene rings, still on opposite sides of the molecule, Scheme 1.1. These isomers are only visible in high field NMR and can prove to be very difficult to separate. However, this separation is essential as it has been shown that they can have drastically different properties.[26-28] In some cases, fortuitous separation can be achieved by column chromatography after further functionalisation,[26] however, more often repeated recrystallizations of the dibromo PDI are necessary in order to give pure 1,7- isomer,[29] greatly increasing the difficulty of synthesis.

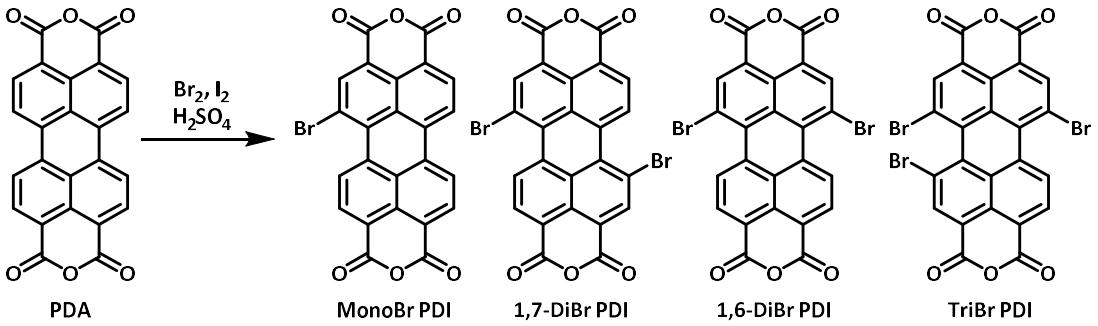

Scheme 1.1. Reaction products formed following bromination of PDA. The mono- and tri-substituted analogues can be removed by column chromatography but separation of the dibrominated isomers is more problematic.

Once halogenation has been achieved further reactions are then possible to introduce the desired functionality. Nucleophilic substitutions allow the introduction of, for example, amino-,[30] phenoxy-[31], thio-[32] and cyano-[33] groups whilst Suzuki,[34] Sonogashira[35] and Stille[36] couplings give the potential for a huge array of different substitutions by C-C bond formation. Extension of the PDI core has been achieved by substitution of dibromo PDI with terminal alkyne followed by catalytic hydrogenation

of triple bonds[37] or by Suzuki cross coupling to introduce pyridyl-groups followed by light promoted cyclisation.[38]

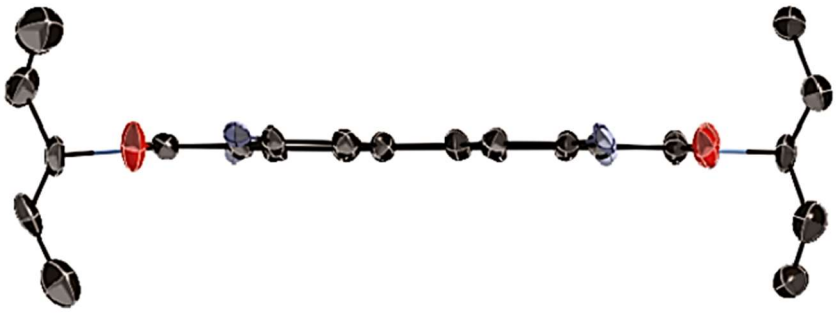

Figure 1.4. X-ray crystal structure showing the side view of an ortho-substituted PDI displaying the planarity of the core. Ortho-groups and hydrogen atoms removed for clarity.[39]

Selective functionalisation of the ortho-positions was only reported in 2009 by Osuka and co-workers with the reaction of PDIs in a Ru-catalysed C-H activation reaction giving alky- and aryl-substituted PDIs.[40, 41] The synthesised PDIs possessed increased solubility to the parent PDIs despite being shown crystallographically to have retained their planar structure, Figure 1.4. Whilst this synthetic method has proven to be a powerful tool in the synthesis of new PDIs there are some drawbacks such as; low yields with some substituents, the reactivity of the catalyst reducing the number of potential functional groups and the sole formation of C-C bonds. To address these issues, the Müllen and Shinokubo groups independently devised a new strategy by reacting the PDIs with bispinacolato diboron (B_2Pin_2), using a Ru or Ir catalyst, to give PDIs tetra-substituted with boronic esters, Figure 1.5.[39, 42] These PDIs increased the scope of ortho-substitution drastically with the potential to introduce various aryl- and heterocyclic groups by Suzuki cross couplings, oxidation to introduce heteroatoms directly onto the core of the PDI and iodination in order to increase the potential for further reactions such as nucleophilic substitution. Ortho-substitution has been utilised to create PDIs that are mechanochromic,[43] display slip-stacking for organic photovoltaics (OPVs),[44] are water soluble[45] and undergo PET.[46] Interestingly, all of these reports utilise the Ru

catalysed C-C bond formation method. To date, there are no subsequent publications repeating the work functionalising the PDI with boronic esters.

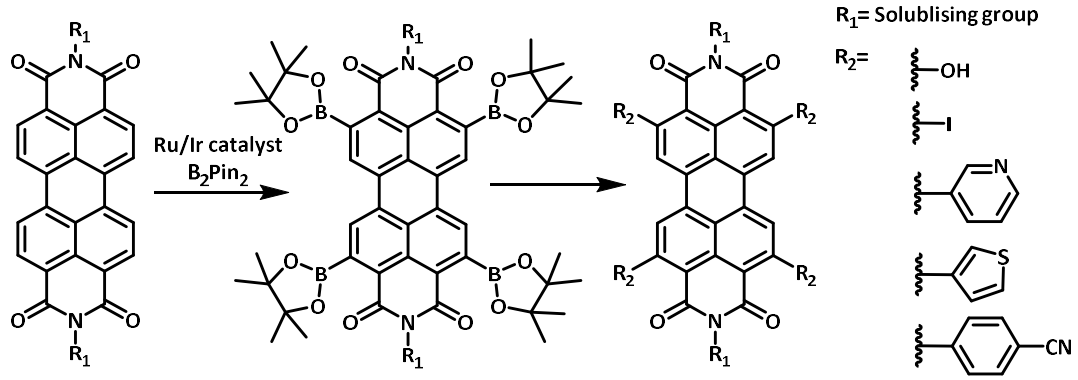

Figure 1.5. Synthesis of ortho-substituted PDIs *via* functionalisation with a boronic ester.

1.1.2. Optical and Redox Properties

Non bay-substituted PDIs possess a peak absorption at around 530 nm, associated with the S_0-S_1 transition, which displays vibrational structure, Figure 1.6.[47] Emission spectra reveal fluorescence, with a small Stokes shift, that is usually a mirror image of absorption with quantum yields of up to 100 %. The introduction of bay-substituents distorts the vibronic structure of the absorption, amplifies the S_0-S_2 transition and can reduce the fluorescence quantum yield due to distortion of the planar perylene core.[47] Electron withdrawing substituents have minor effects on the absorbance maximum whereas electron donating groups can induce significant bathochromic shifts.[48] Ortho-substituents have a similar, although less pronounced, effect on the absorbances apart from the case of the tetra-hydroxy substituted PDI where intramolecular hydrogen bonding with the carbonyl increases the electron withdrawing properties of the imide resulting in a blue shift in the absorption.[39] Fluorescence is preserved in most ortho-substituted cases with the tetra-boronic ester PDI exhibiting a fluorescence quantum yield of 0.18 in the solid state, rationalised by the bulky pinacolboryl groups reducing intermolecular interactions.[39]

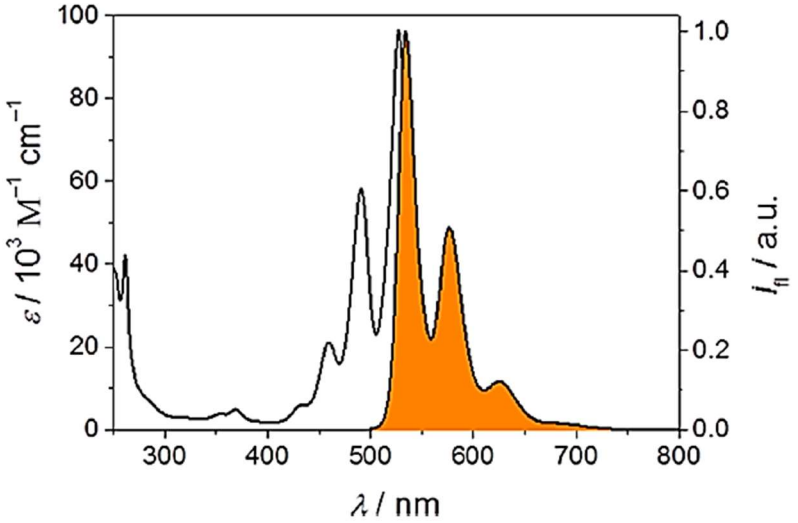

Figure 1.6. Typical absorption (white) and emission (orange) spectra of a non-bay substituted PDI displaying vibronic structure.[3]

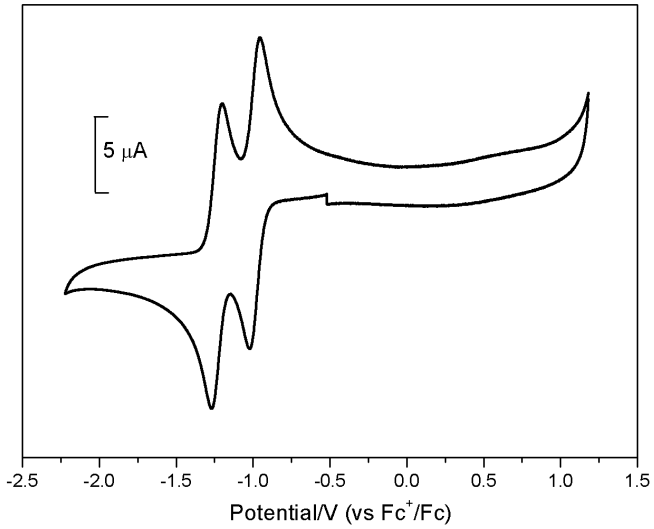

Figure 1.7. Typical cyclic voltammogram of a non-bay substituted PDI displaying two reductions and no oxidations.[49]

PDIs can be considered as electron poor and can easily be reduced. Non-bay substituted PDIs typically display two reversible reductions at around 1.0 and 1.2 V (*vs*. Fc^+/Fc) and no oxidations, Figure 1.7. Bay-substituents, as well as introducing their own localised oxidations and reductions, can affect the potential of the processes located on the PDI. Electron withdrawing groups make reduction potentials more positive,[50] with a 1,6,7,12-tetrachloro-2,5,8,11-tetracyano PBI synthesised by Würthner and co-workers having the most positive reduction potential to date of -0.07 V (*vs*. Fc^+/Fc)

allowing stabilisation of the anion under ambient conditions,[51] whilst electron donating groups make these potentials more negative.[52] Ortho-substitution has the same effect with alkylamine groups making the reduction potentials more negative and iodine atoms making them more positive.[42]

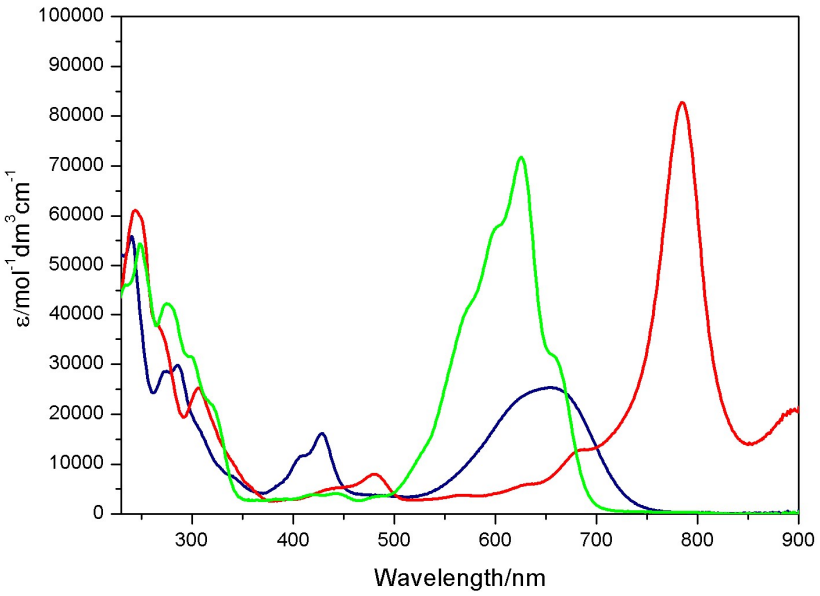

Figure 1.8. UV/vis spectroelectrochemical measurements showing the absorption profiles of the neutral (blue), anion (red) and dianion (green) of a bay-substituted PDI.[26]

Spectroelectrochemical measurements show that reduction has a dramatic effect on the absorption properties; reduction to the monoanion is accompanied by a significant red shift, often into the near infrared, accompanied by an increase in absorption coefficient whilst the second reduction process induces a blue shift often to a wavelength similar to the neutral absorption or between the neutral and first reduction, Figure 1.8.[26, 53] Spectroelectrochemistry not only shows the behaviour of PDIs upon reduction but can be a useful tool in assigning redox processes, observed in cyclic voltammetry, to individual components of the molecule in multichromophoric systems, such as the PDI-fullerene dyad and triad synthesised by Champness and co-workers.[34]

1.1.3. Applications

Harnessing the Sun's power in order to convert it to electricity is an ever expanding field of research, of the many new technologies being developed organic photovoltaics (OPVs) are a promising route to achieving this.[54] Whilst the efficiency of silicon based solar cells has not yet been achieved, OPVs have several advantages such as synthetic versatility, solubility, high absorption coefficients and structural flexibility, with PDIs becoming promising materials for use as the acceptor part in these devices.[55]

PDIs have been incorporated into OPVs by the sublimation of insoluble PDIs into flat heterojunction (FHJ) cells, several examples of such devices were made with copper phthalocyanine as the donor compound with PDI as the acceptor.[56] The groups at the imide nitrogen were varied and it was found that increasing the steric bulk leads to a raising of the open circuit voltage due to greater interfacial dipole moments. However, the steric bulk also decreases the donor-acceptor interactions resulting in an increase in resistance; leading to very little change in overall efficiency of the devices. Improving the solubility of the PDIs allows incorporation into bulk heterojunction (BHJ) cells, where the donor and acceptor are mixed together, allowing excitons easy access to the donor-acceptor interface, however, the π-π stacking between the PDI molecules proved to be problematic due to charge recombination reducing the efficiency of the devices. Bay-substitution, inducing a twist in the PDI core, has gone some way to supress this leading to improved efficiencies.[57] The synthesis of polymers and oligomers where the PDI is connected, *via* bay substitution, to the acceptor is another way of reducing stacking and increasing efficiency such as the PDI-dithienothiophene polymer, shown in Figure 1.9, which possesses a power conversion efficiency of 1.5%.[58]

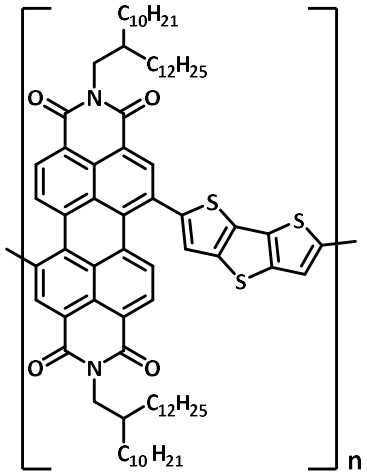

Figure 1.9. PDI-dithienothiophene polymer used in a BHJ cell.

PDIs have also been incorporated into dye sensitized solar cells (DSSCs). The synthesis of 'push-pull' systems bearing electron donating groups can improve efficiency by broadening the absorption and increasing the electron density on the PDI core thus improving the electron injection from the dye to the conduction band of the device, PDIs containing phenoxy- and piperidyl- moieties were synthesised for this purpose.[59] Efficiency of these devices has remained low due to the presence of the electron withdrawing imides at each end of the molecule preventing directed energy transfer to the conduction band of the device. Perylene monoimides (PMIs), therefore, suggest better potential for this application with a sensitizer containing a PMI acceptor, triphenylamine donor and thiophene spacer giving a 96 % conversion of absorbed photons to electrons resulting in a sevenfold increase in energy conversion efficiency, Figure 1.10.[60]

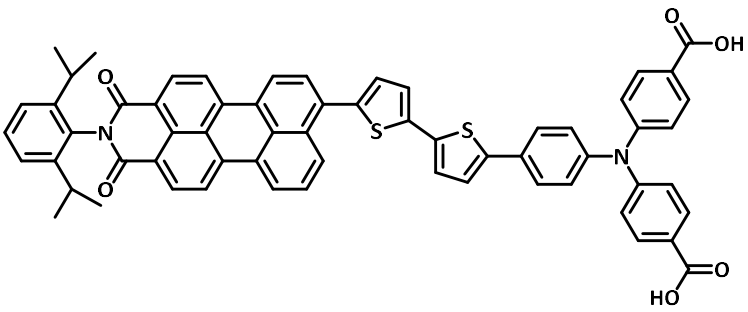

Figure 1.10. 'Push-pull' PMI with excellent photon to electron conversion efficiency.

The desire for low cost, large area and flexibility in electronics, for uses in displays and sensors, has led to the intense interest in the area of organic field effect transistors (OFETs).[61] PDIs suggest great promise for this area of research due to their stability, low lying LUMOs and reversible reductions.[62, 63] One of the main challenges in the fabrication of OFETs is the stability of the generated anions to oxidants, such as oxygen and water. The low lying LUMO of unsubstituted PDIs greatly reduces this instability and the possibility of functionalising the PDIs further makes them even more attractive for use as the semiconductors in these devices. The introduction of electron withdrawing groups, in order to further lower the LUMO energy, is a common method in the synthesis of PDIs for OFETs with bay-substitution of cyano-,[64] fluoro-[65] and chloro-groups[66] resulting in excellent ambient stability accompanied by electron mobilities of up to 1.18 $cm^2V^{-1}s^{-1}$. The addition of fluorinated alkyl chains to the imide-position is another common method to increase the stability of the OFETs caused by closer packing preventing the diffusion of air and water into the channel.[67] The previous examples are all made *via* vacuum deposition giving excellent long range crystalline order. This process is, however, time consuming. Therefore, spin coating and printing have been developed to aid scale up of the devices in order to improve economic viability. Spin coating results in more amorphous materials therefore lower electron mobilities. PDI containing polymers have been synthesised to increase the long range order following spin coating resulting in reasonable electron mobilities of up to 0.0013 $cm^2V^{-1}s^{-1}$ although ambient stability is difficult to achieve.[36, 68]

The potential for fluorescence above 500 nm to minimise the autofluorescence background of cells, stability, non-toxicity and chemical versatility of PDIs had led to their exploitation in various biological systems such as protein tagging and single protein spectroscopy.[47] A prerequisite for use in this type of system is water solubility.

Whilst this had been achieved *via* imide functionalisation it was accompanied by quenching of fluorescence due to hydrophobic aggregation.[69] The incorporation of hydrophilic sulfonic acid groups or polyglycerol dendrons at the bay-area of a PDI was found to supress this aggregation whilst maintaining water solubility, therefore, allowing high fluorescence quantum yields.[70, 71] The introduction of one group to allow bioconjugation, achieved by asymmetric imide substitution, such as meleimide groups able to form amide bonds with lysine[72] or nitrilotriacetic acid to complex to nickel(II),[73] resulted in highly fluorescent PDI based labels for biological systems, Figure 1.11.

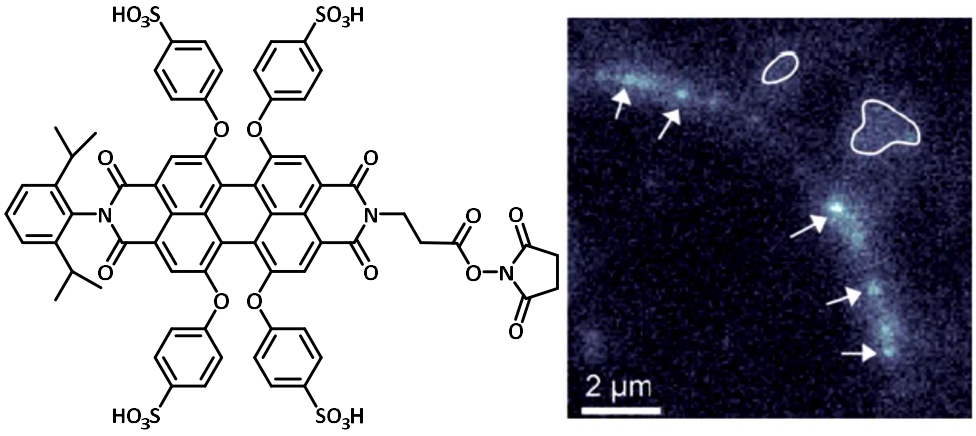

Figure 1.11. Water soluble PDI based biolabel for lysine in DNA (left) and fluorescence image showing enzymes labelled with the PDI (right).[72]

1.2. Thesis Outline

This thesis details the synthesis of PDIs *via* functionalisation of the imide-, bay-, ortho- and carbonyl-regions. The synthesised molecules then undergo detailed optical, electronic and photophysical investigations to fully elucidate their properties. Chapter 2 describes the bay-area amine substitution of a PDI followed by the tetra-thionation of the imide carbonyls resulting in two of the first examples of PDIs with absorption maxima in the near infrared. Chapter 3 details the synthesis of seven multichromophoric PDI-BODIPY systems, substituted at the bay area symmetrically and asymmetrically

and at the ortho-positions. The properties of the molecules are fine-tuned by the introduction of methyl- and catecholate-groups to the BODIPYs and any charge transfer processes are investigated. In Chapter 4 two PDIs bearing platinum acetylide complexes are synthesised and their ability to undergo intersystem crossing to generate triplet excited states is investigated. Chapter 5 summarises the results presented in this thesis and brings the work to a conclusion.

1.3. References

1. M. Kardos, *Patent 276357*, 1913.
2. F. Wurthner, *Chem. Commun.*, 2004, 1564-1579.
3. F. Würthner, C. R. Saha-Möller, B. Fimmel, S. Ogi, P. Leowanawat and D. Schmidt, *Chem. Rev.*, 2016, **116**, 962-1052.
4. C. Huang, S. Barlow and S. R. Marder, *J. Org. Chem.*, 2011, **76**, 2386-2407.
5. G. Klebe, F. Graser, E. Hädicke and J. Berndt, *Acta. Cryst. B*, 1989, **45**, 69-77.
6. H. Langhals, *Heterocycles*, 1995, **40**, 477 - 550.
7. C. Ramanan, A. L. Smeigh, J. E. Anthony, T. J. Marks and M. R. Wasielewski, *J. Am. Chem. Soc.*, 2011, **134**, 386-397.
8. C. Backes, C. D. Schmidt, F. Hauke, C. Böttcher and A. Hirsch, *J. Am. Chem. Soc.*, 2009, **131**, 2172-2184.
9. F. Biedermann, E. Elmalem, I. Ghosh, W. M. Nau and O. A. Scherman, *Angew. Chem. Int. Ed.*, 2012, **51**, 7739-7743.
10. Y. Liu, K.-R. Wang, D.-S. Guo and B.-P. Jiang, *Adv. Funct. Mater.*, 2009, **19**, 2230-2235.
11. Z. Chen, B. Fimmel and F. Wurthner, *Org. Biomol. Chem.*, 2012, **10**, 5845-5855.
12. E. H. A. Beckers, S. C. J. Meskers, A. P. H. J. Schenning, Z. Chen, F. Würthner and R. A. J. Janssen, *J. Phys. Chem. A*, 2004, **108**, 6933-6937.
13. H. Tröster, *Dyes Pigments*, 1983, **4**, 171-177.
14. C. Xue, R. Sun, R. Annab, D. Abadi and S. Jin, *Tetrahedron Lett.*, 2009, **50**, 853-856.
15. J. Wang, A. Kulago, W. R. Browne and B. L. Feringa, *J. Am. Chem. Soc.*, 2010, **132**, 4191-4196.
16. B. J. Slater, E. S. Davies, S. P. Argent, H. Nowell, W. Lewis, A. J. Blake and N. R. Champness, *Chem. Eur. J.*, 2011, **17**, 14746-14751.
17. Y. Wu, R. M. Young, M. Frasconi, S. T. Schneebeli, P. Spenst, D. M. Gardner, K. E. Brown, F. Würthner, J. F. Stoddart and M. R. Wasielewski, *J. Am. Chem. Soc.*, 2015, **137**, 13236-13239.
18. P. D. Frischmann, V. Kunz, V. Stepanenko and F. Würthner, *Chem. Eur. J.*, 2015, **21**, 2766-2769.
19. P. Spenst and F. Würthner, *Angew. Chem. Int. Ed.*, 2015, **54**, 10165-10168.
20. G. Seybold and G. Wagenblast, *Dyes Pigments*, 1989, **11**, 303-317.
21. A. Bohm, H. Arms, G. Henning and P. Blaschka, *Ger. Pat. Appl., Vol. DE 19547290 A1*, 1997.
22. W. Qiu, S. Chen, X. Sun, Y. Liu and D. Zhu, *Org. Lett.*, 2006, **8**, 867-870.
23. P. Rajasingh, R. Cohen, E. Shirman, L. J. W. Shimon and B. Rybtchinski, *J. Org. Chem.*, 2007, **72**, 5973-5979.
24. Y. Kumar, S. Kumar, S. Kumar Keshri, J. Shukla, S. S. Singh, T. S. Thakur, M. Denti, A. Facchetti and P. Mukhopadhyay, *Org. Lett.*, 2016, **18**, 472-475.
25. M. Sadrai, L. Hadel, R. R. Sauers, S. Husain, K. Krogh-Jespersen, J. D. Westbrook and G. R. Bird, *J. Phys. Chem.*, 1992, **96**, 7988-7996.
26. G. Goretzki, E. S. Davies, S. P. Argent, W. Z. Alsindi, A. J. Blake, J. E. Warren, J. McMaster and N. R. Champness, *J. Org. Chem.*, 2008, **73**, 8808-8814.
27. M. J. Ahrens, M. J. Tauber and M. R. Wasielewski, *J. Org. Chem.*, 2006, **71**, 2107-2114.

28. R. K. Dubey, A. Efimov and H. Lemmetyinen, *Chem. Mater.*, 2011, **23**, 778-788.
29. F. Würthner, V. Stepanenko, Z. Chen, C. R. Saha-Möller, N. Kocher and D. Stalke, *J. Org. Chem.*, 2004, **69**, 7933-7939.
30. Y. Zhao and M. R. Wasielewski, *Tetrahedron Lett.*, 1999, **40**, 7047-7050.
31. Y. Chen, Y. Feng, J. Gao and M. Bouvet, *J. Colloid Interface Sci.*, 2012, **368**, 387-394.
32. M.-J. Lin, M. Schulze, K. Radacki and F. Wurthner, *Chem. Commun.*, 2013, **49**, 9107-9109.
33. B. A. Jones, M. J. Ahrens, M.-H. Yoon, A. Facchetti, T. J. Marks and M. R. Wasielewski, *Angew. Chem. Int. Ed.*, 2004, **43**, 6363-6366.
34. T. W. Chamberlain, E. S. Davies, A. N. Khlobystov and N. R. Champness, *Chem. Eur. J.*, 2011, **17**, 3759-3767.
35. B. Dhokale, P. Gautam and R. Misra, *Tetrahedron Lett.*, 2012, **53**, 2352-2354.
36. X. Zhan, Z. a. Tan, B. Domercq, Z. An, X. Zhang, S. Barlow, Y. Li, D. Zhu, B. Kippelen and S. R. Marder, *J. Am. Chem. Soc.*, 2007, **129**, 7246-7247.
37. U. Rohr, P. Schlichting, A. Böhm, M. Gross, K. Meerholz, C. Bräuchle and K. Müllen, *Angew. Chem. Int. Ed.*, 1998, **37**, 1434-1437.
38. W. Jiang, Y. Li, W. Yue, Y. Zhen, J. Qu and Z. Wang, *Org. Lett.*, 2010, **12**, 228-231.
39. T. Teraoka, S. Hiroto and H. Shinokubo, *Org. Lett.*, 2011, **13**, 2532-2535.
40. S. Nakazono, S. Easwaramoorthi, D. Kim, H. Shinokubo and A. Osuka, *Org. Lett.*, 2009, **11**, 5426-5429.
41. S. Nakazono, Y. Imazaki, H. Yoo, J. Yang, T. Sasamori, N. Tokitoh, T. Cédric, H. Kageyama, D. Kim, H. Shinokubo and A. Osuka, *Chem. Eur. J.*, 2009, **15**, 7530-7533.
42. G. Battagliarin, C. Li, V. Enkelmann and K. Müllen, *Org. Lett.*, 2011, **13**, 3012-3015.
43. N. Mizoshita, T. Tani and S. Inagaki, *Adv. Mater.*, 2012, **24**, 3350-3355.
44. P. E. Hartnett, A. Timalsina, H. S. S. R. Matte, N. Zhou, X. Guo, W. Zhao, A. Facchetti, R. P. H. Chang, M. C. Hersam, M. R. Wasielewski and T. J. Marks, *J. Am. Chem. Soc.*, 2014, **136**, 16345-16356.
45. G. Battagliarin, M. Davies, S. Mackowiak, C. Li and K. Müllen, *ChemPhysChem*, 2012, **13**, 923-926.
46. L. E. Shoer, S. W. Eaton, E. A. Margulies and M. R. Wasielewski, *J. Phys. Chem. B*, 2015, **119**, 7635-7643.
47. T. Weil, T. Vosch, J. Hofkens, K. Peneva and K. Müllen, *Angew. Chem. Int. Ed.*, 2010, **49**, 9068-9093.
48. Z. Chen, U. Baumeister, C. Tschierske and F. Würthner, *Chem. Eur. J.*, 2007, **13**, 450-465.
49. N. Pearce, *PhD Thesis, University of Nottingham*, 2016.
50. B. A. Jones, A. Facchetti, M. R. Wasielewski and T. J. Marks, *J. Am. Chem. Soc.*, 2007, **129**, 15259-15278.
51. S. Seifert, D. Schmidt and F. Wurthner, *Chem. Sci.*, 2015, **6**, 1663-1667.
52. A. S. Lukas, Y. Zhao, S. E. Miller and M. R. Wasielewski, *J. Phys. Chem. B*, 2002, **106**, 1299-1306.
53. A. G. Slater, E. S. Davies, S. P. Argent, W. Lewis, A. J. Blake, J. McMaster and N. R. Champness, *J. Org. Chem.*, 2013, **78**, 2853-2862.
54. C. Li, M. Liu, N. G. Pschirer, M. Baumgarten and K. Müllen, *Chem. Rev.*, 2010, **110**, 6817-6855.

55. C. Li and H. Wonneberger, *J. Adv. Mater*, 2012, **24**, 613-636.
56. P. Erwin and M. E. Thompson, *Appl. Phys. Lett.*, 2011, **98**, 223305.
57. G. D. Sharma, P. Suresh, J. A. Mikroyannidis and M. M. Stylianakis, *J. Mater. Chem.*, 2010, **20**, 561-567.
58. X. Zhan, Z. a. Tan, E. Zhou, Y. Li, R. Misra, A. Grant, B. Domercq, X.-H. Zhang, Z. An, X. Zhang, S. Barlow, B. Kippelen and S. R. Marder, *J. Mater. Chem.*, 2009, **19**, 5794-5803.
59. J. Fortage, M. Séverac, C. Houarner-Rassin, Y. Pellegrin, E. Blart and F. Odobel, *J. Photochem. Photobiol. A*, 2008, **197**, 156-169.
60. A. Nattestad, A. J. Mozer, M. K. R. Fischer, Y. B. Cheng, A. Mishra, P. Bauerle and U. Bach, *Nat. Mater.*, 2010, **9**, 31-35.
61. T. M. Figueira-Duarte and K. Müllen, *Chem. Rev.*, 2011, **111**, 7260-7314.
62. Z. Liu, G. Zhang, Z. Cai, X. Chen, H. Luo, Y. Li, J. Wang and D. Zhang, *Adv. Mater.*, 2014, **26**, 6965-6977.
63. F. Wurthner and M. Stolte, *Chem. Commun.*, 2011, **47**, 5109-5115.
64. B. A. Jones, A. Facchetti, M. R. Wasielewski and T. J. Marks, *Adv. Funct. Mater.*, 2008, **18**, 1329-1339.
65. R. Schmidt, M. M. Ling, J. H. Oh, M. Winkler, M. Könemann, Z. Bao and F. Würthner, *Adv. Mater.*, 2007, **19**, 3692-3695.
66. M. Gsänger, J. H. Oh, M. Könemann, H. W. Höffken, A.-M. Krause, Z. Bao and F. Würthner, *Angew. Chem. Int. Ed.*, 2010, **49**, 740-743.
67. J. H. Oh, L. Shuhong, B. Zhenan, R. Schmidt and F. Wurthner, *Appl. Phys. Lett.*, 2007, **91**, 212107.
68. S. Huttner, N. Sommer and M. Thelakkat, *Appl. Phys. Lett.*, 2008, **92**, 093302.
69. H. Langhals, W. Jona, F. Einsiedl and S. Wohnlich, *Adv. Mater.*, 1998, **10**, 1022-1024.
70. C. Kohl, T. Weil, J. Qu and K. Müllen, *Chem. Eur. J.*, 2004, **10**, 5297-5310.
71. S. K. Yang, X. Shi, S. Park, S. Doganay, T. Ha and S. C. Zimmerman, *J. Am. Chem. Soc.*, 2011, **133**, 9964-9967.
72. K. Peneva, G. Mihov, F. Nolde, S. Rocha, J.-i. Hotta, K. Braeckmans, J. Hofkens, H. Uji-i, A. Herrmann and K. Müllen, *Angew. Chem. Int. Ed.*, 2008, **47**, 3372-3375.
73. K. Peneva, G. Mihov, A. Herrmann, N. Zarrabi, M. Börsch, T. M. Duncan and K. Müllen, *J. Am. Chem. Soc.*, 2008, **130**, 5398-5399.

Chapter 2. Thionated Perylene Diimides with Intense Absorbance in the Near Infrared

2.1. Introduction

2.1.1. Near Infrared Absorbing Dyes

The portion of the electromagnetic spectrum between 750 nm and 2500 nm is known as the near infrared (NIR) region. Whilst there are countless examples of materials that interact with ultraviolet (UV) or visible light, materials that absorb or fluoresce in the NIR region are considerably less well known. Interest in the area is increasing as more routes to, and applications of, these materials are discovered.[1]

The synthesis of NIR absorbing materials can be achieved by manipulating the energy levels of the molecules. Reducing the HOMO-LUMO energy gap sufficiently will induce a red shift in the absorbance of radiation into the NIR with two of the most popular routes for doing this being extending the conjugation of the molecule and creating donor-acceptor (D-A) systems. These techniques have been applied to many different types of compound to synthesise NIR dyes such as squaraines,[2] boron dipyrromethenes (BODIPYs),[3] benzobis(1,2,5-thiadiazole) derivatives,[4] conjugated polymers,[5] porphyrins[6, 7] and, discussed below, rylene diimides.

2.1.1.1. Rylene Diimides with Absorbance in the NIR

The extension of the conjugation of the aromatic core in rylene diimides has been thoroughly studied with the aim of pushing the absorption from the UV/vis region, seen in naphthalene diimides (NDIs) and perylene diimides (PDIs), into the NIR.[8] Insertion of additional naphthalene units into the core of the PDI has been achieved by complex combinations of cross coupling reactions to give terrylene diimides (TDIs),[9] quaterrylene diimides (QDIs),[10] pentarylene diimides (5DIs)[11] and hexarylene diimides

(HDIs), Figure 2.1.[11] It was found that a bathochromic shift of around 100 nm was observed for each additional naphthalene unit, pushing the absorption maxima from *ca.* 580 nm for PDI to 953 nm for HDI. In conjunction with this bathochromic shift, a tenfold increase in extinction coefficient was also observed, from 30,000 to 300,000 $mol^{-1}dm^3cm^{-1}$. The 'R' groups at the imide nitrogen and the bay positions could be varied to increase the solubility of the molecules. Whilst this approach is very successful in creating NIR absorbing rylene diimides, the synthesis and characterisation are very difficult and solubility is often also problematic.

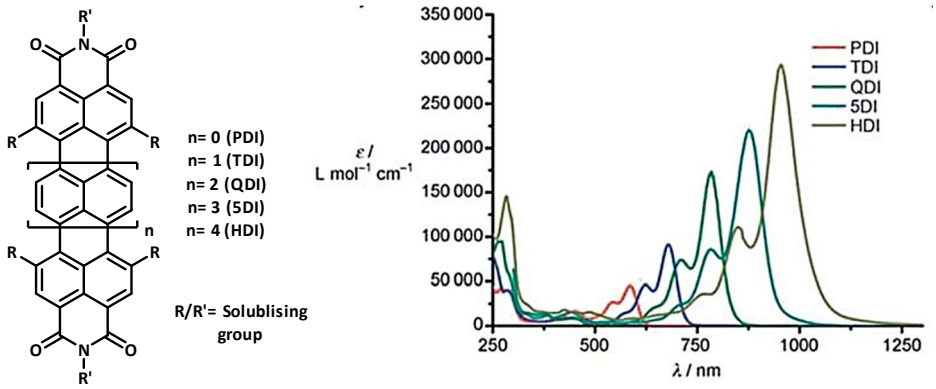

Figure 2.1. Structures of the longitudinally extended family of rylene diimides (left) and UV/vis/NIR spectra showing increasing wavelength of absorption and extinction coefficient with increasing 'n' (right).[8]

Introducing electron donor groups, such as phenoxy-[12] and amino-derivatives,[13] onto the electron deficient PDI core has been shown to induce a bathochromic shift due to the formation of D-A systems. In conjugated D-A systems, hybridisation of the donor and acceptor orbitals occurs, this raises the energy of the HOMO in the donor and lowers the level of the LUMO in the acceptor leading to a reduction in the HOMO-LUMO gap.[14] In one case, this shift was found to be sufficient for a PDI to absorb in the NIR when Langhals and co-workers synthesised a PDI with electron donating nitrogen atoms at the 1-,6-,7- and 12- positions, Figure 2.2.[15] The nitrogen atoms on each side were joined into six membered rings, further amplifying the electron donation

and hence the bathochromic shift. The absorption maximum was found to be significantly red shifted *versus* unsubstituted PDI from 525 nm to 785 nm, just into the NIR. Before the study reported in this thesis, the PDI synthesised by Langhals and co-workers was the only example of a neutrally charged PDI with an absorption maximum in the NIR.

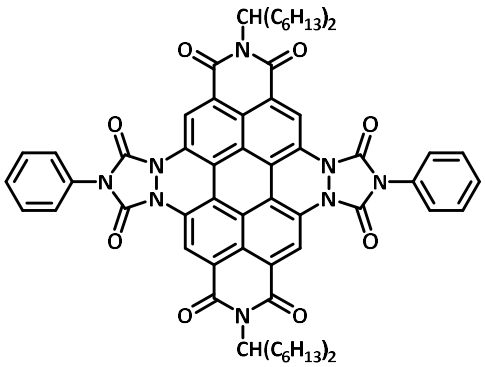

Figure 2.2. Structure of the only previous neutrally charged PDI with an absorbance in the NIR.

Whilst phenoxy-substituted PDIs do not absorb in the NIR, if the hydroxyl-substituent is deprotonated to an oxy-anion the electron donation is enhanced and the bathochromic shift increased. Würthner's halochromic di(hydroxyphenyl)-substituted PDI absorbs at 578 nm in neutral conditions however upon basification of the solution with tetrabutylammonium hydroxide (TBAH) there is a colour change, from red to orange, accompanied by a significant bathochromic shift of 607 nm to 1185 nm, Scheme 2.1.[16] This deprotonation was found to be fully reversible upon the addition of trifluoroacetic acid (TFA) with the neutral UV/vis and ^{1}H NMR spectra being regenerated. Chemical oxidation of the dianion with one equivalent of [$Pb(OAc)_4$] results in a further red shift for the monoradical to 1396 nm whilst two equivalents gives the diradical which is blue shifted back to 800 nm.[17]

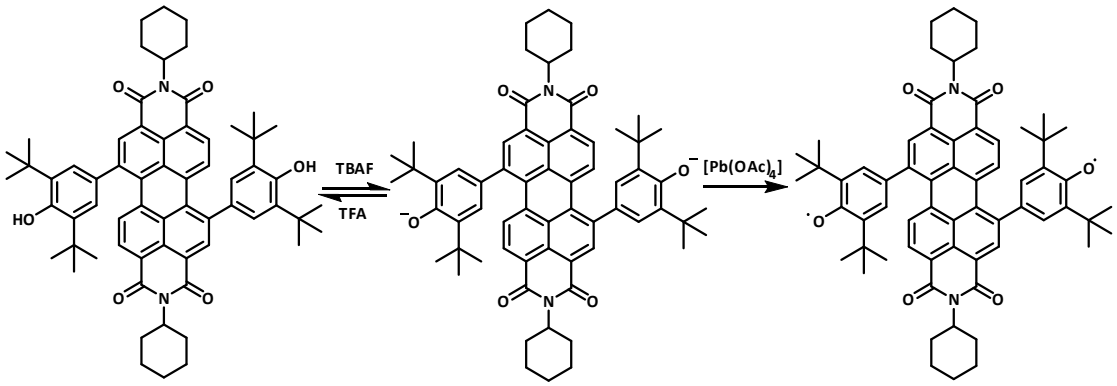

Scheme 2.1. Reaction of a diphenoxy-PDI with TBAF to the dianion, followed by chemical oxidation to the diradical.

The combination of conjugation extension and formation of a D-A system has been combined to synthesise extended rylene diimides bearing electron donating substituents. The reaction of brominated TDIs and QDIs with piperidine results in piperidyl-substituted extended rylene diimides with absorptions at 819 nm and 910 nm respectively.[18]

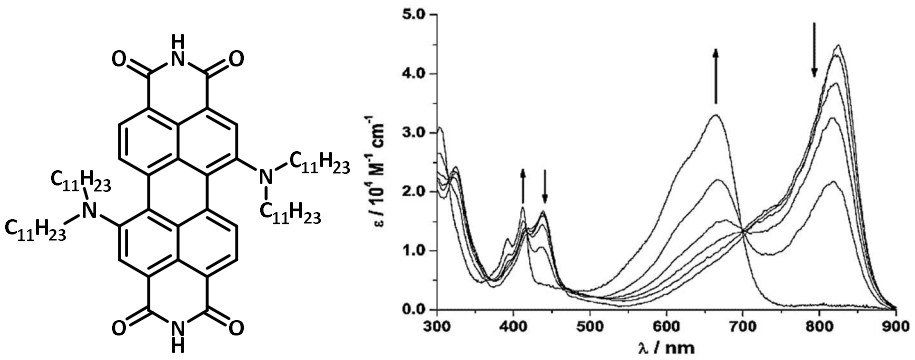

Figure 2.3. Structure of the J-aggregating PDI (left) and UV/vis/NIR absorption spectra showing the change in absorbance upon heating the PDI in methylcyclohexane (right).[19] Arrows indicate progress of dissociation.

A slightly more unusual approach to NIR absorbing PDI dyes is the synthesis of PDIs bearing substituents that allow J-aggregation[20] of the molecules leading to a bathochromic shift. A PDI substituted at the bay-position with tricosan-12-amine displays a typical absorption for amino-substituted PDIs of 702 nm in dichloromethane (DCM), Figure 2.3.[19] However, when the non-polar methylcyclohexane is used as the

solvent J-aggregation occurs leading an increase in the wavelength of absorption to 822 nm. This stacking interaction was found to be fully reversible upon heating as the molecules dissociate to individual monomers and the UV/vis spectrum again resembles that of the molecule in DCM.

2.1.1.2. Applications of NIR Dyes

One of the main challenges facing the world today is the production of energy whilst minimising the emission of greenhouse gasses. Many new technologies are being developed to this end with one area of growing interest being organic photovoltaics (OPVs)[21] including dye sensitised solar cells (DSSCs)[22] and bulk heterojunction (BHJ) cells.[23] Whilst the performance of these devices are constantly being improved there is a fundamental problem in their design that, whilst the majority of the dye materials being synthesised absorb in the UV/vis region of the spectrum, over 50 % of the sun's radiation lies in the NIR.[24] This mismatch between the absorption spectrum of the dye and the solar emission spectrum could be improved by extending the absorption of the dyes into the NIR.[25]

The majority of research into BHJ cells has centred on polymeric donor materials. Whilst polymers have superior film forming properties to non-polymeric materials, small molecules have the advantage of ease of synthesis and purification, however, power conversion efficiencies (PCEs) have remained low. Nguyen and co-workers synthesised a D-π-A-π-D molecule with benzofuran as the donor and a diketopyrrolopyrrole as the acceptor, Figure 2.4.[26] Whilst the absorption maxima (in a film) of this molecule lies at 660 nm, the broad absorption extends well into the NIR. This broad absorption combined with a good match between the molecule's frontier

orbitals and those of the fullerene acceptor lead to the highest PCE (4.4 %) in any small molecule system BHJ cell to date.

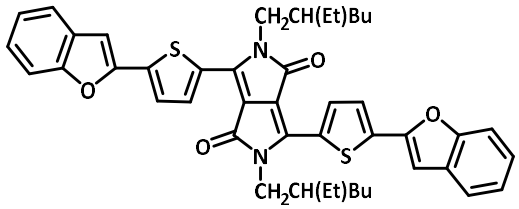

Figure 2.4. NIR absorbing diketopyrrolopyrrole based small molecule with a PCE of 4.4 % in a BHJ cell.

Traditionally, investigations into the dyes used in DSSCs have focused on Ru^{II} complexes.[27] However, Ru is a rare and expensive metal making these dyes neither cost effective nor environmentally friendly.[28] In the search for a metal free organic dye, BODIPYs are emerging as a potential replacement for Ru complexes due to their broad range of absorption, high quantum yield, good solubility and excellent photostability.[29] Akkaya and co-workers synthesised a series of NIR absorbing BODIPY based dyes with the aim of incorporation into DSSCs.[30] All of these dyes displayed high absorption maxima, between 650 nm and 800 nm, leading to impressive overall efficiencies up to 2.46 %, currently the best for a BODIPY based DSSC. This result demonstrates that extending the wavelength of absorption into the NIR can indeed substantially increase the efficiency of DSSCs. The efficiencies of the BODIPY sensitisers in this series displayed a large variation. These differences could be attributed to; access to the triplet excited stated leading to degradative chemical reactions, flexibility of the molecules allowing vibrational losses in energy and poor orientation of anchoring groups resulting in inefficient electron injection. This shows that, whilst increasing the wavelength of absorption is a worthwhile aim in seeking to improve the efficiency of DSSCs, many other variables contribute to the overall performance of the device making careful molecular design imperative.

Organic light emitting diodes (OLEDs) have found uses in many devices, such as optical displays, due to their emission in the visible region.[31] More recently interest has grown in NIR OLEDs with potential applications such as optical communication,[32] night vision, readable displays and sensors.[33] Lanthanides have previously been one of the main sources of NIR emissive material[34] paving the way for the creation of cheaper materials to take their place. Four D-π-A-π-D molecules were synthesised by Ma and co-workers with a benzo(1,2-c:4, 5-c')bis((1,2,5)thiadiazole) (BBTD) acceptor, various diaryl amino-groups as donors and either phenyl- or thiophene-groups acting as π-spacers, Figure 2.5.[35] All four were found be thermally stable and able to sublime making them suitable for vapour deposition in OLED fabrication. The three phenyl linked compounds displayed an absorption at ~700 nm and an emission at ~1050 nm, however, the absorption and emission of the thiophene-spaced derivative was red shifted by ~250 nm to 945 nm and 1285 nm respectively. Once the materials were fabricated into OLEDs, their external quantum efficiency was measured with values up to 0.28 % being achieved, higher than most other NIR OLED devices.

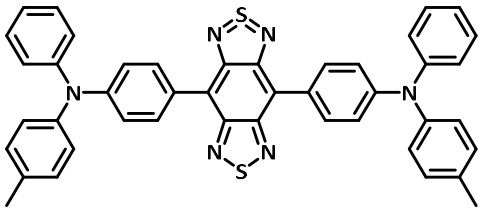

Figure 2.5. BBTD based dye with an emission at 1050 nm and an external quantum efficiency of 0.28 %.

2.1.2. Towards a NIR Absorbing PDI Dye

The results reported in this Chapter combine two different approaches to induce a bathochromic shift in a PDI resulting in a PDI with an absorption maxima in the NIR.

2.1.2.1. Secondary Amine Substitution

The first approach is the substitution of the bay area of a PDI with a secondary amine which, as discussed above, leads to the formation of a D-A system with the amine as a donor and the PDI as the acceptor. The secondary amine chosen in this case was morpholine which, following work previously carried out by Champness and co-workers, was known to induce a significant bathochromic shift.[36] The reaction of morpholine with dibromo PDI gives two isomers (1,6- and 1,7-) of dimorpholino-substituted PDI with absorption maxima at 628 nm and 653 nm respectively, Figure 2.6 and Figure 2.7. This variation in absorption can be observed in the difference in colour of the two isomers, the 1,6- isomer is blue and the 1,7- isomer is green. Cyclic voltammetry of the two isomers reveals the two reduction potentials to have both become more negative by 0.2 V due to the electron donation from the morpholine.[36] Additional oxidation processes are also observed in both cases, the 1,6- isomer displaying three oxidations the first of which was found to be reversible, the 1,7- isomer only possessing one oxidation, found to be a two electron process and only reversible at 233 K.

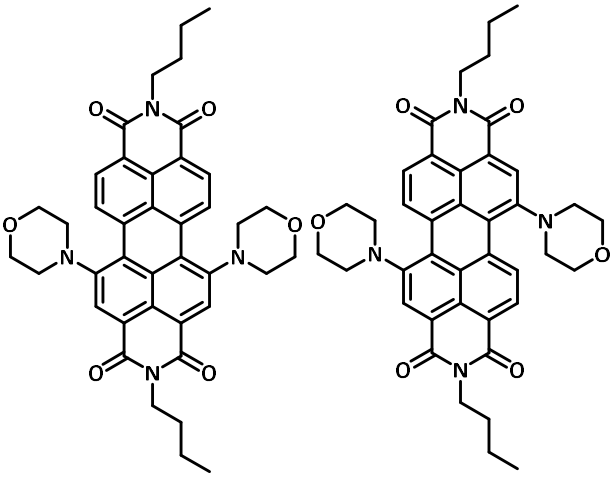

Figure 2.6. Structures of the 1,6- (left) and 1,7- (right) dimorpholino-substituted PDIs.

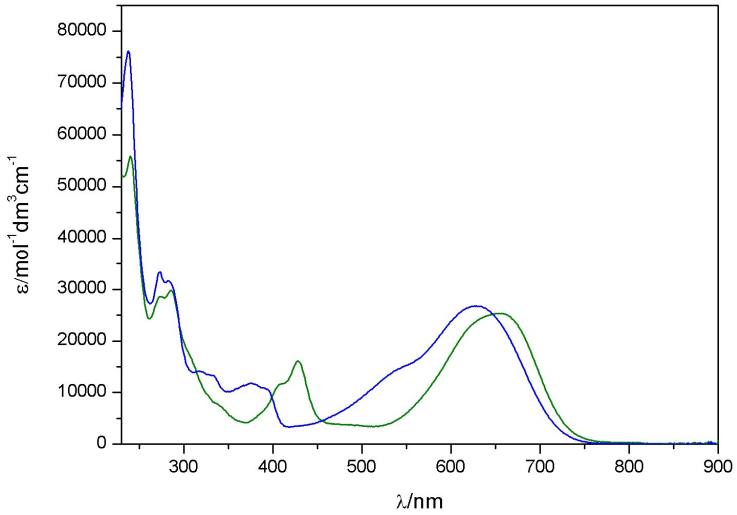

Figure 2.7. UV/vis absorption spectra of the 1,6- (blue) and 1,7- (green) dimorpholino-substituted PDIs in DCM.[36]

2.1.2.2. Thionation of Rylene Diimides

The substitution of oxygen for other Group 16 elements has been shown to be an effective way of tuning the optoelectronic properties of molecules by altering their frontier orbitals without affecting the overall structure of the molecule.[37-39] DFT studies on bithiophene based oligomers suggest that substitution with Group 16 elements, moving down the group from oxygen to tellurium, results in a lowering of the LUMO energy thus a lowering of the HOMO-LUMO gap inducing a bathochromic shift.[40] Within the last few years, the application of this technique to rylene diimides has become increasingly popular with the first example published being a patent by Facchetti and co-workers in 2011.[41] This patent reports the treatment of varied NDIs and PDIs with either Lawesson's or Davy Reagent resulting in the thionation of the imide carbonyls. These reactions mainly yielded mono- and di-thionated products with only trace amounts of tri- or tetra-thionated product isolated, insufficient quantities for full optical and electrochemical characterisation.

The first in-depth study of the properties of a full series of thionated rylenes was undertaken by Tilley and co-workers in 2014 when they synthesised a set of mono- to tetra-thionated PDIs, Scheme 2.2.[42] They found that the reaction of a PDI, solubilised with a 3-hexylundecyl chain at the imide nitrogen, with five equivalents of Lawesson's Reagent resulted in mostly tri- and tetra-thionation of the PDI. When the number of equivalents was decreased the mono- and di-thionated products were favoured with two disubstituted isomers, *cis*- and *trans*-, also separable by column chromatography. UV/vis studies revealed that the wavelength of absorption increased with each additional sulfur substitution resulting in a bathochromic shift of 179 nm between the non-thionated and tetra-thionated species. A cyclic voltammetric investigation showed a decrease in the reduction potential with each degree of thionation accompanied by a decrease in the potential between the first and second reduction on the PDI. Unexpectedly, no fluorescence was observable for any of the thionated PDIs, this was investigated by ultrafast transient absorbance (TA) spectroscopy revealing that the PDI was undergoing rapid intersystem crossing (ISC) to a triplet excited state. When incorporated into organic field effect transistors (OFETs), the electron mobility of the PDIs was found to increase for each additional sulfur with the tetra-thionated compound having an electron mobility two orders of magnitude higher than the non-thionated PDI.[43] This increase was attributed to the enhancement of solid state properties and intermolecular interactions caused by the thionation.

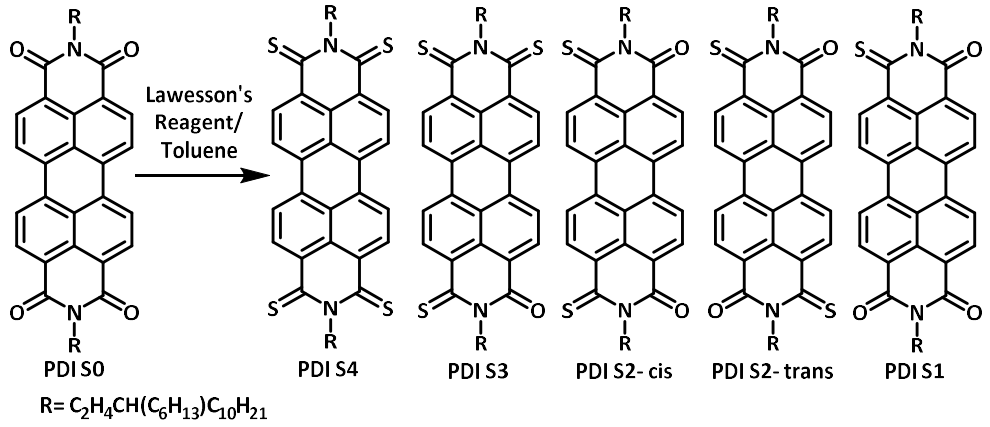

Scheme 2.2. The reaction of **PDI S0** with Lawesson's Reagent to form mono- to tetra-thionated PDIs.

In 2015, three studies investigating the thionation of NDIs were published. Two focussed on the improved electron mobility of thionated NDIs when incorporated into OFETs[44, 45] whilst the other demonstrated that core substitution of the NDIs restricted the thionation of the carbonyl proximal to the substitution, promoting exclusive formation of the *trans*-isomer over the *cis*-.[46] In all three cases, bathochromic shifts and decreases in reduction potentials upon thionation were observed. Interestingly the choice of group at the imide nitrogen appears to play a part in the degree of thionation. When the branched 2-ethyhexyl chain is used no tetra-thionation is observed, however, in the case of the unbranched dodecyl chain the tetra-thionated product can be separated in a 9 % yield. A careful choice of imide group is therefore vital to ensure sufficient solubility whilst not hindering thionation due to excessive steric bulk.

2.1.3. Aims and Objectives

As discussed at length in Chapter 1 PDIs possess various properties highly desirable for a number of interesting applications. One of the most promising directions for this research involves the incorporation of PDIs into OPVs. The performance of OPVs has been shown to increase when the wavelength of absorption of these materials is extended into the NIR, therefore the synthesis of a PDI with an absorbance in this region

is a most worthwhile target. Of the different approaches put forward to achieve this aim there is currently only one example of a PDI with an absorbance in the NIR whist neutral in common organic solvents.

To this end, a combination of secondary amine substitution followed by imide carbonyl thionation of a PDI was carried out and the resulting molecules investigated by optical and electrochemical methods, including UV/vis/NIR spectroscopy, cyclic voltammetry, EPR spectroscopy and spectroelectrochemistry, to fully elucidate their properties and to give an insight into their potential suitability for incorporation into OPVs.

2.2. Results and Discussion

2.2.1. Synthesis

The synthesis of the two NIR absorbing PDI dyes **2.5** and **2.6** first required the formation of the tetra-carboxyl analogues **2.3** and **2.4**. This was achieved in three steps from the perylene dianhydride (PDA) starting material following a known procedure[36] as shown in Scheme 2.3.

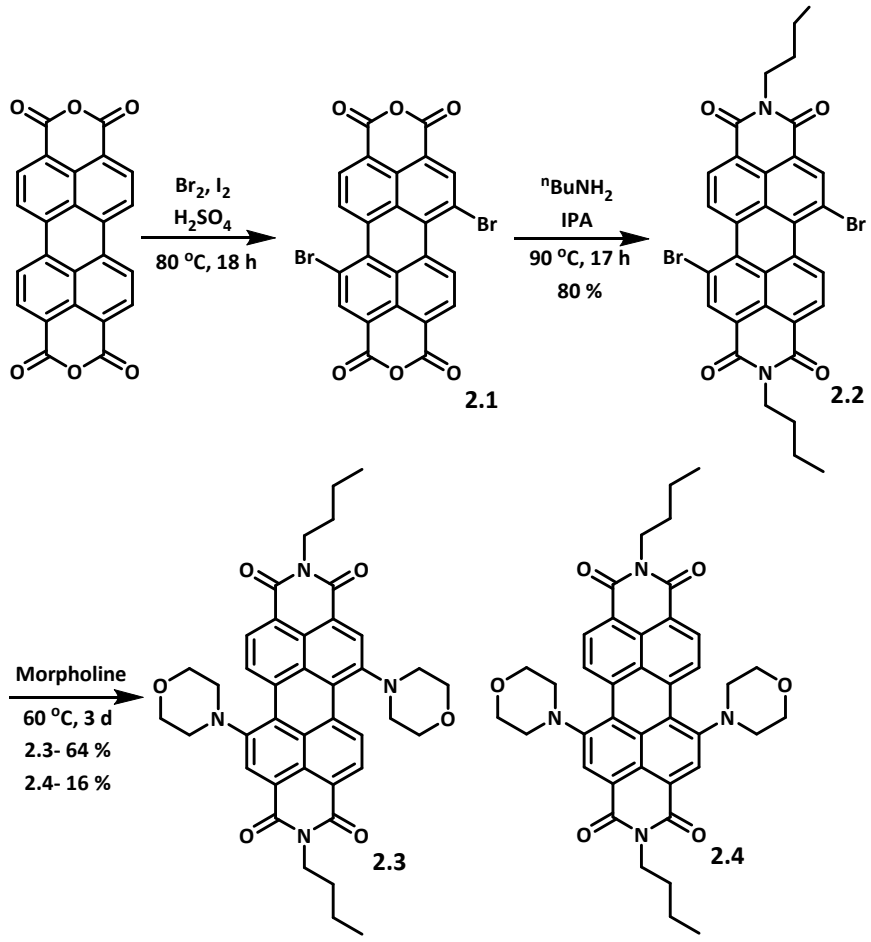

Scheme 2.3. Synthesis of the two dimorpholino-substituted PDIs **2.3** and **2.4** from PDA. **2.1** and **2.2** are represented as the major 1,7- isomer for clarity.

PDA was reacted with Br_2 in sulfuric acid with iodine as a catalyst to give **2.1** as a mixture of mono-, di- and tri-substituted adducts. At this stage, **2.1** is highly insoluble making the separation of these PDIs impossible by standard methods, therefore, the

crude product was used in the next step without further purification. **2.1** was then imidized by reacting with n-butyl amine in isopropyl alcohol (IPA) to give **2.2**. At this stage, the mono- and tribromo adducts could be easily removed by column chromatography to give dibromo PDI in a yield of 80 %, However, the 1,6- and 1,7-isomers were still inseparable. **2.2** was heated in morpholine, acting as both reagent and solvent, for three days to give a mixture of **2.3** and **2.4**, which could be separated by column chromatography, to give the pure products in 64 % and 16 % yields respectively.

Single crystals of **2.4** were grown by layered diffusion between methanol and a chloroform solution of the target compound. X-ray structural determination revealed the conformational arrangement of the molecule in the solid state and further confirmed the 1,6- arrangement of the morpholine moieties, Figure 2.8. The single crystal structure of **2.3** has been reported previously.[36]

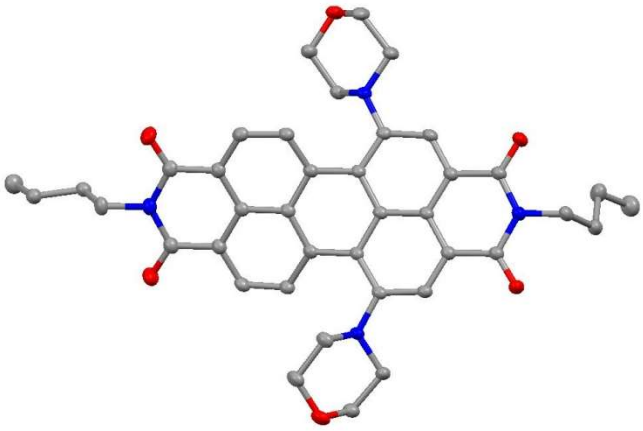

Figure 2.8. View of the single crystal structure of **2.4** showing the 1,6- arrangement of the morpholine moieties. Grey- carbon, blue- nitrogen, red- oxygen. H-atoms removed for clarity. Ellipsoids drawn at 50 % probability.

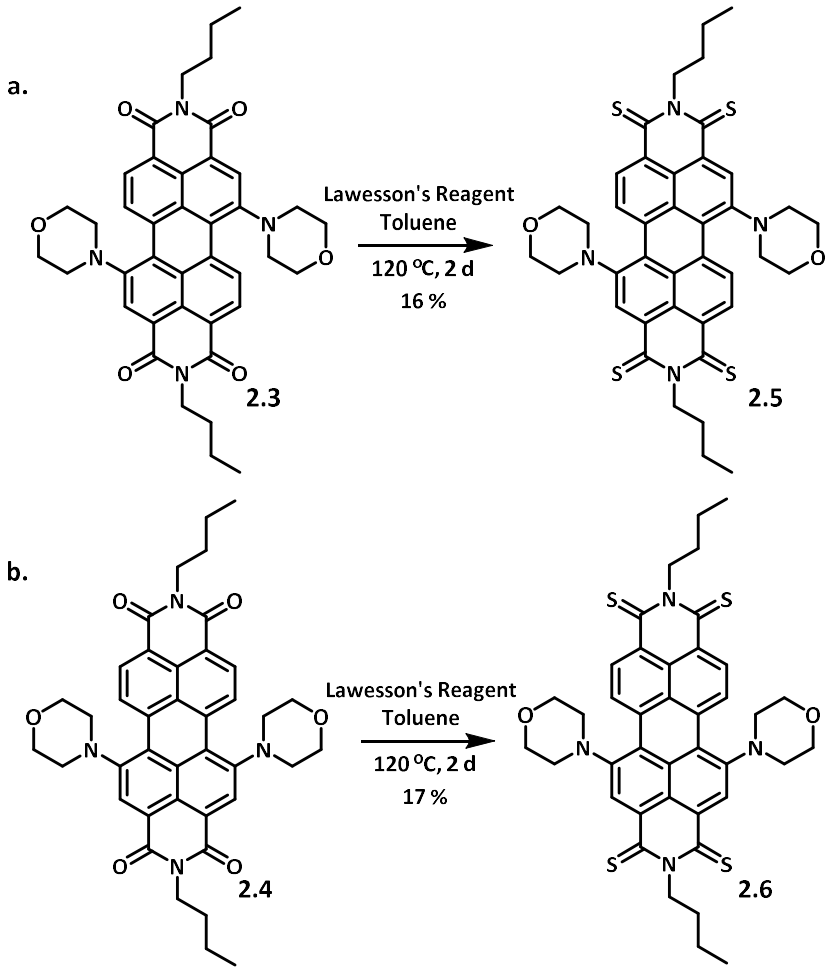

Scheme 2.4. Synthesis of NIR absorbing PDI dyes **2.5** (a) and **2.6** (b) by thionation of their tetra-carbonyl equivalents.

The final step in the synthesis of the NIR absorbing PDIs involved the reaction of **2.3** and **2.4** with Lawesson's reagent in toluene to give the tetra-thionated products **2.5** and **2.6**, Scheme 2.4. The yields of these two reactions were found to be low however they could be slightly improved by stopping the reaction after one day, purifying by column chromatography and re-reacting the lesser substituted products with more Lawesson's reagent. This was found to give higher yields than simply leaving the reaction to run for two days. The presence of tri-thionated PDI was observed by mass spectrometry and NMR spectroscopy; however, unlike previous examples with no bay substitution, two isomers exist and it was not found to be possible to separate them. Interestingly, these reaction conditions were applied to the analogous PDIs, but with a cyclohexyl-

group at the imide position. However, only small amounts of tri-thionation and no tetra-thionation were observed. This is most likely due to steric effects and indicates how important the correct choice of solubilising group is.

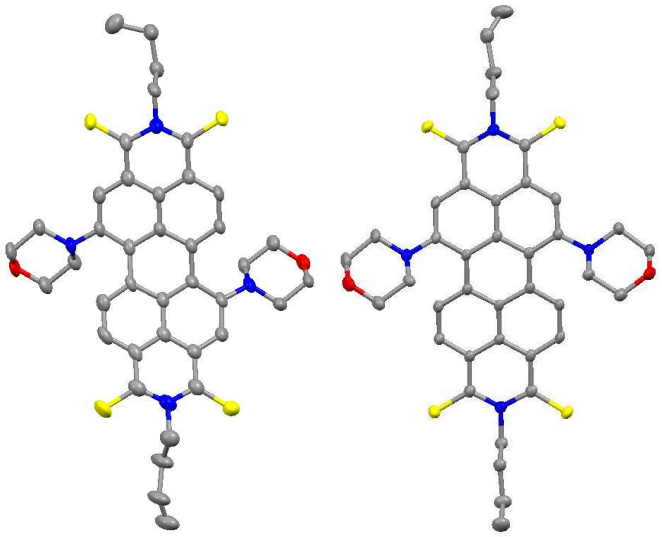

Figure 2.9. Views of the single crystal structures of **2.5** (left) and **2.6** (right). Grey- carbon, blue- nitrogen, red- oxygen, yellow- sulfur. H-atoms removed for clarity. Ellipsoids drawn at 50 % probability.

Single crystals of **2.5** and **2.6** were grown by layered diffusion between hexane and a solution of the target compound in chloroform/TFA. X-ray structural determination again confirmed the isomeric arrangement of the morpholine in the two isomers, Figure 2.9. The full thionation of the molecules was also shown; these structures represent the first reported for any thionated PDI. The two isomers of the thionated PDIs display different stacking interactions in the solid state, Figure 2.10 and Figure 2.11. **2.5** stacks in twisted pairs of molecules with the main π-π interaction being between two molecules in the pair, the morpholine moieties are pushed out of the pair thus preventing further π-interactions with other pairs of PDIs. **2.6** stacks in offset columns with one naphthalene ring π-stacking with the molecule above it and the other naphthalene ring π-stacking with the molecule below it. This stacking distance was measured as 3.33 Å (measured between planes generated on interacting naphthalene rings), similar to the π-π stacking distance measured in pyrolytic graphite of 3.36 Å.[47]

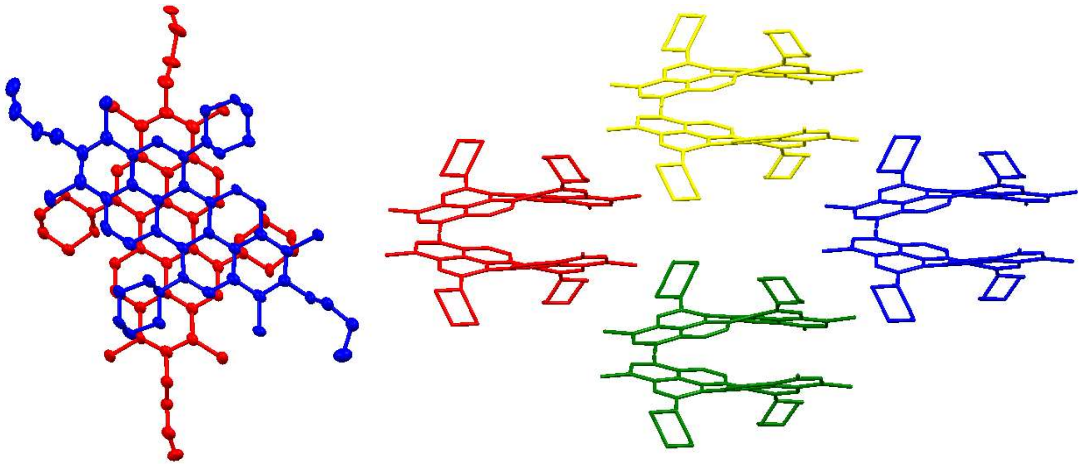

Figure 2.10. Top view of a stacked pair of molecules of **2.5** (left) and side view of four stacked pairs of **2.5** showing no π-interaction between the pairs (right). H-atoms removed in both cases with the butyl-chins also removed on the right. Ellipsoids drawn at 50 % probability.

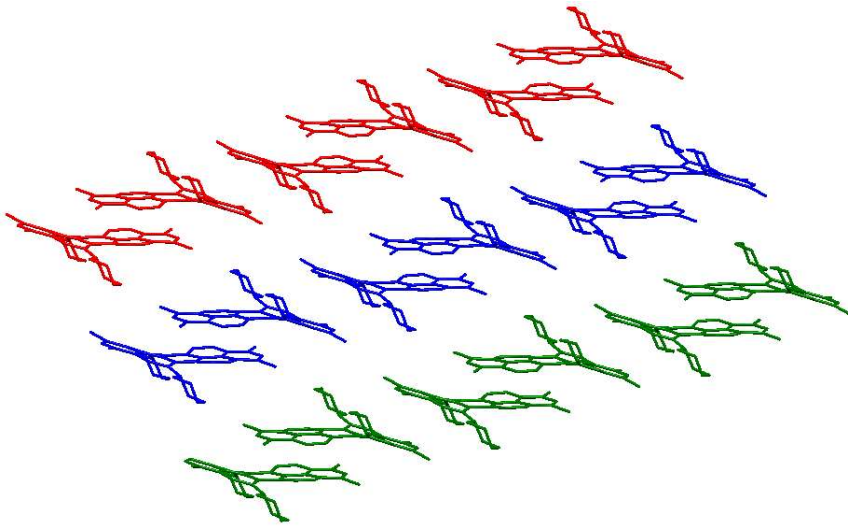

Figure 2.11. Side view showing stacking of offset columns of **2.6**. Hydrogen atoms and butyl-chains removed for clarity.

2.2.2. Optical and Electrochemical Investigation of NIR PDI Dyes

UV/vis/NIR spectroscopy revealed that the dual approach of secondary amine substitution and thionation has indeed been successful in pushing the absorption maxima into the NIR, Figure 2.12. The absorption of **2.5** peaks at 864 nm displaying a bathochromic shift of 211 nm versus **2.3** and 160 nm versus Tilley's tetra-thionated

PDI S4, Scheme 2.2. The combination of morpholine substitution and thionation was found to have a dramatic increase in the wavelength of absorption versus Tilley's non-thionated **PDI S0** of 339 nm. The previous highest wavelength of absorption of a neutrally charged PDI was found in Langhals' tetra-nitrogen substituted PDI[15] (Figure 2.2, page 21) at 785 nm, 79 nm lower than **2.5**. **2.6** has an absorption maxima at 838 nm, red-shifted 212 nm relative to its non-thionated counterpart **2.4** (almost identical to the difference between **2.5** and **2.3**), and 134 nm higher than the unsubstituted tetra-thionated **PDI S4**. The molar extinction coefficients for both thionated PDIs increased by *ca.*10,000 $mol^{-1}dm^3cm^{-1}$ in comparison to their non-thionated analogues.

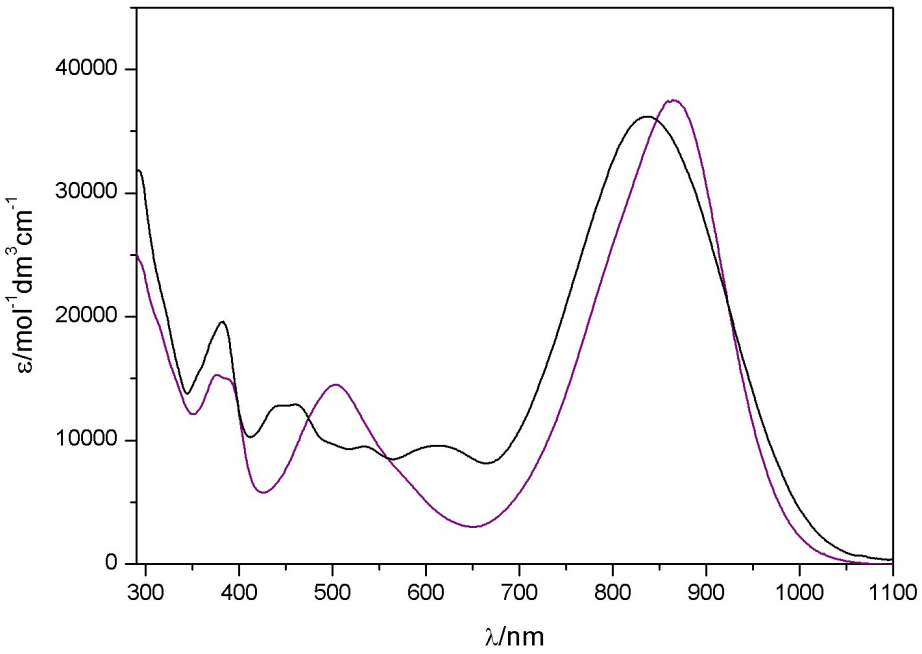

Figure 2.12. UV/vis/NIR absorption spectra of **2.5** (purple) and **2.6** (black) in DCM. c = 2.52 x 10^{-5} (**2.5**) and 2.3 x 10^{-5} $mol^{-1}dm^3cm^{-1}$ (**2.6**).

2.5 is purple in both solid state and solution but **2.6** is an unexpected black colour. This black colour can be explained by the absorbance observed across the range from above 1000 nm to 230 nm showing that **2.6** not only has an intense absorption in the NIR, but also absorbs across the entire visible region. This suggests excellent potential for incorporation into light harvesting devices. Black PDIs are extremely unusual with

previous examples being the result of solid state packing effects rather than intrinsic electronic properties of discrete molecules.[48, 49] Figure 2.13 shows the colour change, due to the progressive bathochromic shift, occurring along the synthetic pathway from dibromo PDI **2.2** to the two thionated PDIs **2.5**/**2.6** demonstrating how simple modifications can drastically change the optical properties of the PDIs.

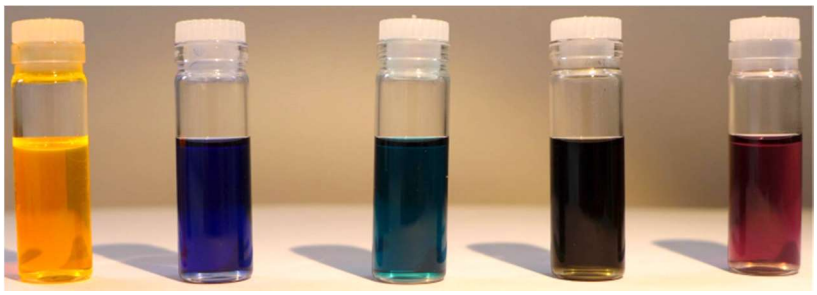

Figure 2.13. Solutions of PDI species in DCM. From left to right **2.2**, **2.4**, **2.3**, **2.6**, **2.5**.

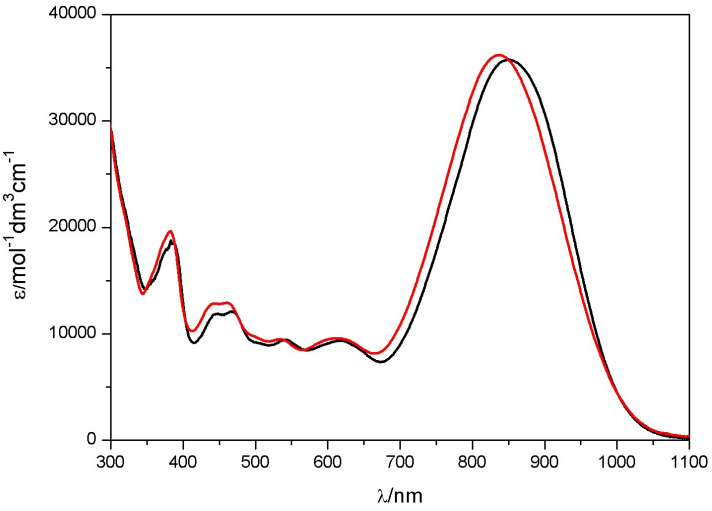

Figure 2.14. UV/vis/NIR absorption spectra of **2.5** in dichlorobenzene (black) and DCM (red). c = 2.67 x 10^{-5} (DCB) and 2.52 x 10^{-5} $mol^{-1}dm^3cm^{-1}$ (DCM).

In order to probe the effect of reduction upon the optical properties of **2.5** and **2.6**, their electrochemical behaviour was investigated by cyclic voltammetry, UV/vis/NIR spectroelectrochemistry and coulometry/EPR spectroscopy. It is well documented that upon reduction of PDIs, the major adsorption band shifts significantly to lower energy[36,50-52] and it was anticipated that in the case of **2.5** and **2.6** this would result in a significant shift into the NIR. Unexpectedly, upon thionation the solubility of the PDIs

was severely reduced. Electrochemical studies on **2.6** were possible in DCM at 1 mM concentrations. However, the solubility of **2.5** dropped to a level that made cyclic voltammetry in this solvent problematic. It was found that 1,2-dichlorobenzene (DCB) was a suitable alternative and very little change in the absorption properties of **2** were observed between the two solvents, Figure 2.14.

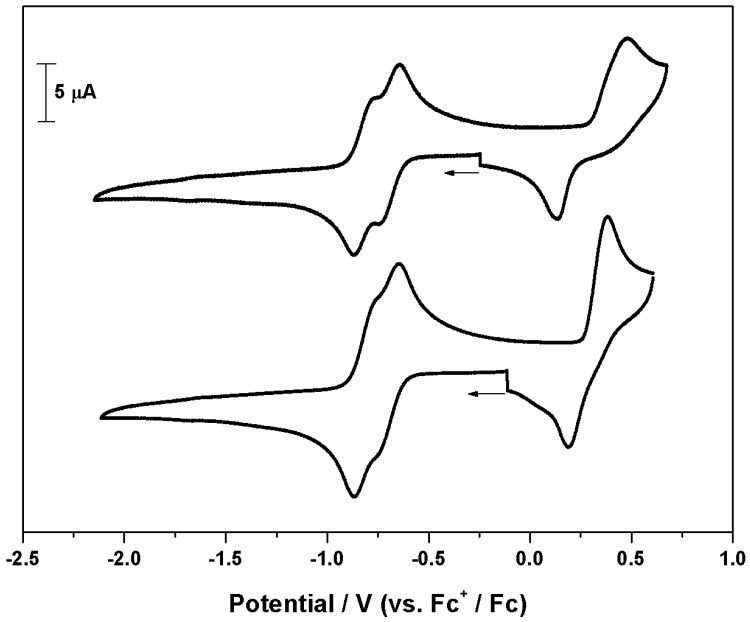

Figure 2.15. Cyclic voltammograms of **2.5** (bottom) and **2.6** (top) recorded in DCB containing $[Bu_4N][BF_4]$ (0.4 M).

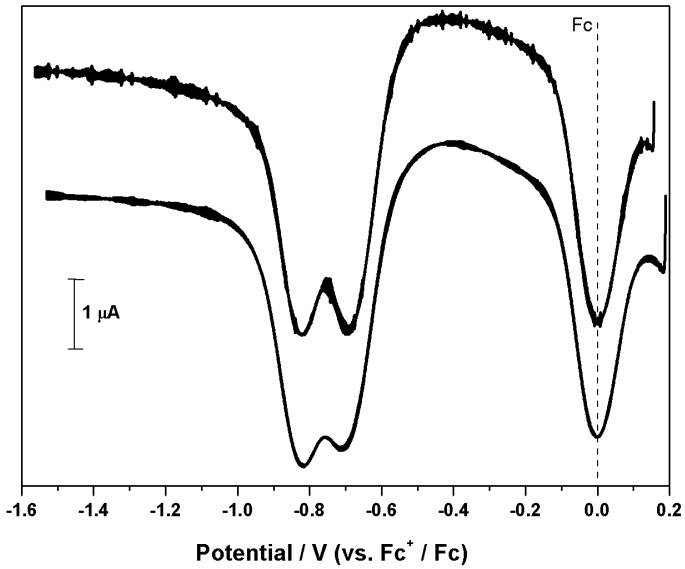

Figure 2.16. Square wave voltammograms of **2.5** (bottom) and **2.6** (top) recorded in DCB containing $[Bu_4N][BF_4]$ (0.4 M).

Compound	Solvent	1st Reduction	2nd Reduction
2.5	DCB	-0.71	-0.82
2.6	DCB	-0.70	-0.82
2.6	DCM	-0.61	-0.71
2.3[36]	DCM	-1.11	-1.29
2.4[36]	DCM	-1.11	-1.30

Table 2.1. Reduction potentials for thionated PDIs *versus* non-thionated dimorpholino-substituted PDIs. All potentials reported as $E_{1/2}$ (= $(E_p^a + E_p^c)/2$) in V *vs*. Fc^+/Fc at 0.1 Vs^{-1} scan rate and quoted to the nearest 0.01 V.

Cyclic voltammetric investigations of **2.5** and **2.6**, in DCB, revealed two closely overlapped reduction processes, Figure 2.15. The potentials of these reductions were determined from square wave voltammetry as -0.71 and -0.81 V for **2.5** and -0.69 and -0.82 V for **2.6**, (*vs*. Fc^+/Fc), Figure 2.16 and Table 2.1. The potentials observed for the two isomers are very similar, matching the behaviour exhibited by the reductions of **2.3** (-1.11 and -1.29 V) and **2.4** (-1.11 and -1.30 V) (*vs*. Fc^+/Fc).[36] The recording of cyclic and square wave voltammetry data for **2.6** in DCM gave a direct comparison with analogous measurements on **2.4**. In DCM the same two reductions noted for **2.6** in DCB were present but the potentials were shifted to -0.61 and -0.71 V (*vs*. Fc^+/Fc) for the first and second reductions respectively. Importantly, comparison of the first reduction of the thionated and non-thionated species, **2.6** *versus* **2.4** in DCM, reveal a shift of *ca*. 0.50 V to less negative potentials for the thionated analogue and this is accompanied by a small drop in the separation between the first and second reduction processes which may indicate a decrease in coulombic interaction in $\mathbf{2.6^{2-}}$. These results are consistent with those reported for *N*,*N*'-di(3-hexylundecyl)-perylene-3,4:9,10-tetracarboxylic diimide **PDI S0** (-0.68 and -0.91 V) and its tetra-thionated analogue **PDI S4** (-0.23 and -0.33 V) recorded in DCM (*vs*. Fc^+/Fc).[42] An oxidation process is also observed in the cyclic voltammogram of both **2.5** and **2.6**. However, neither were found to be electrochemically reversible in the scan rate range 0.02 – 0.3 Vs^{-1}. Therefore, these

oxidation processes were not subject to further investigations by spectroscopic techniques.

Coulometry confirmed the first reductions of **2.5** and **2.6** were one-electron processes and the solutions were observed to acquire a blue colour. Solutions of **2.5**$^{\bullet-}$ and **2.6**$^{\bullet-}$ were both found to be EPR active and gave signals consistent with the generation of radical anions with g_{iso} values of 2.0107 and 2.0105, respectively, Figure 2.17. Both of these g_{iso} values have increased with respect to **2.3**$^{\bullet-}$ and **2.4**$^{\bullet-}$ resulting from larger π-spin population due to an increase in spin-orbit coupling, an effect promoted by the presence of heavy (S *versus* O) atoms. As with **2.3**$^{\bullet-}$ and **2.4**$^{\bullet-}$, no hyperfine splittings were observed in the EPR spectra. The second reduction process of both species was also probed using EPR spectroscopy. Direduction leads to the formation of even more intensely blue solutions, however these solutions were found to be EPR silent, with only small residual signals attributed to the presence of **2.5**$^{\bullet-}$ and **2.6**$^{\bullet-}$ (5% and 14% respectively).

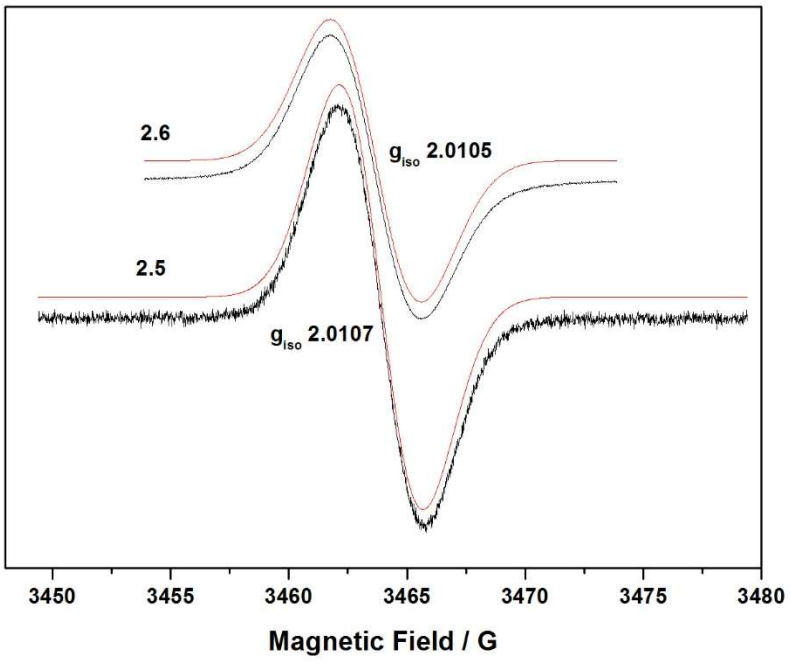

Figure 2.17. EPR spectra (black) for **2.5** and **2.6** with simulated spectra overlaid (red). Spectra simulated using Gaussian lineshape with a linewidth of 3.85 G (**2.5**) and 3.55 G (**2.6**).

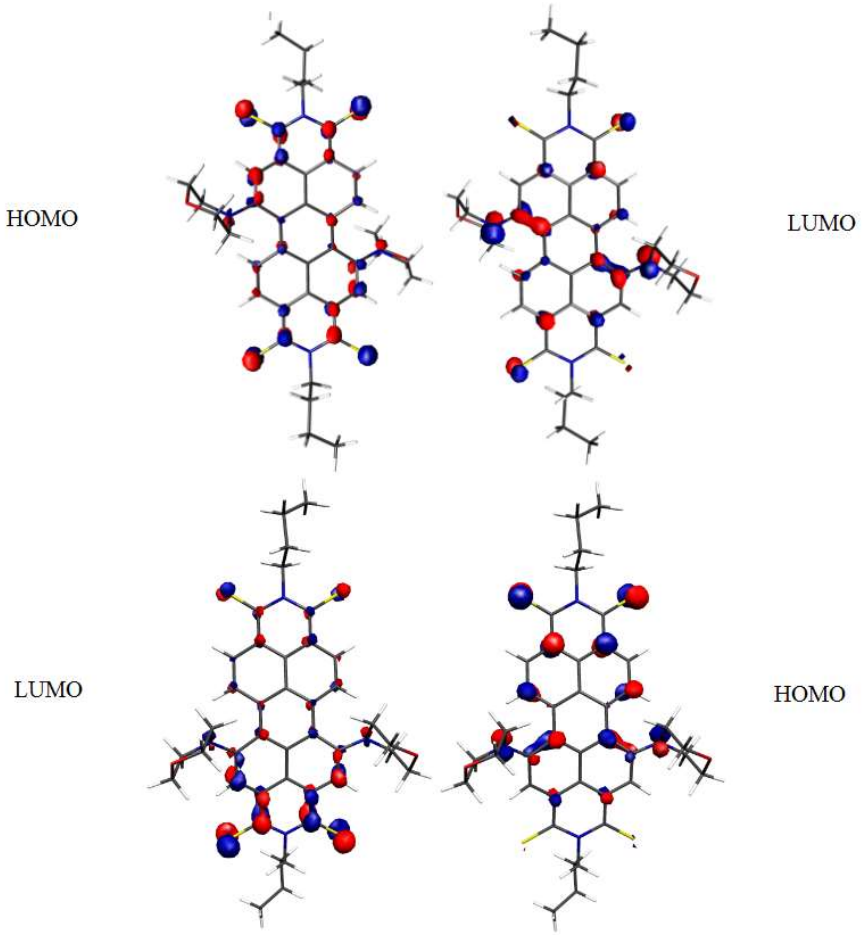

Figure 2.18. DFT calculated MO isosurfaces for **2.5** (top) and **2.6** (bottom).

Density Functional Theory (DFT) calculations were carried out using the B3LYP/6-31G* basis set. The geometry optimized structures showed the expected twist in the perylene core due to the steric bulk of the morpholine, Figure 2.18. The LUMO energies of **2.5** and **2.6** were calculated as -3.75 eV and -3.76 eV respectively, consistent with the first reduction potentials being almost identical. This result matches that of **2.3** and **2.4** which were also found to be identical.[36] The HOMO energy levels were calculated as -5.27 eV for **2.5** and -5.31 eV for **2.6**. The difference of 0.04 eV cannot be directly compared to the oxidation potentials due to the irreversibility of the processes. The 1,6-isomer having a lower HOMO energy than the 1,7- isomer is in keeping with the measurements for **2.3** and **2.4**. The molecular orbital (MO) isosurfaces for **2.5** show the HOMO and the LUMO to be a similar shape to the equivalent diagrams for **2.3** but with

more electron density lying on the sulfur atoms, further suggesting increased spin-orbit coupling due to the heavy sulfur atoms. The MO isosurfaces of **2.6** show the electron density mainly lies around the naphthalene ring bearing the morpholine subunits in the LUMO but in the HOMO the electron density is mainly on the unsubstituted naphthalene ring. Again, more electron density lies on the sulfur atom than in the case of **2.4**.

The reduction behaviour of **2.5** and **2.6** was probed further by spectroelectrochemical methods with both the *in situ* one- and two-electron reductions of **2.5** and **2.6** followed by UV/vis/NIR spectroscopy, Table 2.2. The results reported here are all carried out in DCB. The equivalent measurements for **2.6** were also carried out in DCM with very little change in absorption behaviour observed. Upon first reduction, the main band corresponding to the neutral species reduced in intensity with new bands forming, red shifted by 98 nm to 962 nm for **2.5**$^{\bullet-}$, Figure 2.19, and 116 nm to 954 nm for **2.6**$^{\bullet-}$, Figure 2.20, mimicking the behaviour of **2.3** and **2.4** following reduction. The extinction coefficients for these two new bands doubled in intensity compared to the neutral species. An additional considerably lower energy peak was observed at 1568 nm for **2.5**$^{\bullet-}$ and 1491 nm for **2.6**$^{\bullet-}$. Absorption bands in the NIR have been observed previously for PDI radicals, for example in a tetrachloro-tetracyano-PDI monoanion reported by Würthner and co-workers,[53] but the wavelengths observed here are at lower energy and in the short wave infrared (SWIR) region (1400 nm – 3000 nm), the first reported examples of such absorption in PDIs.

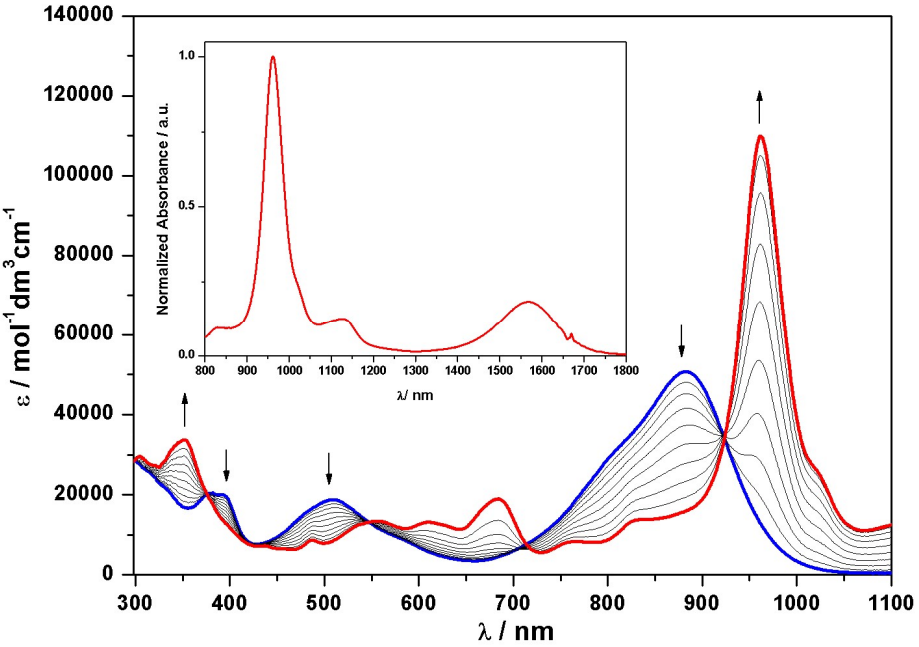

Figure 2.19. UV/vis/NIR absorption spectra recorded in DCB containing $[Bu_4N][BF_4]$ (0.4 M) using spectroelectrochemical methods for **2.5** at 273 K showing the inter-conversion of **2.5** (blue) to **2.5**$^{\bullet-}$ (red). Arrows indicate the progress of the reduction. c = 2.05 x 10^{-4} $mol^{-1}dm^3cm^{-1}$. Inset shows expanded spectrum displaying absorption in the SWIR.

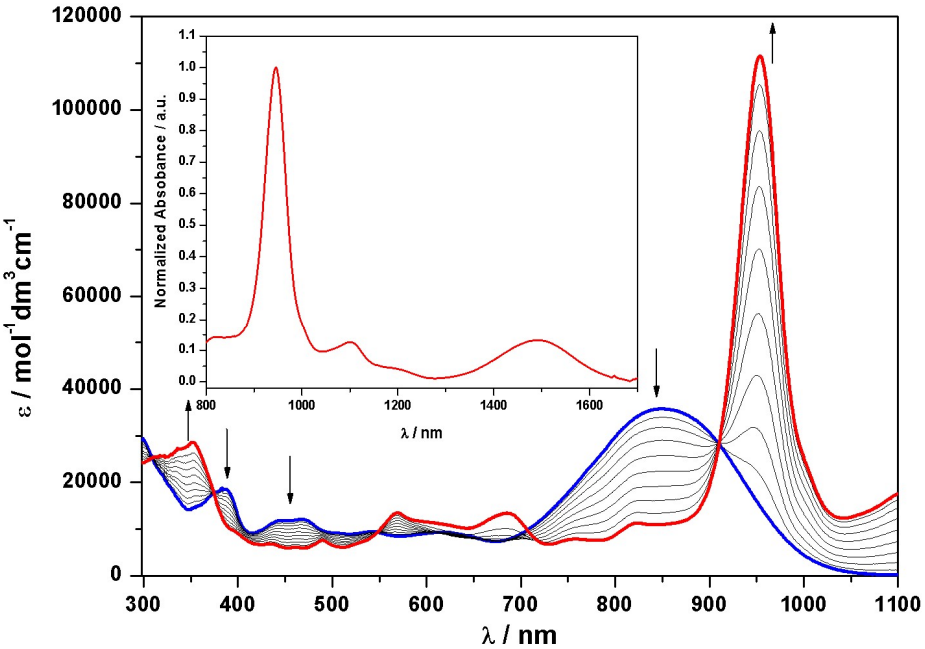

Figure 2.20. UV/vis/NIR absorption spectra recorded in DCB containing $[Bu_4N][BF_4]$ (0.4 M) using spectroelectrochemical methods for **2.6** at 273 K showing the inter-conversion of **2.6** (blue) to **2.6**$^{\bullet-}$ (red). Arrows indicate the progress of the reduction. c = 2.00 x 10^{-4} $mol^{-1}dm^3cm^{-1}$. Inset shows expanded spectrum displaying absorption in the SWIR.

As the second reduction proceeded, the $\mathbf{2.5}^{\bullet-}$ and $\mathbf{2.6}^{\bullet-}$ peaks diminished in intensity and new bands corresponding to the $\mathbf{2.5}^{2-}$ and $\mathbf{2.6}^{2-}$ species were formed, blue shifted to 684 nm and 687 nm respectively, Figure 2.21 and Figure 2.22. The blue shift from the monoanion to the dianion of PDIs is well documented, with the main dianion absorbance often lying between the main band of the anion and the neutral species.[50-52] However, in this case this shift is even more pronounced with the dianion's absorbance appearing 180 nm and 151 nm below that of **2.5** and **2.6** respectively. The dianion absorbances also appear to show vibrational structure, often seen in neutral PDIs, but missing from the broad featureless absorptions of **2.5** and **2.6**. Both reductions of **2.5** and **2.6** were shown to be reversible as the neutral spectra were fully regenerated upon reoxidation.

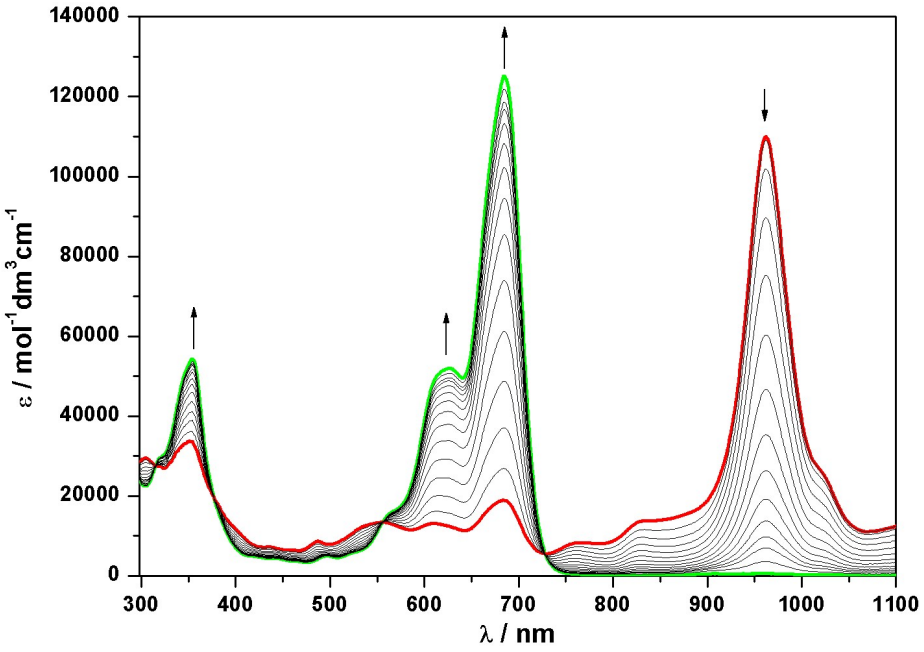

Figure 2.21. UV/vis/NIR absorption spectra recorded in DCB containing $[Bu_4N][BF_4]$ (0.4 M) using spectroelectrochemical methods for **2.5** at 273 K showing the inter-conversion of $\mathbf{2.5}^{\bullet-}$ (red) to $\mathbf{2.5}^{2-}$ (green). Arrows indicate the progress of the reduction. c = 2.05 x 10^{-4} $mol^{-1}dm^3cm^{-1}$.

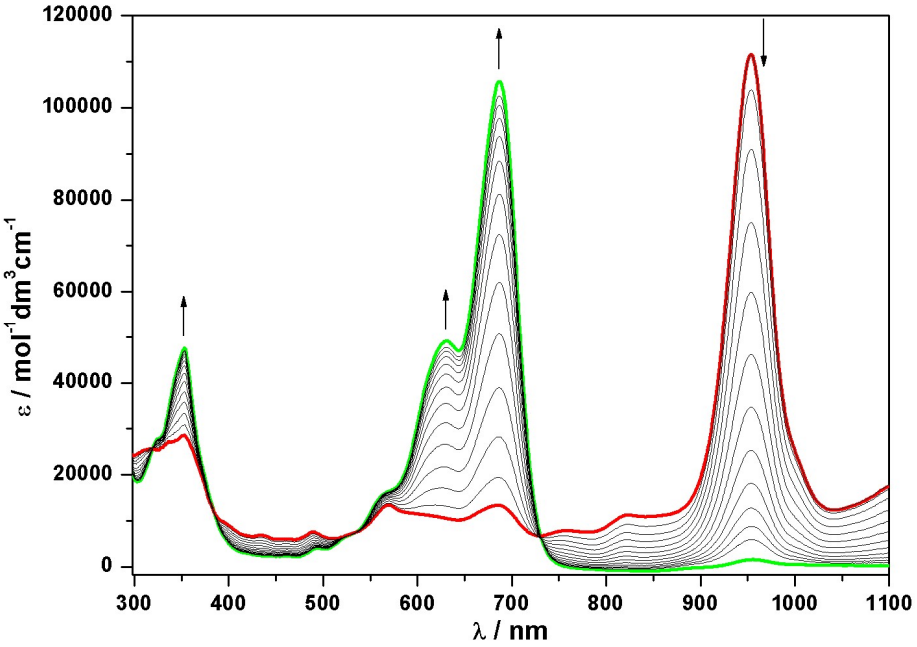

Figure 2.22. UV/vis/NIR absorption spectra recorded in DCB containing $[Bu_4N][BF_4]$ (0.4 M) using spectroelectrochemical methods for **2.6** at 273 K showing the inter-conversion of $\mathbf{2.6^{\bullet-}}$ (red) to $\mathbf{2.6^{2-}}$ (green). Arrows indicate the progress of the reduction. c = 2.00 x 10^{-4} $mol^{-1}dm^3cm^{-1}$.

	Neutral	Anion	Dianion
2.5	394 (2.0), 508 (1.9), 881 (5.1)	351 (3.4), 557 (1.3), 829 (1.4), 962 (11), 1128*, 1568*	354 (5.4), 626 (5.2), 685 (1.3)
2.6	383 (1.9), 468 (1.2), 850 (3.6)	352 (2.9), 570 (1.3), 821 (1.1), 954 (1.1), 1097*, 1484*	353 (4.7), 631 (4.9), 687 (1.1)

Table 2.2. UV/vis/NIR spectroscopic data for **2.5** and **2.6** measured at 273 K in DCB from spectroelectrochemistry. * indicates it was not possible to measure molar extinction coefficient. All values λ_{max}/nm (ε x10^5/$mol^{-1}dm^3cm^{-1}$).

2.3. Conclusions

Two PDIs with absorption maxima in the NIR have been synthesised by a combination of secondary amine substitution and thionation. This method is considerably simpler than many of the previous examples of NIR absorbing rylene diimides. X-ray crystal structures were collected giving the first examples of structures of thionated PDIs and revealing contrasting packing behaviour in the solid state between the two isomers. The absorbances at 864 nm and 838 nm, for **2.5** and **2.6** respectively, are only the second in the NIR for any neutrally charged PDI and the highest to date. In both cases, cyclic voltammetry revealed a shift to less negative reduction potentials and a decrease in the gap between first and second reduction. Oxidations were observed but were not found to be reversible over scan rate range 0.02 – 0.3 Vs^{-1} so were not probed any further. Upon first reduction, UV/vis/NIR spectroelectrochemistry revealed a significant red shift further into the NIR accompanied by a doubling of extinction coefficient. Bands in the SWIR were also present, the first examples of this in a PDI. Second reduction shifted the absorbance to a lower wavelength than the neutral species and reoxidation revealed all of these processes to be fully reversible. One of the PDIs, **2.6**, displayed an unexpected black colour in solution and in the solid state. UV/vis/NIR studies revealed this to be due to a broad range of absorbance from well into the NIR right across the UV and visible regions. This suggests excellent potential for this PDI to be incorporated into light harvesting devices such as OPVs.

Figure 2.23 displays structures of the PDIs discussed in this Chapter in order of increasing wavelength of absorption. It shows how the absorption maxima can be bathochromically shifted by amine substitution at the bay-area[15, 36] and imide carbonyl thionation[42] which, when combined, result in the PDIs reported in this Chapter with the

highest absorption maxima of any neutrally charged discrete PDI to date. Inducing a bathochromic shift into the NIR has also been possible by the formation of extended rylene diimides requiring complex synthesis and difficult purification[8] and the formation J-aggregating PDIs which only display high wavelength of absorbance in non-polar solvents.[19] The highest wavelengths of absorption observed to date utilise first the deprotonation of two phenoxy- groups bound to the bay are of the PDI[16] followed by chemical monoreduction to give a charged species with an absorption of 1396 nm.

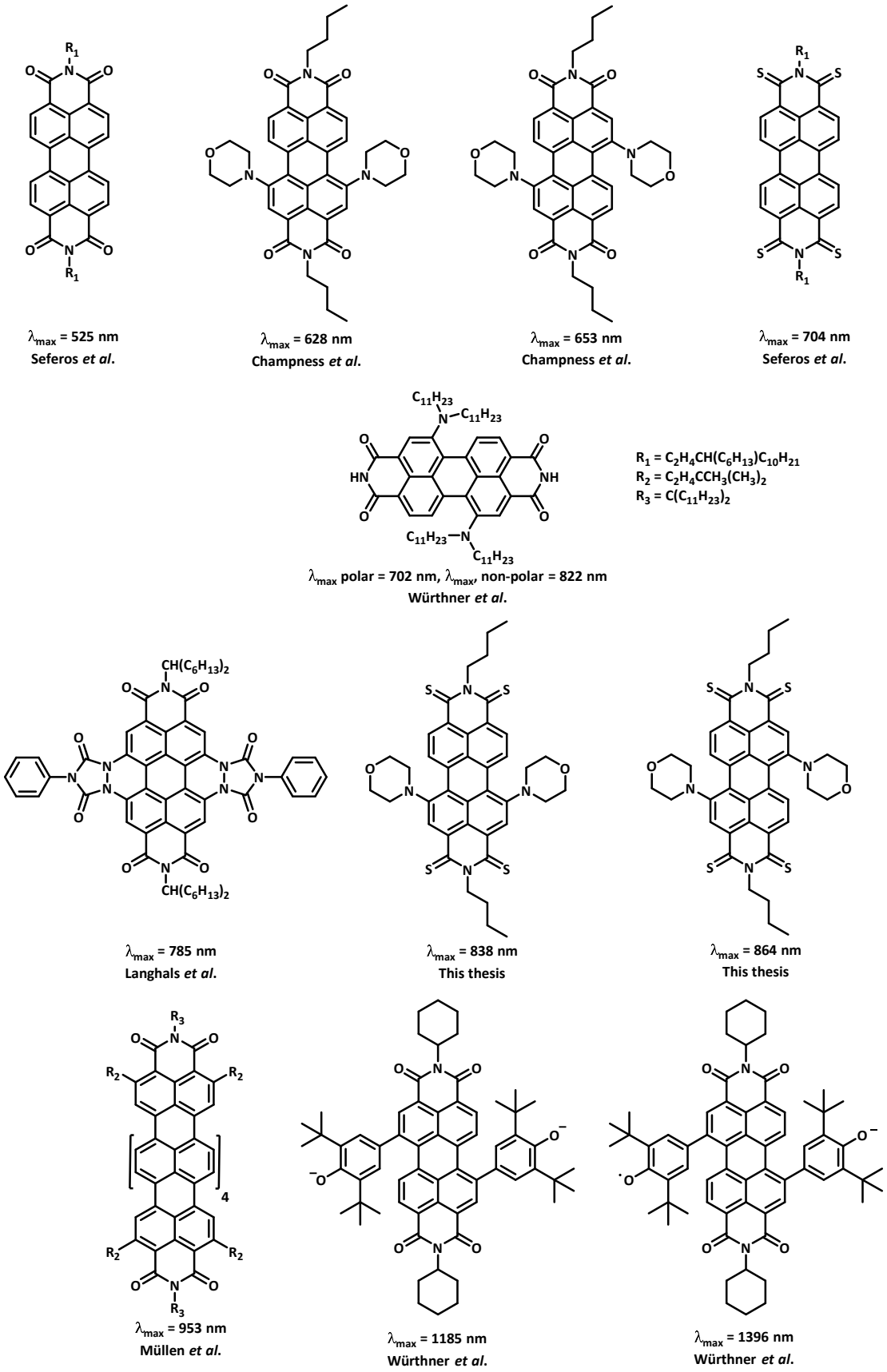

Figure 2.23. Structures of PDIs discussed in this chapter displayed in order of increasing absorption maximum.

2.4. Experimental

General Experimental Methods

All starting materials were purchased from Sigma Aldrich or Fisher Scientific and were used without further purification unless otherwise stated. Column chromatography was performed on silica gel (Merck silica gel 60, 0.2–0.5 mm, 50–130 mesh). Reactions using dry solvents (Sigma Aldrich) were carried out utilising standard Schlenk techniques. The ^{1}H and ^{13}C NMR spectra were obtained on a Bruker 400 MHz spectrometer. MS spectra were determined on a VoyagerDE-STR spectrometer (MALDI-TOF) with DCTB as the matrix, a Bruker microTOF II spectrometer (ESI) or a JEOL GCv4G spectrometer (FI).

Synthesis of dibromo perylene dianhydride (2.1)

Synthesis adapted from a literature procedure.[54] Perylene-3,4:9,10-tetracarboxylic dianhydride (12.0 g, 30.6 mmol), iodine (290 mg, 1.2 mmol) and sulfuric acid (98 %, 170 mL) were premixed and stirred at room temperature for 2 h. The reaction mixture was then heated to 80 ºC and bromine (3.66 mL, 71.1 mmol) was added dropwise over 1.5 h. The reaction mixture was reacted further at 80 ºC for 17 h. The reaction mixture was cooled to room temperature and the excess bromine was displaced by N_2. The mixture was poured into ice water and the precipitate collected by filtration then washed with water and methanol. The crude product **2.1** was dried in an oven overnight yielding a wet brick red solid (16.9 g). This was used for subsequent steps without further purification. MS(MALDI-TOF) $[M]^-$: 630.3 (tribromo-PDA), 550.1 (dibromo-PDA, major product), 470.1 (monobromo-PDA).

Synthesis of *N,N'*-di(n-butyl)-1,7(6)-dibromo-3,4:9,10-perylenetetracarboxylic diimide (2.2)

2.1 (3.00 g, 4.36 mmol), n-butyl amine (1.5 mL, 10.8 mmol) and IPA (50 mL) were heated to reflux for 17 h. The mixture was cooled to room temperature and poured into HCl (2 M). Chloroform was added and the organic extract was washed twice with HCl (2 M) and once with water before drying over $MgSO_4$ and removal of the solvent under reduced pressure. The crude product was purified by column chromatography (SiO_2, chloroform:hexane 9:1) to give **2.2**, in a mixture of 1,6- and 1,7- isomers, as a red powder (2.88 g, 4.36 mmol, 80 %). ^{1}H NMR ($CDCl_3$, 400 MHz): δ = 9.45 (d, *J*=8.2 Hz, 2 H), 8.89 (s, 2 H), 8.67 (d, *J*=8.2 Hz, 2 H), 4.17 - 4.28 (m, 4 H), 1.69 - 1.80 (m, 4 H), 1.48 (q, *J*=8.0 Hz, 4 H), 1.01 ppm (t, *J*=7.3 Hz, 6 H). ^{13}C NMR ($CDCl_3$, 101 MHz): δ = 163.1, 162.8, 162.3, 161.9, 138.0, 137.9, 133.0, 132.8, 132.6, 132.2, 130.2, 129.9, 129.8, 129.1, 128.4, 128.0, 127.8, 127.6, 126.8, 126.0, 123.3, 123.1, 122.7, 122.3, 121.6, 120.7, 40.7, 40.5, 40.4, 30.2, 30.1, 30.1, 20.4, 20.3, 20.3, 13.8 ppm. MS(MALDI-TOF) $[M]^-$: calcd for $C_{32}H_{24}Br_2N_2O_4$ 660.4, found 660.0.

Synthesis of *N,N'*-di(n-butyl)-1,7-dimorpholino-3,4:9,10-perylenetetracarboxylic diimide (2.3) and *N,N'*-di(n-butyl)-1,6-dimorpholino-3,4:9,10-perylenetetracarboxylic diimide (2.4)

Synthesis adapted from a literature procedure.[36] A mixture of **2.2** (1.79 g, 2.71 mmol) and morpholine (50 mL) were heated to 65 ºC for three days. The mixture was cooled to room temperature and slowly poured into HCl (2 M). Chloroform was added and the organic extracts were washed twice with HCl (2 M) and once with water before drying over $MgSO_4$ and removal of the solvent under reduced pressure. The crude product was purified by column chromatography (SiO_2, chloroform:acetone 97:3) to give the 1,7-

isomer, **2.3**, as a green microcrystalline powder (1.17g, 1.74 mmol, 64 %) and the 1,6-isomer, **2.4**, as a blue powder (304 mg, 0.451 mmol, 16 %). **2.3**- ^{1}H NMR ($CDCl_3$, 400 MHz): δ = 9.67 (d, *J*=8.3 Hz, 2 H), 8.41 (d, *J*=8.3 Hz, 2 H), 8.33 (s, 2 H), 4.24 (t, *J*=7.5 Hz, 4 H), 3.83 - 4.01 (m, 8 H), 3.38 (d, *J*=12.0 Hz, 4 H), 3.06 (t, *J*=9.9 Hz, 4 H), 1.75 (quin, *J*=7.6 Hz, 4 H), 1.49 (dq, *J*=15.0, 7.4 Hz, 5 H), 1.02 ppm (t, *J*=7.3 Hz, 6 H). ^{13}C NMR ($CDCl_3$, 101 MHz): δ = 163.2, 163.1, 149.7, 134.5, 129.6, 127.9, 124.2, 123.5, 122.7, 122.6, 122.6, 121.3, 66.4, 51.3, 40.5, 30.2, 20.4, 13.9 ppm. MS(MALDI-TOF) $[M]^-$: 672.5. **2.4**- ^{1}H NMR ($CDCl_3$, 400 MHz): δ = 9.88 (d, *J*=8.3 Hz, 2 H), 8.63 (d, *J*=8.3 Hz, 2 H), 8.40 (s, 2 H), 4.22 (q, *J*=8.0 Hz, 4 H), 3.86 - 4.00 (m, 8 H), 3.29 (d, *J*=12.2 Hz, 4 H), 3.03 - 3.16 (m, 4 H), 1.76 (sxt, *J*=7.6 Hz, 4 H), 1.39 - 1.55 (m, 4 H), 1.01 ppm (t, *J*=7.3 Hz, 6 H). ^{13}C NMR ($CDCl_3$, 101 MHz): δ = 163.5, 163.5, 152.1, 135.4, 131.7, 130.7, 128.8, 128.3, 124.3, 123.7, 123.5, 121.9, 121.5, 120.9, 66.5, 51.7, 40.4, 40.3, 30.3, 30.2, 20.4, 20.3, 13.9, 13.8 ppm. MS(MALDI-TOF) $[M]^-$: calcd for $C_{40}H_{40}N_4O_6$ 672.3, found 672.5.

Synthesis of *N,N'*-di(n-butyl)-1,7-dimorpholino-3,4:9,10-perylenetetrathio diimide (2.5)

2.3 (1.00 g, 1.49 mmol) and Lawesson's Reagent (3.60 g, 8.91 mmol) were dissolved in dry toluene (200 mL) and heated to reflux, under an inert atmosphere, for two days. The solution was cooled to room temperature and poured into NaOH (100 mM) then the organic extract was washed with water three times. The solution was dried over $MgSO_4$ and the solvent removed under reduced pressure. The crude product was purified by column chromatography (SiO_2, chloroform:EtOAc 97:3) to give **2.5** as a dark purple powder (175 mg, 0.237 mmol, 16 %). ^{1}H NMR ($CDCl_3$/TFA-d, 400 MHz): δ = 9.18 (d, *J*=8.7 Hz, 2 H), 8.57 (d, *J*=8.7 Hz, 2 H), 8.38 (s, 2 H), 5.21 - 5.44 (m, 5 H),

3.85 - 4.14 (m, 8 H), 3.02 - 3.32 (m, 4 H), 1.82 - 2.04 (m, 5 H), 1.55 (sxt, *J*=7.4 Hz, 5 H), 1.08 ppm (t, *J*=7.3 Hz, 7 H); ^{13}C NMR ($CDCl_3$/TFA-d, 126 MHz): δ = 187.3, 149.3, 134.9, 133.3, 128.8, 128.3, 127.4, 123.8, 121.8, 119.4, 66.4, 55.6, 51.5, 27.5, 20.1, 13.8 ppm; HRMS(MALDI-TOF) $[M]^+$: calcd for $C_{40}H_{40}N_4O_2S_4$ 736.2034, found 736.2016.

Synthesis of *N,N'*-di(n-butyl)-1,6-dimorpholino-3,4:9,10-perylenetetrathio diimide (2.6)

2.4 (445 mg, 0.661 mmol) and Lawesson's Reagent (1.60 g, 3.96 mmol) were dissolved in dry toluene (100 mL) and heated to reflux, under an inert atmosphere, for two days. The solution was cooled to room temperature and poured into NaOH (100 mM) then the organic extract was washed with water three times. The solution was dried over $MgSO_4$ and the solvent was removed under reduced pressure. The crude product purified by column chromatography (SiO_2, chloroform:EtOAc 97:3). Any unreacted tri-thionated PDI was re-reacted with 1.5 equivalents of Lawesson's reagent before work up and purification by the above method. Both crops were combined to give **2.6** as a black powder (85 mg, 0.115 mmol, 17 %). ^{1}H NMR ($CDCl_3$, 400 MHz): δ = 9.71 (d, *J*=8.8 Hz, 2 H), 8.92 (d, *J*=8.8 Hz, 2 H), 8.60 (s, 2 H), 5.25 - 5.43 (m, 4 H), 3.84 - 4.02 (m, 8 H), 3.29 (d, *J*=11.8 Hz, 4 H), 2.96 - 3.11 (m, 4 H), 1.84 - 2.03 (m, 4 H), 1.45 - 1.56 (m, *J*=15.4, 7.7 Hz, 4 H), 1.03 (t, *J*=7.3 Hz, 3 H), 1.04 ppm (t, *J*=7.4 Hz, 3 H). ^{13}C NMR ($CDCl_3$, 101 MHz): δ = 188.7, 188.1, 151.9, 137.1, 134.6, 130.8, 129.5, 128.1, 127.9, 125.2, 125.1, 123.7, 123.0, 116.8, 66.4, 55.2, 55.0, 51.9, 27.6, 27.5, 20.1, 20.1, 13.8, 13.8 ppm. HRMS(MALDI-TOF) $[M]^+$: calcd for $C_{40}H_{40}N_4O_2S_4$ 736.2034, found 736.2032.

Electrochemical and Optical Investigations

UV/visible absorption spectra were recorded on a Perkin-Elmer Lambda 25 spectrometer.

Cyclic voltammetric and coulometric studies were carried out using an Autolab PGSTAT20 potentiostat. DCM was freshly distilled under an atmosphere of dinitrogen from calcium hydride. $[NBu_4][BF_4]$ was prepared by literature methods.[55] Standard cyclic voltammetry was carried out under an atmosphere of argon using a three-electrode arrangement in a single compartment cell. A glassy carbon working electrode, a Pt wire secondary electrode and a saturated calomel reference electrode, chemically isolated from the test solution *via* a bridge tube containing electrolyte solution and fitted with a porous vycor frit, were used in the cell. The solutions were 10^{-3} M in test compound and 0.4 M in $[NBu_4][BF_4]$ as supporting electrolyte. Redox potentials are quoted *versus* the ferrocenium–ferrocene couple used as an internal reference. Compensation for internal resistance was not applied.

Bulk electrolysis experiments, at a controlled potential, were carried out using a two-compartment cell. The Pt/Rh gauze basket working electrode was separated from the wound Pt/Rh gauze secondary electrode by a glass frit. A saturated calomel reference electrode was bridged to the test solution through a vycor frit orientated at the centre of the working electrode. The working electrode compartment was fitted with a magnetic stirrer bar and the test solution was stirred rapidly during electrolysis. The solutions used were 0.4 M in $[NBu_4][BF_4]$ as supporting electrolyte and 10^{-3} M in test compound and were prepared using Schlenk line techniques. Electrolysed solutions were transferred to quartz tubes, *via* a teflon canula, for analysis by EPR spectroscopy. EPR spectra were recorded on a Bruker EMX spectrometer.

The UV/vis spectroelectrochemical experiments were carried out with an optically transparent electrochemical cell (modified quartz cuvette, optical pathlength: 0.5 mm). A three-electrode configuration, consisting a Pt/Rh gauze working electrode, a Pt wire secondary electrode (in a fritted PTFE sleeve) and a saturated calomel electrode, chemically isolated from the test solution *via* a bridge tube containing electrolyte solution and terminated in a porous frit, was used in the cell. The potential at the working electrode was controlled by a Sycopel Scientific Ltd DD10M potentiostat. The UV/vis spectra were recorded on a Perkin Elmer Lambda 16 spectrophotometer. The cavity was purged with dinitrogen and temperature control at the sample was achieved by flowing cooled dinitrogen across the surface of the cell. For UV/vis/NIR measurements the reduced species were generated in the same way and the spectra were recorded on a Perkin-Elmer Lambda 750 spectrometer.

X-Ray Crystallography

Single crystals of **2.4**, **2.5** and **2.6** were grown by layered diffusion between a chloroform solution of the target compound and hexane. Single crystal diffraction data was collected at 120(2) K on a Rigaku FR-E+ Very High Flux Diffractometer using monochromated Mo Kα radiation for **2.4** or a Bruker GV1000 spectrometer using mirror monochromated Cu Kα radiation for **2.5** and **2.6**. All structures were solved using Olex2,[56] the structures were solved with the ShelXT[57] structure solution program using Direct Methods and refined with the ShelXL[58] refinement package using Least Squares minimisation.

In the structure of **2.5**, disordered solvent chloroform could not be reasonably modelled to give convergence and the data was processed using SQUEEZE,[59] which gave an estimate of 118 e- per cell, corresponding to about two chloroform molecules per

asymmetric unit. These molecules were then added to the sum formula. Three butyl chains, containing atoms 61A to 64A (chain 1), 61B to 64B (chain 2), and 51A to 54A (chain 3), are disordered over two positions and their respective occupancies were refined competitively. Chain 1 and chain 3 converged to ratios of 0.43:0.57 while chain 2 converged to a ratio of 0.40:0.60. Chemically equivalent bonds of the disordered atoms were restrained to be approximately equal to each other and those of the ordered equivalent. Enhanced rigid bond and similarity restraints were applied to the thermal parameters of the disordered atoms. Antibumping restraints were applied to prevent close intermolecular H-H interactions due to vaguely located disordered hydrogen atoms.

In the structure of **2.6**, the butyl chain, containing atoms 51 to 54, is disordered over two positions and its occupancy was refined competitively converging to a ratio of 55:45. Chemically equivalent bonds of the disordered atoms were restrained to be approximately equal to each other and those of the ordered equivalent. Enhanced rigid bond and similarity restraints were applied to the thermal parameters of the disordered atoms.

Crystal data for **2.4**: $C_{40}H_{40}N_4O_6 \cdot CHCl_3$. Monoclinic, space group *P*21/*c*, a = 12.7735(2), b = 8.38150(10), c = 32.1723(5) Å, β = 111.6840(10)°, V = 3200.66(8) Å^3, Z = 4, D_{calc} = 1.396g cm^{-3}, μ = 0.767 mm^{-1}, F(000) = 1424. A total of 12505 reflections were collected, of which 6283 were unique, with R_{int} = 0.016. Final R_1 (wR_2) = 0.0436 (0.1269) with GOF = 1.04.

Crystal data for **2.5**: $C_{40}H_{40}N_4O_2S_4.CHCl_3$. Triclinic, space group *P*-1, a = 12.8268(14), b = 13.2644(13), c = 24.5245(7) Å, α = 96.008(5), β = 95.267(6), γ = 118.650(11)° , V = 3593.1 (6) Å^3, Z = 4, D_{calc} = 1.473 g cm^{-3} , μ = 3.81 mm^{-1} , F(000) = 1668. A total of

28315 reflections were collected, of which 14170 were unique, with R_{int} = 0.133. Final R_1 (wR_2) = 0.149 (0.416) with GOF = 1.26.

Crystal data for **2.6**: $C_{40}H_{40}N_4O_2S_4 \cdot CHCl_3$. Triclinic, space group *P*-1, a = 10.5929(5), b = 13.3915(8), c = 15.0416(8) Å, α = 93.393(5), β = 105.711(5), γ = 107.519(5)°, V = 1935.59(19) $Å^3$, Z = 2, D_{calc} = 1.469g cm^{-3}, μ = 4.51 mm^{-1} , F(000) = 892. A total of 14080 reflections were collected, of which 7626 were unique, with R_{int} = 0.051. Final R_1 (wR_2) = 0.061 (0.166) with GOF = 1.02.

Density Functional Theory

DFT calculations were carried out using the B3LYP/6-31G* basis set and all calculations were performed with Gaussian 03 Revision D. 01.[60]

2.5. References

1. G. Qian and Z. Y. Wang, *Chem. Asian. J.*, 2010, **5**, 1006-1029.
2. L. Hu, Z. Yan and H. Xu, *RSC Adv.*, 2013, **3**, 7667-7676.
3. W. Zhao and E. M. Carreira, *Angew. Chem. Int. Ed.*, 2005, **44**, 1677-1679.
4. G. Qian, B. Dai, M. Luo, D. Yu, J. Zhan, Z. Zhang, D. Ma and Z. Y. Wang, *Chem. Mater.*, 2008, **20**, 6208-6216.
5. A. Ajayaghosh, *Chem. Soc. Rev.*, 2003, **32**, 181-191.
6. A. Abuteen, S. Zanganeh, J. Akhigbe, L. P. Samankumara, A. Aguirre, N. Biswal, M. Braune, A. Vollertsen, B. Roder, C. Bruckner and Q. Zhu, *Phys. Chem. Chem. Phys.*, 2013, **15**, 18502-18509.
7. J. R. Sommer, A. H. Shelton, A. Parthasarathy, I. Ghiviriga, J. R. Reynolds and K. S. Schanze, *Chem. Mater.*, 2011, **23**, 5296-5304.
8. L. Chen, C. Li and K. Mullen, *J. Mater. Chem. C*, 2014, **2**, 1938-1956.
9. F. Nolde, J. Qu, C. Kohl, N. G. Pschirer, E. Reuther and K. Müllen, *Chem. Eur. J.*, 2005, **11**, 3959-3967.
10. Y. Geerts, H. Quante, H. Platz, R. Mahrt, M. Hopmeier, A. Bohm and K. Mullen, *J. Mat. Chem.*, 1998, **8**, 2357-2369.
11. N. G. Pschirer, C. Kohl, F. Nolde, J. Qu and K. Müllen, *Angew. Chem. Int. Ed.*, 2006, **45**, 1401-1404.
12. H. Zhao, Y.-Y. Zhang, H. Xu, Z.-M. He, Z.-L. Zhang and H.-M. Zhang, *Tetrahedron*, 2015, **71**, 7752-7757.
13. K.-Y. Chen, C.-W. Chang and H.-Y. Tsai, *Materials*, 2015, **8**, 4943-4960.
14. G. Brocks and A. Tol, *Synt. Met.*, 1996, **76**, 213-216.
15. H. Langhals and P. Blanke, *Dyes Pigments*, 2003, **59**, 109-116.
16. M.-J. Lin, B. Fimmel, K. Radacki and F. Würthner, *Angew. Chem. Int. Ed.*, 2011, **50**, 10847-10850.
17. D. Schmidt, M. Son, J. M. Lim, M.-J. Lin, I. Krummenacher, H. Braunschweig, D. Kim and F. Würthner, *Angew. Chem. Int. Ed.*, 2015, **54**, 13980-13984.
18. A. C. Grimsdale and K. Müllen, *Angew. Chem. Int. Ed.*, 2005, **44**, 5592-5629.
19. H. Wang, T. E. Kaiser, S. Uemura and F. Wurthner, *Chem. Commun.*, 2008, 1181-1183.
20. F. Würthner, T. E. Kaiser and C. R. Saha-Möller, *Angew. Chem. Int. Ed.*, 2011, **50**, 3376-3410.
21. K. A. Mazzio and C. K. Luscombe, *Chem. Soc. Rev.*, 2015, **44**, 78-90.
22. M. Grätzel, *J. Photoch. Photobio. C*, 2003, **4**, 145-153.
23. M. C. Scharber and N. S. Sariciftci, *Prog. Polym. Sci.*, 2013, **38**, 1929-1940.
24. H. Xiang, J. Cheng, X. Ma, X. Zhou and J. J. Chruma, *Chem. Soc. Rev.*, 2013, **42**, 6128-6185.
25. A. Mishra, M. K. R. Fischer and P. Bäuerle, *Angew. Chem. Int. Ed.*, 2009, **48**, 2474-2499.
26. B. Walker, A. B. Tamayo, X.-D. Dang, P. Zalar, J. H. Seo, A. Garcia, M. Tantiwiwat and T.-Q. Nguyen, *Adv. Funct. Mater.*, 2009, **19**, 3063-3069.
27. Y. Qin and Q. Peng, *Int. J. Photoenergy*, 2012, **2012**, 21.
28. B. E. Hardin, H. J. Snaith and M. D. McGehee, *Nat. Photon.*, 2012, **6**, 162-169.
29. S. P. Singh and T. Gayathri, *Eur. J. Org. Chem.*, 2014, **2014**, 4689-4707.

30. S. Kolemen, O. A. Bozdemir, Y. Cakmak, G. Barin, S. Erten-Ela, M. Marszalek, J.-H. Yum, S. M. Zakeeruddin, M. K. Nazeeruddin, M. Gratzel and E. U. Akkaya, *Chem. Sci.*, 2011, **2**, 949-954.
31. J. H. Burroughes, D. D. C. Bradley, A. R. Brown, R. N. Marks, K. Mackay, R. H. Friend, P. L. Burns and A. B. Holmes, *Nature*, 1990, **347**, 539-541.
32. N. Tessler, V. Medvedev, M. Kazes, S. Kan and U. Banin, *Science*, 2002, **295**, 1506-1508.
33. C. Borek, K. Hanson, P. I. Djurovich, M. E. Thompson, K. Aznavour, R. Bau, Y. Sun, S. R. Forrest, J. Brooks, L. Michalski and J. Brown, *Angew. Chem. Int. Ed.*, 2007, **46**, 1109-1112.
34. J. Kido and Y. Okamoto, *Chem. Rev.*, 2002, **102**, 2357-2368.
35. G. Qian, Z. Zhong, M. Luo, D. Yu, Z. Zhang, Z. Y. Wang and D. Ma, *Adv. Mater.*, 2009, **21**, 111-116.
36. G. Goretzki, E. S. Davies, S. P. Argent, W. Z. Alsindi, A. J. Blake, J. E. Warren, J. McMaster and N. R. Champness, *J. Org. Chem.*, 2008, **73**, 8808-8814.
37. S. Lévesque, D. Gendron, N. Bérubé, F. Grenier, M. Leclerc and M. Côté, *J. Phys. Chem. C*, 2014, **118**, 3953-3959.
38. G. L. Gibson, T. M. McCormick and D. S. Seferos, *J. Phys. Chem. C*, 2013, **117**, 16606-16615.
39. Y. Yamashita, K. Ono, M. Tomura and S. Tanaka, *Tetrahedron*, 1997, **53**, 10169-10178.
40. H. Ammar Aouchiche, S. Djennane and A. Boucekkine, *Synthetic Met.*, 2004, **140**, 127-133.
41. J. Quinn, Y. Zheng, Z. Chen, H. Usta, C. Newman, H. Yan and A. Facchetti, *US 2011/0155247 A1*, 2011.
42. A. J. Tilley, R. D. Pensack, T. S. Lee, B. Djukic, G. D. Scholes and D. S. Seferos, *J. Phys. Chem. C*, 2014, **118**, 9996-10004.
43. A. J. Tilley, C. Guo, M. B. Miltenburg, T. B. Schon, H. Yan, Y. Li and D. S. Seferos, *Adv. Funct. Mater.*, 2015, **25**, 3321-3329.
44. W. Chen, J. Zhang, G. Long, Y. Liu and Q. Zhang, *J. Mater. Chem. C*, 2015, **3**, 8219-8224.
45. L. M. Kozycz, C. Guo, J. G. Manion, A. J. Tilley, A. J. Lough, Y. Li and D. S. Seferos, *J. Mater. Chem. C*, 2015, **3**, 11505-11515.
46. F. S. Etheridge, R. Fernando, J. A. Golen, A. L. Rheingold and G. Sauve, *RSC Adv.*, 2015, **5**, 46534-46539.
47. H.-K. Jeong, Y. P. Lee, R. J. W. E. Lahaye, M.-H. Park, K. H. An, I. J. Kim, C.-W. Yang, C. Y. Park, R. S. Ruoff and Y. H. Lee, *J. Am. Chem. Soc.*, 2008, **130**, 1362-1366.
48. P. Yan, A. Chowdhury, M. W. Holman and D. M. Adams, *J. Phys. Chem. B*, 2005, **109**, 724-730.
49. F. Würthner, C. Bauer, V. Stepanenko and S. Yagai, *Adv. Mater.*, 2008, **20**, 1695-1698.
50. T. W. Chamberlain, E. S. Davies, A. N. Khlobystov and N. R. Champness, *Chem. Eur. J.*. 2011, **17**, 3759-3767.
51. B. A. Llewellyn, A. G. Slater, G. Goretzki, T. L. Easun, X.-Z. Sun, E. S. Davies, S. P. Argent, W. Lewis, A. Beeby, M. W. George and N. R. Champness, *Dalton Trans.*, 2014, **43**, 85-94.
52. A. G. Slater, E. S. Davies, S. P. Argent, W. Lewis, A. J. Blake, J. McMaster and N. R. Champness, *J. Org. Chem.*, 2013, **78**, 2853-2862.
53. S. Seifert, D. Schmidt and F. Wurthner, *Chem. Sci.*, 2015, **6**, 1663-1667.

54. M. Franceschin, A. Alvino, V. Casagrande, C. Mauriello, E. Pascucci, M. Savino, G. Ortaggi and A. Bianco, *Bioorg. Med. Chem.*, 2007, **15**, 1848-1858.
55. J. Kubas, *Inorg. Synth.*, 1990, **28**, 68.
56. O. V. Dolomanov, L. J. Bourhis, R. J. Gildea, J. A. K. Howard and H. Puschmann, *J. Appl. Cryst.*, 2009, **42**, 339-341.
57. G. M. Sheldrick, *Acta. Cryst. A.*, 2008, **64**, 112-122.
58. G. M. Sheldrick, *Acta. Cryst. C*, 2015, **71**, 3-8.
59. A. L. Spek, *Acta Crystallogr.*, 2009, **65**, 148-155.
60. M. J. Frisch, G. W. Trucks, H. B. Schlegel, G. E. Scuseria, M. A. Robb, J. R. Cheeseman, G. Scalmani, V. Barone, B. Mennucci, G. A. Petersson, H. Nakatsuji, M. Caricato, X. Li, H. P. Hratchian, A. F. Izmaylov, J. Bloino, G. Zheng, J. L. Sonnenberg, M. Hada, M. Ehara, K. Toyota, R. Fukuda, J. Hasegawa, M. Ishida, T. Nakajima, Y. Honda, O. Kitao, H. Nakai, T. Vreven, J. A. Montgomery Jr., J. E. Peralta, F. Ogliaro, M. J. Bearpark, J. Heyd, E. N. Brothers, K. N. Kudin, V. N. Staroverov, R. Kobayashi, J. Normand, K. Raghavachari, A. P. Rendell, J. C. Burant, S. S. Iyengar, J. Tomasi, M. Cossi, N. Rega, N. J. Millam, M. Klene, J. E. Knox, J. B. Cross, V. Bakken, C. Adamo, J. Jaramillo, R. Gomperts, R. E. Stratmann, O. Yazyev, A. J. Austin, R. Cammi, C. Pomelli, J. W. Ochterski, R. L. Martin, K. Morokuma, V. G. Zakrzewski, G. A. Voth, P. Salvador, J. J. Dannenberg, S. Dapprich, A. D. Daniels, Ö. Farkas, J. B. Foresman, J. V. Ortiz, J. Cioslowski and D. J. Fox, *Gaussian 03, ReVision D. 01; Gaussian Inc., Wallingford CT*, 2004.

Chapter 3. Perylene Diimide-BODIPY Dyads and Triads

3.1. Introduction

3.1.1. BODIPY Dyes

3.1.1.1. Synthesis and Properties of BODIPYs

4,4-Difluoro-4-borata-3a-azonia-4a-aza-s-indacene, known hereafter as BODIPY, was first synthesised in 1968[1] but it was not until the 1980s that the potential applications of this class of dye started to be realised, creating an area of research that is still expanding to this day.[2, 3] The basic structure of unsubstituted BODIPY is shown in Figure 3.1 along with its IUPAC numbering system and more common α/β/meso labelling system. One of the main attractions of the BODIPY is its excellent synthetic versatility as it is possible to easily functionalise all eight of these positions.

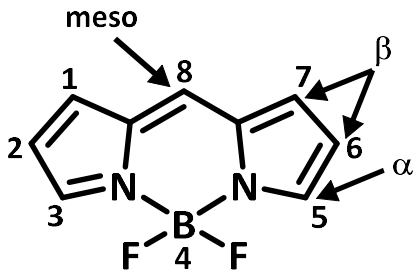

Figure 3.1. Basic structure of BODIPY with two labelling systems shown.

The general synthesis of BODIPY is derived from well-known porphyrin chemistry and involves the condensation of pyrrole with an acid chloride or aldehyde to give a dipyrromethene (in the case of aldehydes an additional oxidation step is required), followed by reaction with a base then complexation with boron trifluoride diethyl etherate ($BF_3.OEt_2$) to yield the BODIPY, Figure 3.2. This synthetic pathway allows easy incorporation of many different functionalities to the meso position of the BODIPY as a huge range of aldehydes and acid chlorides are available. Meso-

substituents bearing further reactive sites, such as halogens, are a potential route to adding further functionality as the BODIPY core is stable to varied harsh reaction conditions.[4-6] The condensation can also be performed with functionalised pyrroles allowing α and β functionality to be introduced. A common method to increase the stability of BODIPYs is to introduce alkyl groups at these positions preventing unwanted polymerisation or porphyrin formation reactions from occurring.

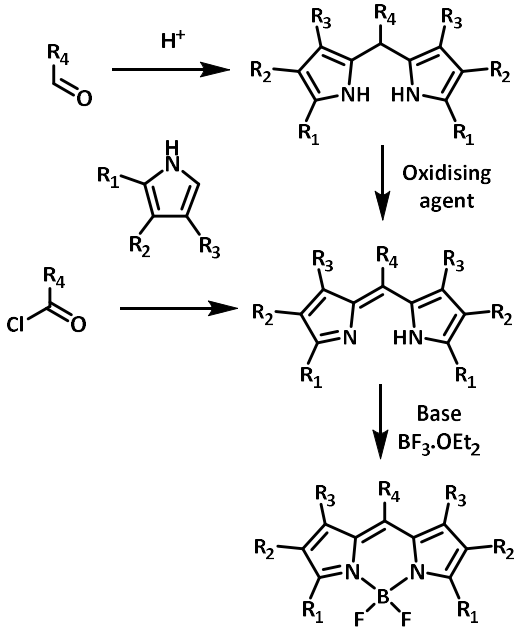

Figure 3.2. General synthesis of symmetric BODIPYs from aldehydes (top) and acid chlorides (bottom).

Asymmetric BODIPYs can by synthesised by the reaction of a carbonyl containing pyrrole with a pyrrole bearing no substitution at the 2-position, leading to the potential for BODIPYs with six different groups attached to the pyrrole units. Further modification of the BODIPY framework is possible by electrophilic[7] or nucleophilic[8] substitution, methyl-group activation,[9] cross coupling reactions[10] and the formation of aza-BODIPYs which bear an additional nitrogen atom replacing the methylene bridge.[11] The substitution of the fluorine atoms was first reported by Murase and co-workers when they used phenyl magnesium chloride to replace the fluorine atoms with aryl groups.[12] Since then various other aryl-[13] and ethynyl-substituted[14] BODIPYs have

been synthesised even leading to asymmetrically substitution at this position imparting chirality to the boron atom.[13] Substitution of the fluorine atoms has also been achieved *via* reactions with alkoxy- and aryloxy-groups catalysed by Lewis acids.[14, 15]

The intense research into the synthesis of BODIPYs is driven by their numerous desirable properties. BODIPYs tend to possess a sharp absorbance and fluorescence in the UV/vis range with high extinction coefficients ($\varepsilon > 50{,}000$ $mol^{-1}dm^3cm^{-1}$) and high fluorescence quantum yields accompanied by excellent photo- and chemostability.[16] The absorption and emission of BODIPYs can be extended into the near infrared (NIR) by the introduction of electron donating moieties,[17] increasing the rigidity of the structure[18] and extending the conjugation of the molecule.[19] Introduction of halogens onto the BODIPY core results in the 'heavy atom' effect allowing the molecule to access the triplet excited state.[20]

3.1.1.2. Applications of BODIPYs

The photo- and chemo-robustness, absorption and intense fluorescence in the UV/vis region and low toxicity of BODIPYs has resulted in the synthesis of many BODIPYs for use as fluorescent indicators.[21] There are currently numerous examples of this type of system for the detection of pH,[22] metal cations,[23, 24] anions[25] and, as discussed below, biomolecules. Glutathione is the most abundant cellular thiol and plays a crucial role in maintaining the redox status of biological systems.[26] However, abnormal levels can lead to cancer, ageing and heart problems.[27] The detection of glutathione in the body is therefore a highly worthwhile aim. There are several existing sensors that can preferentially detect glutathione and other cellular thiols, such as cysteine and homocysteine, from other biological amino acids although the detection of glutathione over these other thiols has proven difficult in living systems.[28] In 2012, Yang and co-

workers synthesised a BODIPY asymmetrically substituted with a chlorine atom.[29] In the presence of glutathione, cysteine or homocysteine the chlorine will undergo a halogen-thiol nucleophilic substitution resulting in a quenching of the fluorescence of the chloro-BODIPY at 556 nm and the appearance of a new band at 588 nm, Figure 3.3. Cysteine or homocysteine bound to the BODIPY will then undergo a further intramolecular displacement reaction between the amino groups and thiol group to result in an amino-substituted BODIPY, again resulting in a new fluorescence peak at 564 nm. This reaction does not occur in the glutathione bound BODIPY so the fluorescence profile remains the same indicating the presence of glutathione over cysteine and homocysteine. Tests of this BODIPY system were carried out *in vivo* confirming the BODIPY's cell permeability and capability for selective detection of glutathione.

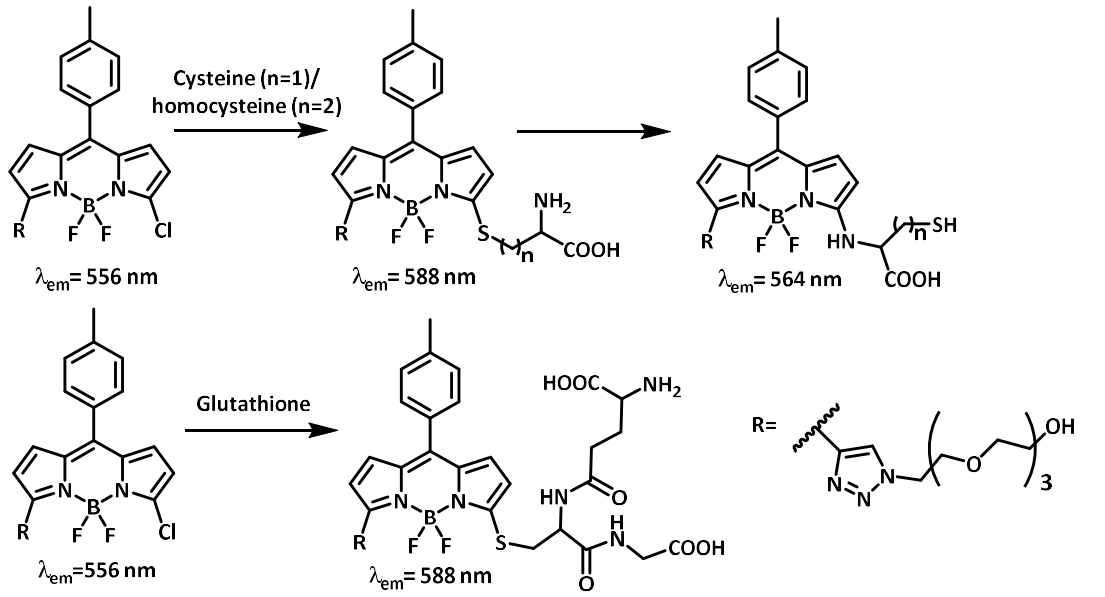

Figure 3.3. Reaction of the BODIPY sensor with cysteine or homocysteine (top) and glutathione (bottom).

Photodynamic therapy (PDT) is an emerging technique for the treatment of cancers which works by irradiating a photosensitising drug which can undergo intersystem crossing (ISC) to a triplet excited state.[30] This triplet excited state can react with ground

state triplet oxygen exciting it to singlet oxygen which is highly damaging to surrounding tissues. This effect is highly localised due to targeting of the radiation source and the short half-life of singlet oxygen. Although not currently approved for clinical use in PDT, the ability of halogenated BODIPYs to access the triplet excited state,[31] due to the 'heavy atom' effect, combined with their high extinction coefficients, low toxicity, good cellular uptake and synthetic versatility gives them excellent potential to be used as the photosensitiser in this technique in the future.[32] The addition of iodine at the 2- and 6-positions of the BODIPY core allows for the generation of singlet oxygen from triplet oxygen, however iodine atoms at the 3- and 5-positions surprisingly lowers the quantum yield of singlet oxygen generation, therefore, is detrimental to PDT.[33]

Akkaya and co-workers synthesised BODIPYs substituted at the boron centre with styryl-groups bearing pyrene which are able to bind non-covalently to single walled carbon nanotubes, Figure 3.4a.[34] Whilst this non-covalent interaction resulted in a small decrease in singlet oxygen quantum yield, nanotubes of this kind are known to be internalised by mammalian cells making a system with the potential for intercellular delivery of the PDT sensitiser. One potential side effect of PDT is the prolonged light sensitivity of the dyes. In an attempt to minimise this effect, O'Shea and co-workers synthesised an aza-BODIPY dye functionalised with a non-conjugated amine, Figure 3.4b.[35] When this amine is not protonated, any excitation of the BODIPY undergoes rapid relaxation due to photoinduced electron transfer (PET) shutting down any triplet excited state generation. The interstitial fluid surrounding tumours is slightly acidic, thus protonating the amine, stopping the PET and allowing singlet oxygen generation to occur making this BODIPY a therapeutically selective PDT photosensitiser.

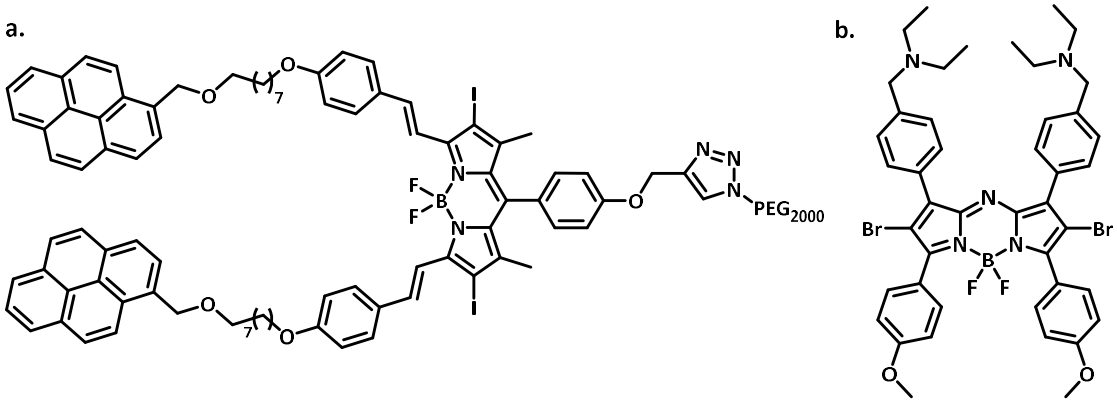

Figure 3.4. BODIPY based PDT sensitisers with ability to bind to carbon nanotubes for drug delivery (a) and turn on activity in a therapeutically selective environment (b).

When two or more different chromophores are covalently attached to one another, there is the potential for the formation of light harvesting cassettes where one chromophore, the 'donor', absorbs light at a specific wavelength then passes this energy on to another 'acceptor' chromophore from which this energy is emitted at a longer wavelength. This effect is commonly seen in nature during photosynthesis and has potential applications in solar energy production.[36] There are two main mechanisms for this energy transfer; through space or through bond. In through space light harvesting devices, the donor and acceptor chromophores are usually separated by alkyl-chains to remove any conjugation, energy transfer therefore relies upon fluorescence resonance energy transfer (FRET), due to spectral overlap between the donor emission and the acceptor absorbance, with the degree of energy transfer being dependant on the distance between these two moieties. In 2007, Qian and co-workers synthesised a three component energy transfer cassette containing three different BODIPYs synthesised *via* 'click' reactions, Figure 3.5.[37] Each of these BODIPYs possesses an absorbance at a different wavelength (red- 501 nm, green- 568 nm and purple- 647 nm, see Figure 3.5 for colours) giving the molecule a broad range of absorbance across the visible spectrum. Upon photoexcitation of either the red or green BODIPY only minimal fluorescence was observed from these two chromophores with a large fluorescence associated with the purple BODIPY observed. The quantum yields measured for excitation of the molecule

at all three absorption wavelengths showed very little variation compared to a model compound of the purple BODIPY, suggesting almost complete energy transfer from donor to acceptor.

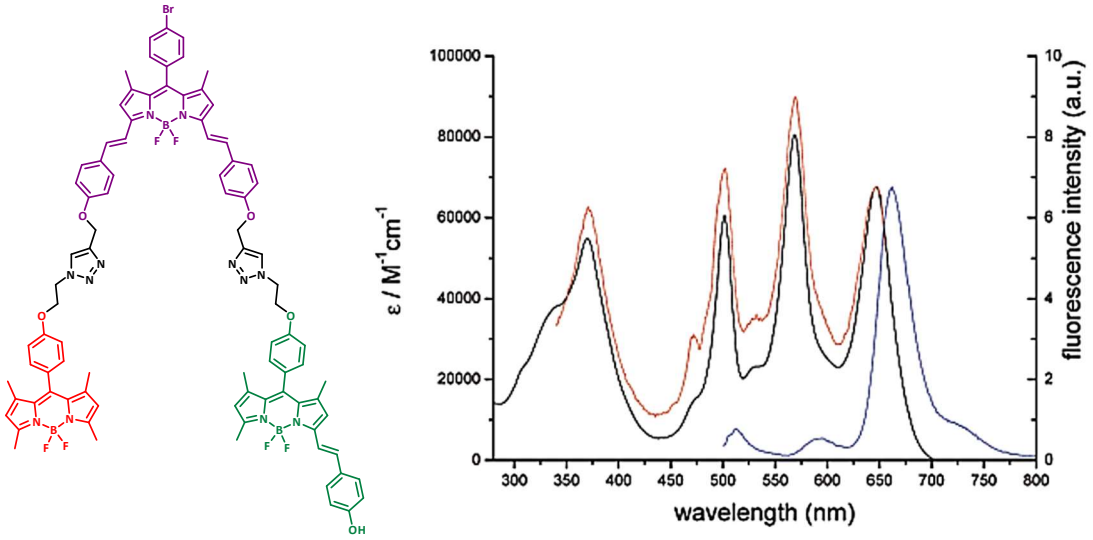

Figure 3.5. Structure of light harvesting cassette containing three different BODIPY chromophores (left) and absorption (black), emission (blue) and excitation (red) spectra of the BODIPY cassette (right).[37]

Through-bond cassettes are created when the chromophores are attached *via* conjugated linkers. The energy transfer in these systems is affected by steric interactions between the donor and acceptor causing torsional constraints reducing rate and efficiency of energy transfer, the nature of the HOMOs and LUMOs, the site of attachment and the nature of the linker.[38] Lindsey and co-workers synthesised linear molecular photonic wires consisting of a BODIPY donor covalently connected to a free base porphyrin *via* a zinc metallated porphyrin 'wire', Figure 3.6.[39] Upon excitation of the donor energy, transfer of 76 % efficiency occurs leading to emittance from the free base porphyrin despite a 90 Å separation between donor and acceptor. Lindsey and co-workers calculated that if this energy transfer was through space, the transfer efficiency would only be 6 %, proving the transfer is indeed through bond. These systems were further modified by the addition of an 'on/off' gate in the form of a porphyrin metallated with magnesium.[40] When the magnesium is in its oxidised state, fluorescence is quenched

via intramolecular charge transfer (ICT), however, when reduced the gate is turned on and the free base porphyrin fluoresces following energy transfer of 80 % efficiency.

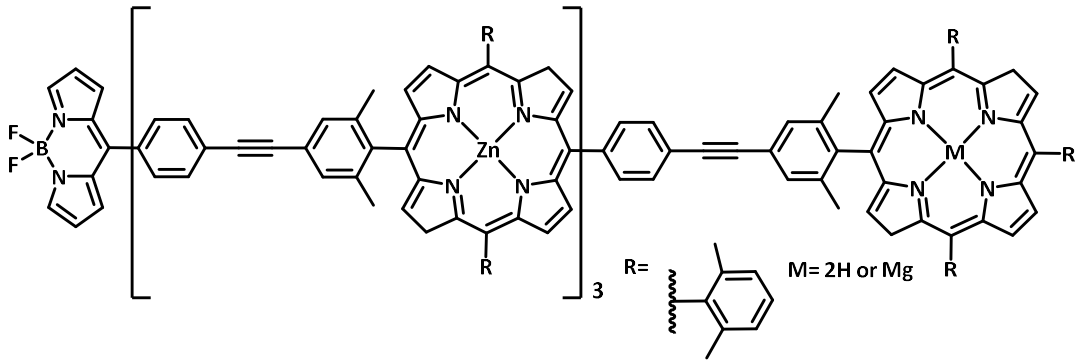

Figure 3.6. Structure of BODIPY-porphyrin molecular photonic wire.

3.1.2. Perylene Diimide-BODIPY Systems

At the outset of the studies described in this Chapter (2014), there were only two examples in the literature of systems composed of covalently bound BODIPYs and perylene diimides (PDIs), both synthesised by Akkaya and co-workers.[41, 42] The first of these two systems consisted of a PDI tetra-substituted at the bay position with BODIPY connected by long, non-conjugated, chains synthesised *via* 'click' chemistry.[41] UV/vis spectroscopic studies on this compound revealed an absorption spectrum with a peak maximum at 526 nm, with a very large extinction coefficient of 240,000 $mol^{-1}dm^3cm^{-1}$, corresponding to the four BODIPYs and a smaller peak at 588 nm, with an extinction coefficient of 45,000 $mol^{-1}dm^3cm^{-1}$, corresponding to the PDI. Upon excitation at 526 nm, no BODIPY fluorescence is observed due to FRET from the BODIPY donor to the PDI acceptor. The PDI possess a fluorescence peak at 618 nm and, upon excitation of the molecule at 526 nm, this peak is seen to increase in intensity 3.5 fold *vs*. excitation at 588 nm (removing the BODIPY contribution) demonstrating that this system is a highly efficient light harvester over a wide range of the visible spectrum.

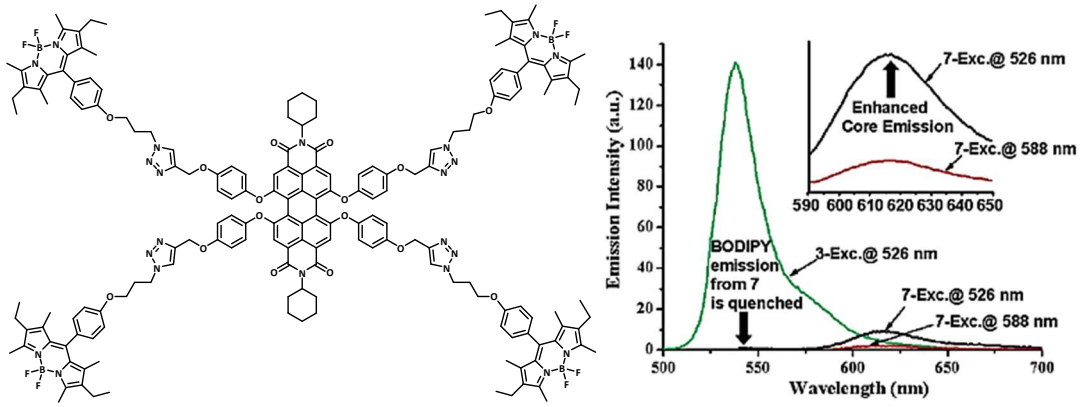

Figure 3.7. Structure of the first of Akkaya's light harvesting PDI-BODIPY systems (left) and the fluorescence spectra demonstrating the efficient energy transfer (right).[41] Green line- BODIPY model emission, red line- emission of PDI model, black line- emission of PDI-BODIPY system of an optically matched solution.

The second system synthesised in this series is similar to the first. However, there is a branch in the chain between each BODIPY and the PDI core allowing eight rather than four BODIPYs to be attached.[42] An increase in the length of the chain is also necessary due to the greater complexity of the synthesis. This system displayed an increase in extinction coefficient of 60 %, rather than the expected 2 fold increase, suggesting interchromophoric interactions between the BODIPYs. The emission spectrum again showed quenching of the BODIPY fluorescence. However, this quenching was not as complete as in the previous example, suggesting less efficient energy transfer, most likely due the larger distance between the PDI and BODIPY chromophores. The PDI fluorescence was enhanced 4-fold, only a modest increase *vs*. the four BODIPY system, again suggesting a reduction in the efficiency of the energy transfer. Energy transfer rates were calculated for the four and eight BODIPY systems giving values of 1.77 x 10^{10} and 6.77 x 10^{9} s^{-1}, respectively. These results indicate that whilst doubling the number of donor chromophores improves the antenna effect of the system the increase is only modest due to the larger distance between the PDI and the BODIPYs.

In 2015, Elmali and co-workers published the first examples of BODIPYs connected to a PDI centre *via* an aryl linker, Figure 3.8.[43] A bay functionalised PDI-BODIPY dyad and triad were synthesised with methyl-groups substituted at the 1-,3-,5- and 7-positions of the BODIPY and iodine at the 2- and 6-positions. Interestingly the PDI 1,6- and 1,7- isomers, formed during the bromination reaction, were not separated despite the different isomers having the potential to possess different properties.[44-46] Upon excitation of the BODIPY, quenching of the BODIPY emission was observed with the remaining emission assigned to the PDI, suggesting FRET to the PDI is occurring. However, when the fluorescence intensity of this emission is compared to that of a reference PDI the quantum yield is seen to drastically decrease indicating that, following FRET, PET occurs resulting in a charge separated state and quenching of the fluorescence. The presence of the iodine atoms on the BODIPY allows ISC resulting in the formation of a triplet excited state, as demonstrated by the production of singlet oxygen. The triplet state is generated on the BODIPY chromophore then undergoes intramolecular triplet-triplet energy transfer (TTET) to form the PDI triplet excited state with a long lived lifetime of 150 μs, confirmed by nanosecond transient absorption spectroscopy. This lifetime is considerably longer than that of PDIs covalently bound to Pt[47] or Ir[48] atoms, that allow access to the triplet excited state by the 'heavy atom' effect, as the effect also increases the rate of the spin forbidden T_1-S_0 relaxation thus decreasing the excited state lifetime. Cyclic voltammetry was used to probe the electrochemical properties of the systems revealing three reductions, two located on the PDI core with the third located on the BODIPY at a more negative potential, and an oxidation lying on the BODIPY. The combination of these techniques allowed the production of a Jablonski diagram displaying all of the competing processes present in

these systems, Figure 3.8. Following excitation the BODIPY acts as both a singlet energy donor and a spin converter whilst the PDI is a singlet/triplet energy acceptor.

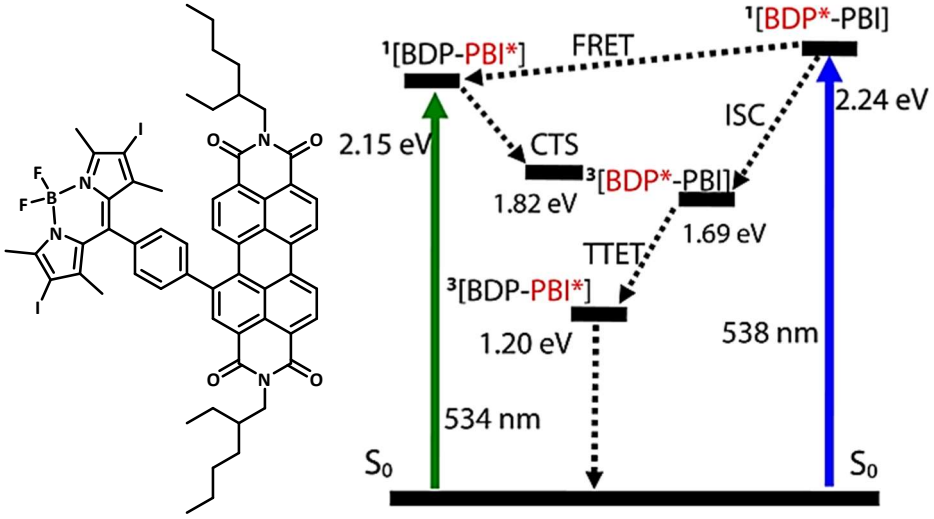

Figure 3.8. Structure of PDI-BODIPY dyad (left) and Jablonski diagram for the system (right).[43]

3.1.3. Aims and Objectives

The results reported in this Chapter describe the synthesis of a series of PDI-BODIPY systems. A dyad and triad consisting of a bay substituted PDI functionalised with an unsubstituted BODIPY were synthesised along with an ortho-substituted PDI-BODIPY pentad. The series was further extended by the synthesis of a dyad and triad bearing methyl-BODIPYs in an attempt to stabilise the electrochemical reductions of the BODIPY moieties and further manipulate the electrochemistry. Additional functionality was introduced to boron centres of the unsubstituted PDI-BODIPY dyad and triad by substituting the fluorine atoms with di(tert-butyl) catecholate groups with the intention of incorporating an additional oxidation process, isolated form the PDI and BODIPY part of the molecule by a node at the boron atom, in the hope of inducing charge separated states following PET.

The optical and electrochemical properties of these molecules were probed *via* UV/vis spectroscopy, fluorescence spectroscopy, cyclic voltammetry, density functional theory and spectroelectrochemistry. These measurements were used to investigate the nature of any energy or charge transfer occurring, the location of the redox processes in the molecules and the absorption behaviour of the molecules upon oxidation and reduction.

3.2. Results and Discussion

3.2.1. Synthesis

3.2.1.1. Perylene Diimide-BODIPYs

The synthesis of the PDI-BODIPY triad **3.4** was achieved in five steps from the PDA starting material, Scheme 3.1. Previously, the synthesis of PDI-BODIPY systems has involved the synthesis of the PDI and BODIPY units separately then utilised 'click' chemistry or Suzuki cross coupling reactions to join the constituent parts together.[42, 43] In this study, the BODIPY is synthesised *in situ* on the PDI core.

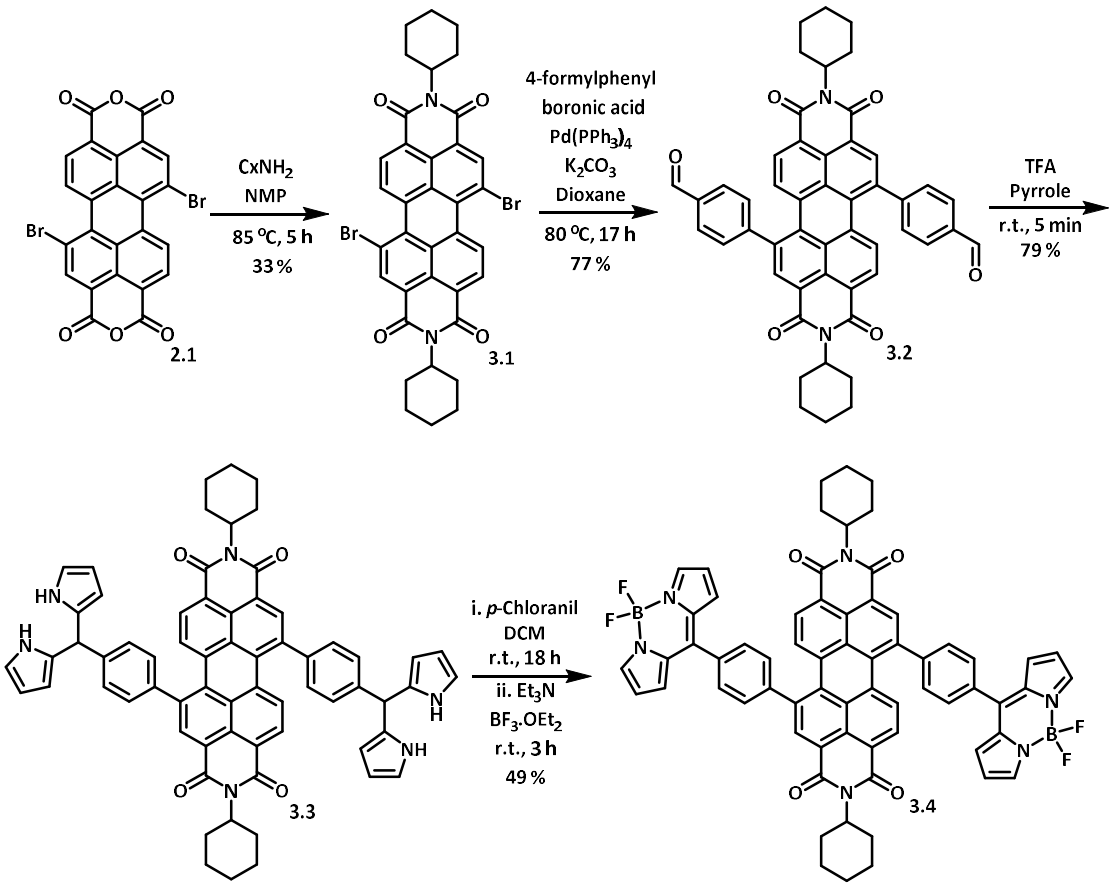

Scheme 3.1. Synthesis of the PDI-BODIPY triad **3.4** from **2.1**.

The synthesis of **2.1** is discussed in Chapter 2. As discussed in Chapter 1, the separation of the 1,6- and 1,7- isomers of bay substituted PDIs is a recurring problem. In some cases (as in Chapter 2), the isomers are fortuitously separable by column chromatography. However, in most cases this is not possible and therefore separation must be achieved by other means. To that end **2.1**, was reacted with cyclohexyl amine in *N*-methyl-2-pyrrolidone (NMP) to give **3.1** as a mixture of mono-, di- and tri-bromo PDI with both di-substituted isomers present. The mono- and tri-bromo adducts could be separated by column chromatography leaving a mixture of the 1,6- and 1,7-dibromo PDI. The 1,7- isomer was then purified by a series of layered recrystallisations between the target compound in chloroform with methanol as the antisolvent.[49] With each recrystallisation, the proportion of 1,6- isomer was reduced until, after five recrystallisations, regioisomerically pure 1,7-**3.1** was isolated in a 33 % yield, Figure 3.9. Small amounts of 1,6- isomer are difficult to differentiate from the 1,7- isomer in chloroform-d, even in high field NMR, however benzene-d_6 was found to induce a change in the chemical shift of the isomers, separating them from one another, proving the pure product was obtained.

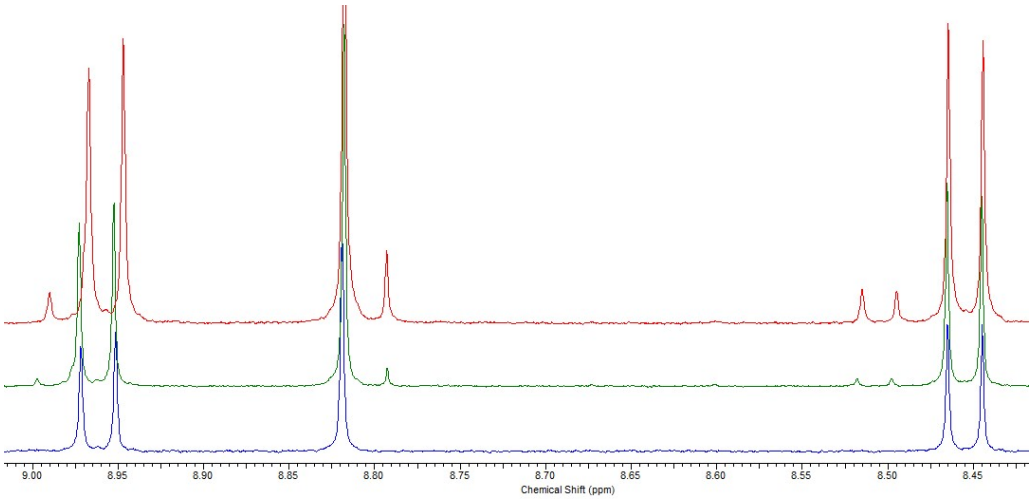

Figure 3.9. ^{1}H NMR spectra (in C_6D_6) of the aromatic region of **3.1** showing the removal of the 1,6-isomer by repeated recrystallisations. Red- after 1 recrystallisation, green- after 3 recrystallisations, blue- after 5 recrystallisations.

Crystals of **3.1** of suitable quality for analysis by single crystal X-ray diffraction were grown by slow diffusion of methanol into a solution of the compound in chloroform. A single crystal structure of *N*,*N*′-bis(cyclohexyl)-1,7-dibromo-PDI has been reported previously[49] as a dichloromethane (DCM) solvate, and the structure obtained was very similar in most respects to the structure obtained here. However, in this case the compound crystallises in an alternative space group, $P2_1/c$, as opposed to $P\bar{1}$, and is not a solvate, Figure 3.10. As a result, an alternative packing arrangement of pairs of **3.1** is observed but in all other respects the bond lengths, angles and twisting of the perylene are similar in the two structures. The structure is reported here mainly as confirmation that the isomer isolated is indeed the in the 1,7-arrangement.

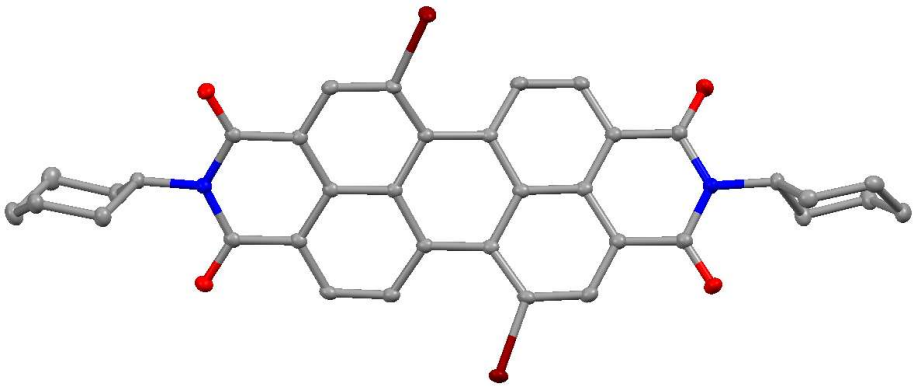

Figure 3.10. View of the X-ray crystal structure of **3.1** displaying the 1,7-arrangement of the bromine atoms. Grey- carbon, blue- nitrogen, red- oxygen, brown- bromine. H-atoms removed for clarity. Ellipsoids drawn at 50 % probability.

3.1 was reacted with 4-formylphenyl boronic acid *via* a Suzuki cross coupling to give **3.2** as a highly fluorescent bright pink solid and solution. The di(benzaldehyde)-PDI was then reacted with pyrrole, as a reagent and solvent, with trifluoroacetic acid (TFA) as a catalyst to form the di(dipyrromethane)-PDI **3.3** in a 79 % yield. The final step in the synthesis of **3.4** combines two processes; first the oxidation of the dipyrromethane group to a dipyrromethene group followed by complexation with $BF_3.OEt_2$. The most common oxidising agent selected for these reactions is 2,3-dichloro-5,6-

dicyanobenzoquinone (DDQ). However, in this case DDQ gave very low yields so a milder alternative, *p*-chloranil was used instead. The yield could be further improved by stopping the reaction following the oxidation with *p*-chloranil after 18 hours, working up the reaction mixture and removing any unreacted starting materials and decomposition products by column chromatography, before redissolving in DCM and adding the triethylamine and $BF_3.OEt_2$ to give **3.4** in a yield of 49 %.

Single crystals of **3.4** were grown by layered diffusion between a chloroform solution of the target compound and methanol. X-ray structural determination revealed the conformational arrangement of the molecule in the solid state showing the molecules stack in pairs with slightly offset stacking between the perylene cores, Figure 3.11. The BODIPY moieties are sterically pushed away from one another, enabled by the twist in the perylene core, and are themselves twisted nearly perpendicular to the PDI. No examples of crystal structures of PDI-BODIPY systems have been reported previously.

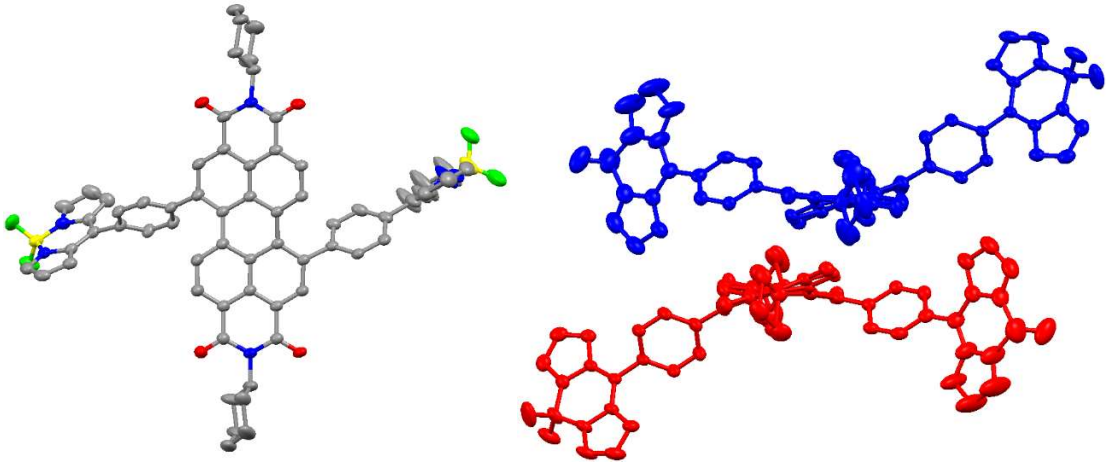

Figure 3.11. Left- view of the single crystal structure of **3.4**. Grey- carbon, blue- nitrogen, red- oxygen, yellow- boron, green- fluorine. Right- View down the N-N axis of the PDI displaying packing of two molecules of **3.4** showing the BODIPY moieties pushed away from one another. H-atoms removed for clarity. Ellipsoids drawn at 50 % probability.

The synthesis of the asymmetrically substituted PDI-BODIPY dyad **3.8** was achieved by a similar route to **3.4**, in six steps from the PDA starting material, Scheme 3.2.

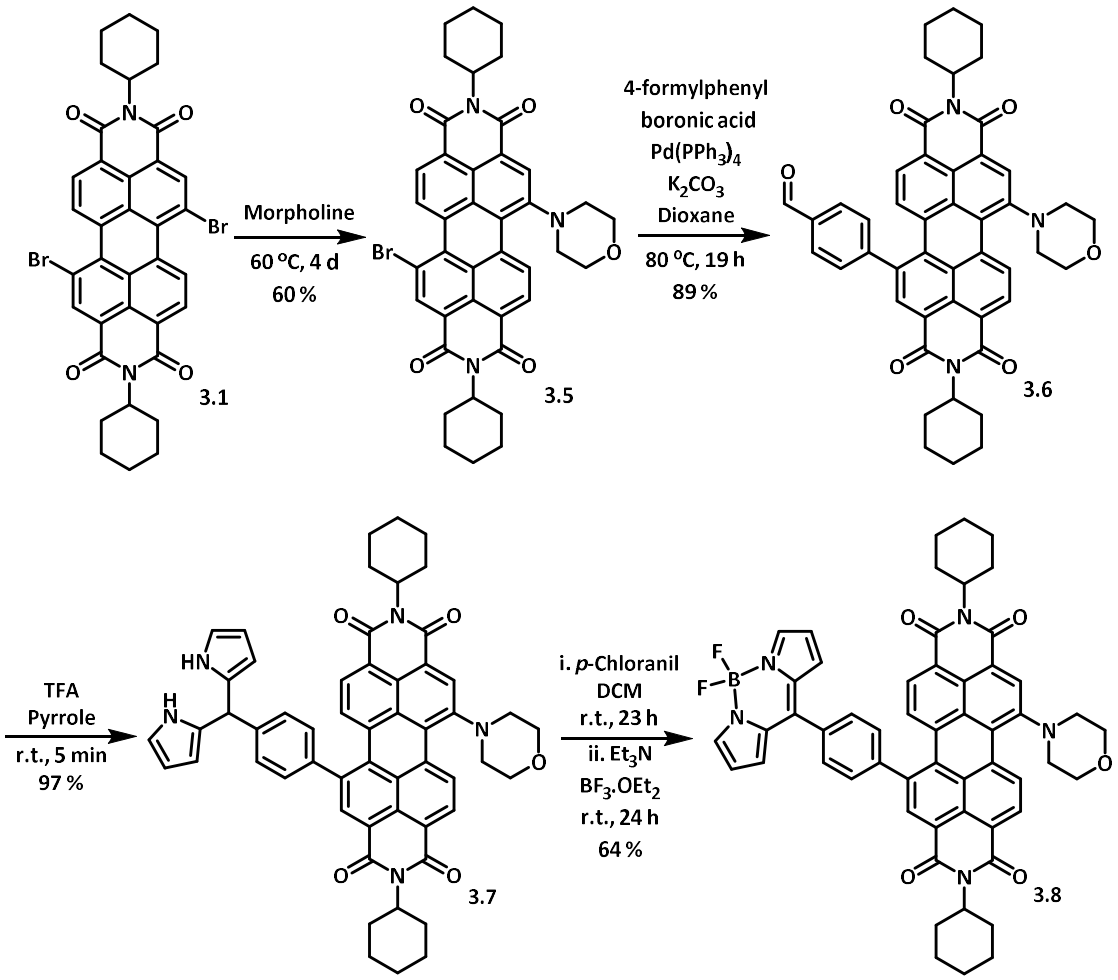

Scheme 3.2. Synthesis of the asymmetrically substituted PDI-BODIPY dyad **3.8** from **3.1**.

The synthesis of **3.5** was fortuitously achieved whilst attempting to synthesise the dimorpholino-substituted equivalent. After four days reacting **3.1** in morpholine as a reagent and solvent (the same conditions used to synthesise the n-butyl analogue **2.3**), the reaction had not proceeded to completion giving the main product of the reaction as the mono-substituted **3.5** in a yield of 60 %. This was found to be reliably reproducible. **3.5** then underwent a Suzuki cross coupling with 4-formylphenyl boronic acid to give **3.6**. Reaction with pyrrole gave **3.7** in a 97 % yield followed by oxidation with *p*-chloranil and complexation with $BF_3.OEt_2$ to give **3.8** in a 64 % yield.

Single crystals of **3.8** were grown by layered diffusion between a chloroform solution of the target compound and methanol. X-ray structural determination revealed the conformational arrangement of the molecule in the solid state showing a twisting of the perylene core with the BODIPY lying just out of plane with the PDI, Figure 3.12. The molecule stacks in pairs with the bulky BODIPY moieties positioning themselves as far away from one another as possible.

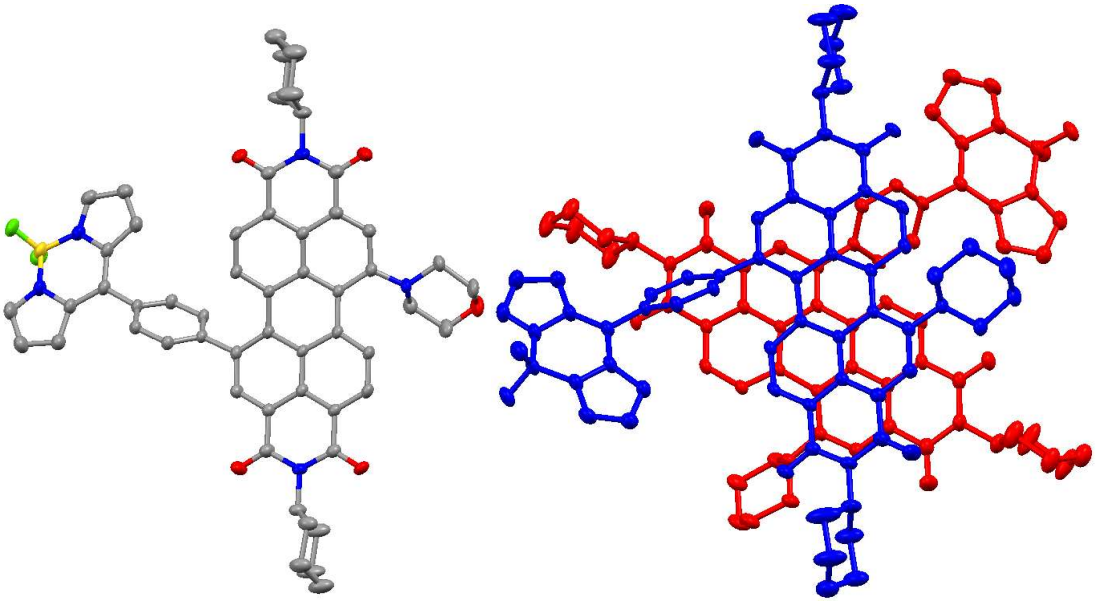

Figure 3.12. Left- view of the single crystal structure of **3.8**. Grey- carbon, blue- nitrogen, red- oxygen, yellow- boron, green- fluorine. Right- Packing of two molecules of **3.8** with BODIPY moieties pointing in opposite directions. H-atoms removed for clarity. Ellipsoids drawn at 50 % probability.

The synthesis of the ortho-substituted PDI-BODIPY pentad **3.13** was not attempted by the *in situ* route used previously as the four reaction sites for each step were predicted to severely complicate the purification of the compounds and reduce the yield. Instead, the tetra-pinacolato boron (BPin) PDI **3.12**, Scheme 3.4, and the bromo BODIPY **3.10**, Scheme 3.3, were synthesised separately then coupled.

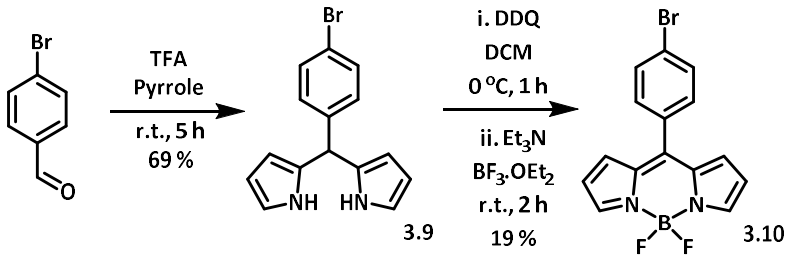

Scheme 3.3. Synthesis of the bromo BODIPY **3.10** for Suzuki cross coupling with **3.12**.

The synthesis of **3.10** was achieved in two steps from the commercially available 4-bromobenzaldehyde by reacting with pyrrole to give **3.9** then DDQ and $BF_3.OEt_2$ to give the target compound in a 19 % yield. The low yield of the final step has been attributed to the decomposition of the $BF_3.OEt_2$ reagent before the reaction. The reaction was not repeated, in order to improve the yield, as sufficient material for the next step was acquired from this reaction.

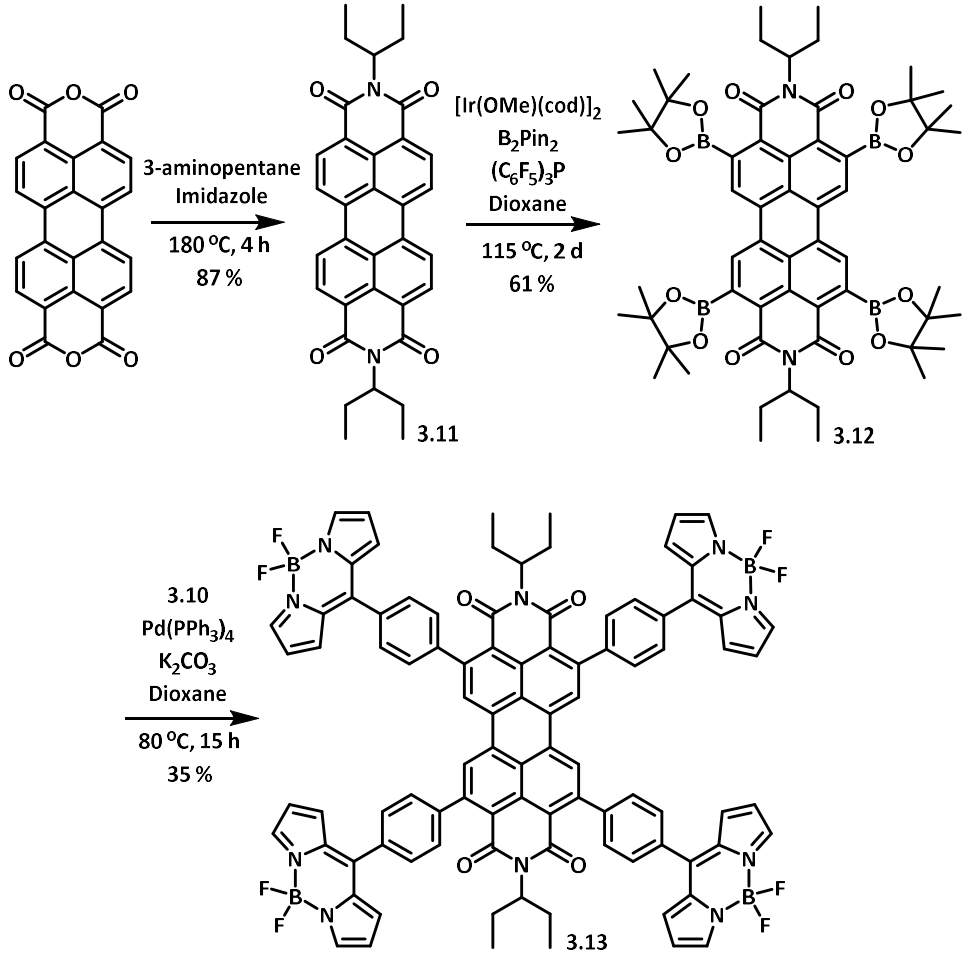

Scheme 3.4. Synthesis of the PDI-BODIPY pentad **3.13** from PDA.

The first step in the synthesis of **3.13** involved the imidization of PDA with 3-aminopentane to give **3.11**. 3-Aminopentane was chosen as, despite being relatively small, it imparts good solubility on PDIs and has more potential for crystallisation than larger groups. The first catalyst used in the reaction of **3.11** with B_2Pin_2 was the Murai catalyst ($RuH_2(CO)(PPh_3)_3$) used by Müllen and co-workers[50] in their synthesis of this molecule. Some tetra-substituted product was formed however there was still large amounts of partially reacted side products remaining. The alternative $[Ir(OMe)(cod)]_2$ catalyst used by Shinokubo and co-workers[51] was then attempted. This catalyst gave a much higher conversion to tetra-substituted product, however, there was still a small amount of the mono-, di- and tri-substituted products remaining. Many different approaches were then used to try to purify **3.12** including column chromatography, recrystallisation, washing with different solvents *etc*. although it was not found to be possible to fully isolate **3.12**. This difficulty in purification may explain that whilst the two papers reporting the synthesis were published five years ago and have been cited around forty times each, there has not been a single paper published reproducing these results to synthesise new, more complex, ortho-substituted PDIs. **3.12** was therefore not isolated before the subsequent Suzuki coupling to **3.10** to give **3.13** in a yield of 35 %.

3.2.1.2. Perylene Diimide-MethylBODIPYs

The *in situ* approach was also applied to the synthesis of **3.18** and was successful. However, the best yields achieved for the dipyrromethane and BODIPY formation steps were found to be 25 % and 16 % respectively, leading to very small amounts of product. Therefore, a different approach was used where the two substituents were synthesised separately and then coupled together, similar to **3.13**, Scheme 3.5 and Scheme 3.6.

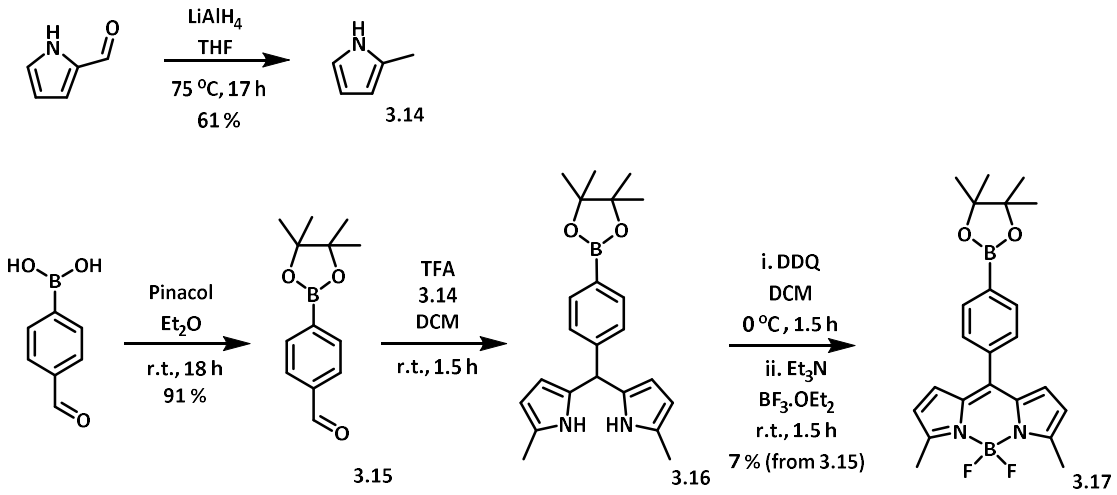

Scheme 3.5. Synthesis of **3.14** from pyrrole-2-carboxaldehyde (top) and **3.17** from 4-formylphenyl boronic acid (bottom).

The first step in the synthesis was the reduction of pyrrole-2-carboxaldehyde with $LiAlH_4$ to **3.14**. 4-Formylphenyl boronic acid was then protected by the reaction with pinacol to give **3.15** which was subsequently reacted with **3.14** and a TFA catalyst in DCM to give **3.16**. At this stage, purification of **3.16** was attempted. However, it decomposed rapidly on silica during column chromatography thus in subsequent attempts **3.16** was used in the next step without further purification. Crude **3.16** was oxidised with DDQ then coordinated to $BF_3.OEt_2$ to give **3.17** in a disappointing 7 % yield from **3.15**.

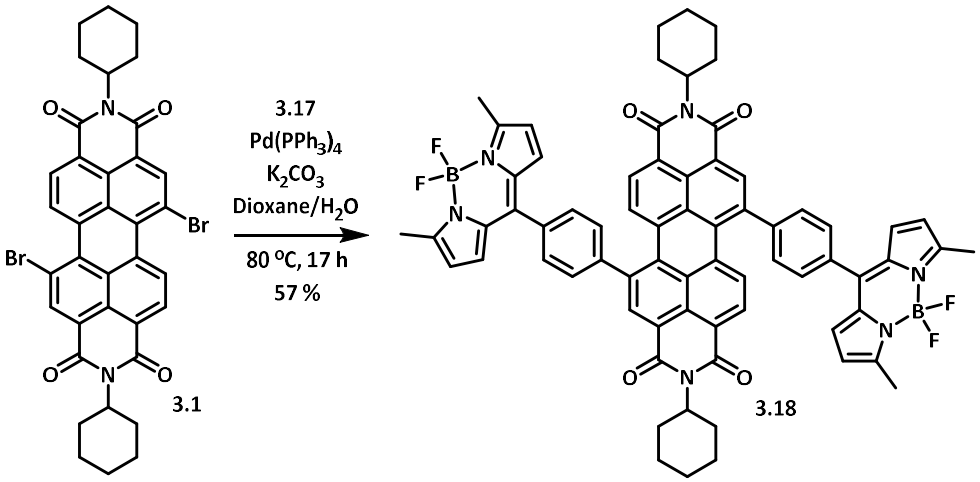

Scheme 3.6. Suzuki cross coupling of **3.1** with **3.17** to give PDI-MethylBODIPY triad **3.18**.

3.18 was then synthesised *via* a Suzuki cross coupling between **3.1** and **3.17**, Scheme 3.6. Toluene/ethanol/water was the first solvent system attempted, however, this resulted in only partial substitution and generation of other side products making purification very difficult. Dioxane/water resulted in much higher conversion and a cleaner reaction allowing **3.18** to be isolated in a 57 % yield.

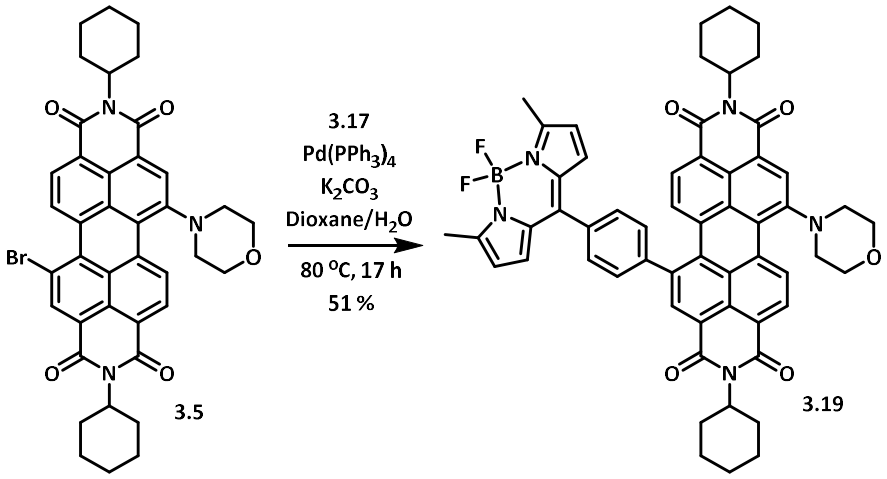

Scheme 3.7. Suzuki cross coupling of **3.5** with **3.17** to give the PDI-MethylBODIPY dyad **3.19**.

The asymmetrically substituted PDI-MethylBODIPY dyad **3.19** was synthesised using the same conditions as for **3.18** to give **3.19** in a 51 % yield, Scheme 3.7.

Single crystals of **3.19** were grown by layered diffusion between a chloroform solution of the target compound and methanol. X-ray structural determination revealed the conformational arrangement of the molecule in the solid state showing **3.19** stacks in pairs of molecules, Figure 3.13. Unlike **3.8**, the BODIPY moieties are on the same side in the pair, however, the twist in the perylene core allows the BODIPYs to be pushed some distance away from one another. The BODIPYs also lie more in plane with the perylene core than in the case of **3.19**. There is apparent π–π stacking interaction between one BODIPY in each pair of molecules and a perylene core in the adjacent pair (and *vice versa*) with an approximate stacking distance of 3.5 Å (measured between a

plane on a naphthalene ring on the PDI and a centroid on one of the BODIPY pyrrole rings).

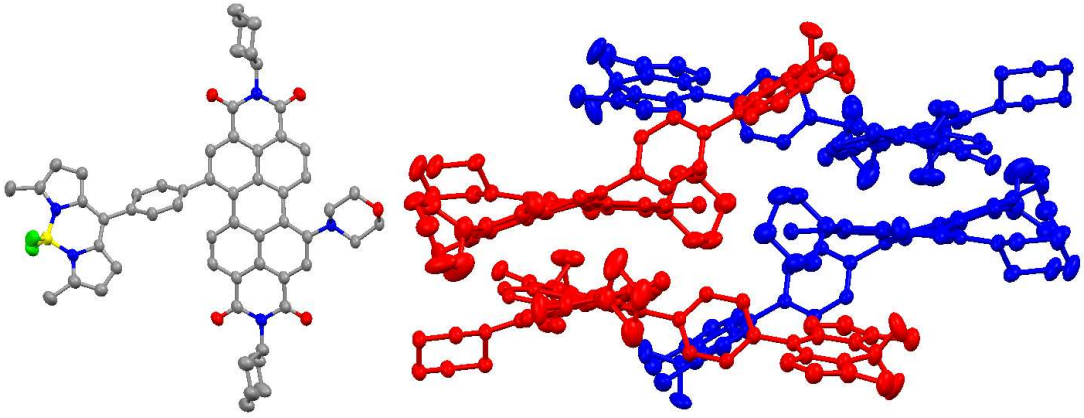

Figure 3.13. Left- view of the single crystal structure of **3.19**. Grey- carbon, blue- nitrogen, red- oxygen, yellow- boron, green- fluorine. Right- Packing of four molecules of **3.19** showing π-stacking between pairs of molecules and the interaction between two pairs. H-atoms removed for clarity. Ellipsoids drawn at 50 % probability.

3.2.1.3. Perylene Diimide-CatecholateBODIPYs

The final two PDI-BODIPYs synthesised were the PDI-CatecholateBODIPY dyad and triad **3.20** and **3.21**. Aluminium trichloride was employed as a Lewis acid to activate the boron-fluorine bonds in **3.4** then 3,5-di(tertbutyl)catechol was added to perform the substitution to **3.20** in a yield of 54 %, Scheme 3.8. **3.21** was synthesised in a 55 % yield from **3.8**, by the same method as **3.20**, with aluminium chloride and 3,5-di(tertbutyl)catechol, Scheme 3.9. ^{11}B NMR was a useful tool in the characterisation of the catecholate substituted BODIPYs; the ^{11}B NMR spectrum of **3.4** displays a triplet due to the coupling between the boron and the two spin ½ fluorine atoms. In **3.20**, this coupling is removed resulting in a singlet in the spectrum confirming the fluorine atoms have been substituted by the catecholate.

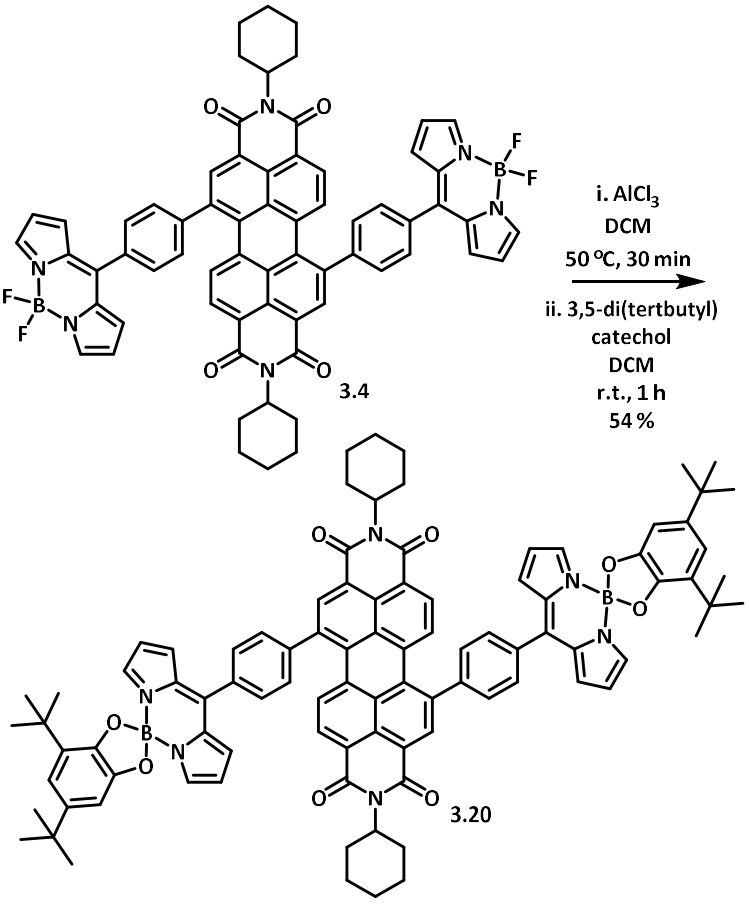

Scheme 3.8. Conversion of **3.4** to PDI-CatecholateBODIPY triad **3.20**.

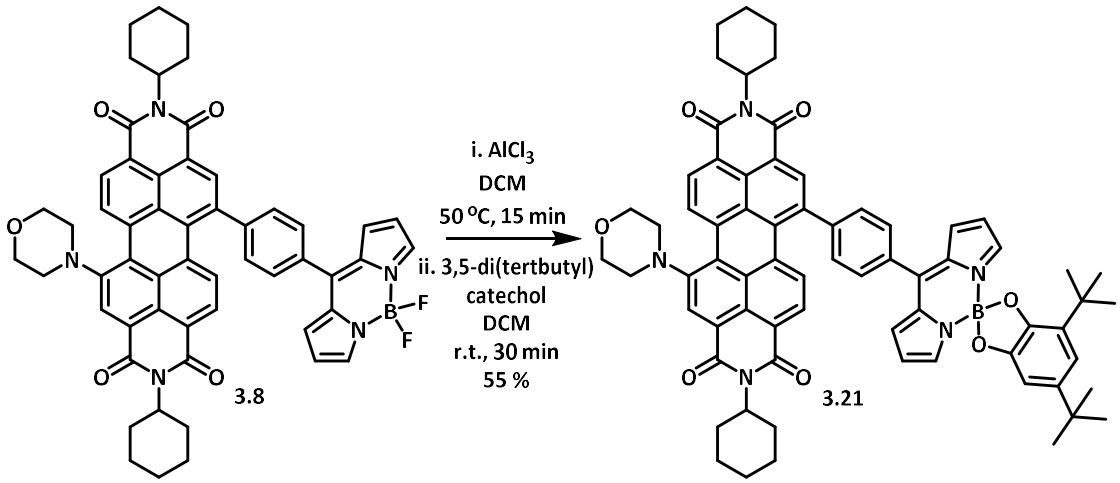

Scheme 3.9. Conversion of **3.8** to PDI-CatecholateBODIPY dyad **3.21**.

3.2.2. Optical and Electrochemical Investigation of Perylene Diimide-BODIPYs

3.2.2.1. Perylene Diimide-BODIPYs

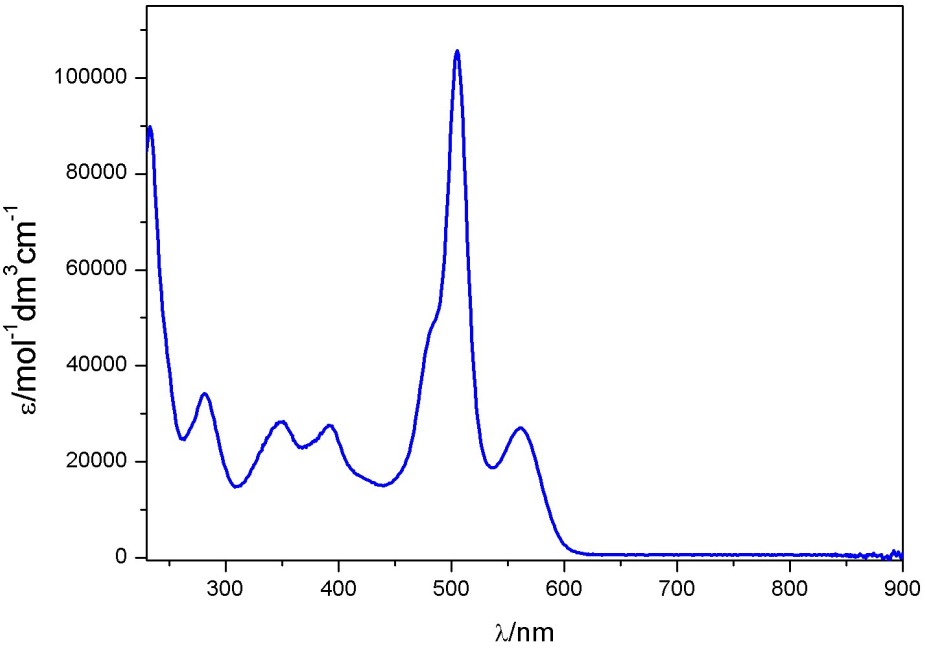

Figure 3.14. UV/vis absorption spectrum of **3.4** in DCM. c = 1.00 x 10^{-5} $mol^{-1}dm^3cm^{-1}$.

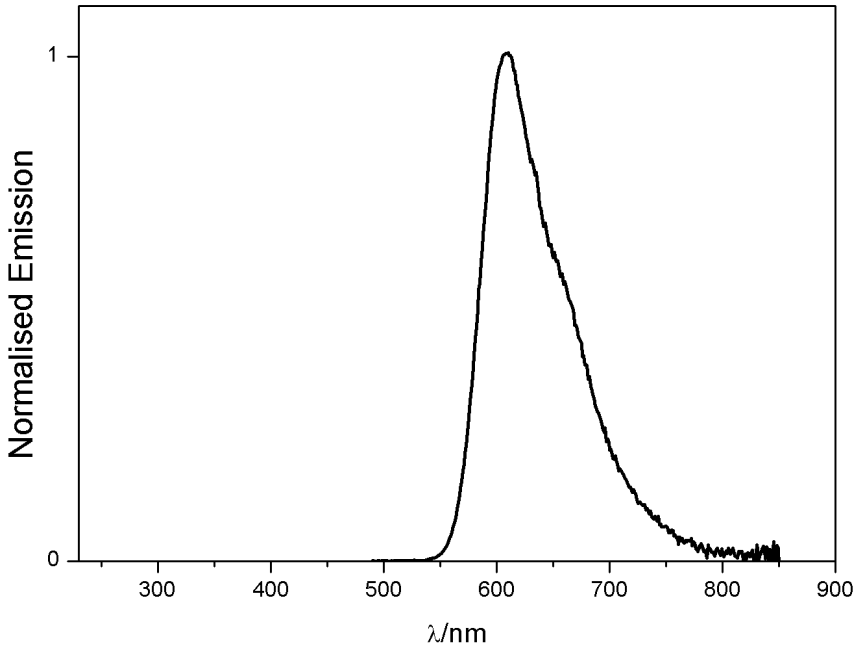

Figure 3.15. Emission spectrum of **3.4** in DCM. Emission recorded following excitation at 480 nm. c = 3.69 x 10^{-8} $mol^{-1}dm^3cm^{-1}$.

The UV/vis spectrum of the dyad **3.4** contains a peak at 505 nm with an extinction coefficient of 106,000 $mol^{-1}dm^3cm^{-1}$, corresponding to the two BODIPY moieties, and a much smaller peak at 562 nm from the PDI with an extinction coefficient of 27,000 $mol^{-1}dm^3cm^{-1}$, Figure 3.14 and Table 3.1. Unlike in the previous PDI-BODIPY system published by Elmali,[43] the PDI and BODIPY absorptions are not completely overlapping making characterisation of the redox process by spectroelectrochemical methods easier. Excitation of the BODIPY chromophore, by irradiation at 480 nm, leads to an emission spectrum containing a single peak at 610 nm, Figure 3.15. This emission is assigned to fluorescence from the PDI[52] rather than the BODIPY[53] suggesting that, upon excitation of the BODIPY, FRET is occurring due to spectral overlap between the BODIPY emission and the PDI absorption leading to emission solely from the PDI. The quantum yield of the emission was calculated as 0.91 suggesting efficient energy transfer to the PDI and that there are no other processes in competition with FRET. The energy transfer results in a Stokes shift of 105 nm *vs*. the BODIPY.

The peak corresponding to the BODIPY in the UV/vis spectrum of **3.8** is at 505 nm, the same as **3.4**, showing that a change in the PDI chromophore has had minimal effect on the BODIPY absorption, Figure 3.16. The extinction coefficient has approximately halved to 50,000 $mol^{-1}dm^3cm^{-1}$ as expected due to only having one BODIPY moiety in the system. The peak corresponding to the PDI has undergone a bathochromic shift of 52 nm to 616 nm, attributable to the electron donating effect of the morpholine, further separating the BODIPY and PDI absorbances. Similarly to the emission of **3.4**, the emission spectrum upon excitation of the BODIPY in **3.8** results in one peak at 741 nm, related to the PDI[54] moiety, again indicating that FRET is occurring, Figure 3.17. In this case, the increased wavelength of emission of the morpholino-substituted PDI

results in a considerable Stokes shift of 236 nm *vs*. the BODIPY with the tail of the emission extending well into the NIR. The fluorescence quantum yield was measured to be 0.05; much lower than **3.4**. This suggests that, following FRET, a PET process is occurring resulting in a $PDI^{\bullet-}$-$BODIPY^{\bullet+}$ charge separated state as seen in Elmali's PDI-BODIPY systems[43] and in an oligothienylenevinylene-fullerene system synthesised by Janssen and co-workers.[55] Transient absorbance measurements are required to fully confirm that these processes are indeed occurring. This PET effect was not observed in **3.4** most likely due to the increased conjugation between the PDI and the BODIPYs, as shown by the communication between the BODIPY moieties in the cyclic voltammetry (see below), removing the capability for charge separation.

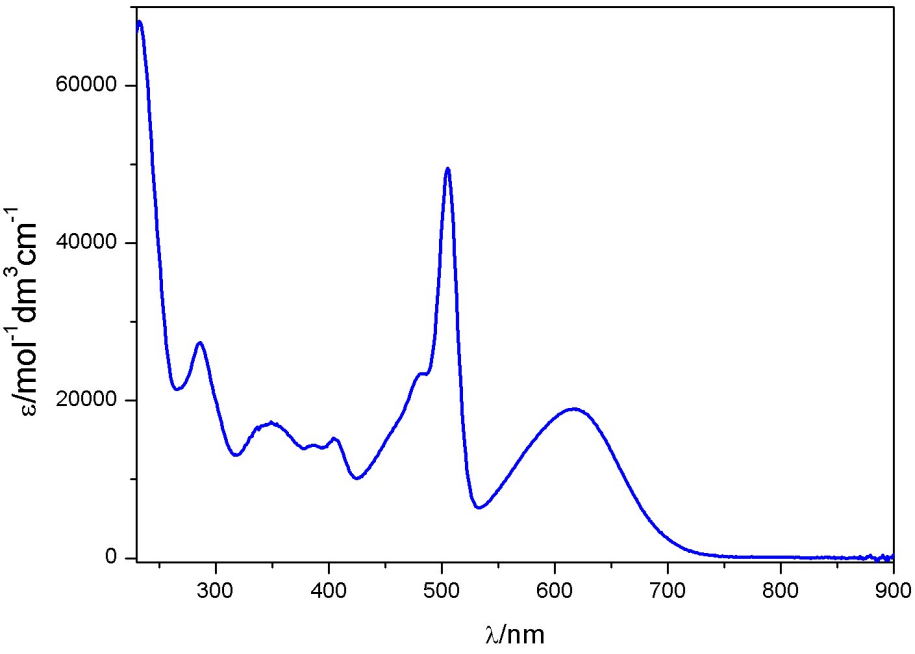

Figure 3.16. UV/vis absorption spectrum of **3.8** in DCM. c = 1.71 x 10^{-5} $mol^{-1}dm^3cm^{-1}$.

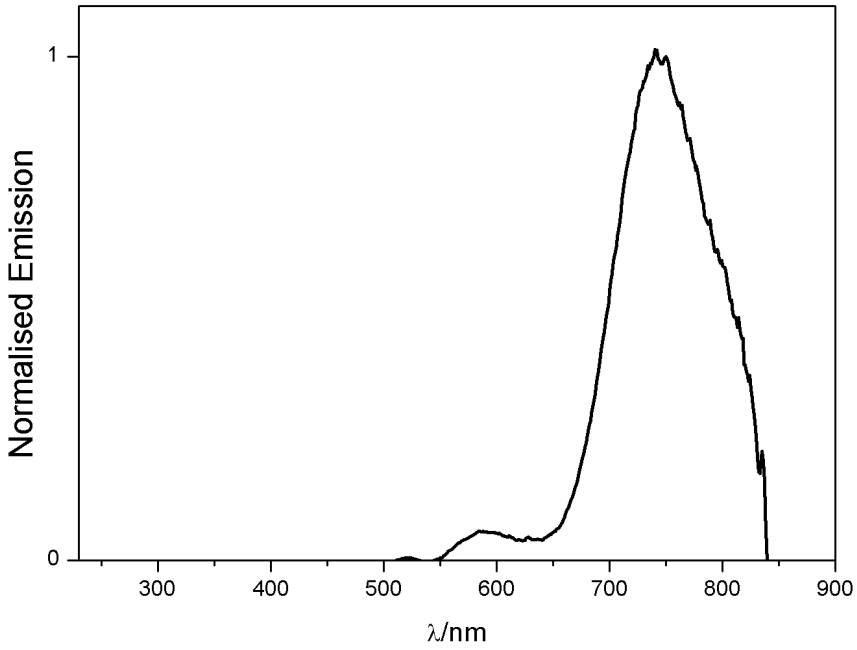

Figure 3.17. Emission spectrum of **3.8** in DCM. Emission recorded following excitation at 480 nm. c = 9.50 x 10^{-7} $mol^{-1}dm^3cm^{-1}$.

A very small hypsochromic shift of 2 nm, within the experimental error of the measurement, is observed in the BODIPY absorption of **3.13** demonstrating that the attachment at the ortho- rather than the bay-position has very little effect on the absorption properties of the BODIPY unit, Figure 3.18. The quadrupling of the number of BODIPYs attached to the PDI, *vs*. **3.8**, is matched by an approximate quadrupling of the extinction coefficient to 180,000 $mol^{-1}dm^3cm^{-1}$. It is not possible to determine the exact position of the absorption maximum for the PDI chromophore, as it is engulfed in the BODIPY absorbance, however this maximum has clearly been hypsochromically shifted by at least 30 nm *vs*. **3.4**. This shift signifies that, whilst the position of substitution of the BODIPY has no effect on the BODIPY absorbance, it has a significant effect on the absorption of the PDI. Emission measurements on **3.13** reveal a PDI based fluorescence, displaying vibrational structure as seen in other ortho-substituted PDIs,[56] with a maximum at 546 nm relating to a Stokes shift of 43 nm *vs.* the BODIPY, Figure 3.19. This emission is attributed to FRET whilst the low quantum

yield of 0.02 suggests that this process is again followed by PET resulting in a charge separated state.

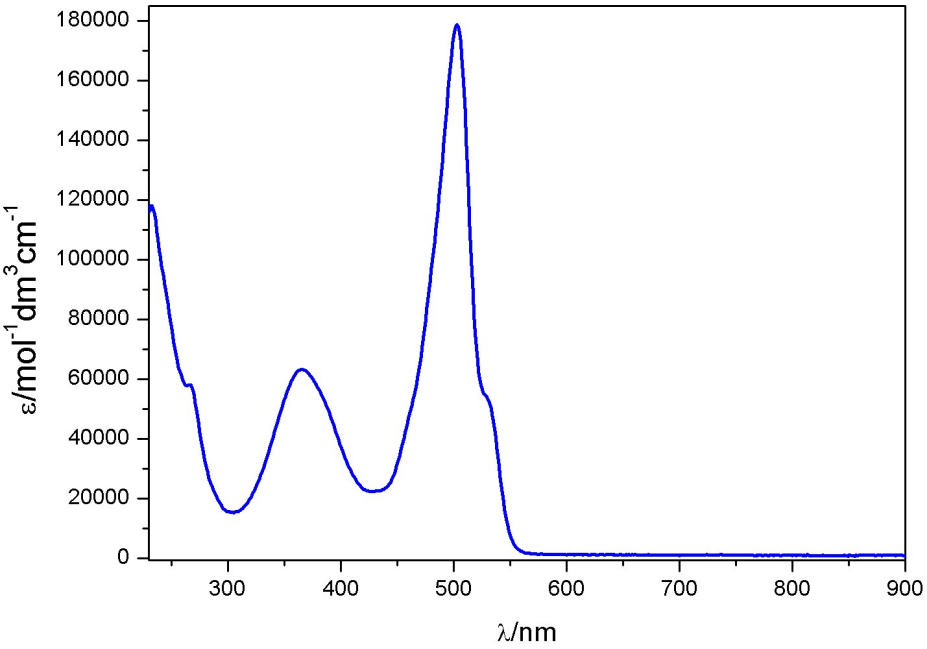

Figure 3.18. UV/vis absorption spectrum of **3.13** in DCM. c = 2.61 x 10^{-6} $mol^{-1}dm^3cm^{-1}$.

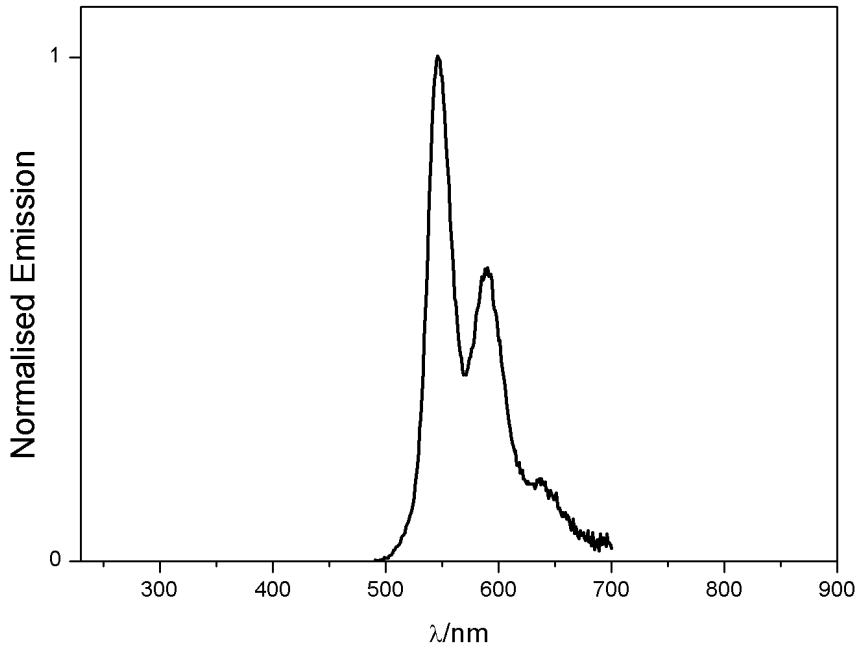

Figure 3.19. Emission spectrum of **3.13** in DCM. Emission recorded following excitation at 480 nm. c = 2.54 x 10^{-7} $mol^{-1}dm^3cm^{-1}$.

Compound	λ_{max} BODIPY	λ_{max} PDI	λ_{em}	Stokes Shift *vs.* BODIPY	Stokes Shift *vs.* PDI	Quantum Yield
3.4	505	562	610	105	48	0.91
3.8	505	616	741	236	125	0.05
3.13[a]	503	-	546	43	-	0.02

Table 3.1. Summary of the optical properties of **3.4**, **3.8** and **3.13** measured in DCM. All wavelengths reported in nm. All emissions measured after excitation at 480 nm. [a] λ_{max} could not be calculated due to overlap of the BODIPY and PDI absorptions.

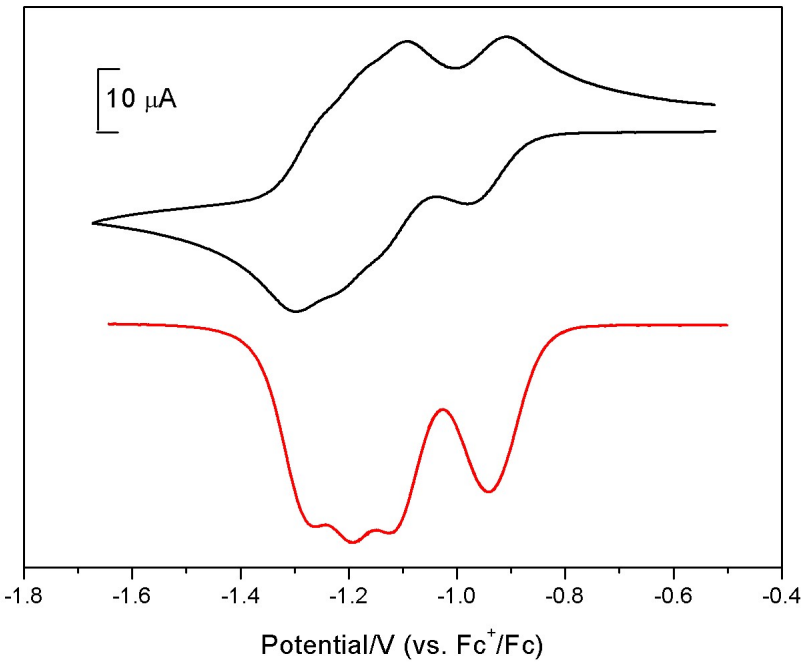

Figure 3.20. Cyclic (black) and square wave (red) voltammograms of **3.4** recorded in DCM containing $[Bu_4N][BF_4]$ (0.4 M).

Cyclic voltammetric investigations on **3.4** were expected to show two one-electron reductions from the PDI and a single two-electron reduction from the two BODIPYs. However, four separate reduction processes are resolvable in the square wave voltammogram at -0.94, -1.12, -1.19 and -1.26 V (*vs.* Fc/Fc^+), Figure 3.20 and Table 3.2. All four reductions were found to be electrochemically reversible in the scan rate range 0.02 – 0.3 Vs^{-1}. The presence of an additional reduction process has been observed previously, in a 1,7-di(cobalt-dithiolene)-PDI,[57] assigned to communication

across the conjugated PDI core; when one cobalt-dithiolene is reduced this affects the reduction potential of the other. It appears the same effect is occurring in the case of **3.4**. In the PDI-BODIPY systems synthesised by Elmali and co-workers,[43] oxidations associated with the BODIPY moiety are observed in the cyclic voltammograms. In the case of **3.4**, no oxidations were observed within the solvent window of DCM. This is likely due to the stabilising effect of the electron donating alkyl-groups in Elmali's systems (not present in **3.4**), raising the HOMO level bringing the oxidations into the solvent window.

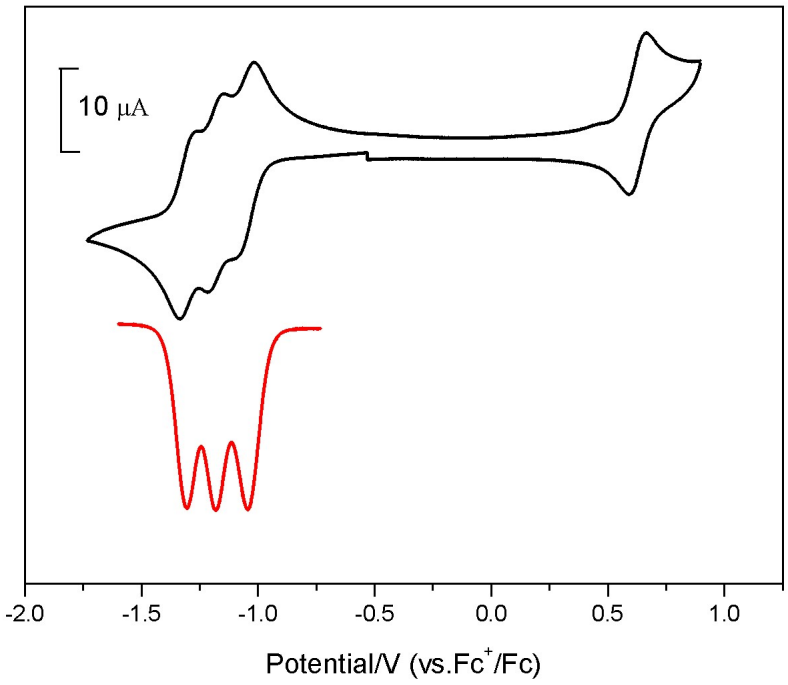

Figure 3.21. Cyclic (black) and square wave (red) voltammograms of **3.8** recorded in DCM containing $[Bu_4N][BF_4]$ (0.4 M).

Cyclic voltammetric investigations on **3.8** reveal three reductions at -1.04, -1.18 and -1.31 V and one oxidation at 0.63 V (*vs.* Fc/Fc^+), Figure 3.21. The three reductions were found to be electrochemically reversible in the scan rate range 0.02 – 0.3 Vs^{-1}. However, the oxidation was not found to be fully reversible. The reduction processes display higher resolution from one another compared to **3.4** but cannot be assigned to the

BODIPY or the PDI without the aid of spectroelectrochemistry, see below. The oxidation of **3.8** is comparable to that of the 1,7-dimorpholino PDI, synthesised by Champness and co-workers,[44] but comes at a more positive potential by 0.20 V due to the lessened electron donating effect of monomorpholino-substitution *vs.* dimorpholino-substitution. This oxidation is unlikely to be associated with the BODIPY as an analogous process would have been observed in the cyclic voltammogram of **3.4**, the prediction that the oxidation lies on the PDI rather than the BODIPY is confirmed by density functional theory (DFT), see below.

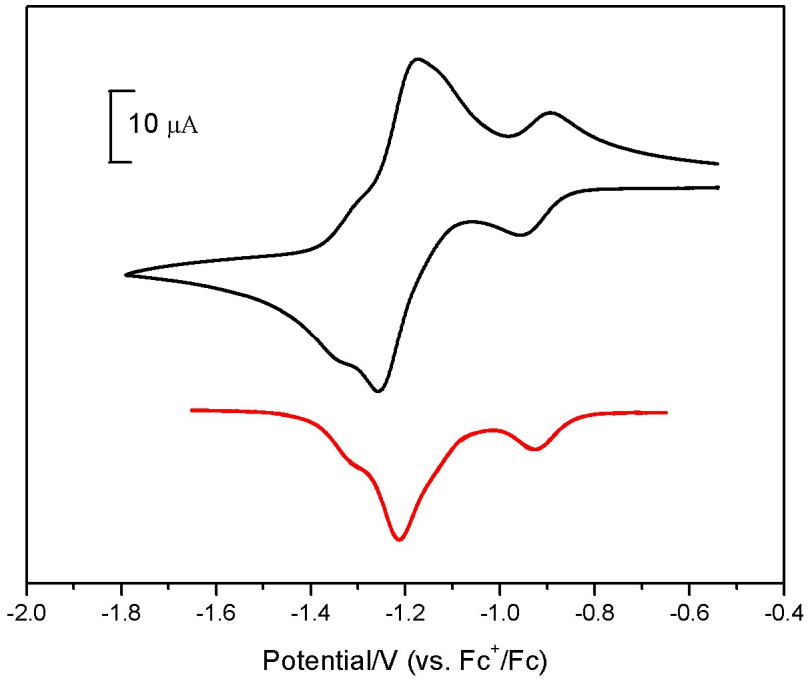

Figure 3.22. Cyclic (black) and square wave (red) voltammograms of **3.13** recorded in DCM containing $[Bu_4N][BF_4]$ (0.4 M).

The cyclic voltammogram of **3.13** displays a reduction at -0.93 V (*vs.* Fc/Fc^+) corresponding, by comparison to **3.4**, to the first reduction on the PDI core, a large process at -1.22 V related to the four one-electron reductions due to the BODIPYs with a shoulder associated with the second reduction on the PDI and no oxidations within the solvent window of DCM. All three processes were found to be electrochemically

reversible in the scan rate range 0.02 – 0.3 Vs^{-1}. There is no evidence of communication between the BODIPY moieties suggesting that positioning them ortho- on the PDI core reduces the conjugation across the PDI between the BODIPYs. Whilst there was very little variation in the position of the BODIPY absorption maxima, depending on whether it was connected at the ortho- or bay- position, there is a slightly more pronounced effect in the reduction potential in the cyclic voltammogram of 0.04 V between **3.8** and **3.13**.

Compound	**Reduction**				**Oxidation**
	1st	**2nd**	**3rd**	**4th**	
3.4	-0.94	-1.12	-1.19	-1.26	-
3.8	-1.04	-1.18	-1.31	-	0.63
3.13	-0.93	-1.22	-	-	-

Table 3.2. Redox potentials for **3.4**, **3.8** and **3.13**. All potentials reported as $E_{1/2}$ (= (E_p^a + E_p^c)/2) in V *vs*. Fc^+/Fc at 0.1 Vs^{-1} scan rate and quoted to the nearest 0.01 V.

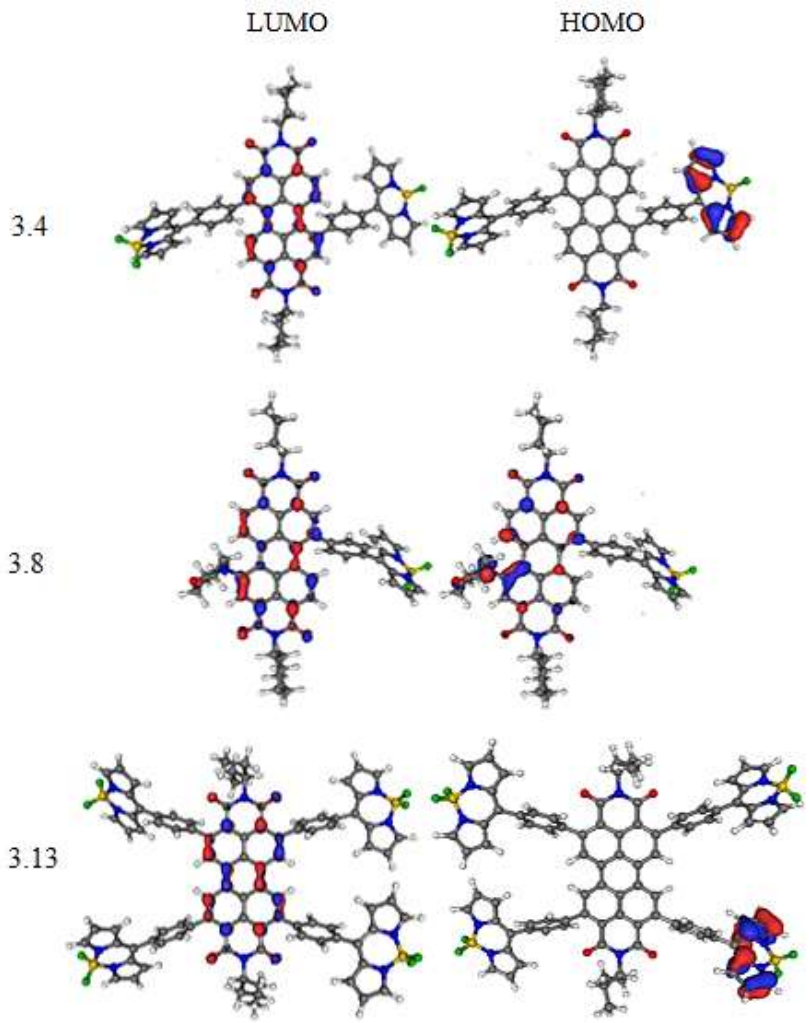

Figure 3.23. Molecular orbital (MO) isosurfaces calculated by DFT **3.4**, **3.8** and **3.13**.

DFT was used to generate MO isosurfaces for the **3.4**, **3.8** and **3.13** in order to identify the locations of the HOMOs and LUMOs and compare the energies of the LUMOs with the potential of the first reductions, Figure 3.23. In all cases, the LUMO was found on the PDI part of the molecule, confirming that the first reduction was indeed based on the PDI. The HOMO of **3.4** and **3.13** is centred on the BODIPY. However it was not possible to compare this to the cyclic voltammetry as no oxidations were observed. The HOMO of **3.8** lies on the PDI with much of the electron density pulled towards the morpholine moiety. This confirms that the oxidation observed in the cyclic voltammetry is indeed analogous with that of the dimorpholino-substituted PDI and lies on the PDI part of the molecule.[44] The energy levels of the LUMOs of **3.4**, **3.8** and **3.13**

were found to be -3.60, -3.34 and -3.91 eV respectively. The LUMO energy of **3.4** being more negative than that of **3.8** is reflected in the more ready reduction of **3.4** *vs*. **3.8.** The difference between **3.4** and **3.13** is also reflected by the experimental observations as **3.13** is easier to reduce than **3.4** however only by 0.1 V suggesting the difference in the calculated LUMOs may be slightly exaggerated.

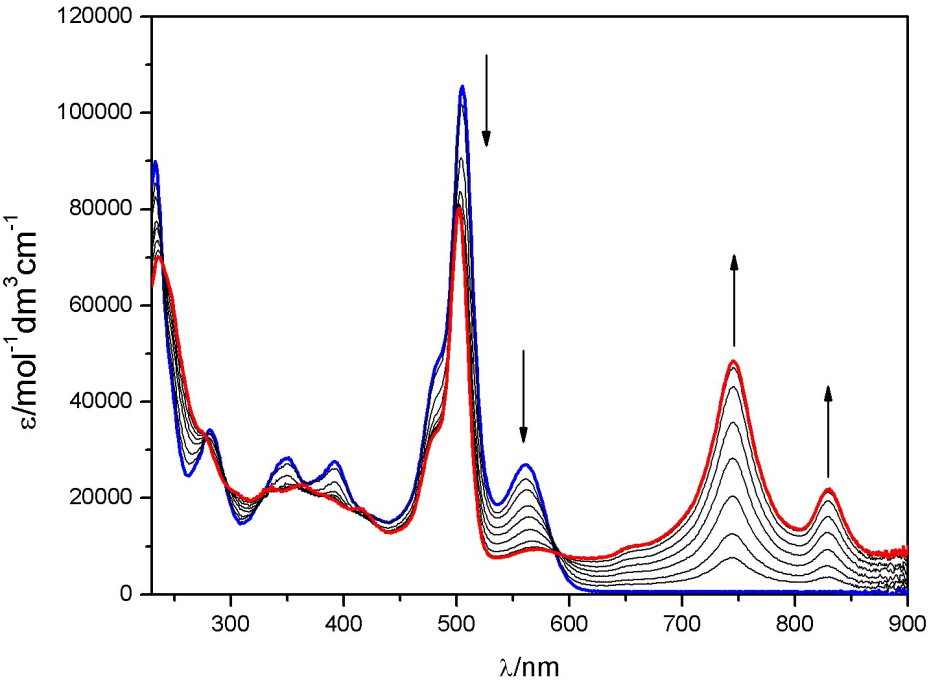

Figure 3.24. UV/vis absorption spectra recorded in DCM containing $[Bu_4N][BF_4]$ (0.4 M) using spectroelectrochemical methods for **3.4** at 243 K showing the inter-conversion of **3.4** (blue) to **3.4**$^{\bullet-}$ (red). c = 1.32 x 10^{-4} $mol^{-1}dm^3cm^{-1}$. Arrows indicate the progress of the reduction.

The nature of these redox process was further probed by *in situ* reduction followed by UV/vis spectroelectrochemistry in DCM with $[^nBu_4N][BF_4]$ as supporting electrolyte, summarised in Table 3.3. Upon application of a potential between the first and second reductions of **3.4**, the absorption band corresponding to the PDI decreases in intensity accompanied by the formation of a band corresponding to a PDI monoradical at 745 nm (ε = 48,000 $mol^{-1}dm^3cm^{-1}$) confirming that the reduction at -0.94 V lies on the PDI, this bathochromic shift upon reduction is well documented, Figure 3.24.[58-60] The formation of a PDI$^{\bullet-}$ band was accompanied by a slight reduction in intensity in the

band corresponding to the neutral BODIPY. This reduction in intensity started as soon as the potential was applied but stopped whilst the PDI band was still decreasing.

Unfortunately, the high degree of overlap between the second to fourth reduction processes of **3.4** meant it was not possibly to individually investigate each one by spectroelectrochemical methods meaning it was not possible to assign each different process to individual parts of the molecule. A potential was therefore applied sufficient to reduce all three remaining processes, Figure 3.25. The peak formed during the first reduction was depleted and replaced by a peak, blue shifted by 123 nm, to 622 nm with a similar extinction coefficient. This peak was assigned to the second reduction on the PDI core.[58-60] At the same time, the peak associated with the neutral BODIPY was also diminished and a peak appearing, with a much smaller extinction coefficient (ε = 36,000 $mol^{-1}dm^3cm^{-1}$), slightly red shifted at 540 nm.[61-63]

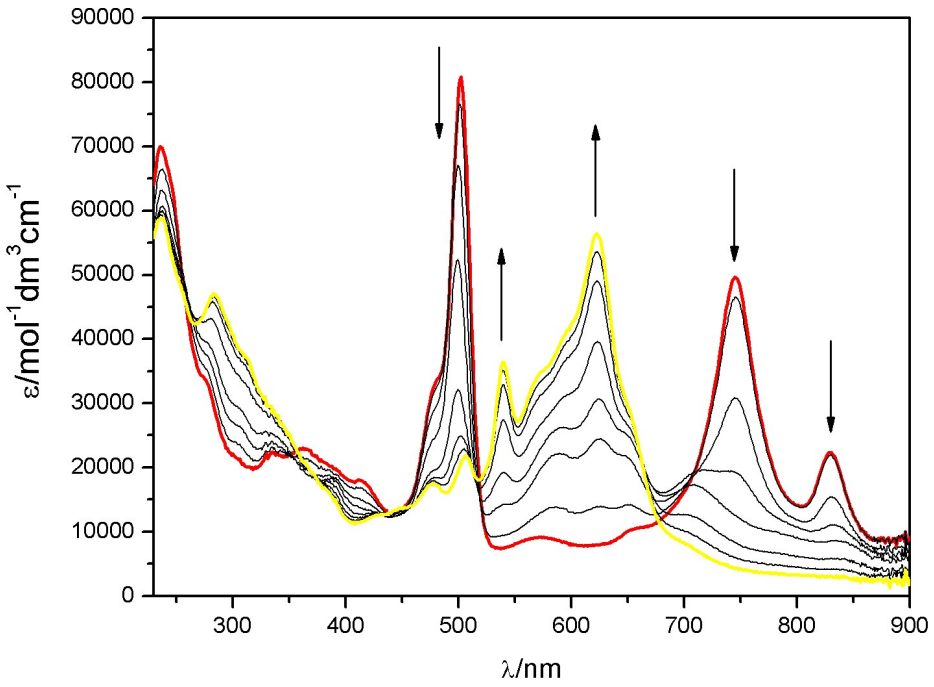

Figure 3.25. UV/vis absorption spectra recorded in DCM containing $[Bu_4N][BF_4]$ (0.4 M) using spectroelectrochemical methods for **3.4** at 243 K showing the inter-conversion of $\mathbf{3.4^{\bullet-}}$ (red) to $\mathbf{3.4^{4-}}$ (yellow). c = 1.32 x 10^{-4} $mol^{-1}dm^3cm^{-1}$. Arrows indicate the progress of the reduction.

Upon regeneration of the neutral spectrum the absorptions corresponding to the PDI chromophore were fully regenerated, however, the BODIPY absorption had diminished in intensity, Figure 3.26. This lack of full regeneration suggests the BODIPY has partially decomposed and is not fully electrochemically reversible.

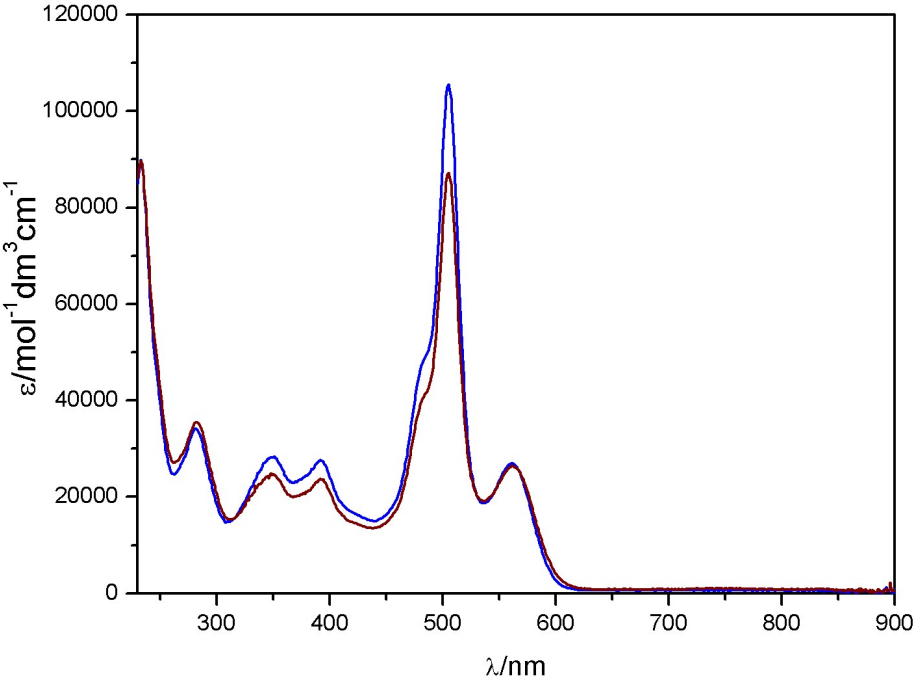

Figure 3.26. UV/vis absorption spectra showing comparison of **3.4** (blue) *vs*. the regenerated molecule after electrochemical reduction (brown). c = 1.32 x 10^{-4} $mol^{-1}dm^3cm^{-1}$.

The separation between the three reduction processes of **3.8** allowed spectroelectrochemical methods to be used to assign each process to individual parts of the molecule. The lack of reversibility shown by the oxidation process during cyclic voltammetry meant that this process was not investigated any further. Upon application of a potential between the first and second reductions, **3.8** displayed similar behaviour to **3.4**; the peak corresponding to the PDI at 616 m was diminished with a new more intense band forming at 766 nm, due to the first reduction on the PDI core, and there was a slight reduction in the intensity of the BODIPY absorption at 505 nm Figure 3.27. This demonstrates that the peak at -1.04 V in cyclic voltammetry is associated with the

first reduction on the PDI core. The difference in absorption maximum of the neutral and first reduced PDI species is 38 nm more pronounced in this case *vs*. **3.4**.

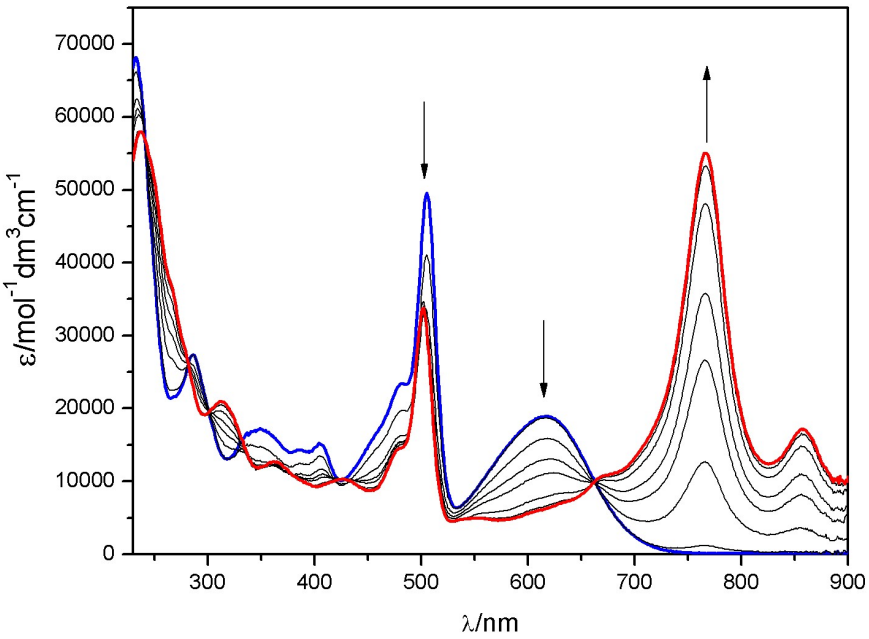

Figure 3.27. UV/vis absorption spectra recorded in DCM containing $[Bu_4N][BF_4]$ (0.4 M) using spectroelectrochemical methods for **3.8** at 243 K showing the inter-conversion of **3.8** (blue) to **3.8**$^{\bullet-}$ (red). c = 2.87 x 10^{-4} $mol^{-1}dm^3cm^{-1}$. Arrows indicate the progress of the reduction.

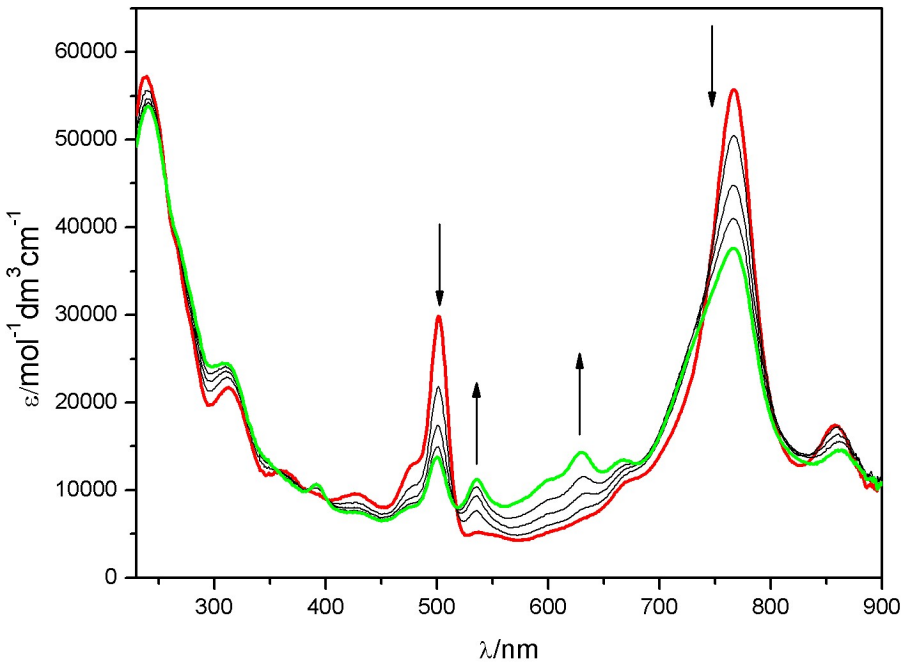

Figure 3.28. UV/vis absorption spectra recorded in DCM containing $[Bu_4N][BF_4]$ (0.4 M) using spectroelectrochemical methods for **3.8** at 243 K showing the inter-conversion of **3.8**$^{\bullet-}$ (red) to **3.8**$^{2-}$ (green). c = 2.87 x 10^{-4} $mol^{-1}dm^3cm^{-1}$. Arrows indicate the progress of the reduction.

Application of a potential between the second and third reductions of **3.8** results in the disappearance of the neutral BODIPY band at 502 nm along with the generation of the first reduced BODIPY band at 536 nm indicating that the reduction at -1.18 V corresponds to the reduction on the BODIPY moiety, Figure 3.28. There is also a slight accompanying decrease in the intensity of the absorption at 766 nm. However, this is assigned to the small potential gap between the second and third reduction resulting in slow formation of $\mathbf{3.8}^{3-}$.

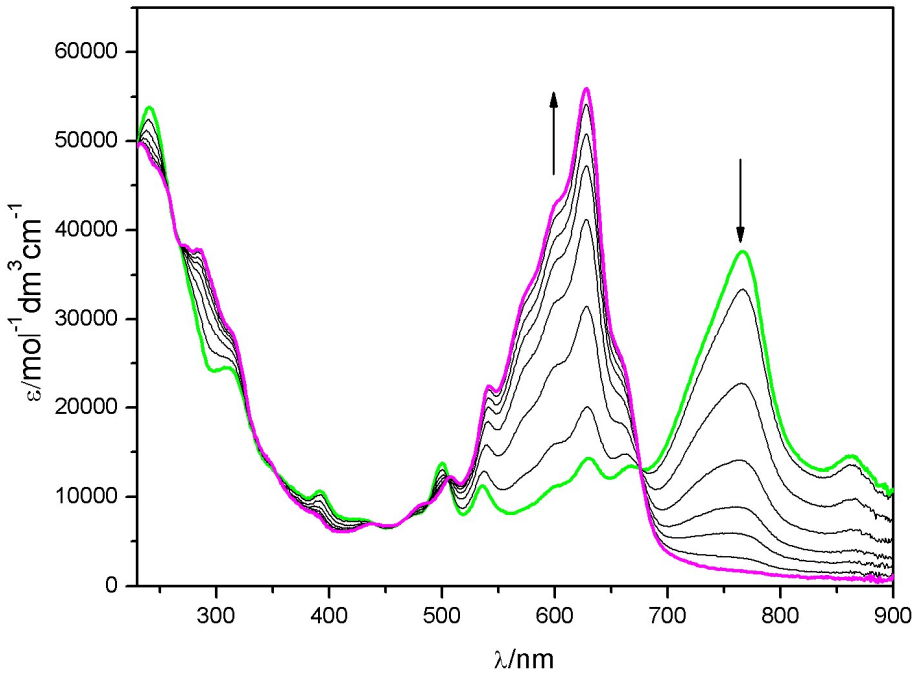

Figure 3.29. UV/vis absorption spectra recorded in DCM containing $[Bu_4N][BF_4]$ (0.4 M) using spectroelectrochemical methods for **3.8** at 243 K showing the inter-conversion of $\mathbf{3.8}^{2-}$ (green) to $\mathbf{3.8}^{3-}$ (pink). c = 2.87 x 10^{-4} $mol^{-1}dm^3cm^{-1}$. Arrows indicate the progress of the reduction.

Applying a potential sufficient to reduce the process at -1.31 V is resultant in the removal of the PDI first reduced peak at 766 nm and the development of a peak related to the second reduction of the PDI at 628 nm, Figure 3.29. The BODIPY reduction is sandwiched between the first and second reduction on the PDI core. The reoxidation of the molecule again resulted in the full regeneration of the PDI absorption band but not

the BODIPY band displaying the BODIPY chromophore's lack of electrochemical reversibility.

The application of a potential sufficient to instigate the first reduction process of **3.13** revealed the reduction in intensity of the absorption corresponding to the PDI and the development of a new band at 723 nm due to the PDI monoanion, Figure 3.30. Once again upon reduction of the PDI there is a decrease in intensity of the absorption of the BODIPY. However, in this case the decrease is much less pronounced than observed for **3.4** and **3.8**.

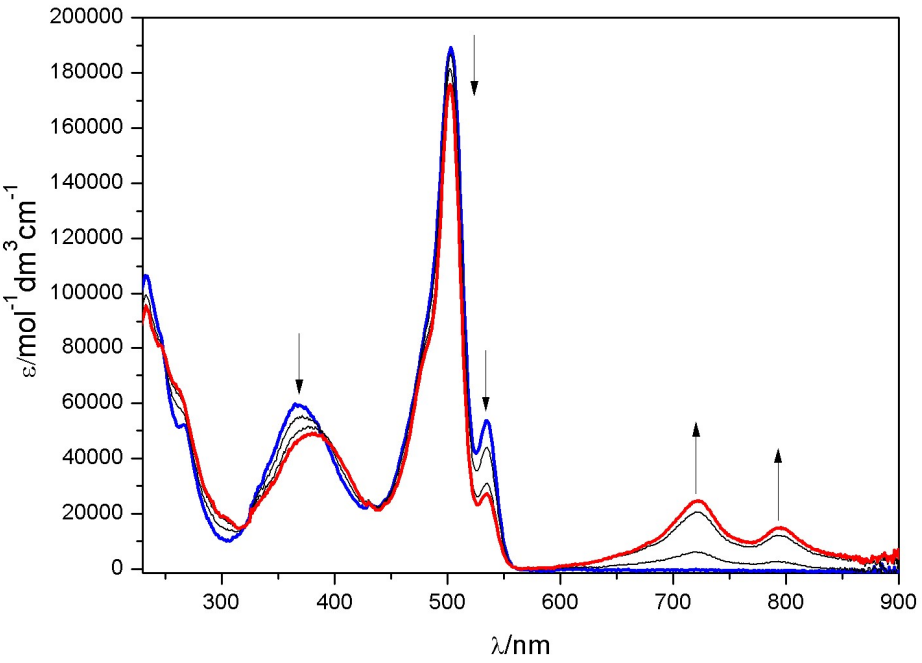

Figure 3.30. UV/vis absorption spectra recorded in DCM containing $[Bu_4N][BF_4]$ (0.4 M) using spectroelectrochemical methods for **3.13** at 243 K showing the inter-conversion of **3.13** (blue) to **3.13**$^{\bullet-}$ (red). c = 7.73 x 10^{-5} $mol^{-1}dm^3cm^{-1}$. Arrows indicate the progress of the reduction.

The overlap between the second and third reductions did not allow for the investigation of these two processes individually therefore a potential sufficient to perform both reductions was applied. Due to the number of processes occurring analysis of the spectra generated is difficult, Figure 3.31. Upon application of the potential, the peaks corresponding to the neutral and anionic PDI are seen to slightly reduce and increase in

intensity respectively, this suggests that the first reduction of the PDI was not complete before the potential was applied. The PDI monoanion peak is then seen to reduce in intensity and a peak at 627 nm is formed, assigned to the PDI dianion. The peak at 603 nm is depleted accompanied by formation of a new peak, slightly red shifted, at 538 nm related to the reduction of the four BODIPY chromophores. The reoxidation of the molecule again resulted in the full regeneration of the PDI absorption band but not the BODIPY band displaying the BODIPY chromophore's lack of electrochemical reversibility.

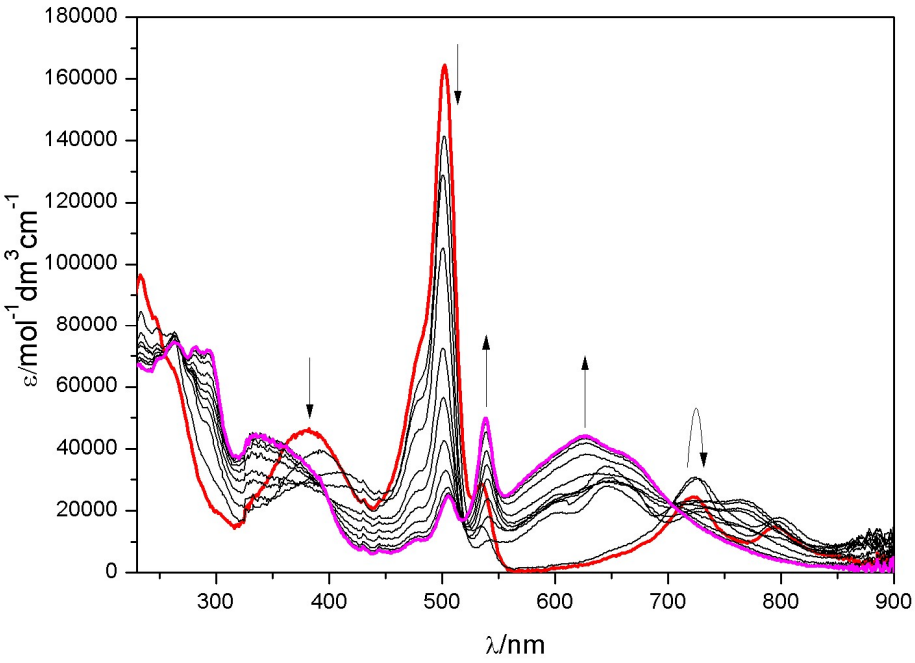

Figure 3.31. UV/vis absorption spectra recorded in DCM containing $[Bu_4N][BF_4]$ (0.4 M) using spectroelectrochemical methods for **3.13** at 243 K showing the inter-conversion of $\mathbf{3.13^{\bullet-}}$ (red) to $\mathbf{3.13^{6-}}$ (pink). c = 7.73 x 10^{-5} $mol^{-1}dm^3cm^{-1}$. Arrows indicate the progress of the reduction.

	Neutral	Reduction			
		1st	2nd	3rd	4th
3.4	281 (3.4), 351 (2.8), 392 (2.8), 505 (10.6), 562 (2.7)	502 (8.0), 745 (4.8), 830 (2.2)	-	-	283 (4.7), 540 (3.6), 622 (5.6)
3.8	286 (2.8), 349 (1.4), 404 (1.3), 505 (3.5), 616 (1.9)	313 (2.1), 502 (3.4), 766 (5.5), 858 (1.7)	309 (2.4), 536 (1.1), 630 (1.4), 765 (3.8), 860 (1.5)	541 (2.2), 628 (5.6)	-
3.13	266 (5.2), 366 (5.9), 503 (18.9), 535 (5.4)	383 (4.9), 502 (17.6), 535 (2.7), 723 (2.5), 795 (1.5)	-	282 (7.3), 505 (2.5), 538 (5.0), 627 (4.4)	-

Table 3.3. UV/vis spectroscopic data for **3.4**, **3.8** and **3.13** measured at 243 K in DCM from spectroelectrochemistry. All values λ_{max}/nm (ε x10^5/mol^{-1}dm^{3}cm^{-1}).

3.2.2.2. Perylene Diimide-MethylBodpipys

UV/vis spectroscopic studies on **3.18** reveal a peak at 513 nm, corresponding to the methyl-BODIPYs, with a large extinction coefficient of 116,000 mol^{-1}dm^{3}cm^{-1}, 10,000 mol^{-1}dm^{3}cm^{-1} higher than **3.4**, Figure 3.32. The electron donating effect of the methyl-groups has induced a slight bathochromic shift in the absorbance *vs*. **3.4** of 8 nm as seen previously in systems containing methylBODIPYs.[62] It is not possible to accurately measure the absorption maximum of the PDI absorption as it is now overlapped by the BODIPY absorption. However, there has clearly been a small hypsochromic shift. This shift is unexpected as only a small modification has been made to the system with this modification more likely to result in a bathochromic shift, due to increased electron donation, suggesting that some other effect is causing the change in wavelength of absorption. Emission measurements reveal **3.18** is not emissive under the experimental conditions. It is likely that the same processes as observed for **3.8** and **3.13**, FRET

followed by PET, are occurring in this case, however, the complete lack of emission suggests the PET process is more efficient resulting in full quenching of fluorescence.

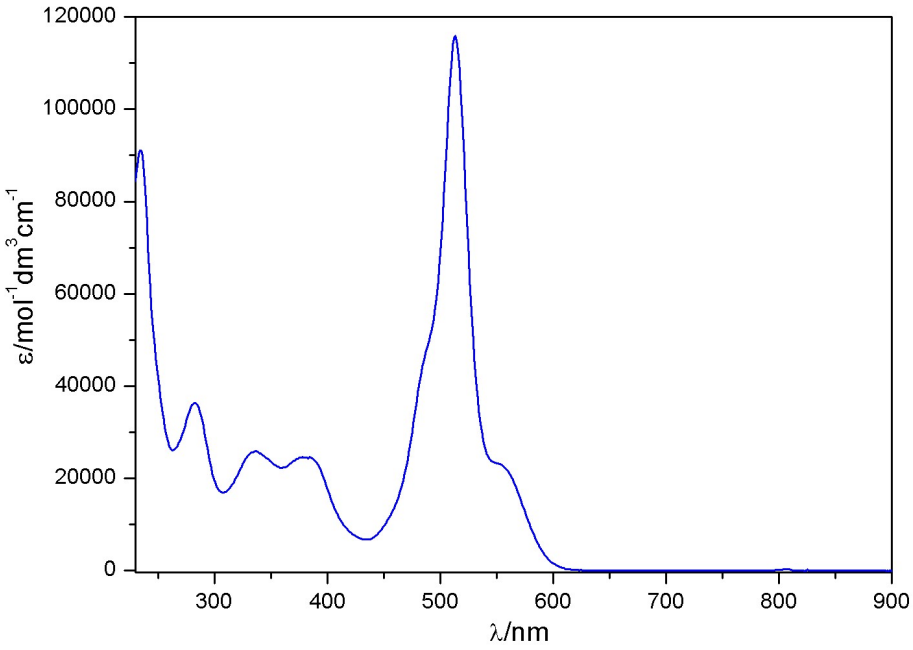

Figure 3.32. UV/vis absorption spectrum of **3.18** in DCM. c = 5.24 x 10^{-6} $mol^{-1}dm^3cm^{-1}$.

In the UV/vis spectrum of **3.19** the BODIPY absorbance is observed at 514 nm, almost identical to that of **3.18**, and is red shifted 9 nm *vs*. **3.8**, again almost identical to the difference between the corresponding absorptions in **3.4** and **3.18**. The extinction coefficient increases by 5,000 $mol^{-1}dm^3cm^{-1}$, exactly half of the increase seen between the di(BODIPY)-substituted systems. The PDI absorption has again been blue shifted. In this instance it is possible to measure that shift as 11 nm *vs*. **3.8** to 605 nm. Emission measurements reveal FRET is occurring resulting in a PDI based fluorescence peak that extends well into the NIR with a maximum at 743 nm, within 2 nm of the corresponding emission in **3.8**, Figure 3.34. The quantum yield of 0.06 suggests this fluorescence is quenched by PET.

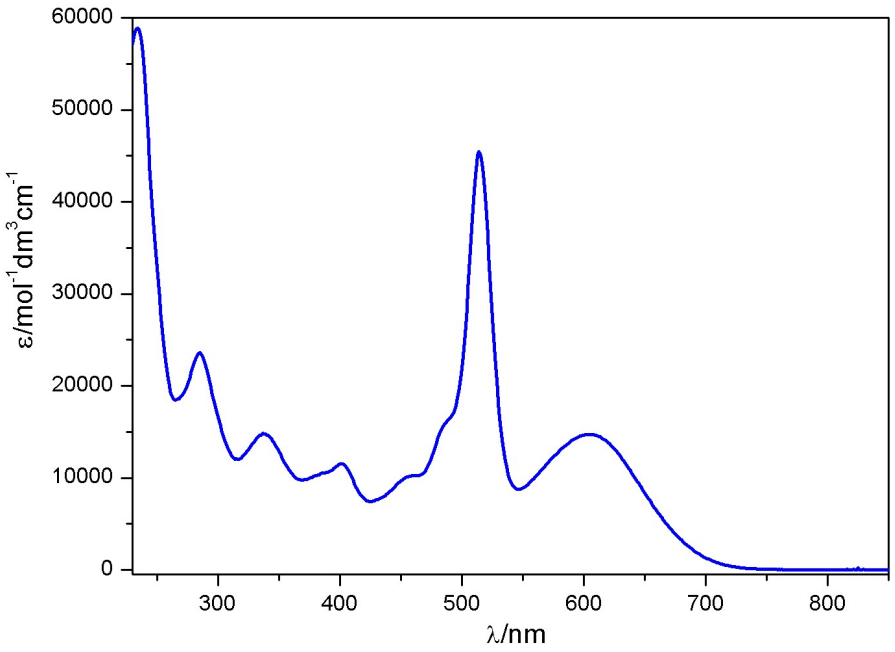

Figure 3.33. UV/vis absorption spectrum of **3.19** in DCM. c = 1.12 x 10^{-5} $mol^{-1}dm^3cm^{-1}$.

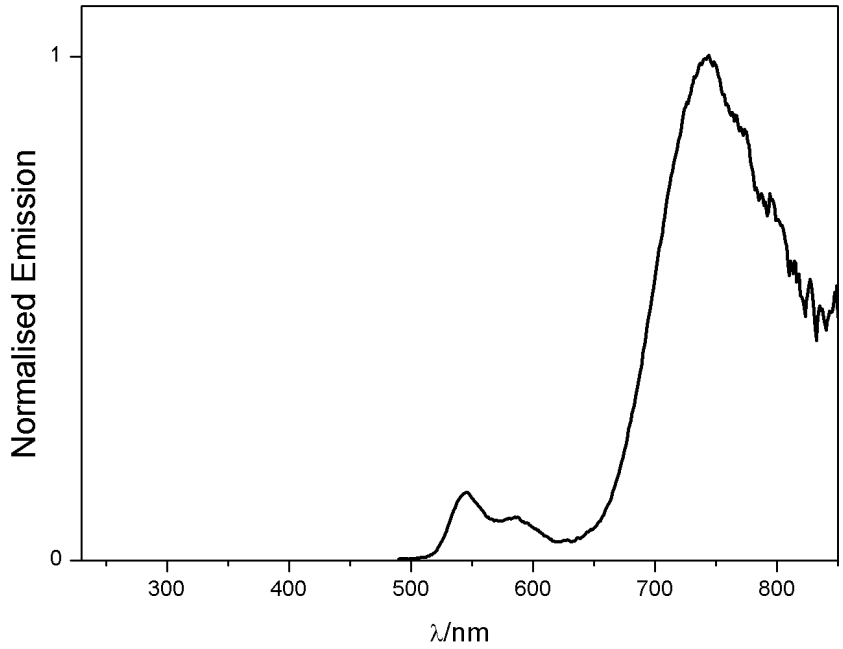

Figure 3.34. Emission spectrum of **3.19** in DCM. Emission recorded following excitation at 480 nm. c = 7.24 x 10^{-7} $mol^{-1}dm^3cm^{-1}$.

One of the main aims in synthesising **3.18** was to attempt to move the reductions located on the BODIPY in **3.4** to a more negative potential, by introduction of the methyl substituents, in order to reduce the overlap between the processes and make interpretation of the communication between BODIPY moieties easier. Cyclic

voltammetry reveals two one-electron reductions at -0.97 and -1.16 V, one two-electron reduction at -1.43 V (*vs.* Fc/Fc^+), all found to be reversible over a scan rate range 0.02 – 0.3 Vs^{-1}, and an oxidation that was found to be irreversible over this scan rate range, Figure 3.35 and Table 3.4. The one-electron reductions correspond to the PDI core, with the reduction at -0.97 V only shifting by 0.03 V *vs*. **3.4**, whilst the two-electron reduction corresponds to the two BODIPY moieties. It is not possible to exactly measure the change in potential of the BODIPY reductions upon addition of the methyl groups, as they could not be exactly assigned in **3.4**, but it is by a minimum of 0.17 V (by comparison to the fourth reduction process in **3.4**). This shows that whilst the addition of methyl-groups had the desired effect of shifting the BODIPY reductions to lower potentials, thus resolving them from the PDI reductions. At the same time, it stopped the communication between them. This suggests the methyl-groups have decreased the degree of conjugation between the BODIPY units across the PDI core. One potential explanation is that the introduction of methyl-groups increases the steric interactions thus restricting the rotation of the BODIPYs and forcing them to lie out of plane with the PDI or phenyl linker. However, this is far more likely in the case of methyl groups at the 1- and 7-positions rather than 3- and 5-positions as in this case. The disruption of the communication is therefore more likely due to changes in the redox potentials of the BODIPY moieties by addition of methyl-groups rather than steric effects.

Due to the irreversibility of the oxidation, this process was not investigated any further. However, this process is likely to be associated with the BODIPY as the addition of alkyl-groups has been shown by Elmali and co-workers[43] to raise the HOMO level of the BODIPY moving the oxidation into the solvent window of the DCM. In the case of **3.18**, the effect is less pronounced, demonstrated by the more positive oxidation

potential *vs*. Elmali's systems, as there are only two methyl-groups on the BODIPY core in **3.18** rather than four for the previously reported system. The HOMO lying on the BODIPY moiety is confirmed by DFT (see below).

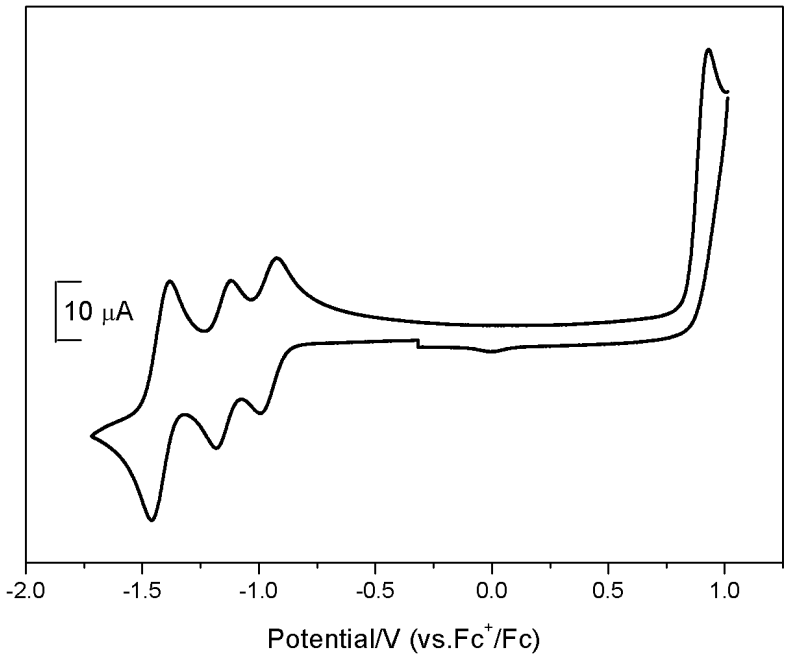

Figure 3.35. Cyclic voltammogram of **3.18** recorded in DCM containing $[Bu_4N][BF_4]$ (0.4 M).

The cyclic voltammogram of **3.19** shows three one-electron reductions at -1.04, -1.23 and -1.43 V and an oxidation at 0.63 V (*vs.* Fc/Fc^+), Figure 3.36. The first two reductions are centred on the PDI core and the third on the BODIPY. The reduction at -1.04 V remains unchanged *vs*. **3.8** but the other PDI reduction has moved by 0.05 V to a more negative potential demonstrating that this reduction is affected by the redox state of the BODIPY. The BODIPY reduction has moved 0.12 V to a more negative potential, the exact same potential as the corresponding reduction of **3.19**, again demonstrating that changes to the PDI core (the meso-substituent) have little or no effect on the BODIPY reductions. The addition of methyl-groups to the BODIPY has moved the BODIPY reduction from between the two PDI reductions to a more negative potential thus decreasing the overlap and enhancing the resolution of the processes. The

oxidation comes at the same potential as the oxidation of **3.8** suggesting this process is associated with the PDI core, confirmed by DFT (see below).

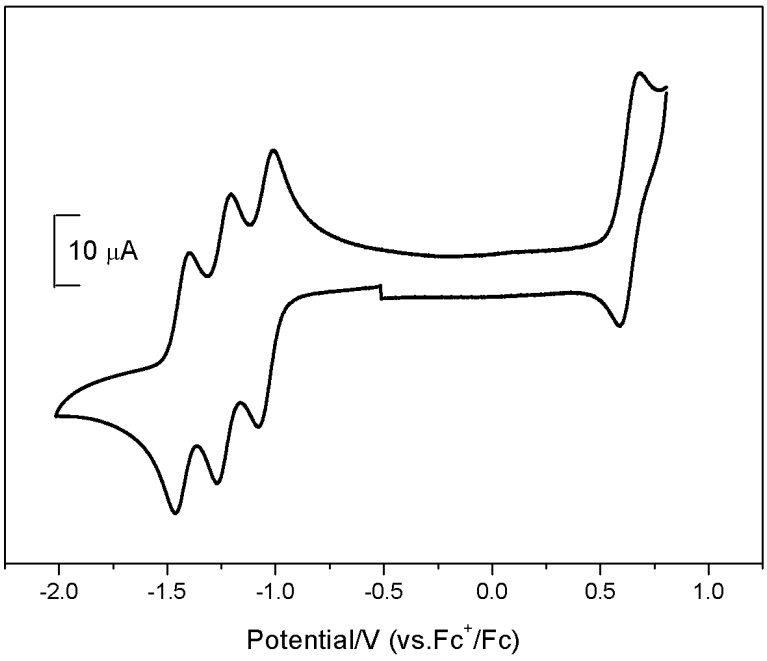

Figure 3.36. Cyclic voltammogram of **3.19** recorded in DCM containing $[Bu_4N][BF_4]$ (0.4 M).

Compound	1st Reduction	2nd Reduction	3rd Reduction	Oxidation
3.18	-0.97	-1.16	-1.43	-
3.19	-1.04	-1.23	-1.43	0.63

Table 3.4. Reduction potentials for **3.18** and **3.19**. All potentials reported as $E_{1/2}$ (= $(E_p^a + E_p^c)/2$) in V vs. Fc^+/Fc at 0.1 Vs^{-1} scan rate and quoted to the nearest 0.01 V.

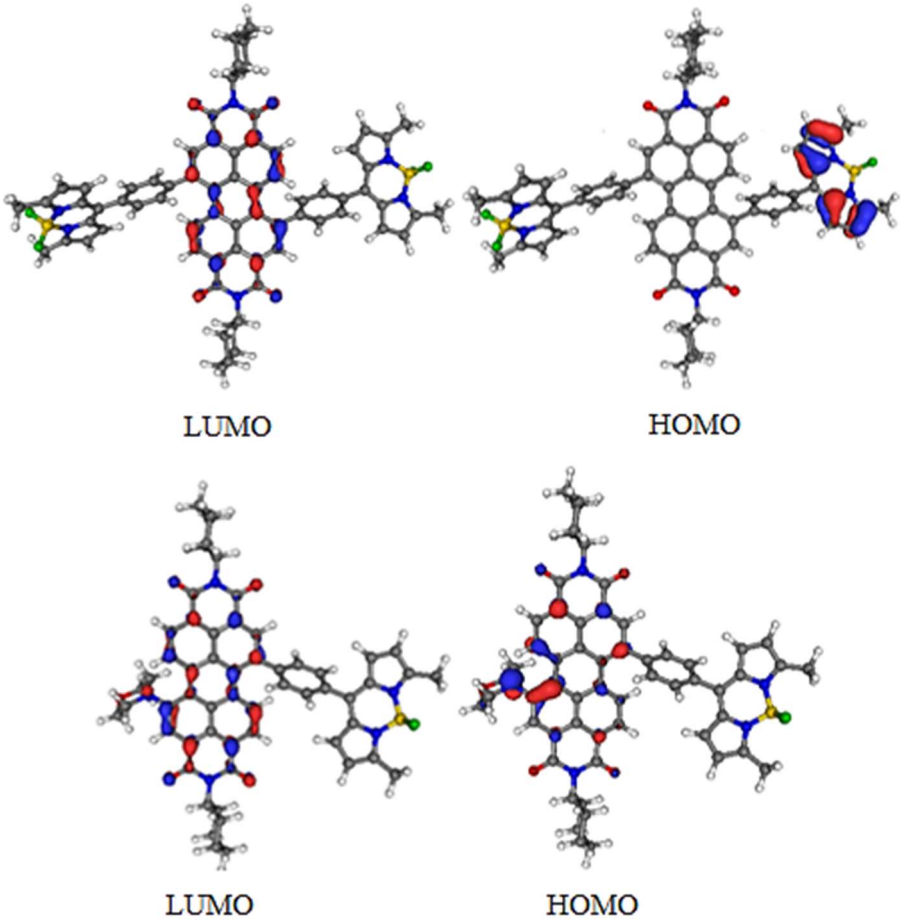

Figure 3.37. MO isosurfaces calculated by DFT **3.18** (top) and **3.19** (bottom).

DFT was again used to calculate MO isosurfaces for **3.18** and **3.19** in order to identify the locations of the HOMOs and LUMOs and compare the energies of the LUMOs with the potential of the first reductions, Figure 3.37. Similarly to the previous PDI-BODIPY systems the LUMO was shown to lie on the PDI in both cases. The LUMO energy for **3.18** was calculated to be -3.51 eV and for **3.19** -3.31 eV reflecting the slightly less negative reduction potential of **3.18**. Once again, in the case of the di(BODIPY)-substituted PDI the HOMO is centred on the BODIPY moiety whilst in the mono(BODIPY)-substituted system the HOMO is on the PDI, confirming that the irreversible oxidations observed are associated with the BODIPY for **3.18** and the PDI core for **3.19**.

The nature of the redox processes of the methylBODIPY-PDIs was further probed by *in situ* reduction followed by UV/vis spectroelectrochemistry in DCM with $[Bu_4N][BF_4]$ as supporting electrolyte. From this point on, the results of the spectroelectrochemistry following reduction are presented in one spectrum for each molecule, showing reduced states of the systems, rather than displaying the interconversion between individual processes. These results are summarised in Table 3.5.

Upon reduction of the first process on **3.18**, the small peak corresponding to the PDI is depleted accompanied by the formation of a band due to the first reduction on PDI at 744 nm, within 1 nm of the analogous process on **3.4**, Figure 3.38. The hypsochromic shift of the neutral PDI absorbance, upon methyl-functionalisation of the BODIPY, is not replicated following reduction. Previously, when the first PDI reduction has been performed the intensity of the BODIPY absorbance has also decreased and not been regenerated upon reoxidation, however, in this case this does not happen. There is a slight increase in the BODIPY absorbance, attributed to bands forming underneath it associated with the PDI anion, and upon reoxidation (of only the anion) the original intensity is re-established. This could suggest that the communication between the BODIPY and the PDI are reduced following the introduction of methyl-groups. An alternative explanation is that the PDI and BODIPY reductions of **3.4** were overlapping causing the BODIPY to be reduced, and to decompose, at the same time as the PDI reduction.

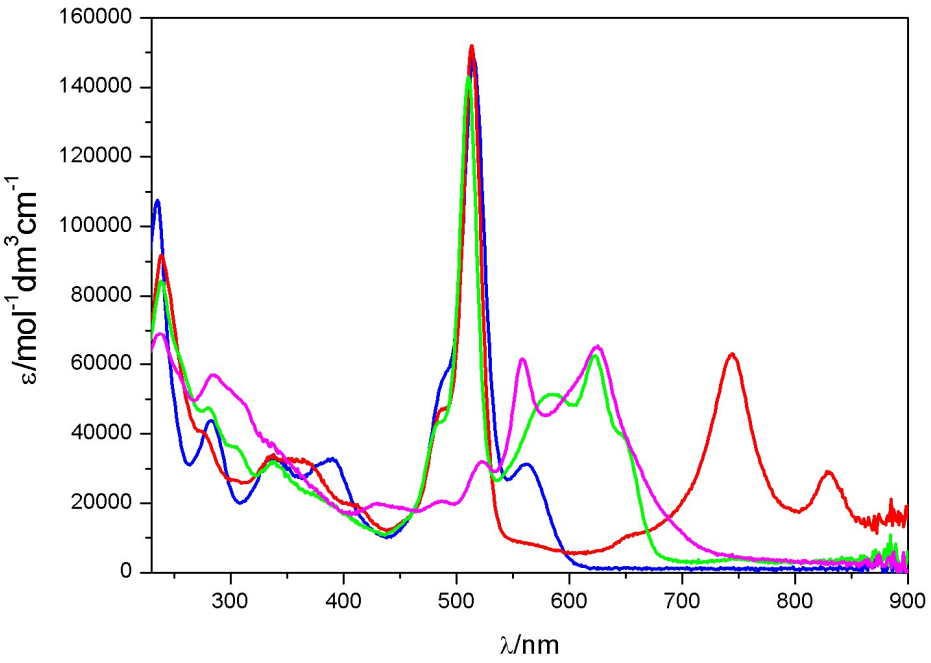

Figure 3.38. UV/vis absorption spectra recorded in DCM containing $[Bu_4N][BF_4]$ (0.4 M) using spectroelectrochemical methods for **3.18** at 243 K showing **3.18** (blue), $\mathbf{3.18^{\bullet-}}$ (red), $\mathbf{3.18^{2-}}$ (green) and $\mathbf{3.18^{4-}}$ (pink). c = 1.17 x 10^{-4} $mol^{-1}dm^3cm^{-1}$.

Application of a potential sufficient to carry out the second reduction process results in the removal of the first PDI reduced band and generation of a blue shifted band due to the second reduction on the PDI core, with a maximum at 623 nm, again almost identical to the corresponding process on **3.4**. Separation of the second PDI and BODIPY reduction of **3.4** was not possible due to the overlap of the processes. Therefore, functionalisation with methyl-groups has allowed a more complete spectroelectrochemical characterisation of the di(BODIPY)-substituted systems to be undertaken. Contrasting to the first reduction, the BODIPY absorbance irreversibly loses a small amount of intensity during this process suggesting the communication or overlap is reinitiated upon second reduction.

Upon reduction of the final process, the BODIPY absorbance disappears accompanied by the formation of the BODIPY radical peak at 558 nm to give the absorbance profile of the fully reduced molecule. Reoxidation results in the same behaviour as seen with

the previously described systems with the PDI absorbances being fully regenerated, showing their electrochemical reversibility, whilst the BODIPY absorption is not fully regenerated due to electrochemical decomposition.

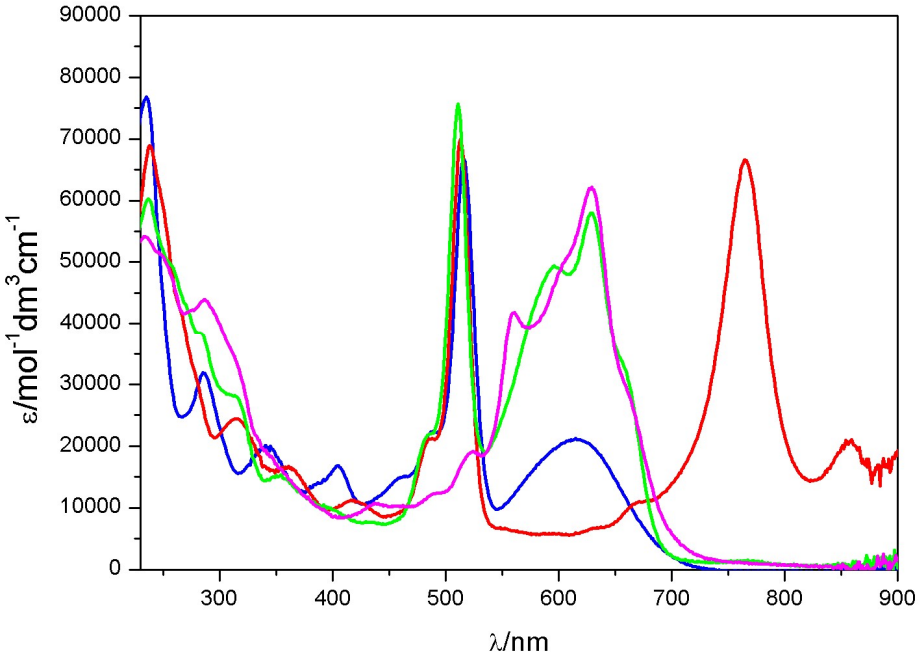

Figure 3.39. UV/vis absorption spectra recorded in DCM containing $[Bu_4N][BF_4]$ (0.4 M) using spectroelectrochemical methods for **3.19** at 243 K showing **3.19** (blue), $\mathbf{3.19^{\bullet-}}$ (red), $\mathbf{3.19^{2-}}$ (green) and $\mathbf{3.19^{3-}}$ (pink). c = 2.93 x 10^{-6} $mol^{-1}dm^3cm^{-1}$.

Reduction of the first two process in **3.19** results in the same behaviour observed previously; loss of the neutral PDI band, formation and removal of a red shifted band corresponding to the first reduction on the PDI then finally the formation of the second reduced PDI absorbance, Figure 3.39. The position of the reduced PDI peaks are again almost identical to the analogous peaks in following reduction of **3.8**. Similarly to **3.18** the intensity of the BODIPY band slightly increases upon PDI reduction and the original profile is reformed upon reoxidation of this process.

Reduction of the final process of **3.19** leads to the removal of the BODIPY absorbance and formation of the red shifted, first reduced BODIPY peak. This confirms that methyl-functionalisation of the BODIPY has moved the reduction process from

between the two PDI reductions to a more negative potential. Upon reoxidation of all three processes the PDI is shown to be fully reversible, however, the BODIPY moiety is not. The oxidation of **3.19** was not investigated spectroelectrochemically as it was not seen to be fully reversible by cyclic voltammetry.

	Neutral	**Reduction**		
		1st	**2nd**	**3rd**
3.18	238 (10.7), 283 (4.4), 336 (3.6), 384 (3.3), 513 (15.5), 561 (3.1)	239 (9.2), 335 (3.3), 513 (15.2), 744 (6.3), 830 (2.9)	238 (8.4), 338 (3.2), 510 (14.3), 583 (5.1), 623 (6.3)	238 (6.9), 284 (5.7), 523 (3.2), 558 (6.2), 625 (6.5)
3.19	235 (7.7), 285 (3.2), 337 (2.0), 402 (1.7), 514 (6.6), 605 (2.1)	238 (6.9), 314 (2.4), 361 (1.7), 513 (9.0), 765 (6.7), 854 (2.1)	237 (6.0), 511 (7.6), 596 (4.9), 628 (5.8)	286 (4.4), 524 (1.9), 562 (4.2), 629 (6.2)

Table 3.5. UV/vis spectroscopic data for **3.18** and **3.19** measured in DCM. All values λ_{max}/nm (ε x10^5/mol^{-1}dm^{3}cm^{-1}).

3.2.2.3. Perylene Diimide-CatecholateBODIPYs

The BODIPY absorption in the UV/vis spectrum of **3.20** is observed at 509 nm, 4 nm higher than **3.4** and 4 nm lower than **3.18**. Whilst the catechol would be expected to be electron donating (in comparison to fluorine), thus inducing a bathochromic shift, the boron acts as a node (see DFT below) preventing this effect from occurring resulting in a very small shift *vs*. **3.4**. The PDI absorption was measured at 552 nm hypsochromically shifted by 10 nm *vs*. **3.4**. The di(t-butyl)catecholate is known to possess an absorption at 285 nm.[62, 63] However, this absorption has a relatively low extinction coefficient (ε ~ 5,000 mol^{-1}dm^{3}cm^{-1}) and cannot be resolved from the more intense absorptions from the BODIPY and PDI chromophores in this system. Note the

peak at 283 nm (ε = 44,000 $mol^{-1}dm^3cm^{-1}$) is also observed in the PDI-BODIPYs discussed above so cannot be assigned solely to the catecholate. When the emission spectrum was collected for **3.20** no emission could be detected, under the experimental conditions, following excitation at 509 nm and 552 nm. This lack of fluorescence has been observed previously in catecholate-BODIPY species[15, 62] and is likely due to a reductive PET mechanism caused by electron transfer from the HOMO on the catechol to the vacated HOMO on the excited PDI or BODIPY resulting in a charge separated state thus preventing fluorescence.

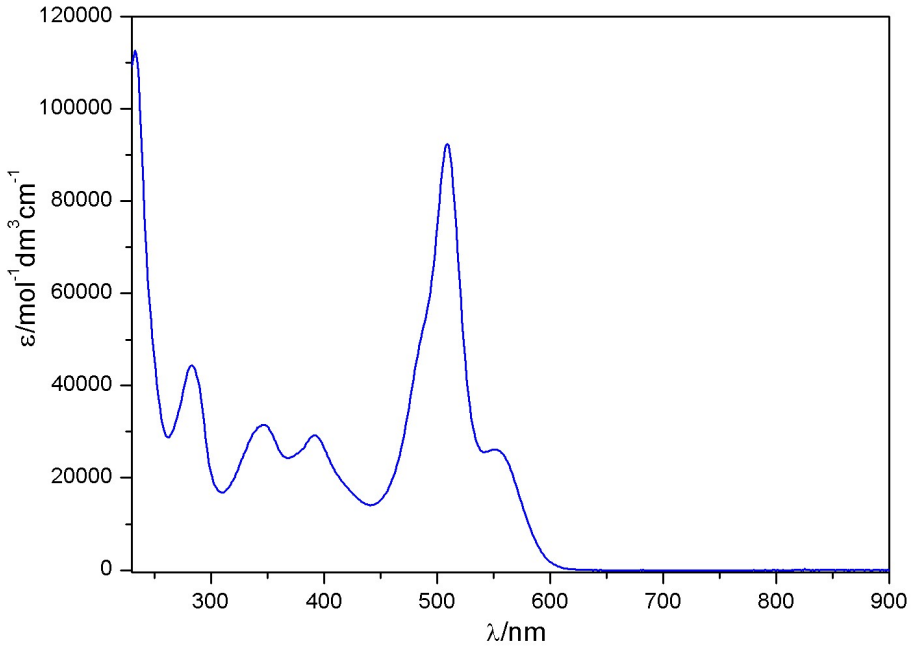

Figure 3.40. UV/vis absorption spectrum of **3.20** in DCM. c = 5.37 x 10^{-6} $mol^{-1}dm^3cm^{-1}$.

In the UV/vis spectrum of **3.21**, the BODIPY absorbance lies at 509 nm, identical to the corresponding absorbance in **3.20**. The PDI chromophore absorbs at 605 nm, the same as **3.19**. Once again, the catecholate absorbance cannot be distinguished from the stronger PDI/BODIPY absorbance. Emission measurements again showed no fluorescence, most likely due to quenching, following PET from the catecholate moiety.

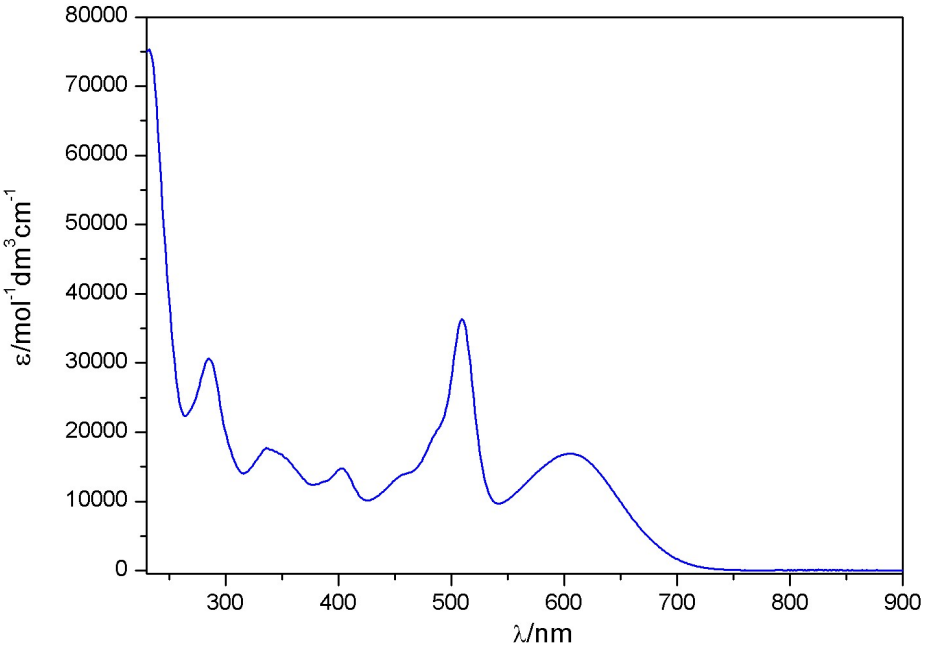

Figure 3.41. UV/vis absorption spectrum of **3.21** in DCM. c = 1.13 x 10^{-5} $mol^{-1}dm^3cm^{-1}$.

The substitution of the fluorine atoms with catecholate was intended to produce a system containing oxidation processes electronically separated from the rest of the molecule. 3,5-Di(t-butyl) catechol was chosen rather than unsubstituted catechol as previous work by Champness and co-workers has shown that the t-butyl groups help to stabilise the oxidation making it electrochemically reversible.[62]

Cyclic voltammetric studies on **3.20** show four one-electron reductions at -0.94, -1.12, -1.20 and -1.26 V and a two-electron oxidation at 0.60 V (*vs.* Fc/Fc^+), Figure 3.42 and Table 3.6. All of these processes were shown to be reversible over a scan rate range 0.02 – 0.3 Vs^{-1}. The reduction processes have almost identical potentials to those displayed by **3.4** showing that the addition of the catecholate has very little effect upon these processes. This can be explained by the presence of a node at the boron atom as shown by DFT (see below). The observation of four rather than three reduction processes shows that the communication between the BODIPY moieties across the PDI core has been preserved upon addition of catecholate. Addition of the catecholate has

had the desired effect of introducing a reversible two-electron oxidation into the system, separated by a node at the boron atom.

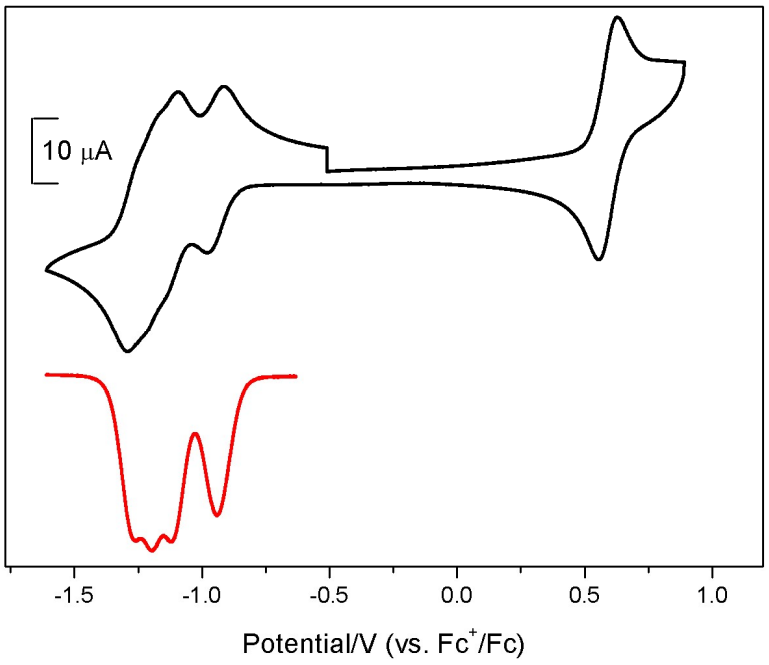

Figure 3.42. Cyclic (black) and square wave (red) voltammograms of **3.20** recorded in DCM containing $[Bu_4N][BF_4]$ (0.4 M).

Cyclic voltammetry shows that **3.21** posses three reversible reductions (over a scan rate range 0.02 – 0.3 Vs^{-1}) at -1.03, -1.16 and -1.29 V and one irreversible oxidation at 0.61 V (*vs.* Fc/Fc^+), Figure 3.43. All four of these processes are within 0.02 V of the analogous **3.8** showing again that the addition of catecholate has very little effect on the redox properties of the BODIPY and the PDI chromophores, due to the node at the BODIPY boron (see DFT). The addition of the catecholate was intended to supply an oxidation that could be investigated independently. However, it appears to overlap exactly with the oxidation seen on **3.8**. The irreversibility of this process is more likely due to the instability of the oxidation on the PDI core rather than that of the catecholate group.

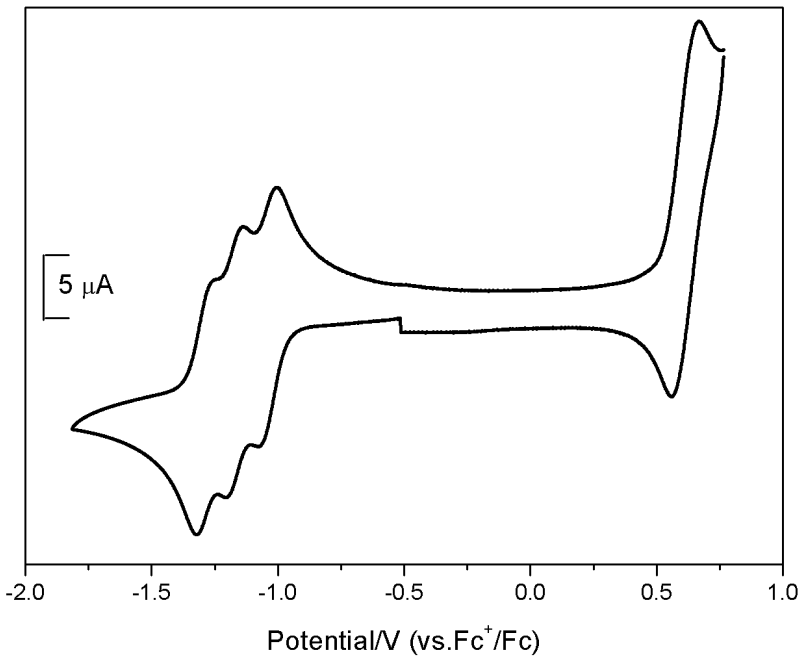

Figure 3.43. Cyclic voltammogram of **3.21** recorded in DCM containing [Bu_4N][BF_4] (0.4 M).

Compound	Reduction				Oxidation
	1st	2nd	3rd	4th	
3.20	-0.94	-1.12	-1.20	-1.26	0.60
3.21	-1.03	-1.16	-1.29	-	0.61

Table 3.6. Reduction potentials for **3.20** and **3.21**. All potentials reported as $E_{1/2}$ (= (E_p^a + E_p^c)/2) in V vs. Fc^+/Fc at 0.1 Vs^{-1} scan rate and quoted to the nearest 0.01 V.

DFT calculated MO isosurfaces of **3.20** and **3.21** show the LUMOs lying on the PDI part of the molecule, confirming the first reduction is centred on the PDI. In contrast to the systems discussed previously in this Chapter, the HOMOs for both of these molecules lie on the catecholate; the boron centre acts as a node isolating the HOMO from the rest of the molecule. This confirms that PET quenching, resulting in a charge separated state, is likely to be the cause of the lack of fluorescence in these systems. The LUMO energies were calculated to be -3.64 and -3.37 eV for **3.20** and **3.21** respectively, matching with the ease of first reduction of **3.20** *vs*. **3.21**. These values are 0.04 eV more negative than were calculated for **3.4** and **3.8** indicating very little change in reduction potential, this observation matches the experimental results. The energy of

the HOMOs of **3.20** and **3.21** were calculated to be -4.86 and -4.79 eV respectively, the HOMOs being at a very similar energy is replicated in the oxidation potentials, however, the overlap between the PDI and BODIPY oxidation in **3.21** makes accurately measuring the catecholate oxidation potential difficult.

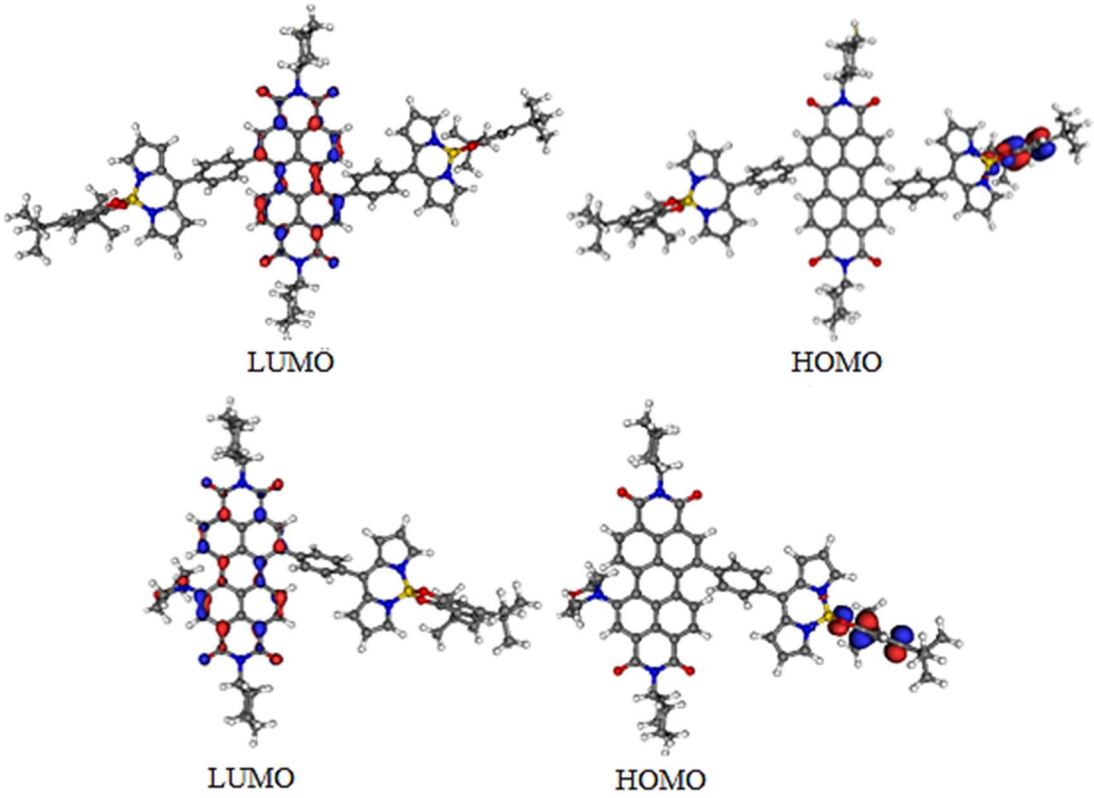

Figure 3.44. MO isosurfaces calculated by DFT **3.20** (top) and **3.21** (bottom).

Spectroelectrochemical methods were used to probe the absorption behaviour of **3.20** and **3.21** upon reduction and, in the case of **3.20**, upon oxidation, Table 3.7. As decomposition of the BODIPY moiety on **3.20** was predicted, the oxidation of the catecholate was the first process to be investigated. The absorption profile generated upon oxidation is not significantly different than the neutral species with the only changes being in the shape and intensity of the peaks between 300-450 nm with no new defined peaks being formed, Figure 3.45. Whilst spectroelectrochemistry does not reveal much about the absorption of the catecholate upon oxidation, it confirms that the process is reversible as the neutral profile is fully regenerated upon reoxidation. The

main absorption peaks corresponding to the BODIPY and PDI are unchanged indicating the oxidation does lie on the catecholate.

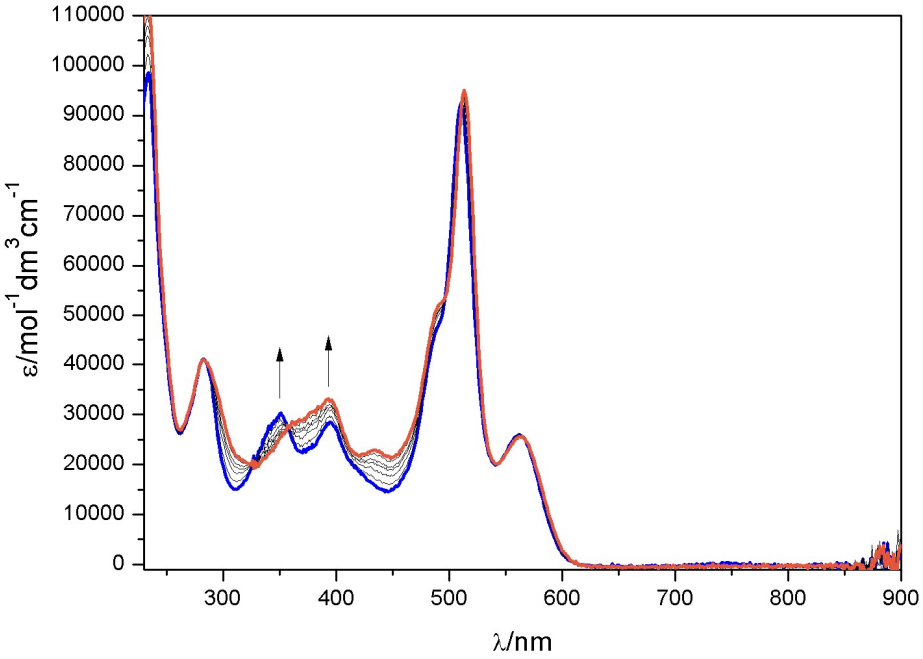

Figure 3.45. UV/vis absorption spectra recorded in DCM containing $[Bu_4N][BF_4]$ (0.4 M) using spectroelectrochemical methods for **3.20** at 243 K showing the inter-conversion of **3.20** (blue) to **3.20**$^{\bullet+}$ (orange). c = 1.38 x 10^{-4} $mol^{-1}dm^3cm^{-1}$. Arrows indicate the progress of the oxidation.

The node at the boron atom means that the behaviour of **3.20** upon reduction is almost identical to that observed for **3.4**, Figure 3.46. The first reduction is assigned to the PDI and the reduction to the tetraanion, necessitated by the overlap of the processes, results in the formation of absorbances corresponding to the reduced BODIPY and the second reduction on the PDI. The peak absorbances corresponded well to those measured for **3.4**. One of the aims of incorporating the catecholate onto the BODIPY was to attempt to stabilise the BODIPY reduction.[62] However, this has not been successful as upon reoxidation the BODIPY absorption is not fully regenerated, although the decrease in intensity is smaller than observed previously suggesting a slight stabilisation effect by the catecholate.

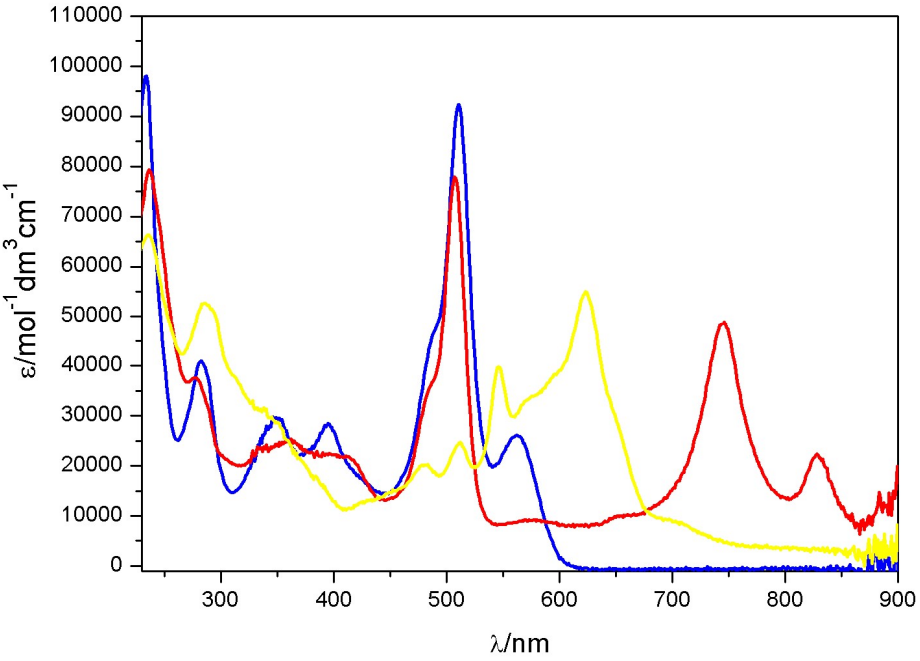

Figure 3.46. UV/vis absorption spectra recorded in DCM containing $[Bu_4N][BF_4]$ (0.4 M) using spectroelectrochemical methods for **3.20** at 243 K showing **3.20** (blue), **3.20**$^{\bullet-}$ (red) and **3.20**$^{4-}$ (yellow). c = 1.38 x 10^{-4} $mol^{-1}dm^3cm^{-1}$.

The UV/vis spectra following reduction of **3.21** are also minimally affected by the addition of catecholate (*vs*. **3.8**), again the BODIPY reduction is seen to be sandwiched between the first and second reduction on PDI with some overlap of the processes resulting in a slight loss of intensity on the first reduced PDI peak during reduction of the BODIPY, Figure 3.47. The catecholate again has a slight, but not complete, stabilisation effect on the BODIPY reduction. The catecholate oxidation was not investigated due to the instability of the underlying PDI oxidation.

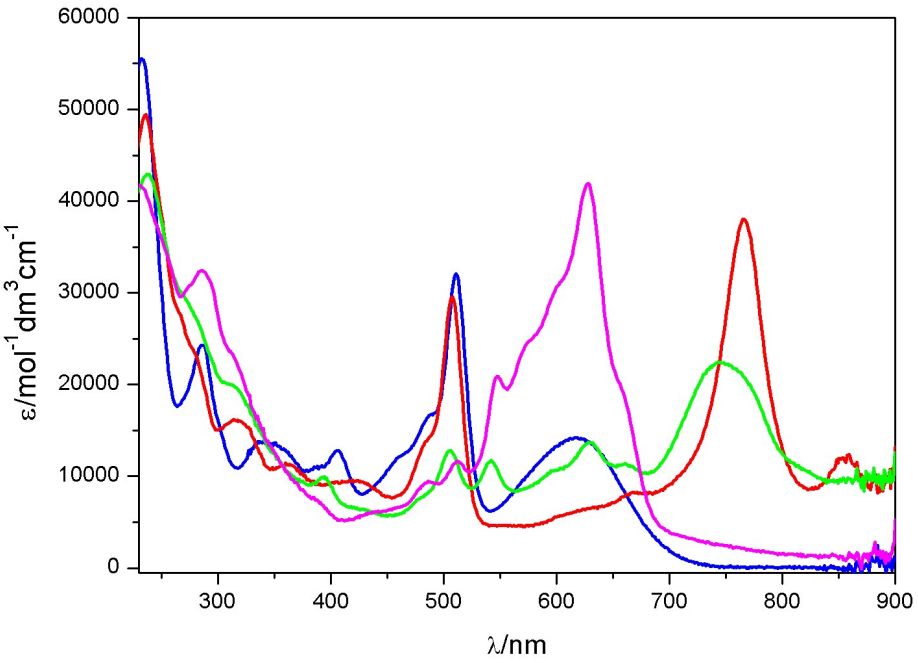

Figure 3.47. UV/vis absorption spectra recorded in DCM containing $[Bu_4N][BF_4]$ (0.4 M) using spectroelectrochemical methods for **3.21** at 243 K showing **3.21** (blue), $\mathbf{3.21^{\bullet-}}$ (red), $\mathbf{3.20^{2-}}$ (green) and $\mathbf{3.20^{3-}}$ (pink). c = 3.92 x 10^{-4} $mol^{-1}dm^3cm^{-1}$.

	Neutral	**Reduction**				**Oxidation**
		1st	**2nd**	**3rd**	**4th**	
3.20	283 (4.1), 347 (3.0), 392 (2.8), 509 (9.2), 552 (2.6)	236 (7.9), 362 (2.5), 507 (7.8), 746 (4.9), 828 (2.2)	-	-	286 (5.3), 483 (2.0), 512 (2.5), 546 (4.0), 623 (5.5)	283 (4.1), 396 (3.3), 513 (9.5), 562 (2.6)
3.21	285 (2.4), 336 (1.4), 403 (1.3), 509 (3.2), 605 (1.4)	236 (4.9), 314 (1.6), 507 (3.0), 766 (3.8), 857 (1.2)	392 (9.9), 505 (1.3), 542 (1.2), 628 (1.4), 744 (2.2)	284 (3.2), 512 (1.2), 547 (2.1), 628 (4.2)	-	-

Table 3.7. UV/vis spectroscopic data for **3.20** and **3.21** measured at 243 K in DCM from spectroelectrochemistry. All values λ_{max}/nm (ε x10^5/$mol^{-1}dm^3cm^{-1}$).

3.3. Conclusions

In total, seven PDI-BODIPY systems have been synthesised; dyads and triads bearing BODIPY, methylBODIPY and catecholateBODIPY at the PDI bay-positions and a pentad ortho-substituted PDI with four BODIPY units. The UV/vis spectra all revealed the expected combinations of the constituent parts of the molecules with morpholine substitution inducing a bathochromic shift onto the PDI, methyl-substituents pushing the BODIPY absorption to a higher wavelength whereas catecholate substitution has very little effect on the absorption profile.

Following excitation of the BODIPY moieties, emission spectra for **3.4**, **3.8**, **3.13** and **3.19** revealed a single fluorescence peak associated with the PDI moiety in all cases. This indicates that, following excitation, FRET is occurring due to the spectral overlap of the BODIPY emission and PDI absorption resulting in exclusive emission from the PDI, as seen in Akkaya's PDI-BODIPY systems.[41, 42] The fluorescence quantum yield of **3.8**, **3.13** and **3.19** is significantly quenched suggesting that, following FRET, a PET process results in the formation of a $PDI^{\bullet-}$-$BODIPY^{\bullet+}$ charge separated state preventing fluorescence. This process has previously been reported in Elmali's PDI-BODIPY systems,[43] however, in Elmali's case the photophysics are additionally complicated by the presence of an iodine atom on the BODIPY resulting in competition between FRET and ISC. The emission of **3.18** is completely quenched most likely due to highly efficient PET following FRET however this cannot be confirmed by emission measurements alone. The quantum yield of the emission of **3.4** is substantially higher than that of **3.8**, **3.13** and **3.19** indicating that it is not possible to form a charge separated state due to a greater degree of conjugation between the BODIPY and PDI moieties, as further indicated by the communication seen in the cyclic voltammetric measurements.

3.20 and **3.21** were found to be non-emissive following excitation of the PDI or BODIPY, this was assigned to PET from the catecholate to the excited BODIPY or PDI resulting in a charge separated state preventing fluorescence from occurring. Transient absorption measurements are currently underway in order to fully elucidate the behaviour of these compounds following excitation.

X-ray crystallography was used to determine the single crystal structures of **3.4**, **3.8** and **3.19**. All three were found to pack into pairs of molecules though the arrangement of the molecules within these pairs was found to differ considerably. In **3.4** the PDI cores are orientated in the same direction with the BODIPY moieties on top of one another but pushed apart by the twist in the perylene core, **3.8** shows the BODIPY moieties on opposite sides of the pair, reducing steric interaction, whilst in **3.19** the pair of molecules are arranged with the BODIPYs on the same side stabilised by a π-interaction with an adjacent pair of molecules.

Cyclic voltammetric investigations on **3.8** and **3.13** displayed the expected three individual reduction processes, with the BODIPY reduction being sandwiched between the two PDI reductions, whilst **3.4** possessed an additional reduction process assigned to communication across the PDI core. The addition of methyl-groups had the desired effect of pushing the BODIPY reduction of **3.18** to a more negative potential, thus resolving it from those of the PDI, allowing full spectroelectrochemical characterisation of each process. However, at the same time this disrupted the communication. No oxidation processes were observed for **3.4** however an irreversible process is present in **3.18**, this process is likely associated with the BODIPY moiety by comparison to other PDI-BODIPY systems[43] and confirmed by DFT. In the case of **3.19**, the methyl-groups pushed the reduction from between the first and second PDI reductions to a more

negative potential than both. The addition of di(t-butyl)catecholate did not affect the potentials of the PDI and BODIPY reductions. In the case of **3.20** the communication seen in **3.4** was maintained and a new two-electron reversible oxidation was introduced. An analogous oxidation was likely introduced into **3.21**, however, this process overlapped with an irreversible process on the PDI core so reversibility could not be confirmed. These oxidations are electronically isolated from the BODIPY and the PDI core by a node at the boron atom. DFT was used to calculate the molecular orbitals in order to confirm the position of the HOMOs and LUMOs and provide a comparison of the LUMO energies to the first reduction potentials of the systems. The oxidation and reduction potentials of all of the compounds reported in this chapter are presented in Table 3.8.

Compound	**Reduction**				**Oxidation**
	1st	**2nd**	**3rd**	**4th**	
3.4	-0.94	-1.12	-1.19	-1.26	-
3.8	-1.04	-1.18	-1.31	-	0.63
3.13	-0.93	-1.22	-	-	-
3.18	-0.97	-1.16	-1.43	-	-
3.19	-1.04	-1.23	-1.43	-	0.63
3.20	-0.94	-1.12	-1.20	-1.26	0.60
3.21	-1.03	-1.16	-1.29	-	0.61

Table 3.8. Summary of the oxidation and reduction potentials of the PDI-BODIPY systems reported in this chapter. All potentials reported as $E_{1/2}$ (= (E_p^a + E_p^c)/2) in V vs. Fc^+/Fc at 0.1 Vs^{-1} scan rate and quoted to the nearest 0.01 V.

Spectroelectrochemistry confirmed the assignments of the redox processes found in cyclic voltammetry to the individual parts of the molecule (PDI or BODIPY) and demonstrates the changes in the absorption properties of the systems upon oxidation and reduction. Formation of the PDI anion resulted in a red shift in the main PDI

absorption accompanied by an increase in intensity, formation of the dianion was accompanied by a blue shift whilst the BODIPY anion induced a slight red shift and a large decrease in intensity of the neutral BODIPY absorption. In all cases, the BODIPY reduction was not found to be electrochemically stable and was not fully regenerated upon reoxidation, however, the PDI absorption profiles were fully electrochemically stable. The only oxidation investigated by spectroelectrochemical methods was the oxidation of the catecholate on **3.20**, whilst dramatic absorption profile changes were not observed, the process was confirmed to be reversible.

3.4. Experimental

For experimental details relating to electrochemical and optical investigations (except emission, see below) and DFT see Chapter 2.

General Experimental Methods

All starting materials were purchased from Sigma Aldrich or Fisher Scientific and were used without further purification unless otherwise stated. Column chromatography was performed on silica gel (Merck silica gel 60, 0.2–0.5 mm, 50–130 mesh). Reactions using dry solvents (Sigma Aldrich) were carried out utilising standard Schlenk techniques. The ^{1}H, ^{13}C and ^{11}B NMR spectra were obtained on a Bruker 400 MHz spectrometer. MS spectra were determined on a VoyagerDE-STR spectrometer (MALDI-TOF) with DCTB as the matrix, a Bruker microTOF II spectrometer (ESI) or a JEOL GCv4G spectrometer (FI).

Emission Measurements

Emission measurements were carried out under ambient conditions on a Horiba FluoroMax-3 spectrometer with a xenon arc lamp as the excitation source. Quantum yields were calculated by plotting the integrated fluorescence intensity *vs*. absorbance of five optically dilute solutions ($\varepsilon < 0.1$ $mol^{-1}dm^{3}cm^{-1}$ at λ_{max}) of the sample and comparing the gradient to that of a known standard (Fluorescein) using the equation: $\phi_x = \phi_{st}\left(\frac{Grad_x}{Grad_{st}}\right)\left(\frac{\eta_x 2}{\eta_{st} 2}\right)$ where the subscripts *st* and *x* denote standard and test respectively, ϕ is the fluorescence quantum yield, *Grad* the gradient from the plot of integrated fluorescence intensity *vs*. absorbance and η the refractive index of the solvent.

3.4.1. Perylene Diimide-BODIPYs

Synthesis of *N,N'*-di(cycloxehyl)-1,7-dibromo-3,4:9,10-perylenetetracarboxylic diimide (3.1)

Synthesis adapted from a literature procedure.[49] A mixture of **2.1** (7.17 g, 13.0 mmol, crude), cyclohexylamine (3.8 mL, 33.2 mmol), acetic acid (3.8 mL) and *N*-methyl pyrrolidone (150 mL) was degassed with N_2 for 10 mins then heated to 85 ^oC, under an inert atmosphere, for 5 h. The reaction mixture was cooled to room temperature and poured into methanol, the resulting precipitate was filtered and washed with methanol. The crude product was adsorbed onto silica and purified by column chromatography (SiO_2, chloroform) to give **3.1**, in a mixture of 1,6-/1,7- isomers (~1:4 molar ratio), as a red powder (3.67 g, 5.15 mmol, 40 %). This mixture of isomers was then further purified by repeated layered recrystallisations (chloroform/methanol) to give **3.1** as the pure 1,7- isomer as red crystals (3.11 g, 4.36 mmol, 33 %). ^{1}H NMR (C_6D_6, 400 MHz): δ = 8.97 (d, *J*=8.2 Hz, 2 H), 8.83 (s, 2 H), 8.46 (d, *J*=8.3 Hz, 2 H), 5.35 (tt, *J*=12.2, 3.8 Hz, 2 H), 2.84 - 2.96 (m, *J*=12.1, 12.1, 12.1, 3.1 Hz, 4 H), 1.78 - 1.93 (m, 8 H), 1.27 - 1.44 ppm (m, 8 H). ^{13}C NMR (C_6D_6, 101 MHz): δ = 163.3, 162.8, 137.9, 132.8, 132.6, 130.0, 129.2, 128.4, 127.0, 123.7, 123.3, 120.7, 54.2, 29.1, 26.5, 25.4 ppm. MS(MALDI-TOF) $[M]^-$: calcd for $C_{36}H2_8Br_2N_2O_4$ 710.0, found 710.1.

Synthesis of *N,N'*-di-(cyclohexyl)-1,7-di(4-benzaldehyde)-3,4:9,10-perylenetetracarboxylic diimide (3.2)

3.1 (200 mg, 0.281 mmol), 4-formylphenyl boronic acid (140 mg, 0.933 mmol), potassium carbonate (800 mg, 5.80 mmol), $Pd(PPh_3)_4$ (40 mg, $3.46x10^{-2}$ mmol) and dioxane (50 mL) were degassed with N_2 for 20 min before heating at 80 ^oC, under an

inert atmosphere, for 17 hours. The solution was cooled to room temperature before the solvent was removed under reduced pressure. The crude product was the purified by column chromatography (SiO_2, chloroform:EtOAc 98:2) to give **3.2** as a pink powder (164 mg, 0.215 mmol, 77 %). ^{1}H NMR ($CDCl_3$, 400 MHz) δ: 10.17 (s, 2 H), 8.60 (s, 2 H), 8.16 (d, *J*=8.0 Hz, 2 H), 8.06 (d, *J*=8.2 Hz, 4 H), 7.70 - 7.80 (m, 6 H), 5.03 (tt, *J*=12.1, 3.4 Hz, 2 H), 2.55 (qd, *J*=12.3, 2.9 Hz, 4 H), 1.93 (d, *J*=12.9 Hz, 4 H), 1.76 (d, *J*=11.7 Hz, 6 H), 1.31 - 1.57 (m, 6 H) ppm. ^{13}C NMR ($CDCl_3$, 101 MHz): δ = 191.7, 163.8, 163.8, 148.4, 139.9, 136.4, 135.0, 134.3, 132.6, 131.7, 131.0, 130.2, 130.0, 129.3, 128.2, 123.5, 123.2, 54.4, 29.4, 26.8, 25.7 ppm. HRMS(FI-TOF) $[M]^+$: calcd for $C_{50}H_{38}N_2O_6$ 762.2730, found 762.2709.

Synthesis of *N,N'*-di-(cyclohexyl)-1,7-di(5-(4-phenyl)dipyrromethane)-3,4:9,10-perylenetetracarboxylic diimide (3.3)

3.2 (120 mg, 0.157 mmol) was dissolved in pyrrole (40 mL) and the solution degassed with N_2 for 15 min. TFA (0.025 mL, 0.327 mmol) was added and the solution was stirred for 5 min before being quenched with triethylamine (3 mL). The solvent was removed under reduced pressure and the crude product was purified by column chromatography (SiO_2, chloroform:EtOAc 94:6) to give **3.3** as purple solid (124 mg, 0.125 mmol, 79 %). ^{1}H NMR ($CDCl_3$,400 MHz): δ = 8.60 (s, 2 H), 8.16 (d, *J*=8.0 Hz, 2 H), 8.10 (br. s., 4 H), 7.86 (d, *J*=8.2 Hz, 2 H), 7.52 (d, *J*=8.2 Hz, 4 H), 7.37 (d, *J*=8.2 Hz, 5 H), 6.81 - 6.87 (m, 4 H), 6.28 (q, *J*=2.8 Hz, 4 H), 5.97 - 6.05 (m, 4 H), 5.64 (s, 2 H), 5.05 (tt, *J*=12.2, 3.7 Hz, 2 H), 2.51 - 2.63 (m, 5 H), 1.89 - 1.97 (m, 4 H), 1.73 - 1.81 (m, 6 H), 1.42 - 1.55 ppm (m, 6 H). The sample was not sufficiently stable to acquire a ^{13}C NMR. HRMS(FI-TOF) $[M]^+$: calcd for $C_{66}H_{54}N_6O_4$ 994.4207, found 994.4193.

Synthesis of *N,N'*-di-(cyclohexyl)-1,7-di(8-(4-phenyl) BODIPY)-3,4:9,10-perylenetetracarboxylic diimide (3.4)

3.3 (120 mg, 0.110 mmol) was dissolved in DCM (25 mL) and the solution was degassed with N_2 for 15 min before *p*-chloranil (87 mg, 0.350 mmol) was added and the solution stirred at room temperature, under an inert atmosphere, for 18 hours. The solvent was removed under reduced pressure and the dipyrrin was purified by column chromatography (SiO_2, chloroform:EtOAc 88:12) to remove any unreacted starting material and *p*-chloranil. The dipyrrin was redissolved in DCM (10 mL) and the solution was degassed with N_2 for 10 min, $BF_3.OEt_2$ (0.25 mL) and triethylamine (0.25 mL) were added and the solution was stirred, under an inert atmosphere, for a further 3 hours. HCl (2 M) was added and the solution was washed twice with HCl, once with water then dried with $MgSO_4$ and the solvent removed under reduced pressure. The crude product was purified by column chromatography (SiO_2, chloroform:EtOAc 97:3) to give **3.4** as a red powder (64 mg, 0.0589 mmol, 49 %). ^{1}H NMR ($CDCl_3$, 400 MHz): δ = 8.68 (s, 2 H), 8.23 (d, *J*=8.2 Hz, 2 H), 8.03 (s, 4 H), 7.92 (d, *J*=8.0 Hz, 2 H), 7.70 - 7.81 (m, 8 H), 7.04 (d, *J*=3.9 Hz, 4 H), 6.62 - 6.72 (m, 4 H), 5.04 (tt, *J*=12.1, 3.5 Hz, 2 H), 2.56 (qd, *J*=1.0 Hz, 4 H), 1.92 (d, *J*=12.7 Hz, 4 H), 1.77 (d, *J*=8.5 Hz, 6 H), 1.37 - 1.55 ppm (m, 6 H). ^{13}C NMR ($CDCl_3$, 126 MHz): δ = 163.6, 163.6, 145.9, 144.7, 144.7, 139.7, 135.1, 134.8, 134.3, 134.2, 132.4, 132.2, 131.3, 130.4, 129.4, 129.3, 129.2, 128.1, 123.2, 123.0, 119.0, 54.1, 29.1, 26.5, 25.4 ppm. ^{11}B NMR ($CDCl_3$, 128 MHz) δ = 0.32 ppm (t, *J*=28.37 Hz). HRMS(FI-TOF) $[M]^+$: calcd for $C_{66}H_{48}B_2F_4N_6O_4$ 1086.3859, found 1086.38538.

Synthesis of *N,N'*-di-(cyclohexyl)-1-bromo-7-morpholino-3,4:9,10-perylenetetracarboxylic diimide (3.5)

3.1 (600 mg, 0.845 mmol) was dissolved in morpholine and the reaction mixture was heated to 60 ºC for 4 days. The solution was cooled to room temperature and poured into HCl (2 M), chloroform was added and the organic extract was washed with HCl and water twice before drying over $MgSO_4$ and removal of the solvent under reduced pressure. The crude product was purified by column chromatography (SiO_2, chloroform:EtOAc 95:5) to give **3.5** as blue crystals (364 mg, 0.506 mmol, 60 %). ^{1}H NMR ($CDCl_3$, 400 MHz): δ = 9.69 (d, *J*=8.3 Hz, 1 H), 9.36 (d, *J*=8.2 Hz, 1 H), 8.80 (s, 1 H), 8.55 (d, *J*=8.3 Hz, 1 H), 8.49 (d, *J*=8.2 Hz, 1 H), 8.46 (s, 1 H), 4.97 - 5.10 (m, *J*=12.1, 12.1, 2.5 Hz, 2 H), 3.83 - 4.02 (m, 4 H), 3.38 (d, *J*=12.2 Hz, 2 H), 3.07 - 3.19 (m, 2 H), 2.49 - 2.64 (m, 4 H), 1.87 - 1.99 (m, *J*=11.8 Hz, 4 H), 1.70 - 1.83 (m, 6 H), 1.31 - 1.55 ppm (m, 6 H). ^{13}C NMR ($CDCl_3$, 101 MHz): δ = 163.8, 163.7, 163.3, 162.8, 151.0, 137.9, 134.5, 133.8, 132.7, 130.6, 129.7, 129.5, 128.4, 127.8, 127.3, 124.4, 124.4, 123.8, 123.6, 123.1, 122.4, 122.0, 121.8, 119.0, 66.4, 54.1, 54.1, 51.6, 29.1, 29.1, 26.5, 26.5, 25.4, 25.4 ppm. HRMS(MALDI-TOF) $[M]^+$: calcd for $C_{40}H_{36}BrN_3O_5$ 717.1838, found 717.1846.

Synthesis of *N,N'*-di-(cyclohexyl)-1-(4-benzaldehyde)-7-morpholino-3,4:9,10-perylenetetracarboxylic diimide (3.6)

A mixture of **3.5** (300 mg, 0.417 mmol), 4-formylphenyl boronic acid (104 mg, 0.693 mmol), potassium carbonate (620 mg, 4.49 mmol), $Pd(PPh_3)_4$ (30 mg, 0.0260 mmol), water (5 mL) and dioxane (90 mL) were degassed for 15 mins then heated to 80 ºC, under an inert atmosphere, for 19 h. The solution was cooled to room temperature and poured into water. The product was extracted into chloroform and washed with water

three times before drying over $MgSO_4$ and removal of the solvent under reduced pressure. The crude product was purified by column chromatography (SiO_2, chloroform:EtOAc 93:7) to give **3.6** as a blue powder (277 mg, 0.372 mmol, 89 %). ^{1}H NMR ($CDCl_3$, 400 MHz): δ = 10.11 (s, 1 H), 9.72 (d, *J*=8.2 Hz, 1 H), 8.59 (d, *J*=8.3 Hz, 1 H), 8.52 (s, 1 H), 8.43 (s, 1 H), 7.96 (d, *J*=8.2 Hz, 1 H), 7.98 (d, *J*=8.3 Hz, 2 H), 7.68 (d, *J*=8.2 Hz, 2 H), 7.59 (d, *J*=8.2 Hz, 1 H), 4.93 - 5.13 (m, 2 H), 3.87 - 4.05 (m, 4 H), 3.38 - 3.51 (m, *J*=12.1 Hz, 2 H), 3.11 - 3.25 (m, 2 H), 2.46 - 2.67 (m, 4 H), 1.86 - 1.99 (m, 4 H), 1.69 - 1.86 (m, 6 H), 1.29 - 1.57 ppm (m, 6 H). ^{13}C NMR ($CDCl_3$, 101 MHz): δ = 191.4, 163.7, 163.7, 163.6, 151.0, 148.4, 138.1, 135.8, 135.3, 134.5, 133.1, 132.9, 131.3, 130.9, 130.8, 129.9, 129.9, 129.0, 128.0, 127.3, 124.7, 124.4, 123.9, 123.2, 122.7, 122.4, 122.3, 121.9, 66.4, 54.0, 54.0, 51.6, 29.1, 26.5, 26.5, 25.4, 25.4 ppm. HRMS(FI-TOF) $[M]^+$: calcd for $C_{47}H_{41}N_3O_6$ 743.2995, found 743.2990.

Synthesis of *N,N'*-di-(cyclohexyl)-1-(5-(4-phenyl)-dipyrromethane)-7-morpholino-3,4:9,10-perylenetetracarboxylic diimide (3.7)

3.6 (298 mg, 0.401 mmol) was dissolved in pyrrole (100 mL) and the solution was degassed with N_2 for 15 min. TFA (32 μL, 0.418 mmol) was added and the solution was stirred for 5 mins, the solution was quenched by the addition of triethylamine (5 mL) followed by stirring for a further 10 mins. The solvent was removed under reduced pressure and the residue was purified by column chromatography (SiO_2, chloroform:EtOAc 92:8) to give **3.7** a blue powder (355 mg, 0.390 mmol, 97 %). ^{1}H NMR ($CDCl_3$, 400 MHz): δ = 9.73 (d, *J*=8.3 Hz, 1 H), 8.55 (d, *J*=8.3 Hz, 1 H), 8.52 (s, 1 H), 8.41 (s, 1 H), 8.07 (br. s., 2 H), 7.97 (d, *J*=8.2 Hz, 1 H), 7.72 (d, *J*=8.2 Hz, 1 H), 7.42 (d, *J*=8.2 Hz, 2 H), 7.30 (d, *J*=8.2 Hz, 2 H), 6.74 - 6.83 (m, 2 H), 6.23 (q, *J*=2.8 Hz, 2 H), 5.96 (br. s., 2 H), 5.58 (s, 1 H), 4.94 - 5.13 (m, 2 H), 3.85 - 4.04 (m, 4 H),

3.36 - 3.50 (m, *J*=12.0 Hz, 2 H), 3.09 - 3.23 (m, *J*=9.7, 9.7 Hz, 2 H), 2.46 - 2.67 (m, 4 H), 1.85 - 1.99 (m, *J*=10.5 Hz, 4 H), 1.69 - 1.85 (m, 6 H), 1.33 - 1.55 ppm (m, 6 H). Acquisition of a ^{13}C NMR was not possible due to the instability of the product in solution. HRMS(MALDI-TOF) $[M]^+$: calcd for $C_{55}H_{49}N_5O_5$ 859.3734, found 859.3694.

Synthesis of *N,N'*-di-(cyclohexyl)-1-(8-(4-phenyl) BODIPY)-7-morpholino-3,4:9,10-perylenetetracarboxylic diimide (3.8)

3.7 (50 mg, 0.0582 mmol) was dissolved in DCM (8 mL) and the solution was degassed with N_2 for 15 min. p-Chloranil (18 mg, 0.0732 mmol) dissolved in DCM (4 mL) was added to the solution dropwise and the solution was stirred, under an inert atmosphere, for 23 h. Triethylamine (0.05 mL) was added followed by $BF_3.OEt_2$ (0.05 mL) and the solution was stirred for a further 24 h. The reaction was quenched by the addition of HCl (2 M) and the organic extracts were washed with HCl twice and water followed by drying over $MgSO_4$ and removal of the solvent under reduced pressure. The crude product was purified by column chromatography (SiO_2, chloroform:EtOAc 95:5) to give **3.8** as a blue powder (34 mg, 0.0375 mmol, 64 %). ^1H NMR ($CDCl_3$, 400 MHz): δ = 9.78 (d, *J*=8.3 Hz, 1 H), 8.56 - 8.67 (m, 2 H), 8.47 (s, 1 H), 8.05 (d, *J*=8.2 Hz, 1 H), 8.00 (s, 2 H), 7.79 (d, *J*=8.2 Hz, 1 H), 7.65 - 7.74 (m, 4 H), 7.00 (d, *J*=4.0 Hz, 2 H), 6.65 (d, *J*=3.3 Hz, 2 H), 4.92 - 5.17 (m, 2 H), 3.88 - 4.08 (m, 4 H), 3.42 - 3.54 (m, *J*=12.0 Hz, 2 H), 3.14 - 3.27 (m, 2 H), 2.44 - 2.70 (m, 4 H), 1.86 - 2.01 (m, *J*=11.3 Hz, 4 H), 1.71 - 1.84 (m, 6 H), 1.38 - 1.57 ppm (m, 6 H). ^{13}C NMR ($CDCl_3$, 101 MHz): δ = 163.8, 163.7, 163.7, 163.7, 151.0, 146.0, 145.0, 144.6, 138.2, 135.5, 134.8, 133.8, 133.5, 132.9, 132.1, 131.3, 130.9, 130.6, 130.1, 129.2, 129.1, 128.1, 127.1, 124.8, 124.4, 123.9, 123.3, 122.8, 122.5, 122.4, 122.0, 119.0, 118.9, 66.4, 54.1, 54.0, 51.6,

29.1, 26.5, 26.5, 25.4, 25.4 ppm. ^{11}B NMR ($CDCl_3$, 128 MHz): δ = 0.03 ppm (t, *J*=28.4). HRMS(MALDI-TOF) $[M]^+$: calcd for $C_{55}H_{46}BF_2N_5O_5$ 905.3560, found 905.3527.

Synthesis of 4-bromophenyl dipyrromethane (3.9)

Synthesis adapted from a literature procedure.[64] 4-Bromo benzaldehyde (3.00 g, 16.22 mmol) was dissolved in pyrrole (100 mL) and the solution was degassed with N_2 for 15 mins. TFA (0.12 mL, 1.57 mmol) was added and the solution was stirred at room temperature, under an inert atmosphere, for 5 h. The reaction was quenched by the addition of sodium hydroxide (2.5 g), the solution filtered and the solvent removed under reduced pressure. The crude product was purified by column chromatography (SiO_2, chloroform:hexane 1:3) and washed with hexane to give **3.9** as a white powder (3.38g, 11.2 mmol, 69 %). ^{1}H NMR ($CDCl_3$, 400 MHz): δ = 7.91 (br. s., 2 H), 7.41 - 7.50 (m, 2 H), 7.05 - 7.14 (m, 2 H), 6.72 (s, 2 H), 6.18 (q, *J*=2.8 Hz, 2 H), 5.85 - 5.94 (m, 2 H), 5.44 ppm (s, 1 H). ^{13}C NMR ($CDCl_3$, 101 MHz): δ = 141.1, 131.8, 131.7, 130.1, 120.8, 117.5, 108.5, 107.4, 43.4 ppm. HRMS(ESI) $[M+Na]^+$: calcd for $C_{15}H_{13}BrN_2Na$ 323.0154, found 323.0151.

Synthesis of 4-bromophenyl BODIPY (3.10)

Synthesis adapted from a literature procedure.[64] **3.9** (2.00 g, 6.64 mmol) was dissolved in DCM (150 mL) and the solution was cooled to 0 ºC and degassed with N_2 for 20 min. DDQ (1.81 g, 7.97 mmol) dissolved in DCM (50 mL) was added to the solution dropwise and the solution was stirred, under an inert atmosphere, for 1 h. Triethylamine (6.5 mL) was added followed by $BF_3.OEt_2$ (5.8 mL) and the solution warmed to room temperature then stirred for a further 2 h. The reaction was quenched by the addition of HCl (2 M) and the organic extracts were washed with HCl twice and water followed by drying over $MgSO_4$ and removal of the solvent under reduced pressure. The crude

product was purified by column chromatography (SiO_2, chloroform:hexane 3:2) to give **3.10** as a red crystalline solid (475 mg, 1.28 mmol, 19 %). ^{1}H NMR ($CDCl_3$, 400 MHz): δ = 7.96 (s, 2 H), 7.63 - 7.76 (m, 2 H), 7.38 - 7.54 (m, 2 H), 6.92 (d, *J*=4.1 Hz, 2 H), 6.57 ppm (d, *J*=3.6 Hz, 2 H). ^{13}C NMR ($CDCl_3$, 101 MHz): δ = 145.7, 144.5, 134.7, 132.6, 131.8, 131.3, 125.5, 118.8, 118.8 ppm. HRMS(ESI) $[M+Na]^+$: calcd for $C_{15}H_{10}BBrF_2N_2Na$ 368.9981, found 368.9983.

Synthesis of *N,N'*-di(1-ethylpropyl)-3,4:9,10-perylenetetracarboxylic diimide (3.11)

Synthesis adapted from a literature procedure.[65] PDA (1.00 g, 2.55 mmol), 3-aminopentane (0.72 mL, 6.19 mmol) and imidazole were heated at 180 ºC for 4 h. The reaction mixture was cooled to room temperature, chloroform was added and the organic layer was washed twice with HCl (2 M) and once with brine. The solution was dried over $MgSO_4$ and the solvent removed under reduced pressure. The crude product was purified by column chromatography (SiO_2, chloroform:methanol 1000:2) to give **3.11** as a red powder (1.183 g, 2.23 mmol, 87 %). ^{1}H NMR ($CDCl_3$, 400 MHz): δ = 8.62 (d, *J*=8.0 Hz, 4 H), 8.53 (d, *J*=8.0 Hz, 4 H), 5.00 - 5.14 (m, *J*=9.5, 9.5, 5.9, 5.9 Hz, 2 H), 2.19 - 2.35 (m, 4 H), 1.89 - 2.04 (m, 4 H), 0.95 ppm (t, *J*=7.5 Hz, 12 H). ^{13}C NMR ($CDCl_3$, 101 MHz): δ = 164.2, 134.3, 131.3, 129.5, 126.3, 123.5, 122.9, 57.7, 25.0, 11.4 ppm. MS(MALDI-TOF) $[M]^-$: calcd for $C_{34}H_{30}N_2O_4$ 530.2, found 530.2.

Synthesis of *N,N'*-Di(1-ethylpropyl)-2,5,8,11-tetra(4,4,5,5-tetramethyl-1,3,2-dioxaborolan-2-yl)perylene-3,4:9,10-tetracarboxylic diimide (3.12)

Synthesis adapted from a literature procedure.[51] **3.11** (2.00 g, 3.77 mmol), $[Ir(OMe)(cod)]_2$ (160 mg, 0.241 mmol), bis(pinacolato)diboron (7.1 g, 28.0 mmol) and tris(pentafluorophenyl)phosphine (310 mg, 0.583 mmol) were dissolved in dry dioxane

(100 mL) and heated at 115 ºC, under an inert atmosphere, for 2 d. The solution was cooled to room temperature and the solvent removed under reduced pressure before the crude product was dry loaded onto silica and purified by column chromatography (SiO_2, chloroform:EtOAc 95:5) to give **3.12** as the major product, with a small amount of lesser substituted products still present, as an orange powder (2.37 g, 2.29 mmol, 61 % crude). ^{1}H NMR ($CDCl_3$, 400 MHz): δ = 8.53 (s, 4 H), 4.86 - 4.99 (m, 2 H), 2.13 - 2.24 (m, 4 H), 1.90 - 2.00 (m, 4 H), 0.93 ppm (t, *J*=7.5 Hz, 12 H). MS(MALDI-TOF) $[M]^-$: calcd for $C_{58}H_{74}B_4N_2O_{12}$ 1034.6, found 1034.4.

Synthesis of *N,N'*-Di(1-ethylpropyl)-2,5,8,11-tetra(8-(4-phenyl)-BODIPY)perylene-3,4:9,10-tetracarboxylic diimide (3.13)

3.12 (95 mg, 0.0918 mmol), **3.10** (175 mg, 0.504 mmol), $Pd(PPh_3)_4$ (21 mg, 0.0182 mmol) and potassium carbonate (280 mg, 2.08 mmol) were dissolved in dioxane (20 mL) and the solution was degassed with N_2 for 20 mins before heating at 80 ºC, under an inert atmosphere, for 15 h. The solution was cooled to room temperature, filtered and the solvent removed under reduced pressure. The crude product was dry loaded onto silica and purification was attempted by column chromatography (SiO_2, chloroform:acetone 98:2) to give **3.13** as a slightly impure red powder (51 mg, 0.0320 mmol, 35 %). Other column conditions attempted included chloroform/methanol, chloroform/acetone and hexane/ethyl acetate of varying ratios. Recrystallisations were attempted from chloroform/hexane and chloroform/methanol. ^{1}H NMR ($CDCl_3$, 400 MHz): δ = 8.61 (s, 4 H), 8.00 - 8.03 (m, 8 H), 7.78 (d, *J*=8.2 Hz, 8 H), 7.67 (d, *J*=8.3 Hz, 8 H), 7.13 (d, *J*=3.7 Hz, 8 H), 6.62 (dd, *J*=4.2, 1.8 Hz, 8 H), 4.81 - 4.91 (m, 2 H), 2.00 - 2.14 (m, 4 H), 1.76 - 1.89 (m, 4 H), 0.93 ppm (t, *J*=7.4 Hz, 12 H). The compound

was not sufficiently soluble for the acquisition of a ^{13}C NMR. MS(MALDI-TOF) $[M]^-$: calcd for $C_{94}H_{66}B_4F_8N_{10}O_4$ 1594.5, found 1594.3.

3.4.2. Perylene Diimide-MethylBODIPYs

Synthesis of 1-methylpyrrole (3.14)

Synthesis adapted from a literature procedure.[66] Pyrrole-2-carboxaldehyde (3.00 g, 53.7 mmol) was dissolved in dry THF (60 mL), the solution was cooled in an ice bath before $LiAlH_4$ (3.60 g, 94.7 mmol) was added slowly. The solution was then heated to 75 ºC and stirred, under an inert atmosphere, for 17 h. The reaction mixture was cooled to room temperature and poured slowly into ice water. EtOAc was added and the organic extract washed with water three times before drying over $MgSO_4$ and removal of the solvent under reduced pressure to give **3.14** as a light yellow oil (2.21 g, 27.2 mmol, 61 %). ^1H NMR ($CDCl_3$, 400 MHz): δ = 7.92 (br. s., 1 H), 6.62 - 6.73 (m, 1 H), 6.16 (q, *J*=2.8 Hz, 1 H), 5.94 (br. s., 1 H), 2.31 ppm (s, 3 H). ^{13}C NMR ($CDCl_3$, 101 MHz): δ = 127.5, 116.2, 108.4, 105.8, 12.9 ppm

Synthesis of 4-formylphenyl pinacol boronic ester (3.15)

Synthesis adapted from a literature procedure.[67] 4-Formylphenyl boronic acid (3.00 g, 20.0 mmol) was dissolved in diethyl ether (35 mL), pinacol (2.81 g, 23.8 mmol) was added and the solution was stirred at room temperature for 18 h. The solution was washed with water three times, dried over $MgSO_4$ and the solvent removed under reduced pressure to give **3.15** as a white crystalline solid (4.223 g, 18.2 mmol, 91 %). ^1H NMR ($CDCl_3$, 400 MHz): δ = 10.05 (s, 1 H), 7.94 - 8.00 (m, *J*=8.0 Hz, 2 H), 7.83 - 7.91 (m, 2 H), 1.37 ppm (s, 12 H). ^{13}C NMR ($CDCl_3$, 101 MHz): δ = 192.6, 138.1, 135.2, 128.7, 84.3, 24.9 ppm.

Synthesis of 8-(4-pinacol boronic ester phenyl)-3,5-dimethyl BODIPY (3.17)

3.15 (2.43 g, 10.5 mmol) was dissolved in DCM (100 mL) and the solution was degassed for 15 mins. TFA (0.15 mL, 1.96 mmol) was added and the solution was stirred for 1.5 h under an inert atmosphere before the reaction was quenched by the addition of triethylamine (0.5 mL) and the solvent removed under reduced pressure to give **3.16**. **3.16** was redissolved in DCM (200 mL) and the solution was cooled in an ice bath and degassed with N_2 for 15 mins. DDQ (2 g, 8.81 mmol), dissolved in DCM (75 mL), was added slowly to the reaction mixture before stirring at 0 ºC for 1.5 h. Triethylamine (7 mL) followed by $BF_3.OEt_2$ (7 mL) were added and the mixture was warmed to room temperature and stirred for a further 1.5 h. The reaction was quenched by the addition of HCl (2 M) and the organic extract was washed with HCl (2 M) once and water twice, dried over $MgSO_4$ and the solvent removed under reduced pressure. The crude product was purified by column chromatography (SiO_2, chloroform), followed by further washing with HCl (2M) to remove triethylamine residues, to give **3.17** as a red powder (291 mg, 0.706 mmol, 7 %). ^{1}H NMR ($CDCl_3$, 400 MHz): δ = 7.92 (d, *J*=8.2 Hz, 2 H), 7.50 (d, *J*=7.9 Hz, 2 H), 6.70 (d, *J*=4.0 Hz, 2 H), 6.27 (d, *J*=4.1 Hz, 2 H), 2.66 (s, 6 H), 1.39 ppm (s, 12 H). ^{13}C NMR ($CDCl_3$, 101 MHz): δ = 157.6, 142.4, 136.7, 134.4, 130.3, 129.6, 119.4, 119.4, 84.1, 24.9, 14.9 ppm. HRMS(ESI) $[M+Na]^+$: calcd for $C_{23}H_{26}B_2F_2N_2NaO_2$ 445.2041, found 445.2040.

Synthesis of *N,N'*-dicycloxehyl-1,7-di(8-(4-phenyl)-3,5-dimethyl BODIPY)-3,4:9,10-perylenetetracarboxylic diimide (3.18)

3.1 (100 mg, 0.140 mmol), **3.17** (124 mg, 0.291 mmol), potassium carbonate (180 mg, 1.30 mmol) and $Pd(PPh_3)_4$ (25 mg, 0.0216) were dissolved in dioxane (25 mL) and water (1 mL), the solution was degassed with N_2 then heated to 90 ºC, under an inert

atmosphere, for 17 h. The solution was cooled to room temperature, dried over $MgSO_4$ and the solvent removed under reduced pressure. The crude product was purified by column chromatography (SiO_2, chloroform:acetone 99:1) to give **3.18** as a red powder (91 mg, 0.0796 mmol, 57 %). ^{1}H NMR ($CDCl_3$, 400 MHz): δ = 8.66 (s, 2 H), 8.21 (d, *J*=8.0 Hz, 2 H), 7.91 (d, *J*=8.5 Hz, 2 H), 7.71 (d, *J*=8.3 Hz, 4 H), 7.66 (d, *J*=8.5 Hz, 4 H), 6.80 (d, *J*=4.0 Hz, 4 H), 6.39 (d, *J*=0.8 Hz, 4 H), 4.95 - 5.11 (m, 2 H), 2.71 (s, 12 H), 2.48 - 2.63 (m, 4 H), 1.92 (d, *J*=12.8 Hz, 4 H), 1.70 - 1.82 (m, *J*=9.0 Hz, 6 H), 1.33 - 1.52 ppm (m, 6 H). ^{13}C NMR ($CDCl_3$, 101 MHz): δ = 163.7, 163.6, 158.2, 143.9, 141.1, 139.9, 135.1, 134.5, 134.4, 134.4, 132.4, 132.1, 130.3, 130.1, 129.4, 129.2, 129.0, 128.0, 123.1, 122.9, 119.9, 54.1, 29.1, 26.5, 25.4, 15.0 ppm. ^{11}B NMR ($CDCl_3$, 128 MHz): δ = 0.98 ppm (t, *J*=30.3). HRMS(FI-TOF) $[M]^+$: calcd for $C_{70}H_{56}B_2F_4N_6O_4$ 1142.4485, found 1142.44798.

Synthesis of *N,N'*-dicycloxehyl-1-(8-(4-phenyl)-3,5-dimethyl BODIPY)-7-morpholino-3,4:9,10-perylenetetracarboxylic diimide (3.19)

3.5 (50 mg, 0.0695 mmol), **3.17** (32 mg, 0.0758 mmol), potassium carbonate (50 mg, 0.362 mmol) and $Pd(PPh_3)_4$ (15 mg, 0.0130 mmol) were dissolved in dioxane (25 mL) and water (1 mL), the solution was degassed with N_2 then heated to 90 ºC, under an inert atmosphere, for 18 h. The solution was cooled, dried over $MgSO_4$ and the solvent removed under reduced pressure. The crude product was purified by column chromatography (SiO_2, chloroform:acetone 98:2) to give **3.19** as a blue/purple powder (33 mg, 0.0353 mmol, 51 %). ^{1}H NMR ($CDCl_3$, 400 MHz): δ = 9.73 (d, *J*=8.2 Hz, 1 H), 8.56 - 8.64 (m, 2 H), 8.44 (s, 1 H), 8.02 (d, *J*=8.2 Hz, 1 H), 7.76 (d, *J*=8.2 Hz, 1 H), 7.63 (d, *J*=8.3 Hz, 2 H), 7.60 (d, *J*=8.8 Hz, 2 H), 6.77 (d, *J*=4.1 Hz, 2 H), 6.36 (d, *J*=2.6 Hz, 2 H), 4.93 - 5.17 (m, 2 H), 3.88 - 4.04 (m, 4 H), 3.45 (d, *J*=11.7 Hz, 2 H), 3.13 -

3.25 (m, 2 H), 2.69 (s, 6 H), 2.46 - 2.62 (m, 4 H), 1.86 - 1.99 (m, 4 H), 1.73 - 1.84 (m, 6 H), 1.37 - 1.54 ppm (m, 6 H). ^{13}C NMR ($CDCl_3$, 101 MHz): δ = 163.8, 163.7, 163.7, 163.7, 158.1, 150.9, 144.1, 141.2, 138.6, 135.4, 134.9, 134.3, 134.2, 133.5, 132.8, 132.0, 130.7, 130.6, 130.1, 130.0, 129.1, 128.9, 128.0, 127.1, 124.8, 124.3, 123.9, 123.2, 122.7, 122.5, 122.3, 122.0, 119.8, 66.4, 54.1, 54.0, 51.6, 29.1, 26.5, 26.5, 25.4, 25.4, 15.0 ppm. ^{11}B NMR ($CDCl_3$, 128 MHz): δ = 0.96 ppm (t, *J*=32.3). HRMS(FI-TOF) $[M]^+$: calcd for $C_{57}H_{50}BF_2N_5O_5$ 933.3873, found 933.3867.

3.4.3. Perylene Diimide-CatecholateBODIPYs

Synthesis of *N,N'*-di-(cyclohexyl)-1,7-di(8-(4-phenyl)-((3,5-di-tertbutyl-catecholate)-BODIPY))-3,4:9,10-perylenetetracarboxylic diimide (3.20)

3.4 (50 mg, 0.0460 mmol) and aluminium chloride (36 mg, 0.270 mmol) were dissolved in dry DCM (20 mL) and heated to reflux, under an inert atmosphere, for 30 min. The reaction mixture was cooled and 3,5-di-tert-butylcatechol (22 mg, 0.0991 mmol) was added and the reaction mixture was stirred for a further 1 h at room temperature. The solvent was removed under reduced pressure and the crude product was purified by column chromatography (SiO_2, chloroform:EtOAc 98:2) to give **3.20** as a red powder (36 mg, 0.0248 mmol, 54%). ^{1}H NMR ($CDCl_3$, 400 MHz): δ = 8.68 (s, 2 H), 8.25 (d, *J*=8.3 Hz, 2 H), 7.95 (d, *J*=8.2 Hz, 2 H), 7.74 - 7.84 (m, 12 H), 7.05 (d, *J*=4.0 Hz, 4 H), 6.78 - 6.85 (m, 4 H), 6.59 (d, *J*=2.6 Hz, 4 H), 4.99 - 5.11 (m, *J*=12.0, 12.0, 3.4, 3.4 Hz, 2 H), 2.47 - 2.65 (m, 4 H), 1.88 - 1.97 (m, 4 H), 1.71 - 1.83 (m, *J*=9.8 Hz, 6 H), 1.38 - 1.52 (m, 24 H), 1.35 ppm (s, 18 H). ^{13}C NMR ($CDCl_3$, 101 MHz): δ = 163.6, 163.6, 150.2, 146.2, 145.7, 145.6, 144.7, 141.7, 139.7, 135.1, 134.8, 134.3, 134.3, 132.4, 132.2, 131.5, 131.5, 130.4, 129.4, 129.3, 129.2, 128.0, 123.2, 123.0, 119.1, 112.8, 105.7, 54.1, 34.6, 34.2, 31.9, 29.5, 29.1, 26.5, 25.4 ppm. ^{11}B NMR ($CDCl_3$, 128 MHz):

δ = 6.67 ppm (s). HRMS(FI-TOF) $[M]^+$: calcd for $C_{94}H_{88}B_2N_6O_8$ 1450.6850, found 1450.6844.

Synthesis of *N,N'*-di-(cyclohexyl)-1-(8-(4-phenyl)-((3,5-di-tertbutyl-catecholate)-BODIPY))-7-morpholino-3,4:9,10-perylenetetracarboxylic diimide (3.21)

3.8 (44 mg, 0.0486 mmol) and aluminium chloride (11 mg, 0.0827 mmol) were dissolved in dry DCM (20 mL) and heated to reflux, under an inert atmosphere, for 15 min. The reaction mixture was cooled and 3,5-di-tert-butylcatechol (13 mg, 0.0586 mmol) was added and the reaction mixture was stirred for a further 30 min at room temperature. The solvent was removed under reduced pressure and the crude product was purified by column chromatography (SiO_2, chloroform:EtOAc 93:7) to give **3.21** as a blue/black powder (29 mg, 0.0267 mmol, 55%). ^{1}H NMR ($CDCl_3$, 400 MHz): δ = 9.78 (d, *J*=8.3 Hz, 1 H), 8.59 - 8.64 (m, 2 H), 8.48 (s, 1 H), 8.06 (d, *J*=8.2 Hz, 1 H), 7.82 (d, *J*=8.2 Hz, 1 H), 7.79 (s, 2 H), 7.67 - 7.75 (m, 4 H), 7.02 (dd, *J*=4.2, 0.9 Hz, 2 H), 6.80 (dd, *J*=4.4, 2.0 Hz, 2 H), 6.57 (dd, *J*=4.1, 1.6 Hz, 2 H), 4.95 - 5.17 (m, 2 H), 3.91 - 4.06 (m, 4 H), 3.48 (d, *J*=11.9 Hz, 2 H), 3.21 (t, *J*=9.6 Hz, 2 H), 2.46 - 2.68 (m, 4 H), 1.90 - 1.99 (m, 4 H), 1.73 - 1.84 (m, 6 H), 1.38 - 1.57 (m, 14 H), 1.35 ppm (s, 9 H). ^{13}C NMR ($CDCl_3$, 101 MHz): δ = 163.8, 163.7, 163.7, 151.0, 150.2, 146.2, 145.8, 145.5, 144.9, 141.7, 138.3, 135.5, 134.9, 134.8, 134.0, 133.5, 132.9, 132.1, 131.6, 131.5, 130.8, 130.7, 130.1, 129.2, 129.2, 128.1, 127.2, 124.8, 124.4, 123.9, 123.3, 122.8, 122.6, 122.4, 122.0, 119.1, 112.8, 105.7, 66.5, 54.1, 54.0, 51.7, 34.6, 34.2, 31.9, 29.5, 29.1, 26.5, 26.5, 25.5, 25.4 ppm ^{11}B NMR ($CDCl_3$, 128 MHz): δ = 6.65 ppm (s). HRMS(FI-TOF) $[M]^+$: calcd for $C_{69}H_{66}BN_5O_7$ 1087.5055, found 1087.5049.

3.4.4. X-Ray Crystallography

Single crystals of **3.1**, **3.4**, **3.8** and **3.19** were grown by layered diffusion between a chloroform solution of the target compound and methanol. Structures were collected on a Rigaku FR-E+ Very High Flux Diffractometer (100 K, MoKα radiation), a XtaLAB Pro: Kappa single diffractometer (120 K, CuKα radiation) GV1000 TitanS2 diffractometer (120 K, CuKα radiation) or the DLS Beamline I19-1 3-circle diffractometer (120 K, Synchrotron) respectively. All structures were solved using Olex2,[68] the structure was solved with the ShelXT[69] structure solution program using Direct Methods and refined with the ShelXL[70] refinement package using Least Squares minimisation.

In **3.4** disordered solvent chloroform could not be reasonably modelled to give convergence and the data was processed using SQUEEZE,[71] which gave an estimate of 415 e- per cell corresponding to approximately six chloroform molecules. These molecules were then added to the sum formula.

In **3.8** disordered solvent chloroform and methanol could not be reasonably modelled to give convergence and the data was processed using SQUEEZE,[71] which gave an estimate of 387 e- per cell, corresponding to about half a chloroform molecule and one methanol molecule per asymmetric unit. These molecules were then added to the sum formula.

In **3.18** chloroform molecules D and E and the cyclohexyl-group containing atoms 61B-66B are disordered over two positions and their occupancy was refined competitively converging to ratios of 68:32, 64:36 and 76:24 respectively. Chloroform C was only partially occupied and its occupancy was refined to 64%. Chloroform C was disordered

over two positions and its occupancy was refined competitively to a ratio of 18:46 totalling 64. Enhanced rigid bond and similarity restraints were applied to the thermal parameters of the disordered atoms.

Crystal data for **3.1**: $C_{36}H_{28}Br_2N_2O_4$, M = 712.42, monoclinic, *P*21/*c*, a = 15.2582(4), b = 11.8210(3), c = 16.0098(11) Å, β = 103.389(7)°, U = 2809.2(2) Å^3, Z = 4, T = 100(2) K, D_{calc} = 1.684 g cm^{-3}, μ = 2.933 mm^{-1}, F(000) = 1440. A total of 33301 reflections were collected, of which 6431 were unique, with R_{int} = 0.031. Final R_1 (wR_2) = 0.0223 (0.0555) with GOF = 1.05.

Crystal data for **3.4**: $C_{73}H_{55}B_2Cl_{21}F_4N_6O_4$ (*M* =1922.30 g/mol): monoclinic, space group $P2_1/n$ (no. 14), *a* = 18.6518(3) Å, *b* = 17.4901(3) Å, *c* = 20.9784(4) Å, *β* = 106.746(2)°, *V* = 6553.4(2) Å^3, *Z* = 4, *T* = 120.00(10) K, μ(CuKα) = 8.665 mm^{-1}, *Dcalc* = 1.948 g/cm^3, 96646 reflections measured with 13697 found to be unique (R_{int} = 0.0582, R_{sigma} = 0.0353) which were used in all calculations. The final R_1 was 0.0570 (I > 2σ(I)) and wR_2 was 0.1693 with GOF= 1.064.

Crystal Data for **3.8**: $C_{57.5}H_{48.5}BCl_{4.5}F_2N_5O_5$ (*M* =1097.85 g/mol): monoclinic, space group *C*2/*c* (no. 15), *a* = 15.3918(3) Å, *b* = 19.8983(4) Å, *c* = 33.5723(8) Å, *β* = 92.671(2)°, *V* = 10271.0(4) Å^3, *Z* = 8, *T* = 120.04(11) K, μ(CuKα) = 2.859 mm^{-1}, *Dcalc* = 1.420 g/cm^3, 47196 reflections measured with 10193 found to be unique (R_{int} = 0.0403, R_{sigma} = 0.0231) which were used in all calculations. The final R_1 was 0.0984 (I > 2σ(I)) and wR_2 was 0.3022 with GOF=1.056.

Crystal Data for **3.19**: $C_{58.8}H_{51.8}BCl_{5.4}F_2N_5O_5$ (*M* =1151.23 g/mol): monoclinic, space group $P2_1/c$ (no. 14), *a* = 16.8997(13) Å, *b* = 16.6487(10) Å, *c* = 39.648(3) Å, *β* = 94.211(7)°, *V* = 11125.0(14) Å^3, *Z* = 8, *T* = 120(2) K, μ(?) = 0.318 mm^{-1}, *Dcalc* = 1.375 g/cm^3, 137855 reflections measured (2.964° ≤ 2Θ ≤ 48.416°), 19640 unique

(R_{int} = 0.1958, R_{sigma} = 0.1231) which were used in all calculations. The final R_1 was 0.1220 ($I > 2\sigma(I)$) and wR_2 was 0.4086 with GOF 1.155.

3.5. References

1. A. Treibs and F.-H. Kreuzer, *Justus Liebigs Ann. Chem.*, 1968, **718**, 208-223.
2. A. Loudet and K. Burgess, *Chem. Rev.*, 2007, **107**, 4891-4932.
3. G. Ulrich, R. Ziessel and A. Harriman, *Angew. Chem. Int. Ed.*, 2008, **47**, 1184-1201.
4. J. Godoy, V. García-López, L.-Y. Wang, S. Rondeau-Gagné, S. Link, A. A. Martí and J. M. Tour, *Tetrahedron*, 2015, **71**, 5965-5972.
5. G. Ulrich and R. Ziessel, *J. Org. Chem.*, 2004, **69**, 2070-2083.
6. A. Coskun and E. U. Akkaya, *J. Am. Chem. Soc.*, 2006, **128**, 14474-14475.
7. T. Yogo, Y. Urano, Y. Ishitsuka, F. Maniwa and T. Nagano, *J. Am. Chem. Soc.*, 2005, **127**, 12162-12163.
8. M. Baruah, W. Qin, R. A. L. Vallée, D. Beljonne, T. Rohand, W. Dehaen and N. Boens, *Org. Lett.*, 2005, **7**, 4377-4380.
9. N. Saki, T. Dinc and E. U. Akkaya, *Tetrahedron*, 2006, **62**, 2721-2725.
10. C.-W. Wan, A. Burghart, J. Chen, F. Bergström, L. B. Å. Johansson, M. F. Wolford, T. G. Kim, M. R. Topp, R. M. Hochstrasser and K. Burgess, *Chem. Eur. J.*, 2003, **9**, 4430-4441.
11. D. Wang, R. Liu, C. Chen, S. Wang, J. Chang, C. Wu, H. Zhu and E. R. Waclawik, *Dyes Pigments*, 2013, **99**, 240-249.
12. S. Murase, A. Tominaga and A. Kohama, *Eur. Pat. 1253151a*, 2002.
13. A. Haefele, C. Zedde, P. Retailleau, G. Ulrich and R. Ziessel, *Org. Lett.*, 2010, **12**, 1672-1675.
14. H. Kim, A. Burghart, M. B. Welch, J. Reibenspies and K. Burgess, *Chem. Commun.*, 1999, 1889-1890.
15. C. Tahtaoui, C. Thomas, F. Rohmer, P. Klotz, G. Duportail, Y. Mély, D. Bonnet and M. Hibert, *J. Org. Chem.*, 2007, **72**, 269-272.
16. K. Umezawa, Y. Nakamura, H. Makino, D. Citterio and K. Suzuki, *J. Am. Chem. Soc.*, 2008, **130**, 1550-1551.
17. A. Burghart, H. Kim, M. B. Welch, L. H. Thoresen, J. Reibenspies, K. Burgess, F. Bergström and L. B. Å. Johansson, *J. Org. Chem.*, 1999, **64**, 7813-7819.
18. W. Zhao and E. M. Carreira, *Angew. Chem. Int. Ed.*, 2005, **44**, 1677-1679.
19. K. Rurack, M. Kollmannsberger and J. Daub, *Angew. Chem. Int. Ed.*, 2001, **40**, 385-387.
20. S. G. Awuah, J. Polreis, V. Biradar and Y. You, *Org. Lett.*, 2011, **13**, 3884-3887.
21. N. Boens, V. Leen and W. Dehaen, *Chem. Soc. Rev.*, 2012, **41**, 1130-1172.
22. K. Rurack, M. Kollmannsberger and J. Daub, *New J. Chem.*, 2001, **25**, 289-292.
23. J.-P. Malval, I. Leray and B. Valeur, *New J. Chem.*, 2005, **29**, 1089-1094.
24. I. Móczár, P. Huszthy, Z. Maidics, M. Kádár and T. Klára, *Tetrahedron*, 2009, **65**, 8250-8258.
25. Z. Ekmekci, M. D. Yilmaz and E. U. Akkaya, *Org. Lett.*, 2008, **10**, 461-464.
26. A. Meister, *J. Biol. Chem.*, 1988, **263**, 17205-17208.
27. S. C. Lu, *Mol. Aspects Med.*, 2009, **30**, 42-59.
28. Y. Guo, X. Yang, L. Hakuna, A. Barve, J. O. Escobedo, M. Lowry and R. M. Strongin, *Sensors*, 2012, **12**, 5940-5950.
29. L.-Y. Niu, Y.-S. Guan, Y.-Z. Chen, L.-Z. Wu, C.-H. Tung and Q.-Z. Yang, *J. Am. Chem. Soc.*, 2012, **134**, 18928-18931.

30. C. A. Robertson, D. H. Evans and H. Abrahamse, *J. Photochem. Photobiol. B*, 2009, **96**, 1-8.
31. J. Zhao, K. Xu, W. Yang, Z. Wang and F. Zhong, *Chem. Soc. Rev.*, 2015, **44**, 8904-8939.
32. A. Kamkaew, S. H. Lim, H. B. Lee, L. V. Kiew, L. Y. Chung and K. Burgess, *Chem. Soc. Rev.*, 2013, **42**, 77-88.
33. M. J. Ortiz, A. R. Agarrabeitia, G. Duran-Sampedro, J. Bañuelos Prieto, T. A. Lopez, W. A. Massad, H. A. Montejano, N. A. García and I. Lopez Arbeloa, *Tetrahedron*, 2012, **68**, 1153-1162.
34. S. Erbas, A. Gorgulu, M. Kocakusakogullari and E. U. Akkaya, *Chem. Commun.*, 2009, 4956-4958.
35. S. O. McDonnell, M. J. Hall, L. T. Allen, A. Byrne, W. M. Gallagher and D. F. O'Shea, *J. Am. Chem. Soc.*, 2005, **127**, 16360-16361.
36. G. D. Scholes, G. R. Fleming, A. Olaya-Castro and R. van Grondelle, *Nat. Chem.*, 2011, **3**, 763-774.
37. X. Zhang, Y. Xiao and X. Qian, *Org. Lett.*, 2008, **10**, 29-32.
38. D. Holten, D. F. Bocian and J. S. Lindsey, *Acc. Chem. Res.*, 2002, **35**, 57-69.
39. R. W. Wagner and J. S. Lindsey, *J. Am. Chem. Soc.*, 1994, **116**, 9759-9760.
40. R. W. Wagner, J. S. Lindsey, J. Seth, V. Palaniappan and D. F. Bocian, *J. Am. Chem. Soc.*, 1996, **118**, 3996-3997.
41. M. D. Yilmaz, O. A. Bozdemir and E. U. Akkaya, *Org. Lett.*, 2006, **8**, 2871-2873.
42. O. A. Bozdemir, M. D. Yilmaz, O. Buyukcakir, A. Siemiarczuk, M. Tutas and E. U. Akkaya, *New J. Chem.*, 2010, **34**, 151-155.
43. Z. Mahmood, K. Xu, B. Küçüköz, X. Cui, J. Zhao, Z. Wang, A. Karatay, H. G. Yaglioglu, M. Hayvali and A. Elmali, *J. Org. Chem.*, 2015, **80**, 3036-3049.
44. G. Goretzki, E. S. Davies, S. P. Argent, W. Z. Alsindi, A. J. Blake, J. E. Warren, J. McMaster and N. R. Champness, *J. Org. Chem.*, 2008, **73**, 8808-8814.
45. M. J. Ahrens, M. J. Tauber and M. R. Wasielewski, *J. Org. Chem.*, 2006, **71**, 2107-2114.
46. R. K. Dubey, A. Efimov and H. Lemmetyinen, *Chem. Mater.*, 2011, **23**, 778-788.
47. E. O. Danilov, A. A. Rachford, S. Goeb and F. N. Castellano, *J. Phys. Chem. A*, 2009, **113**, 5763-5768.
48. J. Sun, F. Zhong and J. Zhao, *Dalton Trans.*, 2013, **42**, 9595-9605.
49. F. Würthner, V. Stepanenko, Z. Chen, C. R. Saha-Möller, N. Kocher and D. Stalke, *J. Org. Chem.*, 2004, **69**, 7933-7939.
50. G. Battagliarin, C. Li, V. Enkelmann and K. Müllen, *Org. Lett.*, 2011, **13**, 3012-3015.
51. T. Teraoka, S. Hiroto and H. Shinokubo, *Org. Lett.*, 2011, **13**, 2532-2535.
52. C. Ramanan, A. L. Smeigh, J. E. Anthony, T. J. Marks and M. R. Wasielewski, *J. Am. Chem. Soc.*, 2012, **134**, 386-397.
53. L. Luo, D. Wu, W. Li, S. Zhang, Y. Ma, S. Yan and J. You, *Org. Lett.*, 2014, **16**, 6080-6083.
54. P. Rajasingh, R. Cohen, E. Shirman, L. J. W. Shimon and B. Rybtchinski, *J. Org. Chem.*, 2007, **72**, 5973-5979.
55. J. J. Apperloo, C. Martineau, P. A. van Hal, J. Roncali and R. A. J. Janssen, *J. Phys. Chem. A*, 2002, **106**, 21-31.
56. S. Nakazono, S. Easwaramoorthi, D. Kim, H. Shinokubo and A. Osuka, *Org. Lett.*, 2009, **11**, 5426-5429.

57. G. Goretzki, E. S. Davies, S. P. Argent, J. E. Warren, A. J. Blake and N. R. Champness, *Inorg. Chem.*, 2009, **48**, 10264-10274.
58. B. A. Llewellyn, A. G. Slater, G. Goretzki, T. L. Easun, X.-Z. Sun, E. S. Davies, S. P. Argent, W. Lewis, A. Beeby, M. W. George and N. R. Champness, *Dalton Trans.*, 2014, **43**, 85-94.
59. A. G. Slater, E. S. Davies, S. P. Argent, W. Lewis, A. J. Blake, J. McMaster and N. R. Champness, *J. Org. Chem.*, 2013, **78**, 2853-2862.
60. T. W. Chamberlain, E. S. Davies, A. N. Khlobystov and N. R. Champness, *Chem. Eur. J.*. 2011, **17**, 3759-3767.
61. V. J. Richards, A. L. Gower, J. E. H. B. Smith, E. S. Davies, D. Lahaye, A. G. Slater, W. Lewis, A. J. Blake, N. R. Champness and D. L. Kays, *Chem. Commun.*, 2012, **48**, 1751-1753.
62. V. Richards, *PhD Thesis, University of Nottingham*, 2014.
63. B. Mangham, *PhD Thesis, University of Nottingham*, 2014.
64. C. Yu, L. Jiao, H. Yin, J. Zhou, W. Pang, Y. Wu, Z. Wang, G. Yang and E. Hao, *Eur. J. Org. Chem.*, 2011, **2011**, 5460-5468.
65. Y. Yang, Y. Wang, Y. Xie, T. Xiong, Z. Yuan, Y. Zhang, S. Qian and Y. Xiao, *Chem. Commun.*, 2011, **47**, 10749-10751.
66. J. T. Tomlinson, G. Park, J. A. Misenheimer, G. L. Kucera, K. Hesp and R. A. Manderville, *Org. Lett.*, 2006, **8**, 4951-4954.
67. M. Nicolas, B. Fabre, G. Marchand and J. Simonet, *Eur. J. Org. Chem.*, 2000, **2000**, 1703-1710.
68. O. V. Dolomanov, L. J. Bourhis, R. J. Gildea, J. A. K. Howard and H. Puschmann, *J. Appl. Cryst.*, 2009, **42**, 339-341.
69. G. M. Sheldrick, *Acta. Cryst. A.*, 2008, **64**, 112-122.
70. G. M. Sheldrick, *Acta. Cryst. C*, 2015, **71**, 3-8.
71. A. L. Spek, *Acta Crystallogr.*, 2009, **65**, 148-155.

Chapter 4. Triplet Excited State Formation in Platinum Substituted Perylene Diimides

4.1. Introduction

4.1.1. The Triplet Excited State

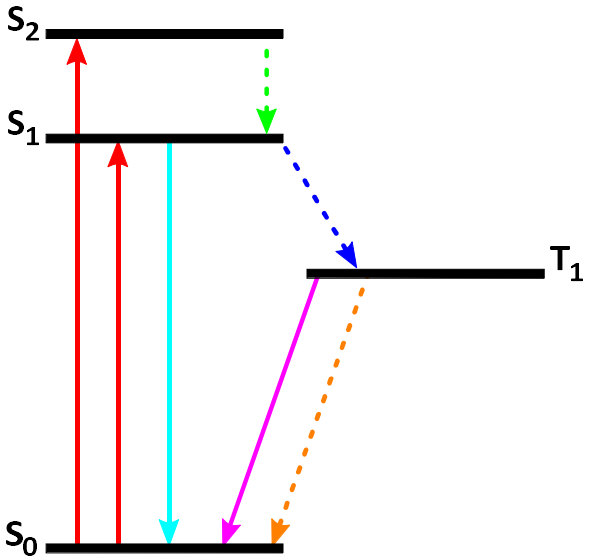

Figure 4.1. Simplified Jablonski Diagram showing possible electronic transitions displaying excitation (red), internal conversion (green), fluorescence (light blue), intersystem crossing (dark blue), non-radiative decay (orange) and phosphorescence (pink). Dashed arrows are non-radiative processes.

The phenomenon of phosphorescence was first correctly interpreted by Terenin in 1943.[1] Since this time, phosphorescence has been exploited in many varied applications and the synthesis of new phosphorescent materials has become a major field of research.[2] Upon absorbance of light, electrons in an organic molecule are excited to a higher energy level in an S_0-S_1 or S_0-S_2 transition. The most common relaxation route is then to decay back to the S_0 ground state (following internal conversion to S_1 in the case of the S_0-S_2 transition) emitting a photon thus exhibiting fluorescence. In some

The work described in this chapter was initiated during a Masters project at the University of Nottingham within the Champness group and was significantly expanded and completed during this PhD.

cases, however, the electron can undergo a spin-forbidden transition from S_1 to the T_1 triplet excited state *via* intersystem crossing (ISC). The decay processes back to the S_0 ground state can then exist as phosphorescence, where a photon is emitted, or as a non-radiative decay process, Figure 4.1. Due to the spin forbidden nature of the T_1-S_0 transition, the lifetimes of phosphorescence are longer than that of standard fluorescence.

The spin forbidden S_1-T_1 transition is often caused by the 'heavy-atom' effect. This effect induces spin-orbit coupling; where the spin magnetic moment of an electron interacts with the magnetic field causing a quantum mechanical mixing of states with different multiplicity and allows the transition to take place.[3] This coupling is proportional to the atomic number of the atoms in the molecule. Therefore, it is more prevalent in the presence of large atoms and is hence known as the 'heavy atom' effect.

Interest in materials with access to the triplet excited state has intensified in recent years due to the possibility of application in several areas. One of the main factors affecting the efficiency of organic photovoltaics (OPVs) is the exciton diffusion length which, in turn, is dependent on exciton mobility and lifetime. Triplet materials, therefore, suggest excellent potential for use in such devices as the spin-forbidden relaxation extends the excitation lifetime. This method has been employed in various OPVs with Pt-porphyrin and Pt-acetylide polymers acting as the triplet donor leading to improvements in efficiency of the devices.[4, 5]

Organic light emitting diodes (OLEDs), first fabricated in 1987,[6] consist of two layers of organic material, one capable of hole transport and the other electron transport.[7] Upon injection of holes and electrons, the charge carriers migrate through the material. When a hole and electron meet, they combine by the electron relaxing back to its ground

state, emitting a photon. In most cases, the electrodes are not capable of spin polarisation of the inserted electrons, resulting in a ratio of 3:1 triplet to singlet excitons. In order to fabricate OLED devices with the potential for up to 100 % internal quantum efficiency, phosphorescent materials, which will allow the triplet to singlet relaxation, are therefore essential.[8] The first example of a phosphorescent OLED contained a porphyrin-platinum dopant allowing 90 % energy transfer resulting in 23 % internal quantum efficiency.[9] Since this point, iridium complexes have become the most studied material for phosphorescent OLEDs as they permit excellent conversion of electrical energy to light[10] and allow the wavelength to be tuned across the entire visible spectrum by modification to the ligands, Figure 4.2.[11]

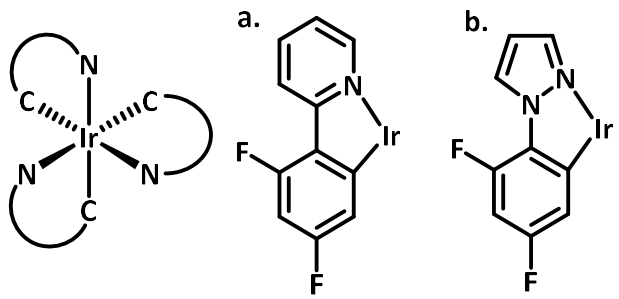

Figure 4.2. Example of two Ir complexes used in phosphorescent OLEDs. A change in ligand from a. to b. results in a 60 nm difference in wavelength of emission.

4.1.2. The Triplet Excited State in Perylene Diimides

The useful properties of molecules that can access the triplet excited state has led to attempts to synthesise perylene diimides (PDIs) that are phosphorescent. This was first achieved in the 1980s by the excitation of a PDI in the presence of an anthracene triplet sensitiser[12] or using methyl iodide as a solvent to induce an 'external heavy atom' effect.[13]

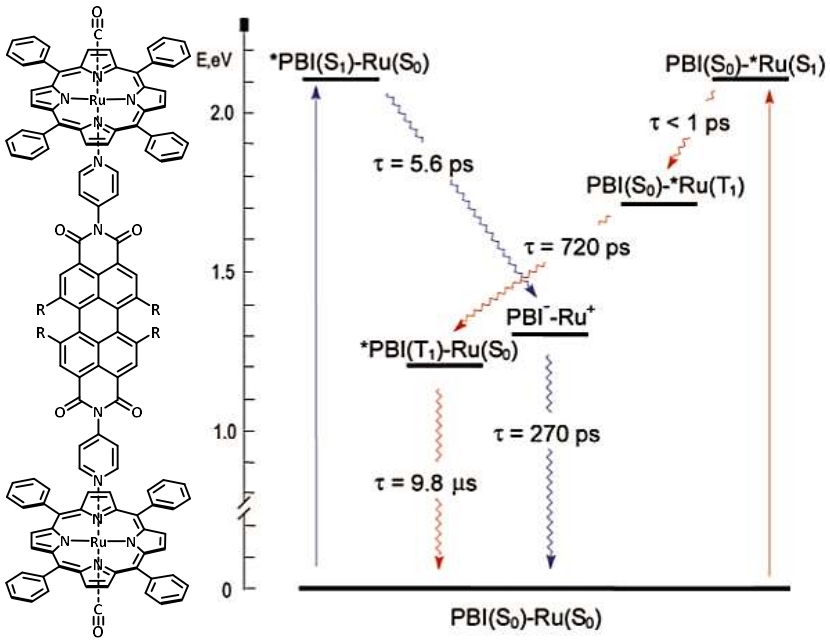

Figure 4.3. Structure of PDI-(Ru-TPP) capable of intramolecular triplet sensitisation, R = 4-t-butylphenoxybenzene, (left) and Jablonski diagram showing the electronic transitions upon excitation of the PDI (blue arrows) and the Ru-TPP (red arrows), (right).[14]

Intramolecular triplet sensitisation has been achieved by Würthner and co-workers by coordinating a PDI, substituted at the imide position with pyridine, to a ruthenium porphyrin (Ru-TPP), capable of accessing the triplet excited state itself, Figure 4.3.[14] Upon excitation of the PDI unit, S_1-S_0 fluorescence is not observed. This was probed by ultrafast time-resolved spectroscopy revealing the presence of absorption bands corresponding to the PDI radical anion and the Ru-TPP radical cation on a sub 50 ps timescale. This suggests charge separation has taken place, due to a reductive photoinduced electron transfer (PET) process, which recombines to the ground state on a 1 ns timescale. Alternatively, upon excitation of the Ru-TPP moiety there is no observable phosphorescence, as seen with a Ru model compound, this was also probed by ultrafast time-resolved spectroscopy. 1 ps after excitation, the Ru-TPP ^{1}T absorbance is observed. 860 ps later the Ru-TPP ^{1}T absorbance disappears, accompanied by a bleaching of the PDI S_0 ground state and formation of a new band at 500 nm. These spectral changes are indicative of triplet-triplet energy transfer from the Ru complex to

form the PDI triplet excited state, with a lifetime measured at 9.8 µs. In this system, a small change in the wavelength of excitation results in a switch from electron to energy transfer leading to a dramatic change in the photophysics. Similar behaviour is observed in a PDI functionalised with an iridium complex at the imide position with triplet-triplet transfer from the complex to the PDI,[15] whilst a PDI functionalised at the imide position with ferrocene accesses the triplet excited state *via* charge recombination following the formation of a charge separated state.[16]

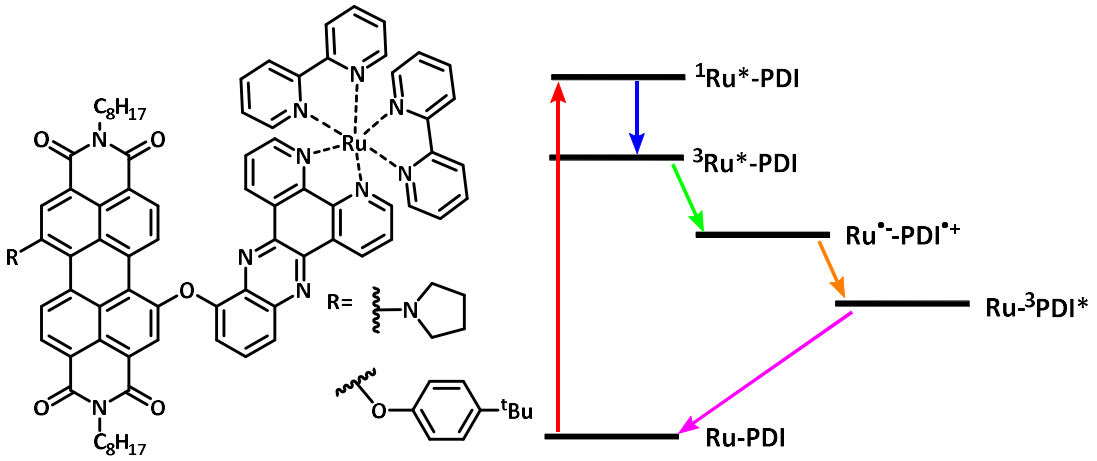

Figure 4.4. Structure of PDIs bay substituted with a Ru complex capable of accessing the triplet excited state (left) and energy level diagram for the pyrrolidinyl-substituted PDI showing behaviour upon excitation of the Ru complex (right). Red arrow- excitation to Ru singlet state, blue arrow- intersystem crossing to Ru triplet state, green arrow- charge separation, orange arrow- charge recombination to PDI triplet state, pink arrow- relaxation to ground state.

Another PDI bearing a Ru complex was synthesised by Lemmetyinen and co-workers. However, in this case the complex was attached to the bay-area of the PDI rather than imide-position.[17] Two different asymmetrically substituted PDIs were synthesised; both with a polypyridyl Ru complex at the 1- position and either a pyrrolidinyl- or phenoxy-substituent at the 7- position, Figure 4.4. In both cases, excitation of the Ru complex resulted in the formation of a charge separated state. However, the electron poor phenoxy-PDI acts as an electron accepter, leading to a $PDI^{\bullet -}$-$Ru^{\bullet +}$ charge separated state, and the electron rich pyrollidinyl-PDI acts an electron donor resulting in a $PDI^{\bullet +}$-

$Ru^{\bullet-}$ charge separated state. Both of these charge separated states then decay to a $^3PDI^*$-Ru triplet state through charge recombination followed by relaxation to the ground state.

Rybtchinski and co-workers were the first to attempt to synthesise a PDI with access to the triplet excited state *via* covalent attachment of a metal to the perylene core. They synthesised a PDI with a palladium complex directly sigma bonded to the bay region of the PDI with the intention of the Pd inducing the 'heavy atom' effect.[18] Unexpectedly, upon excitation the main mode of decay was fluorescence, with a 65 % quantum yield, whilst the triplet state was only yielded in 6 %. This poor intersystem crossing was assigned to weak electronic coupling of the Pd complex with the frontier π-orbitals of the PDI, as shown by DFT calculations.

Efficient formation of the triplet excited state in PDI by covalently attaching a heavy atom to the PDI core was first achieved by Castellano and co-workers in their platinum acetylide PDI systems.[19-21] Four Pt-PDIs have currently been synthesised; two dimers in a square planar *cis*-conformation with the Pt bearing a bipyridyl- or bidentate phosphine ligand, a dimer in a *trans*-conformation with monodentate phosphine ligands and a PDI mono-substituted with a terpyridyl-Pt complex, Figure 4.5. The absorption spectra of all four compounds were dominated by the PDI S_0-S_1 transition but all were non-emissive suggesting full quenching of the PDI singlet state fluorescence, apart from the PDI functionalised with the terpyridyl-Pt complex which displayed residual singlet fluorescence with a quantum yield of 0.014. Ultrafast transient absorption spectra showed this quenching was due to fast intersystem crossing (2-4 ps) to form the triplet excited state on the PDI, which was further confirmed by the generation of singlet oxygen. It was found that the nature of the ligand attached to the Pt centre and the *cis*-/*trans*- arrangement had very little effect on the photophysics of the compounds with

the only changes being in the lifetimes of the excited states which ranged from 246 ns to 1 μs.

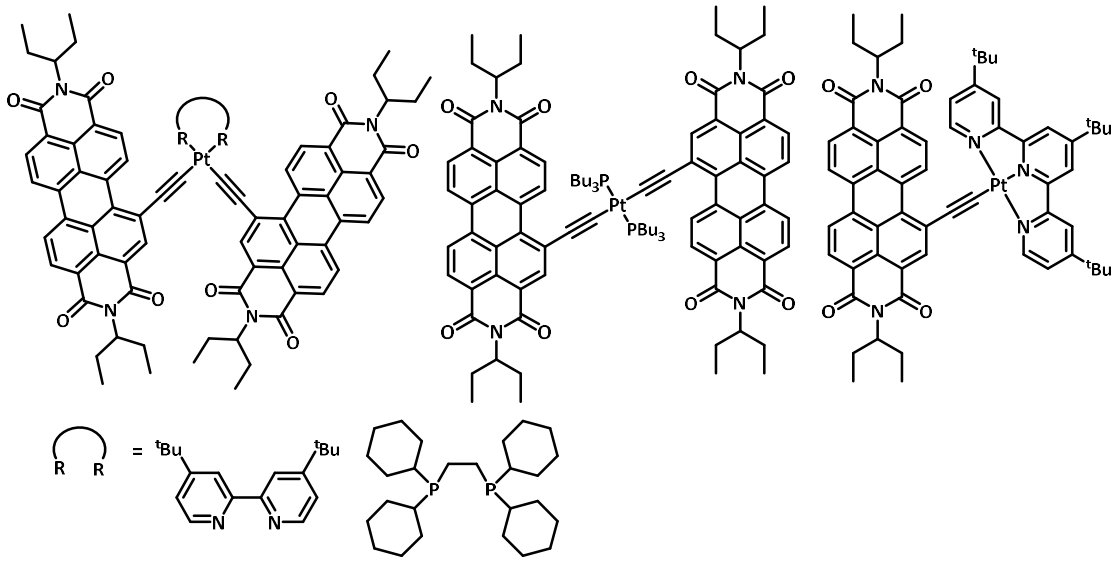

Figure 4.5. Pt-PDIs synthesised by Castellano and co-workers capable of accessing the triplet excited state by the 'heavy atom' effect.

Several other methods have been employed to access the triplet excited state of PDIs that do not require the use of metal complexes. The 'heavy atom' effect is again utilised when the carbonyls on the PDI are substituted with sulfur atoms, as discussed in Chapter 2.[22] Formation of PDIs that are fused at the bay-region to another PDI molecule allows efficient intersystem crossing, resulting in a triplet excited state, due to increased spin-orbit coupling caused by the non-planarity of the extended PDI core.[23] Finally, catenanes comprised of an extended tetracationic cyclophane macrocycles and a macrocycle containing a PDI have been shown to allow energy transfer from the cyclophane to the PDI upon excitation.[24] When the cyclophane macrocycle contains a heavy selenium atom, the generated PDI S_1 state can undergo ISC, due to the 'heavy atom' effect, to the PDI triplet state.

4.1.3. Other Perylene Diimide Metal Complexes

There have been several other PDI based metal complexes synthesised without the ability to form the triplet excited state.[25] The first of these was a molecular square containing PDIs, functionalised with pyridine at the imide region, coordinating to square planar palladium or platinum complexes synthesised by Würthner and co-workers, Figure 4.6.[26] The formation of the squares preserved the absorption, emission and redox properties of the individual monomers. Analogous squares were also synthesised with each PDI bearing four ferrocene groups, giving a supramolecular species containing twenty redox active groups.[27] The absorption, emission and reduction behaviour of the PDIs were unchanged upon square formation, however, an additional process was observed in the reoxidation of the ferrocenes from ferrocenium. This was assigned to the ferrocenium units inhabiting two environments, inside and outside of the square, resulting in different oxidation potentials and two peaks appearing

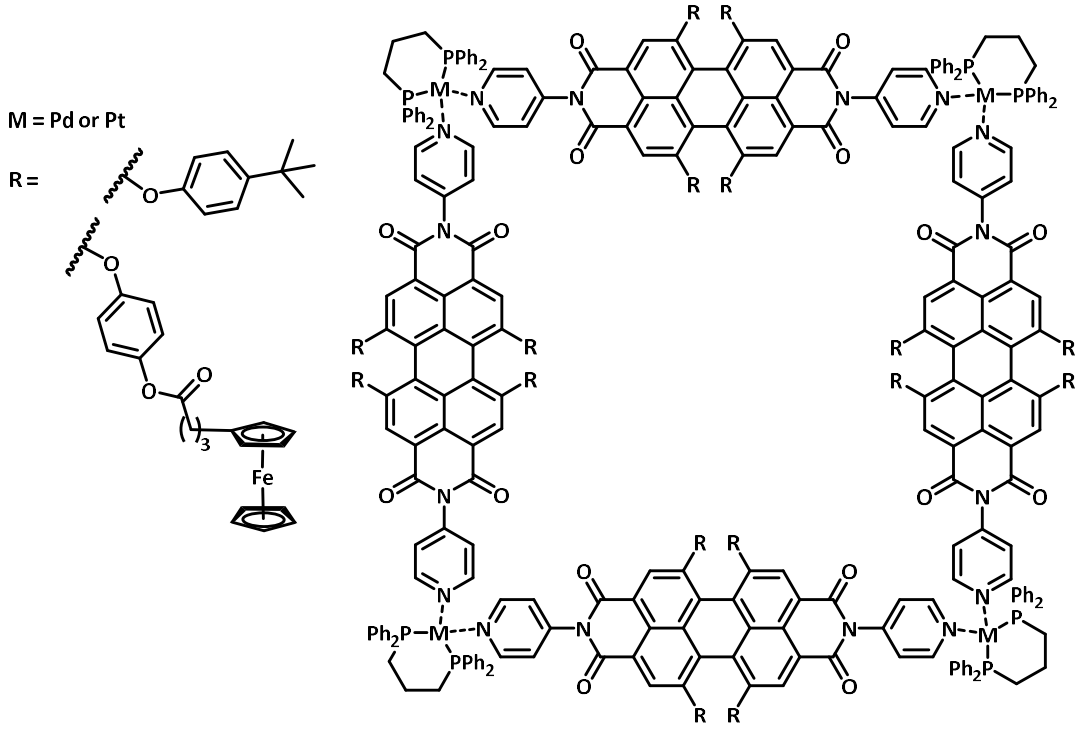

Figure 4.6. Structures of PDI based square coordination complexes.

in the cyclic voltammogram. Müllen and co-workers used a very similar method to synthesise a molecular rectangle, containing two PDIs, by changing the Pt complex used to an anthracene substituted with Pt at the 1- and 8- positions, again there was very little change in the properties of the PDI upon complexation.[28]

In order to further understand, then take advantage of, the complex electron transfer systems used in nature during photosynthesis, simplified mimics of these systems are being synthesised with similar properties such as light harvesting, electron transfer, charge separation and photocatalysis.[29] Systems bearing PDIs and metal centres have received much interest for this application leading to the synthesis of PDIs functionalised at the bay- and imide-positions with metallated porphyrins and phthalocyanines capable of long lived charge separation followed by singlet emission.[30, 31] Similar results were found in a PDI dimer connected, by the bay-area, *via* a ruthenium complex.[32]

In 2009, Champness and co-workers synthesised a series of multistate redox active systems consisting of PDI substituted at the bay-area with ferrocene and cobalt dithiolene.[33] Following separation by column chromatography of the diferrocenyl-PDI, the first crystallographic characterisation of a pair of 1,6- and 1,7-isomers was undertaken. Cyclic voltammetric investigation of the ferrocene-PDI reveals the expected two PDI reductions and a two-electron oxidation located on the ferrocene. In the case of the cobalt-PDI, rather than a single two-electron reduction based on the cobalt dithiolene unit, an additional reduction is observed, assigned to communication between the cobalt units across the conjugated core of the PDI.

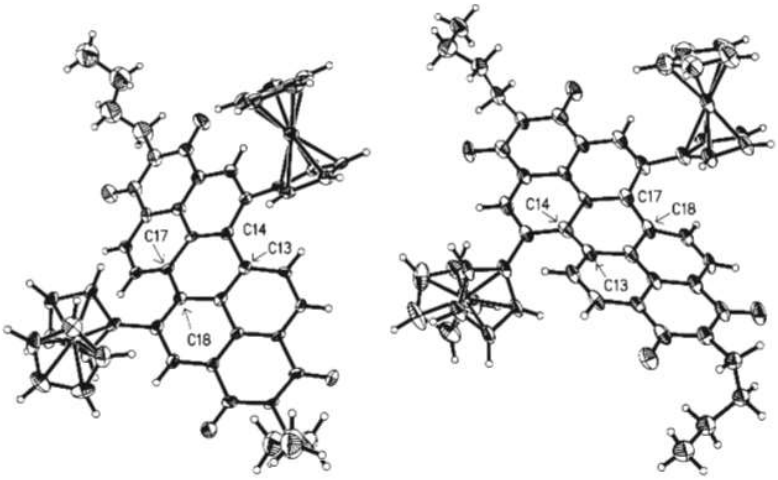

Figure 4.7. Views of X-ray crystal structures of ferrocene substituted PDIs, the first pair of 1,6-/1,7-isomers to be crystallographically characterised.[33]

4.1.4. Aims and Objectives

This Chapter describes the synthesis of a PDI disubstituted with a platinum acetylide complex at the bay-area and an asymmetrically substituted PDI with morpholine at the 1- position and the Pt complex at the 7- position. The optical, electrochemical and photophysical properties of these two compounds are investigated by absorption and emission spectroscopy, cyclic voltammetry, spectroelectrochemistry, transient absorption spectroscopy and singlet oxygen generation measurements. These measurements demonstrate the effect of Pt-substitution on the optical and redox properties of the PDI along with the capability to access the triplet excited state. The introduction of the morpholine to the PDI core will further perturb these properties.

4.2. Results and Discussion

4.2.1. Synthesis

The first stage in the synthesis of the two platinum acetylide substituted PDIs was the synthesis of a suitable platinum complex for incorporation onto the bay-area of the PDI, Scheme 4.1. **4.2**, bearing a chlorine atom for Sonogashira cross coupling, was chosen for this purpose.

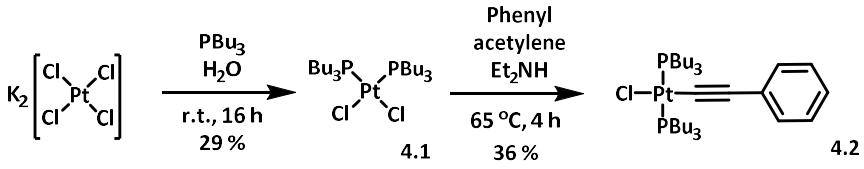

Scheme 4.1. Synthesis of the Pt complex **4.2** for reaction with a PDI.

The first step in the synthesis of **4.2** was the reaction of potassium tetrachloroplatinate with tetra-n-butyl phosphine to give **4.1**, achieved in a 29 % yield. **4.1** was then reacted with phenyl acetylene in diethyl amine to give **4.2**. The ^{13}C NMR spectrum of **4.2** reveals the signals corresponding to the first three carbons in the butyl-chains of the PBu_3 appear as triplets, Figure 4.8. One would expect these signals to be doublets due to coupling to ^{31}P (I = ½) atom. However, phosphorous has a large coupling constant when *trans*- to other ligands.[34] This means the carbon atoms in the butyl-chain are coupling to both phosphorous atoms in the complex leading to second order effects and the appearance of an apparent triplet in the NMR spectrum. The coupling constant to ligands *cis*- to phosphorous are much smaller. Therefore, the second order effects are less apparent, meaning the presence of apparent triplets is typical of a *trans*-arrangement of phosphine ligands.

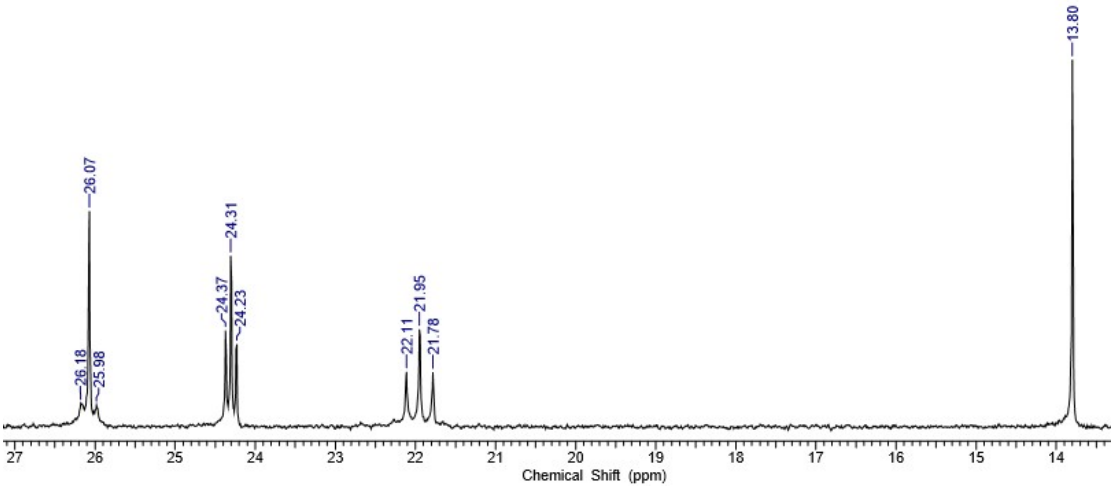

Figure 4.8. Selected view of the ^{13}C NMR spectrum of **4.2** showing the apparent triplets in the butyl chain due to second order effects.

The di(platinum acetylide)-substituted PDI **4.5** was synthesised in five steps from the PDA starting material. The synthesis of 1,7-regiosomerically pure **3.1** is described in Chapter 3.

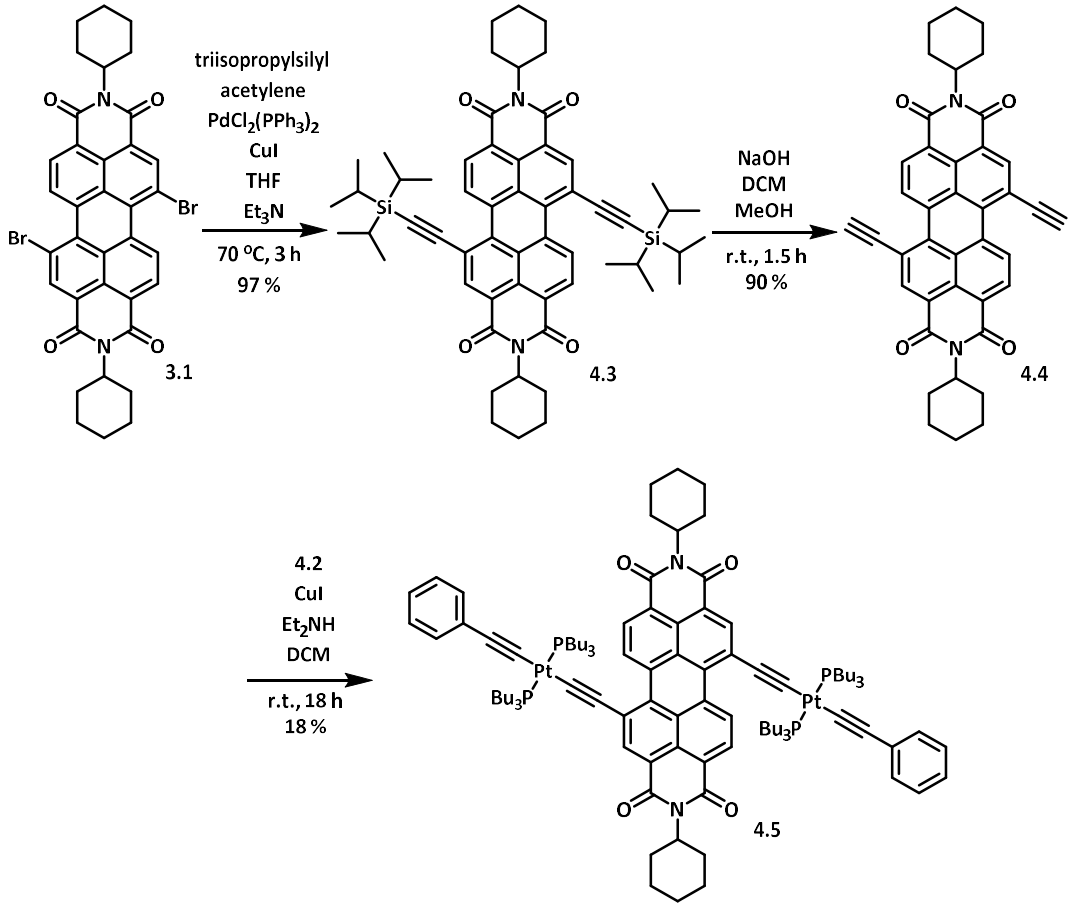

Scheme 4.2. Synthesis of the di(platinum acetylide)-substituted PDI **4.5** from **3.1**.

4.3 was synthesised by a Sonogashira cross coupling reaction between **3.1** and an alkyne group protected with triisopropylsilyl acetylene in a near quantitative yield. Trimethylsilyl (TMS) acetylene was the first choice of protecting group. However, the yield of the cross coupling reaction was surprisingly low. Single crystals, suitable for X-ray crystallographic studies, of **4.3** were grown by layered diffusion between a chloroform solution of the target compound and methanol. X-ray structural determination revealed the conformational arrangement of the molecule in the solid state and confirmed the 1,7-arrangment of the protected acetylene groups, Figure 4.9. The molecules were seen to pack in pairs, similarly to other PDI structures reported in other Chapters, with a large offset between the perylene cores due to the bulky triisopropyl groups.

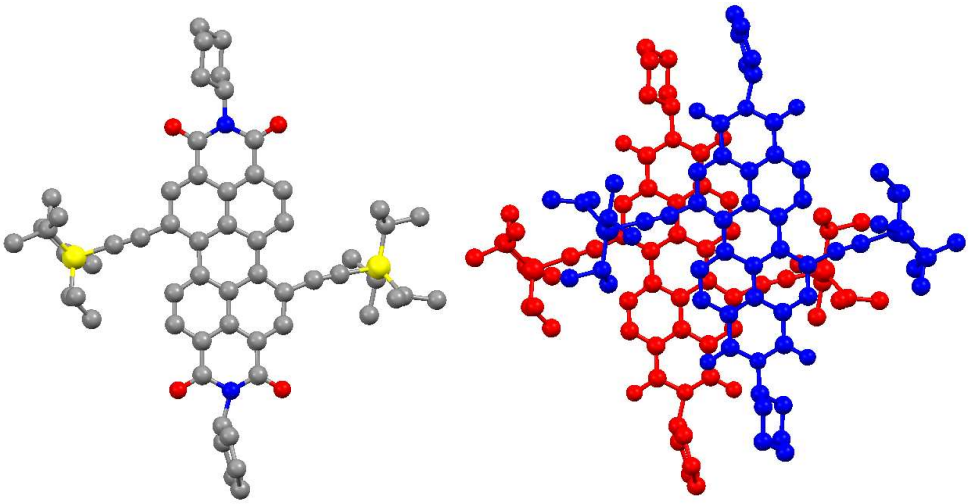

Figure 4.9. View of the X-ray crystal structure of **4.3** (left) and packing of two molecules of **4.3** showing the offset π-π interaction (right). Grey- carbon, blue- nitrogen, red- oxygen, yellow- silicon. H-atoms removed for clarity. This structure was collected and solved by Dr Stephen Argent of the University of Nottingham.

The next step in the synthesis was the deprotection of **4.3** with sodium hydroxide to give **4.4** in a 90 % yield. **4.4** was found to be insoluble in most solvents; therefore characterisation by NMR spectroscopy was not possible. The final step was a Hagihara cross coupling between **4.2** and **4.4** to give **4.5** in a yield of 18 %. Single crystals,

suitable for X-ray crystallographic studies, of **4.5** were grown by layered diffusion between a chloroform solution of the target compound and methanol. X-ray structural determination revealed the conformational arrangement of the molecule in the solid state, Figure 4.10. The bulky Pt complexes completely disrupt the π-π interactions between the perylene cores, removing any stacking between the molecules. Despite the bulk of the bay-substituents the angle between planes generated on the two naphthyl rings in the PDI core was measured to be a relatively small 12°, for comparison the analogous torsion angle in dibromo PDI is 25°. This small angle is attributed to the alkyne group distancing the bulky PBu_3 groups form the PDI core.

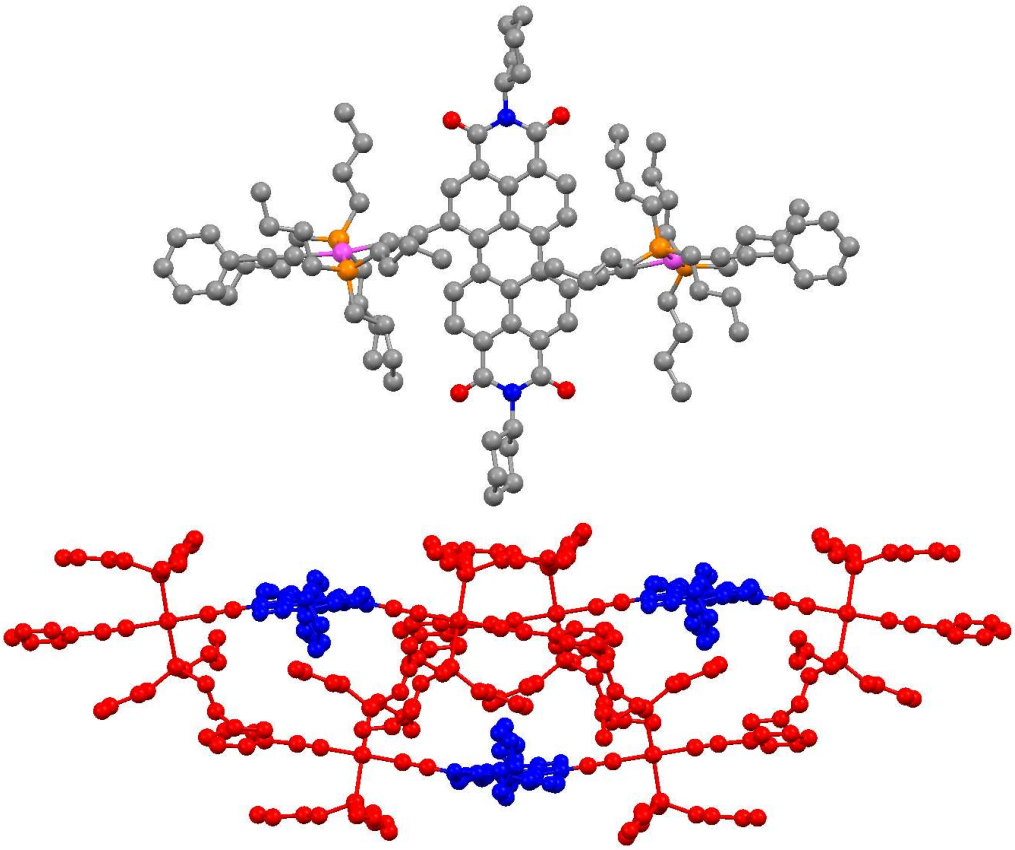

Figure 4.10. View of the X-ray crystal structure of **4.5** (top) and packing of three molecules of **4.5** (bottom) showing the complete disruption of the π-π stacking between the perylene cores (blue) due to the steric bulk of the Pt complexes (red). Grey- carbon, blue- nitrogen, red- oxygen, orange- phosphorous, pink- platinum. H-atoms removed for clarity. This structure was collected and solved by Dr Stephen Argent of the University of Nottingham.

The asymmetrically substituted Pt/morpholino-PDI **4.8** was synthesised by a similar route to **4.5** in six steps from the PDA starting material. Synthesis of **3.5** is described in Chapter 3.

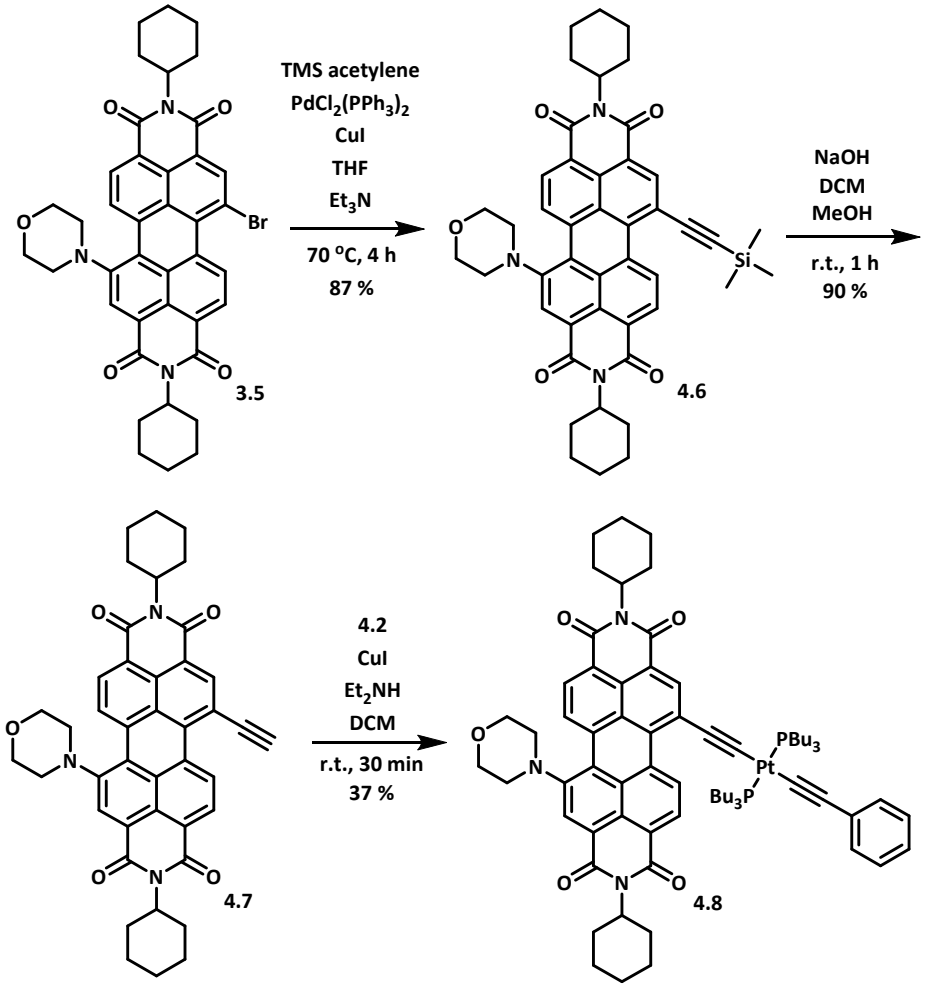

Scheme 4.3. Synthesis of asymmetrically substituted Pt/morpholino-PDI **4.8** from **3.5**.

The Sonogashira cross coupling of **3.5** with TMS acetylene progressed to **4.6** in a yield of 87 %, higher than the comparable reaction with **3.1**, therefore, the use of triisopropylsilyl acetylene was not necessary. Deprotection of **4.6** to **4.7** with sodium hydroxide again worked well with the product in this case being sufficiently soluble for characterisation by NMR spectroscopy due to the increased twist in the PDI core caused by the morpholine moiety. The final step was the Hagihara cross coupling reaction of **4.7** with **4.2** to give **4.8**. When the reaction was left overnight, the yield was found to

be similar to that of **4.5**. However, when the reaction time was reduced to 30 minutes the yield increased to 36 %, suggesting some decomposition of product during the reaction, leading to a reduction in the overall yield.

4.2.2. Optical, Electrochemical and Photophysical Investigation of Platinum Substituted PDIs

UV/vis absorption studies on **4.5** and **4.8** reveal relatively simple absorption profiles with the main absorbance related to the S_0-S_1 excitation, Figure 4.11, Figure 4.12 and Table 4.1. The absorption maximum of **4.5** lies at 625 nm and displays vibrational structure. This absorption has been red shifted *vs.* unsubstituted PDI suggesting the Pt acetylide is electron donating in nature. This red shift upon platinum substitution is also observed in the PDIs reported by Castellano, with absorption maxima at ~570 nm.[19-21] The shift in the case of **4.5** is more pronounced caused by the presence of two electron donating platinum complexes rather than one. The emission spectrum of **4.5** shows a featureless emission with a maximum at 685 nm, corresponding to a Stokes shift of 60 nm. The quantum yield of emission was measured as 0.02, suggesting a severe quenching of emission upon attachment of the Pt complex, whilst the emission lifetime was measured to be 7 ns. The reasonably large Stokes shift (the Stokes shift of the singlet emission from Castellano's terpyridyl-Pt PDI complex was 43 nm)[21] and featureless emissions can be characteristic of the formation of a triplet excited state, however, the lifetime lies between that of the triplet states formed in the non-emissive PDIs synthesised by Castellano and co-workers, of 246 ns – 1 μs, and that of Castellano's terpyridyl-Pt PDI complex singlet emission of 109 ps.[19-21]

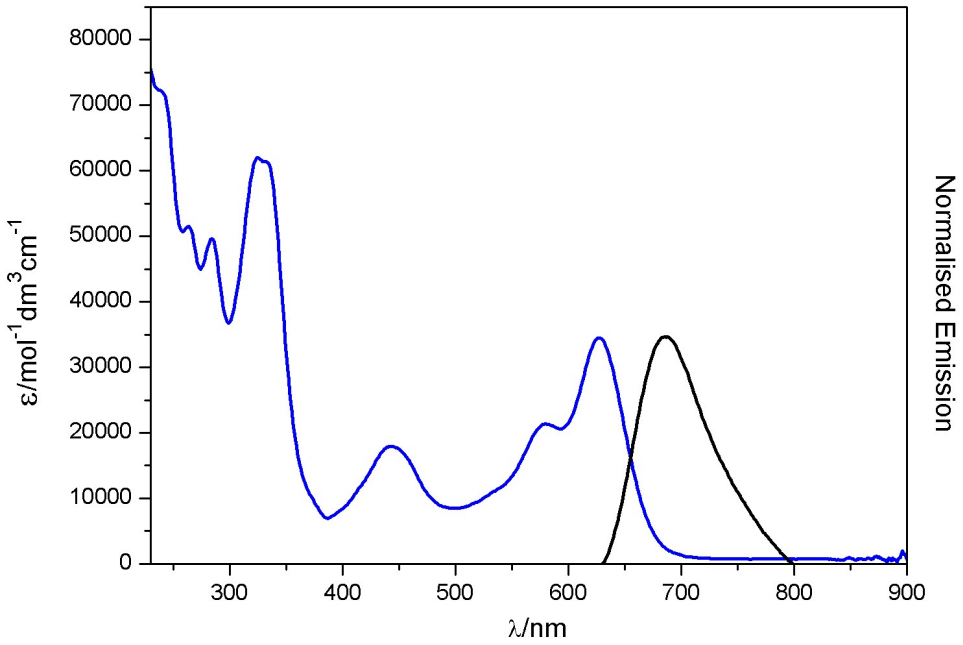

Figure 4.11. UV/vis absorption (blue) and emission (black) spectra of **4.5** in dichloromethane (DCM). Emission spectra recorded with λ_{ex}= 625 nm. c = 2.00 x 10^{-5} (UV) and 1.43 x 10^{-6} $mol^{-1}dm^3cm^{-1}$ (emission).

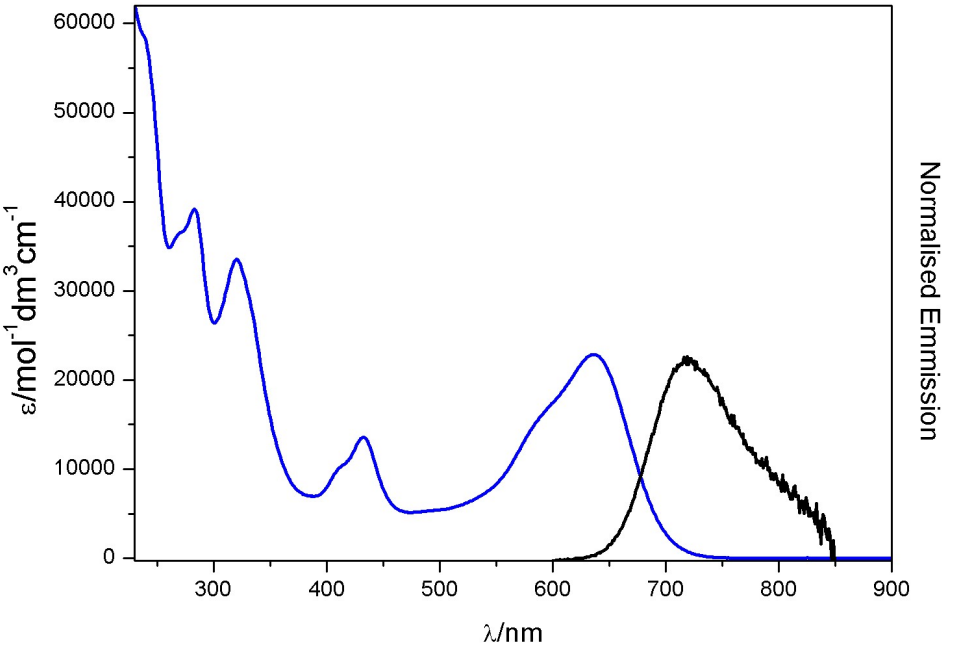

Figure 4.12. UV/vis absorption (blue) and emission (black) spectra of **4.8** in DCM. Emission spectra recorded with λ_{ex}= 590 nm. c = 2.49 x 10^{-5} (UV) and 3.16 x 10^{-6} $mol^{-1}dm^3cm^{-1}$ (emission).

The absorption maximum for **4.8** is at 636 nm and, whilst still displaying vibrational structure, this structure is less well defined than observed for **4.5**. The absorption maximum is red shifted by 16 nm *vs.* **4.5** suggesting that the morpholine is slightly more

electron donating than the Pt acetylide group in **4.8**. Emission measurements on **4.8** reveal an emission with a maximum at 719 nm corresponding to a Stokes shift of 83 nm. The quantum yield of emission was measured to be 0.10 again indicating likely formation of a triplet excited state, however, this quantum yield is considerably higher than that of **4.5** suggesting this triplet excited state formation is less efficient due to the presence of only one 'heavy' platinum atom.

Compound	λ_{max} (nm)	λ_{em} (nm)	Stokes Shift (nm)	Quantum Yield	Lifetime (ns)
4.5	625	685	60	0.02	7
4.8	636	719	83	0.10	-

Table 4.1. Summary of optical properties of **4.5** and **4.8** measured in DCM.

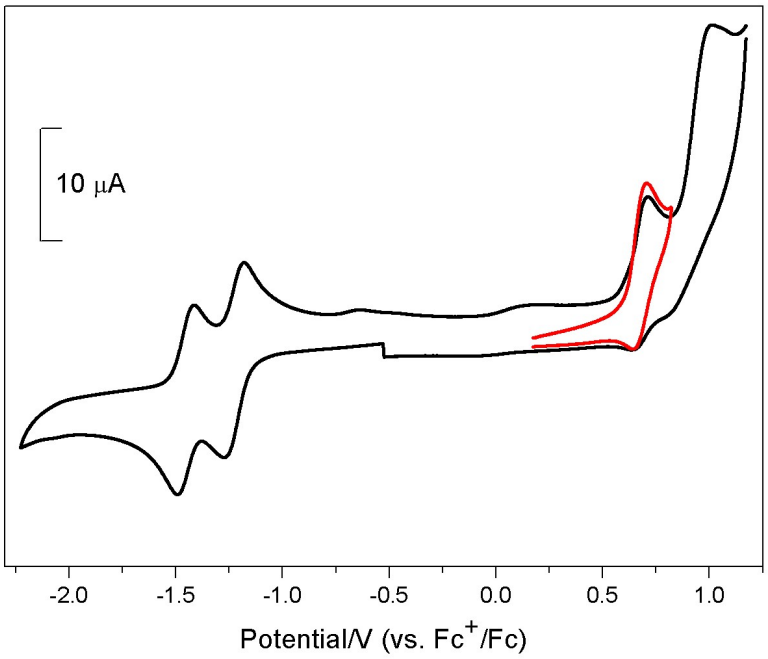

Figure 4.13. Cyclic voltammogram of **4.5** (red line shows first oxidation only) recorded in DCM containing $[Bu_4N][BF_4]$ (0.4 M).

The redox behaviour of **4.5** and **4.8** was probed with cyclic voltammetry and the effect of oxidation and reduction on the absorption profiles of the two molecules was further investigated by spectroelectrochemistry, Table 4.2 and Table 4.3. Cyclic voltammetric investigations on **4.5** revealed the two expected reversible one-electron reductions on

the PDI core at -1.22 and -1.46 V (*vs*. Fc^+/Fc), Figure 4.13. These reduction potentials are more negative than non-bay substituted PDIs and, interestingly, more negative than the dimorpholino-substituted PDIs synthesised by Champness and co-workers.[35] The red shift observed upon exchange of a Pt complex for a morpholine in **4.8** indicated that morpholine is more electron donating than the Pt complex. However, **4.5** possessing more negative reduction potentials than the dimorpholino-substituted PDI suggests the opposite. An oxidation was also observed in the cyclic voltammogram at 0.71 V (*vs*. Fc^+/Fc), not seen in unsubstituted PDIs. Electrochemical reversibility of this process could not be confirmed due to overlap with another oxidation, at a higher potential, which was not found to be reversible.

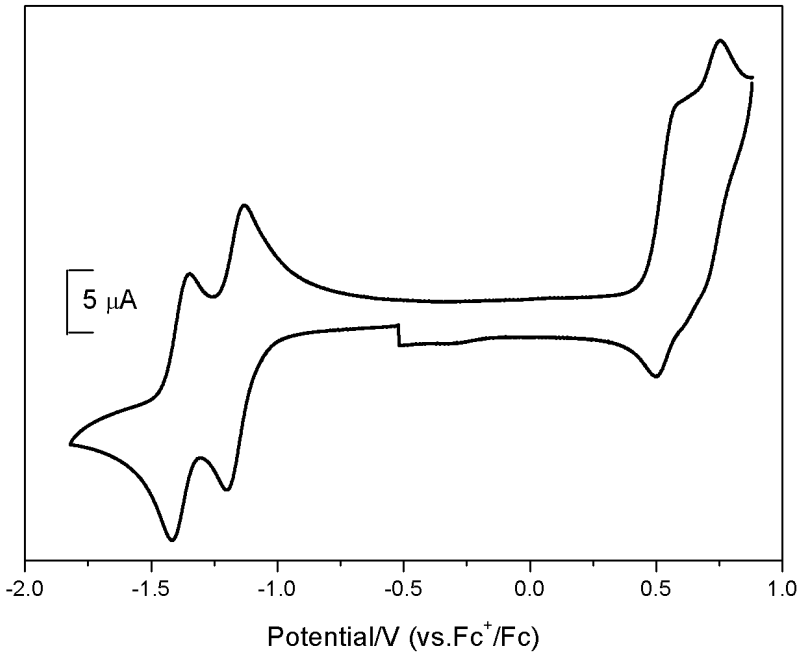

Figure 4.14. Cyclic voltammogram of **4.8** recorded in DCM containing $[Bu_4N][BF_4]$ (0.4 M).

4.8 was found, *via* cyclic voltammetry, to again possess two reversible one-electron reductions, Figure 4.14. The potential of these two process was measured at -1.16 and -1.38 V (*vs*. Fc^+/Fc), less negative than the equivalent reductions in **4.5** by 0.06 and 0.08 V, respectively, but still more negative than the reductions in the dimorpholino-

substituted PDI. Again this result points to the Pt complex being more electron donating than the morpholino group. Two oxidation processes are also observed, however, they are overlapping and were not found to be reversible over a scan rate range 0.02 – 0.3 Vs^{-1} so were not investigated further.

Compound	1st Reduction	2nd Reduction	Oxidation
4.5	-1.22	-1.46	0.71
4.8	-1.16	-1.38	-

Table 4.2. Reduction potentials for **4.5** and **4.8**. All potentials reported as $E_{1/2}$ (= $(E_p^a + E_p^c)/2$) in V *vs.* Fc^+/Fc at 0.1 Vs^{-1} scan rate and quoted to the nearest 0.01 V.

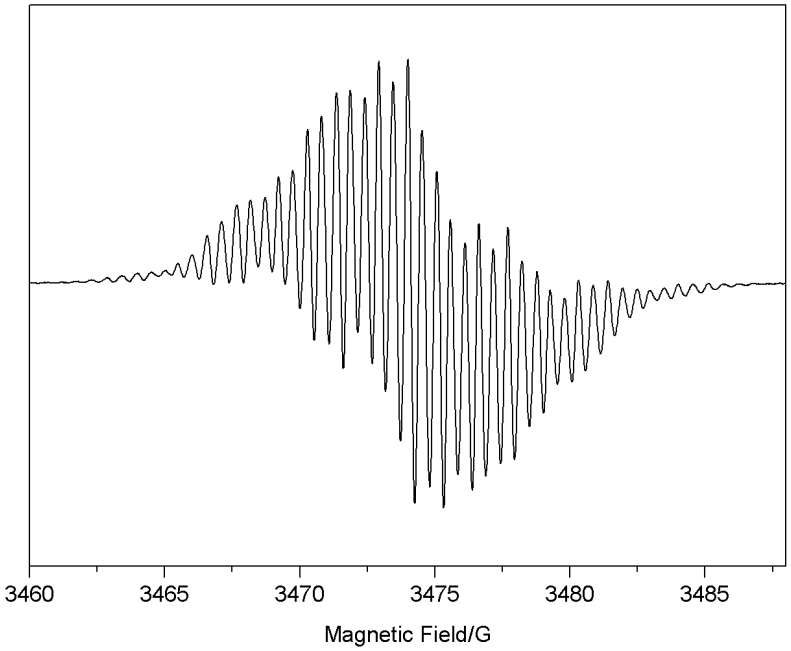

Figure 4.15. Experimental EPR spectra for electrochemically generated **4.5•-** (g_{iso}=2.0044) in DCM containing $[Bu_4N][BF_4]$ (0.4 M) at ambient temperature.

The electrochemical one-electron reduction of **4.5** gave a species that was green in colour and paramagnetic. As a fluid solution, at ambient temperature, EPR spectroscopy gave a signal consistent with the generation of a radical anion (g_{iso} 2.0044). A complex hyperfine splitting pattern was observed for **4.5•−** but this was not simulated satisfactorily. No obvious metal hyperfine coupling was observed in the fluid solution spectrum at ambient temperature suggesting that the unpaired electron density resides mainly around the PDI core.

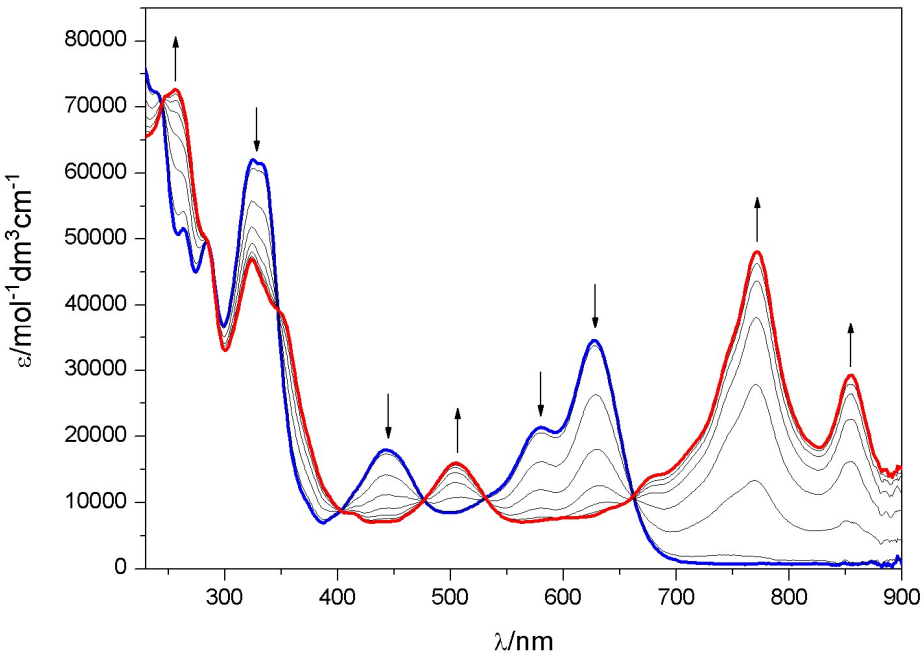

Figure 4.16. UV/vis absorption spectra recorded in DCM containing $[Bu_4N][BF_4]$ (0.4 M) using spectroelectrochemical methods for **4.5** at 273 K showing the inter-conversion of **4.5** (blue) to **4.5**$^{\bullet-}$ (red). c = 3.84 x 10^{-4} $mol^{-1}dm^3cm^{-1}$. Arrows indicate the progress of the reduction.

The one- and two-electron reductions of **4.5** and **4.6** were followed by *in situ* UV/vis spectroelectrochemistry at an optically transparent electrode, Table 4.3. The one-electron reduced radical anion **4.5**$^{\bullet-}$ shows major bands red shifted relative to their parent molecule with a maximum at 771 nm, red shifted by 142 nm, and a series of transitions extending into the near infrared (NIR) region, Figure 4.16. The second reduction blue shifts the spectrum with respect to that of the radical monoanion, with the most intense visible transitions occurring as a series of bands centred around 600 nm, Figure 4.17. This behaviour is highly characteristic of reductions occurring at the PDI core.[36, 37] Oxidation of **4.5** to **4.5**$^{\bullet+}$ was also investigated and new bands, with a maxima at 613 nm, that extended into NIR were noted. However, this oxidation was not electrochemically reversible under the experimental conditions, Figure 4.18. The absorption profile generated upon oxidation is similar to that observed in the dimorpholino-substituted PDI suggesting these processes are analogous and lie on the PDI core.[35]

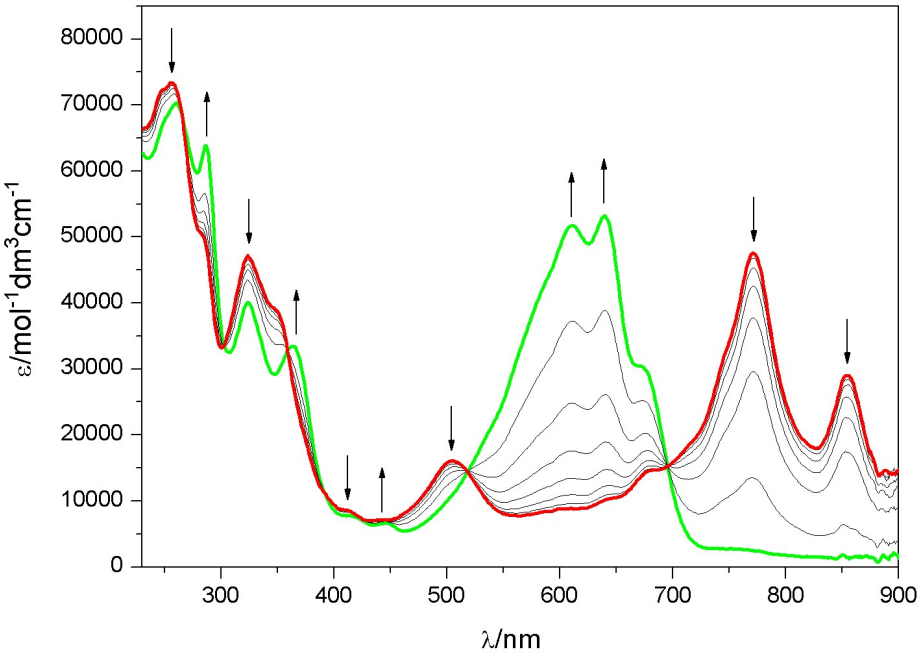

Figure 4.17. UV/vis absorption spectra recorded in DCM containing $[Bu_4N][BF_4]$ (0.4 M) using spectroelectrochemical methods for **4.5** at 273 K showing the inter-conversion of $\mathbf{4.5^{\bullet-}}$ (red) to $\mathbf{4.5^{2-}}$ (green). c = 3.84 x 10^{-4} $mol^{-1}dm^3cm^{-1}$. Arrows indicate the progress of the reduction.

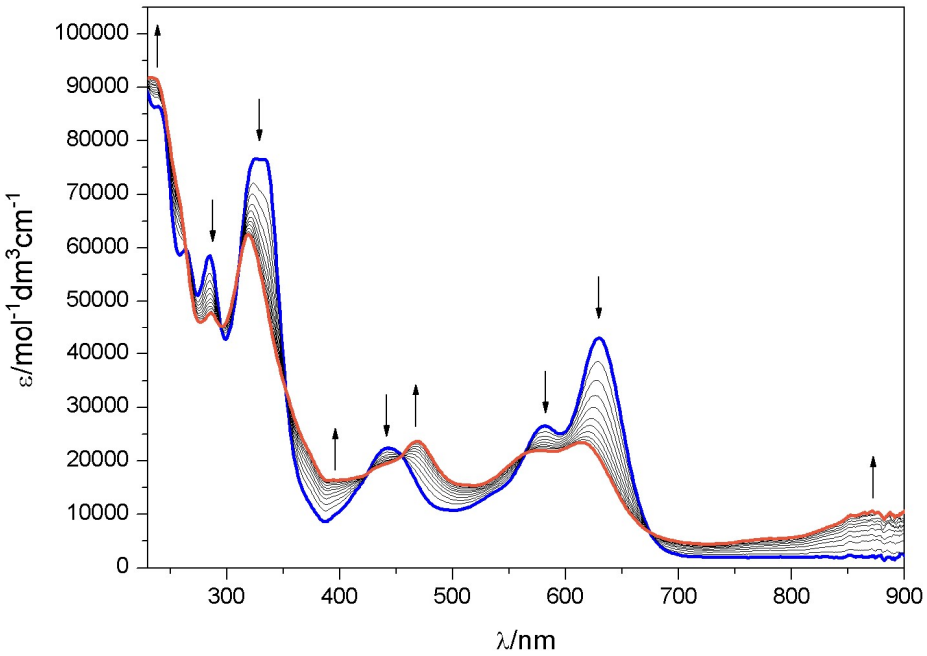

Figure 4.18. UV/vis absorption spectra recorded in DCM containing $[Bu_4N][BF_4]$ (0.4 M) using spectroelectrochemical methods for **4.5** at 243 K showing the inter-conversion of **4.5** (blue) to $\mathbf{4.5^{\bullet+}}$ (orange). c = 3.84 x 10^{-4} $mol^{-1}dm^3cm^{-1}$. Arrows indicate the progress of the oxidation.

The behaviour of **4.8** following first reduction is similar to that of **4.5**. The main absorption band is depleted and is replaced by a more intense band red shifted to 777 nm, Figure 4.19. The magnitude of the red shift of 141 nm is within 1 nm of the corresponding shift in **4.5**, the increase in intensity is, however, more pronounced. Upon second reduction, the main absorption is again blue shifted to around 600 nm with a very similar shape to $\mathbf{4.5}^{2-}$, Figure 4.20. Both of these reductions were found to be fully reversible with the neutral spectra being regenerated upon reoxidation. The only effect the change from a Pt complex to morpholine has on the spectroelectrochemical behaviour is a minor change in the wavelengths of absorption, similar to that seen in the neutral UV/vis spectra.

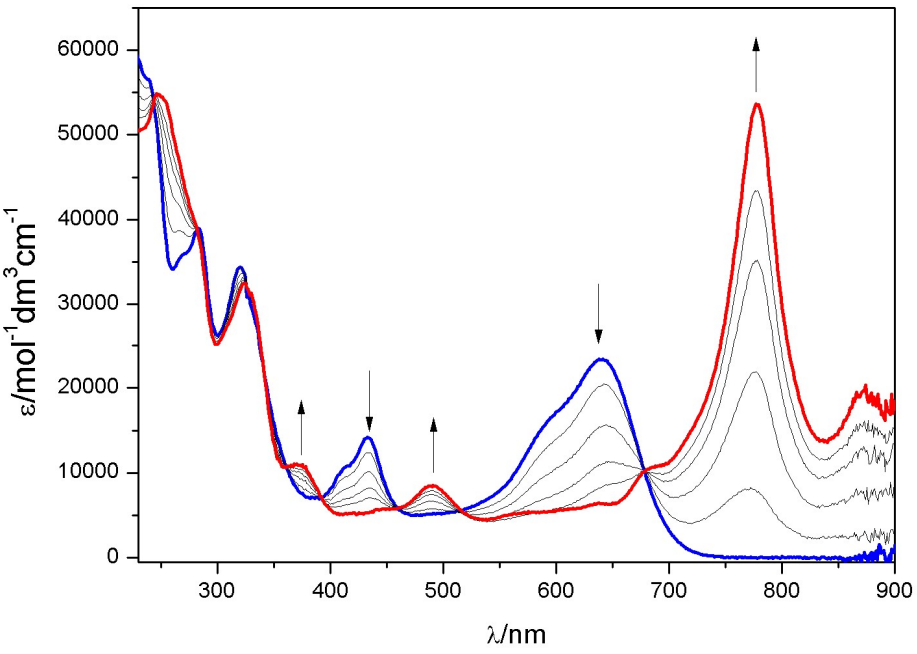

Figure 4.19. UV/vis absorption spectra recorded in DCM containing $[Bu_4N][BF_4]$ (0.4 M) using spectroelectrochemical methods for **4.8** at 273 K showing the inter-conversion of **4.8** (blue) to $\mathbf{4.8}^{\bullet-}$ (red). c = 4.28 x 10^{-4} $mol^{-1}dm^3cm^{-1}$. Arrows indicate the progress of the reduction.

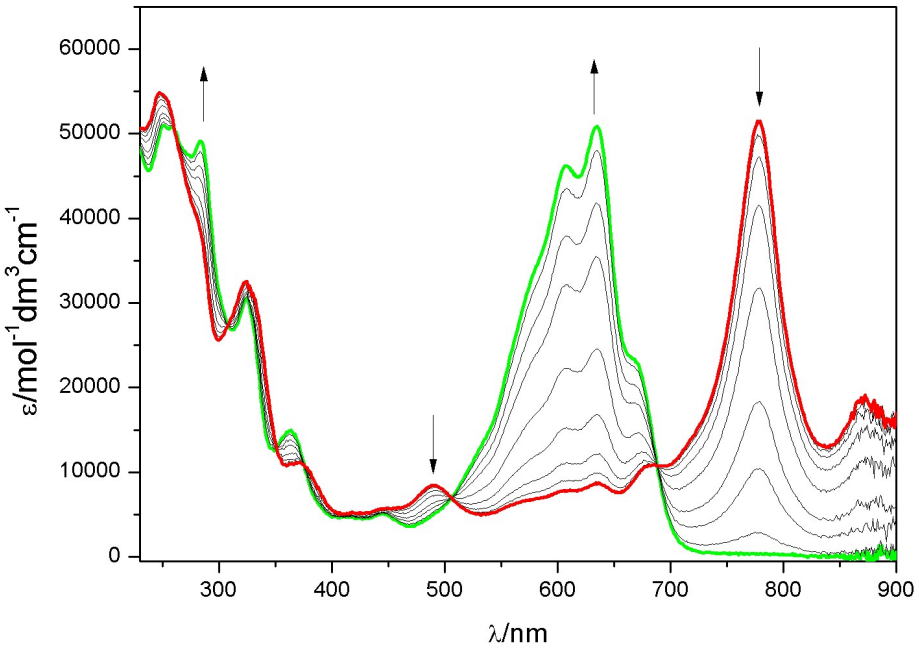

Figure 4.20. UV/vis absorption spectra recorded in DCM containing $[Bu_4N][BF_4]$ (0.4 M) using spectroelectrochemical methods for **4.8** at 273 K showing the inter-conversion of **4.8**$^{\bullet-}$ (red) to **4.8**$^{2-}$ (green). c = 4.28 x 10^{-4} $mol^{-1}dm^3cm^{-1}$. Arrows indicate the progress of the reduction.

	Neutral	Reduction		Oxidation
		1st	2nd	
4.5	263 (3.0), 284 (2.9), 325 (3.6), 443 (1.0), 578 (1.2), 629 (2.0)	257 (4.3), 325 (2.8), 504 (0.9), 771 (2.8), 855 (1.7)	259 (4.1), 287 (3.8), 325 (2.4), 364 (2.0), 447 (0.4), 610 (3.0), 640 (3.1)	286 (2.8), 318 (3.7), 468 (1.4), 577 (1.3), 613 (1.4)
4.8	283 (3.9), 320 (3.4), 432 (1.4), 636 (2.3)	246 (5.5), 324 (3.3), 370 (1.1), 491 (0.85), 777 (5.4)	283 (4.9), 362 (1.5), 608 (4.6), 635 (5.1)	-

Table 4.3. UV/vis spectroscopic data for **4.5** and **4.8** measured at 273 K in DCM from spectroelectrochemistry. All values λ_{max}/nm (ε x10^5/$mol^{-1}dm^3cm^{-1}$).

In order to investigate the nature of the excited state formed upon excitation of **4.5**, singlet oxygen generation experiments were undertaken to probe the potential formation of a triplet excited state. In an air-equilibrated DCM solution, excitation of **4.5** at 532 nm leads to formation of $^1O_2$, detected by its characteristic luminescence at 1275 nm, Figure 4.21. Oxygenating the solution affords $^1O_2$ emission with significantly

higher signal. Confirmation that the emission detected was from $^1O_2$ was obtained by purging the solution of **4.5** for 5 minutes with N_2 gas, after which no emission was detected at 1275 nm. The emission at 1275 nm returned on bubbling the solution for 5 minutes with O_2 gas. The same results (with lower signal intensity) were observed on repeating the experiment at a reduced concentration of **4.5**, further indicating that the complex is acting as a sensitiser for singlet oxygen formation. The lifetime of singlet oxygen emission was determined to be 88 μs, in DCM, consistent with literature values for this solvent.[38] When the experiment was repeated in toluene for **4.5**, a lifetime of 37 μs was recorded, again consistent with literature values.[38]

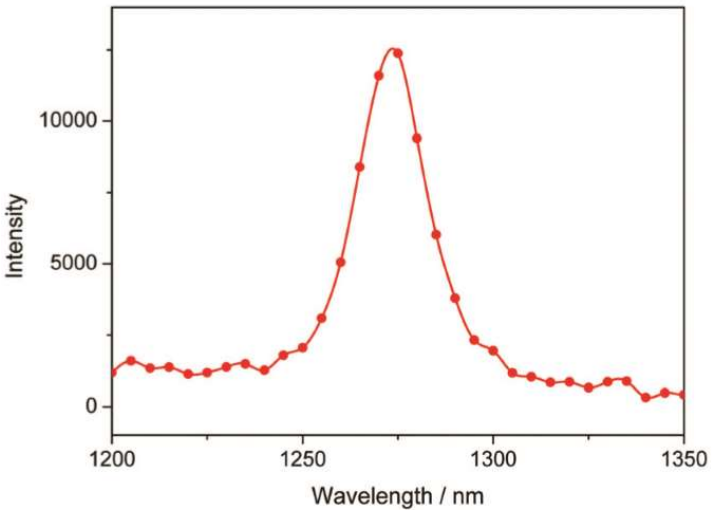

Figure 4.21. Singlet oxygen emission spectrum of **4.5** recorded in oxygenated DCM with λ_{ex} = 337 nm. These measurements were performed by Professor Andrew Beeby of the University of Durham.

The formation of the triplet excited state was then further probed by ultrafast transient absorption spectroscopy. The transient absorption difference spectra at selected delay times of **4.5** following excitation by 400 nm laser pulses are shown in Figure 4.22a. The bands displayed in the spectra are assigned to specific processes by comparison to the previous Pt-PDIs reported by Castellano and co-workers.[19-21] The bands compare well to these compounds, however, they are all slightly red shifted due to the increased wavelength of the S_0-S_1 absorption of **4.5**.

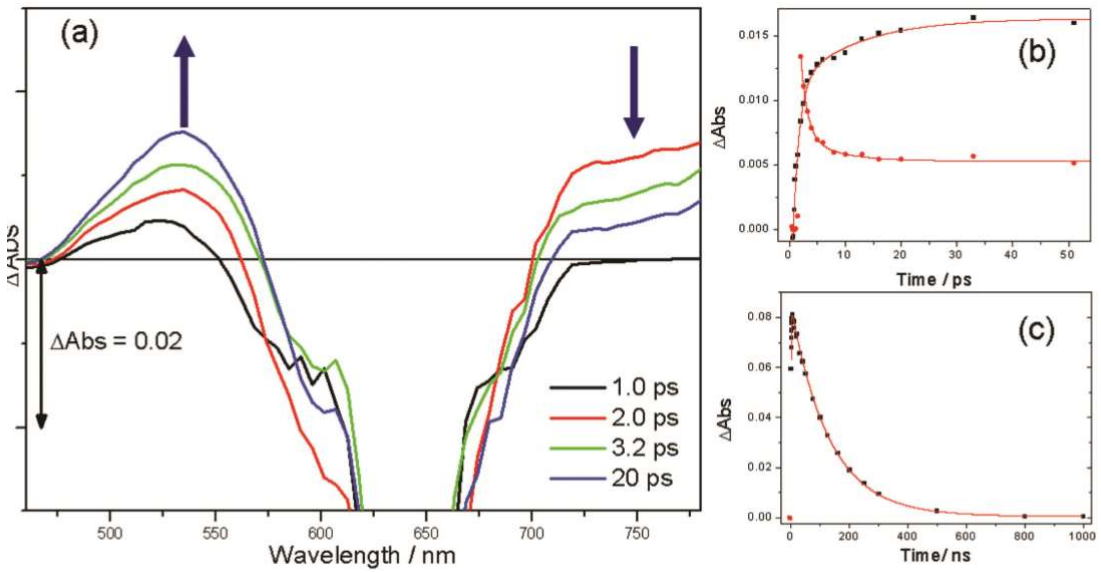

Figure 4.22. (a) Picosecond transient absorption spectra of **4.5** in DCM at selected time delays after 400 nm excitation; (b) ps kinetic traces at 532 nm (black squares) and 760 nm (red circles), and (c) the ns kinetic trace at 505 nm of the same sample after 355 nm excitation. Red lines denote kinetic fits. These measurements were performed by Dr Xue-Zhong Sun and Professor Mike George of the University of Nottingham.

Upon excitation at 400 nm, the ground state absorption at 629 nm is immediately bleached indicating excitation from the ground state is occurring. This bleaching is accompanied by the formation of a new lower energy broad band above 700 nm which is assigned to the singlet excited state of the PDI. This low energy band is then itself bleached, accompanied by the formation of a new band at 532 nm which is assigned to the triplet excited state of the PDI. The growth of this band is at the exact same rate as the bleaching of the low energy band. The triplet absorption at 532 nm increases in intensity on two other timescales. The faster of these can be seen above 10 ps in Figure 4.22b and is attributed to vibrational cooling of the triplet state. The slower growth, over 1 ns, is less clear and has not been assigned to a specific process, Figure 4.22c. The lifetime of the triplet state was measured to be 132 ns which, whilst shorter than those observed by Castellano and co-workers, is considerably longer than would be expected from a singlet excited state. This triplet lifetime is also ~19 times longer than that of the observed emission of **4.4**. This emission has not been successfully assigned

to either the singlet or triplet excited state. The combination of singlet oxygen generation and ultrafast transient absorption spectroscopy has shown that **4.5** is indeed able to access the triplet excited state due to the 'heavy atom' effect following introduction of platinum complexes to the bay-area of the PDI.

4.3. Conclusions

This Chapter describes the synthesis of two PDIs substituted at the bay area with a platinum acetylide complex, **4.5** is substituted with this complex on both sides of the molecule whilst **4.8** is asymmetrically substituted with one of the platinum complexes being replaced by a morpholine moiety. The synthetic pathway was similar in both cases. However, different protecting groups were necessary in order to optimise the yields. X-ray crystal structures of **4.3** and **4.5** displayed how changing the steric hindrance around the core of the PDI affects the twist between the naphthalene units and the packing of the molecules in the solid state.

UV/vis spectroscopic studies revealed the substitution had induced a bathochromic shift in absorbance suggesting the platinum complexes are electron donating. This electron donating effect was further confirmed by the cyclic voltammetry as, in both cases, the two one-electron PDI based reductions were moved to a more negative potential suggesting greater electron density on the PDI core. The incorporation of the platinum complexes introduced oxidation processes although determination of reversibility was not possible. Interestingly, UV/vis spectroscopy suggests that the morpholine is more electron donating, due to a more pronounced bathochromic shift in **4.8**, conversely cyclic voltammetry indicates the opposite as the reductions on **4.5** were measured at a more negative potential.

Spectroelectrochemical methods were used to investigate the effect of oxidation and reduction upon the absorption profiles of the compounds. Both **4.5** and **4.8** exhibited similar behaviour upon formation of their monoanions and dianions as reported previously in this thesis and in the literature. The oxidation of **4.5** resulted in small changes in the absorption profile compared to the neutral species.

Emission spectra revealed both molecules to be emissive, however, this emission was significantly quenched compared to unsubstituted PDIs, suggesting potential formation of the triplet excited state. This was investigated for **4.5** by the generation of singlet oxygen and transient absorption spectroscopy confirming the presence of intersystem crossing, following excitation, to the triplet excited state of the PDI caused by the 'heavy atom' effect due to the covalently linked platinum atom. The lifetime of this state (132 ns) was between that of singlet generating PDIs and other Pt-PDIs capable of accessing the triplet excited state. The emission, which bears the profile of phosphorescence but a lifetime between that of phosphorescence and fluorescence, was not successfully assigned to either process. The equivalent measurements for **4.8** are ongoing.

4.4. Experimental

For experimental details relating to electrochemical and optical investigations (except emission measurements, see below) and DFT see Chapter 2.

General Experimental Methods

All starting materials were purchased from Sigma Aldrich or Fisher Scientific and were used without further purification unless otherwise stated. Column chromatography was performed on silica gel (Merck silica gel 60, 0.2–0.5 mm, 50–130 mesh). Reactions using dry solvents (Sigma Aldrich) were carried out utilising standard Schlenk techniques. The ^{1}H, ^{13}C and ^{31}P NMR spectra were obtained on a Bruker 400 MHz spectrometer. MS spectra were determined on a VoyagerDE-STR spectrometer (MALDI-TOF) with DCTB as the matrix, a Bruker microTOF II spectrometer (ESI) or a JEOL GCv4G spectrometer (FI).

Synthesis of *cis*-di(tri-n-butylphosphine)platinum dichloride (4.1)

Synthesis adapted from a literature procedure.[39] Potassium tetrachloroplatinate (560 mg, 1.35 mmol) was dissolved in water (20 mL) and the solution degassed with N_2 for 15 mins. Tri-n-butyl phosphine (0.81 mL, 3.26 mmol) was added and the solution was stirred at room temperature, under an inert atmosphere, for 16 h. The resulting precipitate was filtered and washed with water before being dissolved in chloroform and dried over $MgSO_4$ and the solvent removed under reduced pressure. The crude product was dissolved in DCM:EtOAc (1:1) and run through a silica plug before trituration with hexane and separation by centrifugation to give **4.1** as a white powder (264 mg, 0.394 mmol, 29 %). ^{1}H NMR ($CDCl_3$, 400 MHz): δ = 1.89 - 2.09 (m, 12 H),

1.40 - 1.59 (m, 24 H), 0.95 ppm (t, *J*=7.2 Hz, 18 H). ^{31}P NMR ($CDCl_3$, 162 MHz): δ = 0.97 ppm (s, satellites *J*= 3520 Hz).

Synthesis of *trans*-phenylethynylchlorobis(tri-n-butylphosphine)platinum (4.2)

Synthesis adapted from a literature procedure.[40] **4.1** (250 mg, 0.373 mmol) was dissolved in diethylamine (10 mL) and the solution was degassed with N_2 for 15 mins, phenyl acetylene (35 µL, 0.313 mmol) was added and the solution was heated to 65 ºC, under an inert atmosphere, for 4 h. The solution was cooled and the solvent removed under reduced pressure. The crude product was purified by column chromatography (SiO_2, chloroform:hexane 1:1) to give **4.2** as a yellow oil (99 mg, 0.135 mmol, 36 %). ^{1}H NMR ($CDCl_3$, 400 MHz): δ = 7.10 - 7.26 (m, 5 H), 1.94 - 2.11 (m, 12 H), 1.56 - 1.62 (m, 12 H), 1.40 - 1.51 (m, 12 H), 0.93 ppm (t, *J*=7.3 Hz, 18 H). ^{13}C NMR ($CDCl_3$, 101 MHz): δ = 130.8, 128.9, 127.9, 125.1, 101.0, 83.0, 26.1 (apparent t, $^1J_{CP}$=11.1 Hz), 24.3 (apparent t, $^2J_{CP}$=6.1 Hz), 21.9 (apparent t, $^3J_{CP}$=16.2 Hz), 13.8 ppm. ^{31}P NMR ($CDCl_3$, 162 MHz): δ = 6.88 ppm (s, satellites *J*= 2375 Hz).

Synthesis of *N,N'*-di-(cyclohexyl)-1,7-triisopropylsilylyacetyl-3,4:9,10-perylenetetracarboxylic diimide (4.3)

3.1 (200 mg, 0.281 mmol) was dissolved in a mixture of dry THF (12 mL) and dry triethylamine (5 mL). $PdCl_2(PPh_3)_2$ (8.4 mg, 0.011 mmol), CuI (3 mg, 0.140 mmol) and (triisopropylsilyl)acetylene (0.25 ml, 1.12 mmol) were added and the mixture was heated at reflux, under an inert atmosphere, for 3 h. The reaction mixture was cooled to room temperature, poured into HCl (2 M), the product was extracted with DCM and the organic layer was washed with water until neutral. The crude product was purified by column chromatography (SiO_2, DCM) to give **4.3** as a red powder (251 mg, 0.274 mmol, 97 %). ^{1}H NMR ($CDCl_3$, 400 MHz): δ = 10.31 - 10.39 (m, 2 H), 8.80 (s, 2 H),

8.60 (d, *J*=8.3 Hz, 2 H), 5.00 - 5.13 (m, 2 H), 2.51 - 2.70 (m, 4 H), 1.91 - 2.00 (m, *J*=12.5 Hz, 4 H), 1.73 - 1.86 (m, 6 H), 1.41 - 1.56 (m, 6 H), 1.22 - 1.31 ppm (m, 42 H). ^{13}C NMR ($CDCl_3$, 101 MHz): δ = 163.6, 163.3, 138.5, 133.9, 130.5, 127.7, 127.6, 127.3, 123.6, 122.5, 119.9, 107.6, 103.8, 54.1, 29.1, 26.5, 25.5, 18.8, 11.4 ppm. HRMS(FI-TOF) $[M]^+$: calcd for $C_{58}H_{70}N_2O_4Si_2$ 914.4874, found 914.4890.

Synthesis of *N,N'*-di-(cyclohexyl)-1,7-ethynyl-3,4:9,10-perylenetetracarboxylic diimide (4.4)

4.3 (220 mg, 0.295 mmol) was dissolved in a mixture of chloroform (15 mL) and methanol (5 mL). NaOH (13 mg) was added and the mixture was stirred at room temperature for 1.5 h. The crude product was separated by filtration, suspended in MeOH, sonicated and the solvent was filtered off giving **4.4** as a purple solid (159 mg, 0.264 mmol, 90 %). The solubility of the product precluded the acquisition of NMR data. HRMS(FI-TOF) $[M]^+$: calcd for $C_{40}H_{30}N_2O_4$ 602.2206, found 602.2205.

Synthesis of *N,N'*-di-(cyclohexyl)-1,7-di(tri-n-butylphosphine)-phenylethynyl-platinum(II)-ethynylen)-3,4:9,10-perylenetetracarboxylic diimide (4.5)

4.4 (80 mg, 0.13 mmol) and **4.2** (194 mg, 0.27 mmol) were dissolved in a mixture of DCM (20 mL) and diethylamine (10 mL). CuI (27 mg) was added and the solution was degassed with N_2 for 15 min and stirred at room temperature, under an inert atmosphere, for 18 hours. The solvent was removed under reduced pressure and the crude product was purified by column chromatography (SiO_2, DCM:petroleum ether 1:1) to give **4.5** as a blue-black powder (48 mg, 0.0240 mmol, 18 %). ^{1}H NMR ($CDCl_3$, 400 MHz): δ = 11.54 (d, *J*=8.4 Hz, 2 H), 9.31 (s, 2 H), 9.10 (d, *J*=8.3 Hz, 2 H), 7.05 - 7.81 (m, 10 H), 5.43 - 5.59 (m, 2 H), 2.93 - 3.11 (m, *J*=11.8 Hz, 4 H), 2.19 - 2.41 (m, 24 H), 1.80 - 1.96 (m, 34 H), 1.51 - 1.57 (m, 24 H), 1.40 (d, *J*=7.5 Hz, 6 H), 1.06 ppm (t, *J*=7.3 Hz,

36 H). ^{13}C NMR ($CDCl_3$, 126 MHz): δ = 164.1, 164.1, 138.7, 135.0, 131.2, 130.8, 128.9, 128.8, 128.0, 127.9, 126.3, 125.4, 125.2, 125.1, 122.4, 121.4, 113.9, 109.8, 106.4, 96.1, 53.6, 29.1, 26.5, 26.4, 25.4, 24.3 (apparent t, $^2J_{CP}$ = 6.8 Hz), 24.1 (apparent t, $^3J_{CP}$ = 17.3 Hz), 13.8 ppm. ^{31}P NMR ($CDCl_3$, 162 MHz): δ = 3.46 (s, satellites *J*= 2331 Hz) ppm. MS(MALDI-TOF) $[M]^-$: 1998.6. CHN calculated for $C_{104}H_{146}N_2O_4P_4Pt_2$, C 62.38 % H 7.35 % N 1.04 %. Found C 62.24 % H 7.24 % N 1.12 %.

Synthesis of *N,N'*-di-(cyclohexyl)-1-trimethylsilylyacetyl-7-morpholino-3,4:9,10-perylenetetracarboxylic diimide (4.6)

3.5 (250 mg, 0.348 mmol), di(triphenylphosphine)palladium dichloride (7 mg, 9.97x10^{-3} mmol) and copper iodide (5 mg, 0.0263 mmol) were dissolved in a mixture of dry THF (30 mL) and dry triethylamine (10 mL). Trimethylsilylacetylene (0.1 mL, 0.7 mmol) was added and the solution was heated to reflux, under an inert atmosphere, for 4 h. The solution was poured into cold HCl (2 M), chloroform was added and the organic extract was washed with water twice. The solution was dried over $MgSO_4$ before the solvent was removed under reduced pressure. The crude product was purified by column chromatography (SiO_2, chloroform:EtOAc 97:3) to give **4.6** as a blue/green powder (222 mg, 0.302 mmol, 87 %). ^{1}H NMR ($CDCl_3$, 400 MHz): δ = 9.89 (d, *J*=8.3 Hz, 1 H), 9.79 (d, *J*=8.3 Hz, 1 H), 8.66 - 8.70 (m, 1 H), 8.54 (d, *J*=8.4 Hz, 1 H), 8.42 - 8.48 (m, 2 H), 5.05 (t, *J*=12.1 Hz, 2 H), 3.83 - 4.01 (m, 4 H), 3.35 (d, *J*=11.9 Hz, 2 H), 3.09 (t, *J*=9.7 Hz, 2 H), 2.50 - 2.66 (m, 4 H), 1.94 (d, *J*=10.8 Hz, 4 H), 1.70 - 1.86 (m, 6 H), 1.49 (q, *J*=12.8 Hz, 4 H), 1.37 (t, *J*=12.9 Hz, 2 H), 0.37 ppm (s, 9 H). ^{13}C NMR ($CDCl_3$, 101 MHz): δ = 163.8, 163.5, 163.3, 151.1, 137.7, 135.2, 135.1, 133.3, 130.7, 129.4, 128.0, 127.9, 127.8, 127.8, 124.6, 124.3, 124.2, 123.6, 123.2, 122.4, 121.8,

121.8, 118.2, 105.5, 104.0, 66.4, 54.1, 53.9, 51.6, 29.2, 29.0, 26.5, 25.5, 25.4 ppm. HRMS(MALDI-TOF) $[M]^+$: calcd for $C_{45}H_{45}N_3O_5Si$ 735.3128, found 735.3090.

Synthesis of *N,N'*-di-(cyclohexyl)-1-ethynyl-7-morpholino-3,4:9,10-perylenetetracarboxylic diimide (4.7)

4.6 (100 mg, 0.136 mmol) was dissolved in a chloroform:methanol mix (15 mL, 2:1), sodium hydroxide (10 mg, 0.25 mmol) was added and the solution was stirred for 1 h. The solution was then filtered to remove the sodium hydroxide and the solvent removed under reduced pressure to give **4.7** as a blue powder (81 mg, 0.122 mmol, 90 %). ^{1}H NMR ($CDCl_3$, 400 MHz): δ = 9.85 (d, *J*=8.2 Hz, 1 H), 9.82 (d, *J*=8.3 Hz, 1 H), 8.74 (s, 1 H), 8.59 (d, *J*=8.3 Hz, 1 H), 8.52 (d, *J*=8.2 Hz, 1 H), 8.49 (s, 1 H), 4.98 - 5.11 (m, *J*=15.3, 8.8, 3.0 Hz, 2 H), 3.87 - 4.02 (m, 4 H), 3.70 (s, 1 H), 3.39 (d, *J*=12.0 Hz, 2 H), 3.08 - 3.20 (m, 2 H), 2.49 - 2.66 (m, *J*=12.4, 12.4, 12.4 Hz, 4 H), 1.87 - 2.00 (m, *J*=12.4 Hz, 4 H), 1.70 - 1.83 (m, 6 H), 1.34 - 1.55 ppm (m, 6 H). ^{13}C NMR ($CDCl_3$, 101 MHz): δ = 163.8, 163.7, 163.5, 163.2, 151.3, 137.9, 135.7, 135.1, 133.0, 131.0, 129.3, 128.3, 128.1, 127.9, 127.8, 124.5, 124.4, 124.1, 123.7, 123.2, 122.2, 121.9, 121.7, 117.0, 85.1, 84.3, 66.4, 54.1, 54.0, 51.6, 29.1, 29.1, 26.5, 25.4, 25.4 ppm. HRMS(MALDI-TOF) $[M]^+$: calcd for $C_{42}H_{37}N_3O_5$ 663.2733, found 663.2737.

Synthesis of *N,N'*-di-(cyclohexyl)-1-di(tri-n-butylphosphine)-phenylethynyl-platinum(II)-ethynylen)-7-morpholino-3,4:9,10-perylenetetracarboxylic diimide (4.8)

4.7 (37 mg, 0.0557 mmol) and **4.2** (43 mg, 0.0584 mmol) were dissolved in a DCM (7 mL) and diethylamine (3 mL). The solution was degassed with N_2 for 15 mins, copper iodide (7 mg, 0.0368 mmol) was added and the solution was stirred at room temperature for 30 mins. The reaction was quenched by the addition of water and the organic extract

was washed with water three times. The solution was dried over $MgSO_4$ and the solvent removed under reduced pressure. The crude product was purified by column chromatography (SiO_2, chloroform:acetone 99:1) to give **4.8** as a green powder (26 mg, 0.0191 mmol, 34 %). ^{1}H NMR ($CDCl_3$, 400 MHz): δ = 10.79 (d, *J*=8.3 Hz, 1 H), 10.01 (d, *J*=8.4 Hz, 1 H), 8.66 (s, 1 H), 8.47 - 8.55 (m, 2 H), 8.45 (d, *J*=8.3 Hz, 1 H), 7.28 - 7.33 (m, 2 H), 7.20 - 7.26 (m, 2 H), 7.10 - 7.18 (m, 1 H), 5.05 (td, *J*=12.0, 3.1 Hz, 2 H), 3.88 - 4.04 (m, 4 H), 3.40 (d, *J*=11.8 Hz, 2 H), 3.06 - 3.17 (m, 2 H), 2.53 - 2.65 (m, 4 H), 2.07 - 2.20 (m, 12 H), 1.89 - 1.95 (m, *J*=12.3 Hz, 4 H), 1.73 - 1.80 (m, 6 H), 1.59 - 1.65 (m, 12 H), 1.36 - 1.51 (m, 18 H), 0.87 ppm (t, *J*=7.3 Hz, 18 H). ^{13}C NMR ($CDCl_3$, 101 MHz): δ = 164.3, 164.1, 163.9, 163.8, 150.3, 138.7, 135.4, 134.6, 131.2, 130.8, 129.7, 128.9, 128.7, 128.4, 127.9, 126.4, 125.5, 125.1, 125.0, 124.5, 124.0, 123.5, 122.9, 122.2, 122.1, 121.4, 113.7, 113.2, 109.8, 106.2, 66.6, 53.8, 53.7, 51.6, 29.1, 26.5, 26.4, 25.5, 24.3 (apparent t, $^2J_{CP}$ = 7.3 Hz), 24.1 (apparent t, $^3J_{CP}$ = 17.6 Hz), 13.8 ppm ^{31}P NMR ($CDCl_3$, 162 MHz): δ = 3.51 ppm (s, satellites *J*= 2328 Hz). HRMS(MALDI-TOF) $[M]^+$: calcd for $C_{74}H_{95}N_3O_5P_2Pt$ 1362.6404, found 1362.6389.

Emission Measurements

Emission measurements were carried out under ambient conditions on a Horiba FluoroMax-3 spectrometer with a xenon arc lamp as the excitation source. Quantum yields were calculated by plotting the integrated fluorescence intensity *vs*. absorbance of five optically dilute solutions ($\lambda_{max} < 0.1$ $mol^{-1}dm^3cm^{-1}$) of the sample and comparing the gradient to that of a known standard ($Ru(bipy)_3Cl_2$ and Cresyl Violet for **4.5** and **4.8** respectively) using the equation: $\phi_x = \phi_{st}\left(\frac{Grad_x}{Grad_{st}}\right)\left(\frac{\eta_x 2}{\eta_{st} 2}\right)$ where the subscripts *st* and *x* denote standard and test respectively, ϕ is the fluorescence quantum yield, *Grad* the gradient from the plot of integrated fluorescence intensity *vs*. absorbance and η the

refractive index of the solvent. Emission lifetime measurements were performed on an Edinburgh Instruments FLS920 spectrometer using the time-correlated single-photon counting technique, with an EPL400 pulsed diode laser (405 nm, pulse width 95 ps) as the excitation source (time resolution *ca*. 1 ns). Solutions were thoroughly freeze–pump–thaw degassed in specially modified 1 × 1 cm quartz cuvettes. Sample concentrations were adjusted to be optically dilute.

Transient Absorption Measurements

Fast Transient Absorption Spectroscopic measurements were performed using a pump-probe method. The probe beam of white light continuum is generated by focusing a small amount of 800 nm (~400 nJ) laser beam into a 4 mm thick Sapphire disk. The picosecond 400 nm pump beam is obtained from a commercial Ti:sapphire oscillator/regenerative amplifier system (Spectra Physics, USA) and a TP-1 harmonic generator (TimePlate Tripler, Minioptic Technology, Inc.) and the time difference (up to 3 ns) between the pump and probe pulses is controlled by an optical delay line. The nanosecond 355 nm pump beam is produced with a Q-switched Nd:YVO laser (ACE-25QSPXHP/MOPA, Advanced Optical Technology, UK) which is electronically synchronised to the Spitfire Pro amplifier. The delay between pump and probe pulses can be controlled with a pulse generator (DG535, Stanford Research System, USA) from 0.5 ns to 100 μs. The white light beam is split into two parts. One part passes through the sample spatially overlapped with the pump beam. Another part serves as a reference to the probe beam fluctuations. The polarization of the pump pulse is set at the magic angle (54.7 degree) relative to the probe pulse to recover the isotropic absorption spectrum. Both parts of the probe beam are monitored by a duel array detector (512 pixels) (Cronin Camera, Spectronic device Ltd, UK). The detector is mounted in the focal plane of a 303 mm Acton spectrograph (Acton, USA) with a 150

g mm^{-1} grating. The pump beam size (~400 μm diameter) is larger than the probe spot (~200 μm diameter). A Harrick solution cell with 2-mm-thick CaF_2 windows is mounted on a motorized cell mount, which moves the cell in x and y dimensions rapidly and continuously.

Singlet Oxygen Generation

Singlet oxygen experiments were performed in DCM, initially air-equilibrated, subsequently oxygenated by bubbling with a steady stream of oxygen for 5 minutes, then deoxygenated by bubbling with N_2 gas for 5 minutes and finally reoxygenated by bubbling with O_2 gas for 5 minutes. Excitation was with a 532 nm Nd:YAG laser (GCR150-10, 10 Hz, 8 ns FWHM, ~45 μJ per pulse at sample). Time-dependent emission traces at 1200, 1275 and 1300 nm (500 μs, 0.5 μs per bin, ~1000 shots per spectrum) were collected at 90° via a monochromator (TRIAX-320), onto a NIR-PMT (Hamamatsu H10330A-45, −750 V, −60 °C) connected to a USB multichannel scalar controlled by LabVIEW.

X-Ray Crystallography

Single-crystal X-ray diffraction experiments were performed on either a Rigaku FR-E+ Ultra High Flux Diffractometer, **4.5**, or a Rigaku FR-E+ Very High Flux Diffractometer, **4.3**. Both structures were collected at 100 K, with the aid of an Oxford Cryosystems Cobra, using Mo Kα radiation (λ = 0.71073 Å). The structures were solved by direct methods using SHELXS97 and refined by full-matrix least squares on F2 using SHELXL97.[41]

Due to weak data arising from poor crystallinity of the crystals of **4.3** rigid bond and similarity restraints were applied to the anisotropic displacement parameters of all

atoms in the structure and the displacement parameters of the isopropyl groups have been restrained to be more isotropic. Disorder was observed in the conformation of cyclohexyl ring and the occupancies of the two components were refined and constrained to sum to unity (major component occupancy 0.55(1)). Geometric similarity restraints were applied to the 1,2 and 1,3 bond lengths of the disordered and ordered cyclohexyl groups reflecting their 2-fold symmetry. The atoms of the two disordered cyclohexyl rings were refined with isotropic displacement parameters. Similarly disorder was observed in the orientation of isopropyl group C88–C90 and the occupancies of the two components were refined and constrained to sum to unity (major component occupancy 0.55(2)). The two components share the position of the methine carbon (C88A/C88B) and one methyl carbon (C89A/C89B). In both cases, cyclohexyl and isopropyl groups, the atoms of the two disordered components were refined with isotropic displacement parameters. Additional geometric similarity restraints were applied to various bond lengths. A residual electron density peak of 1.11 e $Å^{-3}$ is observed 1.56 Å from C86 and is likely to be a result of further unresolved disorder in the triisopropylsilyl group.

Similarly single crystals of **4.5** gave weak data arising from poor crystallinity and rigid bond and similarity restraints were applied to the anisotropic displacement parameters of all atoms in the structure. The C–C 1,2 and 1,3 distances in the butyl chains were all constrained to have values of 1.50 Å and 2.50 Å respectively. The P–C distances, C–O carbonyl distances, C–N imide distances and C–C imide-perylene distances were all restrained to have similar values to their chemically identical equivalents and the terminal phenyl ring has been constrained to have regular hexagonal geometry. A residual electron density peak of 3.46 e $Å^{-3}$ is observed 0.83 Å from Pt1 which is likely to be an artefact caused by deficiencies in the absorption correction for the heavy-metal

containing platy crystal. A further electron density peak of 2.33 e $Å^{-3}$ is observed 1.54 Å from C6, which, although this is within the range of a chemical bond to the perylene core, the peak is in a chemically nonsensical position above the aromatic plane and likely to be a result of unresolved disorder or other experimental artefact.

Crystal data for **4.3**: $C_{58}H_{68}N_2O_4Si_2$, M = 913.32, monoclinic, *P*21/*n*, a = 17.734(8), b = 12.986(5), c = 23.8022(10) Å, β = 111.456(7)°, U = 5102(3) $Å^3$, Z = 4, T = 100(2) K, D_{calc} = 1.189 g cm^{-3}, μ = 0.118 mm^{-1}, F(000) = 1960. A total of 28020 reflections were collected, of which 8667 were unique, with R_{int} = 0.036. Final R_1 (wR_2) = 0.1845 (0.5150) with GOF = 1.91.

Crystal data for **4.5**: $C_{104}H_{146}N_2O_4P_4Pt_2$, M = 2002.29, orthorhombic, *Pbcn* (no. 60), a = 33.88(3), b = 14.178(13), c = 20.595(18) Å, U = 9893(15) $Å^3$, Z = 4, T = 100(2) K, Dcalc = 1.344 g cm^{-3}, μ = 2.939 mm^{-1}, F(000) = 4128. A total of 36399 reflections were collected, of which 8315 were unique, with R_{int} = 0.096. Final R_1 (wR_2)= 0.1490 (0.3850) with GOF = 1.16.

4.5. References

1. A. Terenin, *Acta. Physicochim. URSS*, 1943, **18**, 210.
2. A. Köhler and H. Bässler, *Mater. Sci. Eng. R-Rep.*, 2009, **66**, 71-109.
3. J. C. Koziar and D. O. Cowan, *Acc. Chem. Res.*, 1978, **11**, 334-341.
4. Y. Shao and Y. Yang, *Adv. Mater.*, 2005, **17**, 2841-2844.
5. F. Guo, Y.-G. Kim, J. R. Reynolds and K. S. Schanze, *Chem. Commun.*, 2006, 1887-1889.
6. C. W. Tang and A. A. VanSlyke, *Appl. Phys. Lett.*, 1987, **51**, 913
7. A. Buckley, *Organic Light Emitting Diiodes: Materials, Devices and Applications*, Woodhead Publishing Ltd., 2013.
8. B. Minaev, G. Baryshnikov and H. Agren, *Phys. Chem. Chem. Phys*, 2014, **16**, 1719-1758.
9. M. A. Baldo, D. F. O'Brien, Y. You, A. Shoustikov, S. Sibley, M. E. Thompson and S. R. Forrest, *Nature*, 1998, **395**, 151-154.
10. Y. H. Song, S. J. Yeh, C. T. Chen, Y. Chi, C. S. Liu, J. K. Yu, Y. H. Hu, P. T. Chou, S. M. Peng and G. H. Lee, *Adv. Funct. Mater.*, 2004, **14**, 1221-1226.
11. A. B. Tamayo, B. D. Alleyne, P. I. Djurovich, S. Lamansky, I. Tsyba, N. N. Ho, R. Bau and M. E. Thompson, *J. Am. Chem. Soc.*, 2003, **125**, 7377-7387.
12. W. E. Ford and P. V. Kamat, *J. Phys. Chem.*, 1987, **91**, 6373-6380.
13. E. Z. M. Ebeid, S. A. El-Daly and H. Langhals, *J. Phys. Chem.*, 1988, **92**, 4565-4568.
14. A. Prodi, C. Chiorboli, F. Scandola, E. Iengo, E. Alessio, R. Dobrawa and F. Würthner, *J. Am. Chem. Soc.*, 2005, **127**, 1454-1462.
15. R. D. Costa, F. J. Céspedes-Guirao, H. J. Bolink, F. Fernández-Lázaro, Á. Sastre-Santos, E. Ortí and J. Gierschner, *J. Phys. Chem. C*, 2009, **113**, 19292-19297.
16. M. Supur, M. E. El-Khouly, J. H. Seok, J. H. Kim, K.-Y. Kay and S. Fukuzumi, *J. Phys. Chem. C*, 2010, **114**, 10969-10977.
17. R. K. Dubey, M. Niemi, K. Kaunisto, K. Stranius, A. Efimov, N. V. Tkachenko and H. Lemmetyinen, *Inorg. Chem.*, 2013, **52**, 9761-9773.
18. H. Weissman, E. Shirman, T. Ben-Moshe, R. Cohen, G. Leitus, L. J. W. Shimon and B. Rybtchinski, *Inorg. Chem.*, 2007, **46**, 4790-4792.
19. A. A. Rachford, S. Goeb and F. N. Castellano, *J. Am. Chem. Soc.*, 2008, **130**, 2766-2767.
20. E. O. Danilov, A. A. Rachford, S. Goeb and F. N. Castellano, *J. Phys. Chem. A*, 2009, **113**, 5763-5768.
21. V. Prusakova, C. E. McCusker and F. N. Castellano, *Inorg. Chem.*, 2012, **51**, 8589-8598.
22. A. J. Tilley, R. D. Pensack, T. S. Lee, B. Djukic, G. D. Scholes and D. S. Seferos, *J. Phys. Chem. C*, 2014, **118**, 9996-10004.
23. Y. Wu, Y. Zhen, Y. Ma, R. Zheng, Z. Wang and H. Fu, *J. Phys. Chem. Lett.*, 2010, **1**, 2499-2502.
24. S. T. J. Ryan, R. M. Young, J. J. Henkelis, N. Hafezi, N. A. Vermeulen, A. Hennig, E. J. Dale, Y. Wu, M. D. Krzyaniak, A. Fox, W. M. Nau, M. R. Wasielewski, J. F. Stoddart and O. A. Scherman, *J. Am. Chem. Soc.*, 2015, **137**, 15299-15307.
25. F. N. Castellano, *Dalton Trans.*, 2012, **41**, 8493-8501.

26. F. Wurthner and A. Sautter, *Chem. Commun.*, 2000, 445-446.
27. C.-C. You and F. Würthner, *J. Am. Chem. Soc.*, 2003, **125**, 9716-9725.
28. C. Addicott, I. Oesterling, T. Yamamoto, K. Müllen and P. J. Stang, *J. Org. Chem.*, 2005, **70**, 797-801.
29. M. R. Wasielewski, *J. Org. Chem.*, 2006, **71**, 5051-5066.
30. Á. J. Jiménez, F. Spänig, M. S. Rodríguez-Morgade, K. Ohkubo, S. Fukuzumi, D. M. Guldi and T. Torres, *Org. Lett.*, 2007, **9**, 2481-2484.
31. R. F. Kelley, W. S. Shin, B. Rybtchinski, L. E. Sinks and M. R. Wasielewski, *J. Am. Chem. Soc.*, 2007, **129**, 3173-3181.
32. V. L. Gunderson, E. Krieg, M. T. Vagnini, M. A. Iron, B. Rybtchinski and M. R. Wasielewski, *J. Phys. Chem. B*, 2011, **115**, 7533-7540.
33. G. Goretzki, E. S. Davies, S. P. Argent, J. E. Warren, A. J. Blake and N. R. Champness, *Inorg. Chem.*, 2009, **48**, 10264-10274.
34. P. S. Pregosin and R. W. Kunz, *31P and 13C NMR of Transition Metal Phosphine Complexes*, 1979.
35. G. Goretzki, E. S. Davies, S. P. Argent, W. Z. Alsindi, A. J. Blake, J. E. Warren, J. McMaster and N. R. Champness, *J. Org. Chem.*, 2008, **73**, 8808-8814.
36. T. W. Chamberlain, E. S. Davies, A. N. Khlobystov and N. R. Champness, *Chem. Eur. J.*, 2011, **17**, 3759-3767.
37. A. G. Slater, E. S. Davies, S. P. Argent, W. Lewis, A. J. Blake, J. McMaster and N. R. Champness, *J. Org. Chem.*, 2013, **78**, 2853-2862.
38. K. I. Salokhiddinov, I. M. Byteva and G. P. Gurinovich, *J. Appl. Spectros.*, **34**, 561-564.
39. G. G. Dubinina, R. S. Price, K. A. Abboud, G. Wicks, P. Wnuk, Y. Stepanenko, M. Drobizhev, A. Rebane and K. S. Schanze, *J. Am. Chem. Soc.*, 2012, **134**, 19346-19349.
40. L. Liu, D. Huang, S. M. Draper, X. Yi, W. Wu and J. Zhao, *Dalton Trans.*, 2013, **42**, 10694-10706.
41. G. Sheldrick, *Acta Crystallogr. A*, 2008, **64**, 112-122.

Chapter 5. Conclusions

Three different series of perylene diimides (PDIs) have been synthesised and their optical, electrochemical and photophysical properties have been thoroughly investigated.

A dual approach of secondary amine functionalisation and imide carbonyl thionation was employed to induce a bathochromic shift in a PDI in order to synthesise two of the first examples of PDIs with an absorption maximum in the near infrared (NIR). The work in this Chapter demonstrates how the use of relatively simple synthetic modifications to a PDI can lead to molecules with the potential for application in extremely important areas of technology. The obvious next steps in this project are to incorporate these PDIs into photovoltaic devices in order to investigate how the increase in wavelength and the broad range of absorption affects the performance of these devices. Thionation is becoming an increasingly popular route to vary the properties of molecules, in a simple process, with only small modification to the overall structure. It is not at all surprising that rylene diimides, as one of the most intensely investigated class of dye compound in the last century, are coming to the forefront of this research. The two NIR absorbing PDIs in this Chapter are the first examples of bay substituted PDIs to be thionated, paving the way for a huge array of variations. However, there are still questions to be answered over the yield of the thionation reaction as well as the solubility and stability of the synthesised compounds.

Seven multichromophoric PDI-BODIPY systems have been synthesised, with the nature of the BODIPY and the position it is bound to the PDI varied. Whilst these compounds have fewer obvious direct applications than the thionated PDIs, the covalent attachment of two of the most interesting class of dye compound is a very worthwhile target. One of the most rewarding aspects to this project was the synthetic challenge of the target compounds, whilst both PDIs and BODIPYs are extremely

versatile, both present their own synthetic issues which required a substantial amount of route optimisation to overcome. The synthesis of the tertaBODIPY substituted PDI is achieved *via* ortho-substitution with a boronic ester, this is the first usage of this route since the original publications. There is huge scope for the synthesis of new PDIs with different properties by this method. However, purification of the boronic ester substituted PDI must be optimised before this technique can become commonly utilised. Transient absorption measurements are currently underway in order to fully elucidate the electron and energy transfer processes occurring. These measurements will add to our knowledge of how different chromophores interact, aiding in the development of fundamental understanding in order to mimic photosynthesis and improve the performance of electron transporting organic materials. This project leaves two main topics to be investigated; what is the nature of the communication between moieties across the PDI core and what causes the decomposition of the BODIPYs upon reduction. Addressing these two issues will greatly aid the future research carried out within this field.

The final Chapter in this thesis describes the synthesis and characterisation of two PDIs covalently bound to a platinum acetylide complex. PDIs with the ability to access the triplet excited state are relatively unusual with most examples achieving this by inter- or intramolecular sensitisation. These two compounds allow intersystem crossing by the direct attachment of a ‘heavy atom’ to the core of the PDI, a property possessed by very few other PDIs, with the potential for application in various technological areas. Crystal structures were collected for two of the synthesised PDIs which, similarly to the structures presented in the preceding Chapters, offer a rare and interesting insight into how these molecules interact with one another in the solid state.